Deinking pulp fractionation : characterization and separation of fines by screening

Saurabh Kumar

UNIVERSITÉ DE GRENOBLE

THÈSE

Pour obtenir le grade de

DOCTEUR DE L'UNIVERSITÉ DE GRENOBLE

Spécialité : **Mécanique des fluides Energétique, Procédés**

Arrêté ministériel : 7 août 2006

Présentée par

«Saurabh KUMAR»

Thèse dirigée par **«François JULIEN SAINT AMAND»** et
Codirigée par **«Raphaël PASSAS» et «Benjamin FABRY»**

Préparée au sein du **Laboratoire de Génie des Procédés Papetiers (LGP2)**
dans **l'École Doctorale : I-MEP2 : Ingénierie - Matériaux, Mécanique, Environnement, Energétique, Procédés, Production**

Fractionnement de la pâte désencrée: caractérisation et séparation des éléments fins par classage

Deinking Pulp Fractionation: Characterization and Separation of Fines by Screening

Thèse soutenue publiquement le **«14 Juin 2012»**,
devant le jury composé de:

Mme. Evelyne MAURET
Professeur, Grenoble INP-Pagora, France, Présidente

M. Harald GROSSMANN
Professeur, Université de Dresde, Allemagne, Rapporteur

M. Paulo FERREIRA
Assistant Professeur, Université de Coimbra, Portugal, Rapporteur

M. Frédéric VAULOT
Directeur R&D, Kadant-Lamort, France, Examinateur

M. Benjamin FABRY
Manager, Deinking Process, Centre Technique du Papier, Grenoble, France

M. Raphaël PASSAS
Ingénieur de Recherche, Grenoble INP-Pagora, France, Co-Directeur

M. François JULIEN SAINT AMAND
Directeur Adjoint R&D, Centre Technique du Papier, Grenoble, France, Directeur

CONFIDENTIAL

Abstract

Paper recycling has spread worldwide over the past several decades, reaching a current recovery rate over 70% in the European Union (EU) and leading to the positioning of recovered fibres as the major raw material for paper and board production, even over virgin fibres. Quite half of the recovered fibres are deinked, commonly by froth flotation, in order to remove ink besides other contaminants.

Deinking is a key process in a sustanaible stategy for papermaking. Thus, it is necessary to increase its efficiency, while reducing costs and environmental impact at the same time.

This research target has been pursued in several of some National and European projects in last years and it is also the aim of the work performed in this PhD, which is devoted to studying and optmising the fractionation as a crucial operation for new process designs.

Actually, approximately 30-45% of the whole deinking pulp is composed by the “fine fraction”, defined as the pulp fraction containing particles smaller than 75µm, mainly mineral fillers, cellulosic fines and ink particles. Most of the ink that should be removed from a pulp is present in the “fines”, under the form of isolated particles or linked to inorganic/organic surfaces. Moreover, some of the cellulosic elements contained in the “fines” have important significance to sheet property development. In particular, thin, fibrillar fine type category is more beneficial for mechanical property development than the blocky flake type fraction.

From above considerations, fractionation has been proposed and studied in the present project for a double target: i) to selectively separate fines in deinked pulps and then to apply deinking by flotation only to this fraction, instead of the whole pulp, with the consequent economical benefits, ii) to treat pulp fines and to isolate the most performing fines, for mechanical properties increase.

According to these targets, the work was organised as follows: Firstly, the development of methods for fines characterization, especially for understanding the attachment of ink to mineral filler and cellulosic fines. Secondly, the complete analysis of a specific fractionation technology involving pressure screening with fine perforations. And lastly, the application of the fractionation technology for deinking line simplification and stratified paper manufacture.

Fine sub-fractions analysed by a new manual classification method showed that the major contaminaton of ink occurs in the fraction, which passes an 11µm opening. This particular fraction also contains the finest cellulosic fibrils and flake particles as well as smallest mineral fillers. Visual analysis of the microscopic images revealed the fine fibrils are almost in majority ink free whereas flakes have ink deposition. Mineral fillers have varying degree of ink coverage: partial, complete or totally uninked. A new image analysis module developed showed the possibility to distinguish cellulosic fibrils, flakes and mineral flakes in a fine sub-fraction sample.

Separation of fines by a pressure screening system equipped with a 250µm smooth hole screen plate and solid core rotor show high selectivity towards the separation of fines into the accepts. The long fibres and specks contamination of a model deinking pulp were rejected and a 2-stage fractionation decreased the residual ink content of the long fibres. Analyses revealed that the thickening behaviour of micro-hole screen plate was different in comparison to other aperture types. Higher reject thickening values were obtained in comparison to wedge wire and other smooth-hole sizes reported in the literature. Analysis showed that the screen plate and solid rotor combination followed a plug-flow model with a high degree of fractionation defined as β, with a value of 1.0. It was relatively easier to

pass the chemical pulp fibres in comparison to mechanical pulp fibres. The rotor pressure pulsations were measured to understand the capacity constraints and limited hydraulic loading at higher concentrations. Even though the negative pressure pulse had a high magnitude of about 300kPa, increase in average passing velocity was not possible. Two reasons for this behaviour were analysed. Firstly the increase of the effective passing velocity was non-proportional with an increase of average passing velocity. Secondly at higher pulp concentrations, the pulp mat formation and non-disruption at the reject side led to reduce accept flow hence reduced capacity.

Flotation of the ink containing fines showed similar ink removal efficiency as compared to whole pulp flotation. But the selectivity of ink removal with respect to fibre loss was much higher in comparison to reference pulp mainly due to very low fibre concentration of the fines fraction. The results showed a promising advantage of the use of a micro-hole screen in deinking line rationalization where the fibre and contaminants are separated according to size and then treated. This gave rise to the option of parallel processing, where whole pulp is not treated in all operations but only a fraction is subjected into focussed treatments. A simple simulation showed that 3-stage micro-hole fractionation and fines flotation gave comparable properties as whole pulp flotation.

Lastly, the incidence of fines separation by micro-hole screen plate and their further hydrocyclone fractionation into fibrillar and flake fines types on sheet properties was shown. Incorporation of higher specific area fibrillar fines gave better strength and optical properties. In some cases, they were twice as efficient as the flake type fines.

To conclude, the study highlighted that new optimised deinking lines could be envisaged by introducing a specific fractionation technology and that pulp “fines” can be valorised, with an important impact in future manufacturing concepts as specifically enginnered multilayer papers.

The research leading to these results received partial funding from the European Community's 7th Framework Programme under Grant agreement N°24605 9.

Acknowledgements

Writing some lines of thanks would not justify of how much gratitude I have to the people who helped me shape my thesis from the very beginning until the very end. Without their efforts and time at every step, it would not have been possible to complete my thesis. I take this humble occasion to thank them all.

I am truly indebted, grateful, and thankful to my thesis director Dr. François Julien Saint Amand for his availability, discussions, encouragement, and persistent help.

My deepest appreciation and many thanks to my co-directors Dr. Raphaël Passas and Dr. Benjamin Fabry for their invaluable assistance, support, and guidance.

I thank them for their extreme patience and I was really fortunate to have them as my advisors.

I am also indebted and very much thankful to staff at the recycled fibres laboratories at CTP and the Optical microscope section at PAGORA LGP2. Geneviève Promonet, Max Guillet, Claude Guilmot, Bertine Khelifi, I sincerely thank you all for your immense help in analysis and your sincere dedication at pilot plant operations.

My thanks to Coralie Lefevre and Laurent Cizeron for their efficient help in supplying technical articles.

I would like to take this opportunity to thank my friends Elisa, Davide and their family for their help, guidance, and moral support in my personal and professional life.

I would like to acknowledge and thank every one of them who contributed to the success of my thesis through their help and advice.

Lastly, I would like to thank my family for their support.

Table of Contents

Nomenclature:

Symbols	Definition	Units
C_m	Critical concentration	%
d	Dimension of Bauer McNett square opening	mm
D	Screen basket internal diameter	m
D_h	Cylinder hole internal diameter	m
dp_r	Rotor suction pressure	kPa
lw	Length-weighted fibre length	mm
ERIC	Effective residual ink concentration	ppm
$L_{minimum}$	Minimum fibre length retained on a Bauer McNett mesh	mm
L_{mean}	Mean fibre length retained on a Bauer McNett mesh	mm
$L_{maximum}$	Maximum fibre length retained on a Bauer McNett mesh	mm
IF	Intensity factor	-
C_a	Screen accept concentration	g/L or %
C_r	Screen reject concentration	g/L or %
C_d	Downstream concentration	g/L or %
C_i	Screen inlet concentration	g/L or %
C_{ir}	Recalculated inlet concentration	g/L or %
C_U	Upstream concentration	g/L or %
Cp	Pressure coefficient	-
Cp_w	Power coefficient	-
Cq	Capacity coefficient	-
E_R	Reject efficiency (screening)	%
E_c	Cleanliness efficiency (screening)	%
f	Darcy friction factor	-

FI	Fractionation index	-
h	Profile height	mm
LF	Long fibre content	%
m	Power law consistency coefficient	$Pa.s^n$
n	Power law flow behaviour index	
N	Crowding factor	
P	Passage Ratio	
Pe	Penetration number	
P(l)	Length dependant passage ratio	
P_a	Screen accept pressure	kPa
P_i	Screen inlet pressure	kPa
P_r	Screen reject pressure	kPa
P_F	Passage ratio of ‘homogenous’ class of fibres	
P_K	Passage ratio of contaminants	
Q_a	Screen accept flow,	m^3/s or m^3/h
Q_i	Screen inlet flow,	m^3/s or m^3/h
Q_r	Screen reject flow,	m^3/s or m^3/h
R	Cylinder hole internal radius	m
R_m	Mass reject ratio	m
R_s	Screen basket radius	m
R_r	Rotor solid core radius	m
R_v	Volumetric reject ratio	
SF	Short fibre content	%
T	Thickening factor	-
V_a	Pulp axial velocity	m/s
Ve	Effective passing velocity	m/s
Vp	Passing velocity	m/s

V_s	Downstream slot velocity	m/s
V_t	Rotor tip velocity	m/s
V_u	Upstream slot velocity	m/s
W	Slot width	mm or µm
w	Fibre coarseness	mg/m
β	Degree of fractionation	-
λ	Pulp constant	-
ζ	Ratio of P_K/ P_F	-
ρ	Density of water	kg/m^3
μ	Water dynamic viscosity	mPa.s
L	Cylinder length (basket perforations)	m
ω_f	Fluid flow angular velocity	rd/s
ω_r	Rotor angular velocity	rd/s
x	Flow entrainment ratio = ω_f/ω_r	%

1. Introduction

The pulp and paper industry refers to the production of fibres from wood (bleached and/or unbleached chemical pulps and mechanical pulps) and to the production of paper and board from virgin fibres, recycled fibres (from recovered paper and board) and other raw materials (mainly mineral fillers and pigments, and other additives), as illustrated in Figure 1.

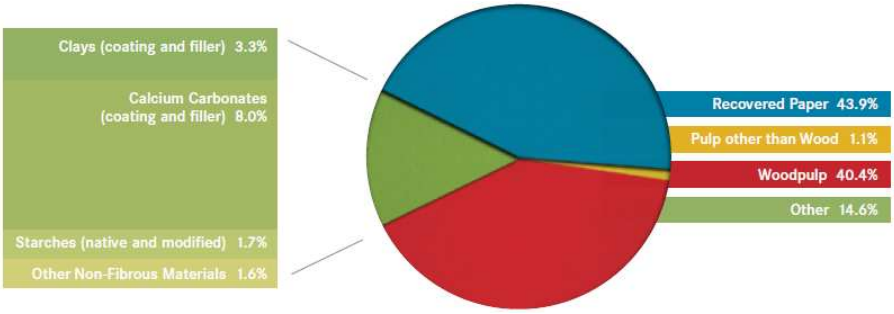

Figure 1: Raw material consumption in paper making in Europe, CEPI 2010 [1]

The European paper and board production, which amounts to about 25% of the global production, is estimated to 95 million tonnes in 2011, according to the latest statistics [2] established by CEPI, the Confederation of European Paper Industries. Graphic paper grades (newsprint and other uncoated and coated paper), represent 43% of the European production, packaging grades (corrugated board, carton board and flexible packaging) 45% and tissue paper 7%, as shown in Figure 2, which also gives the recovered paper utilisation rates for the different grades.

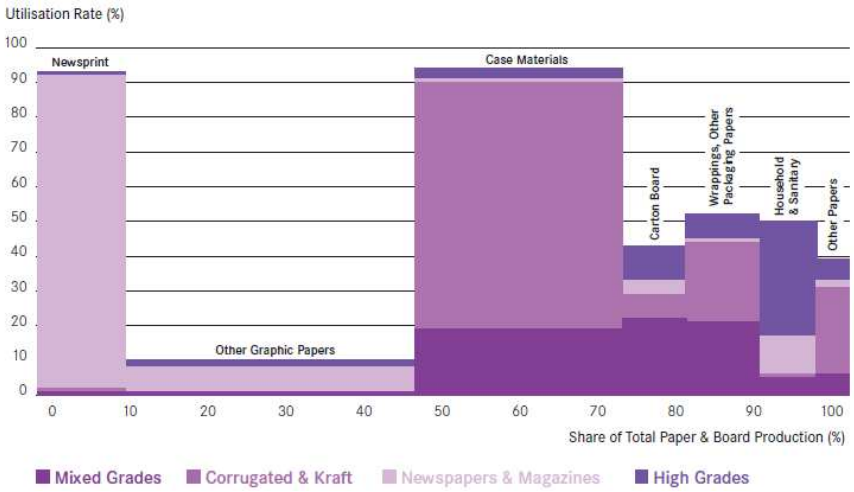

Figure 2: Recovered paper utilisation by sector, CEPI 2010 [3]

Brown packaging papers are efficiently recovered and recycled, especially case materials, while white graphic papers are mainly recycled, after deinking, in newsprint and to a lesser extent in tissue papers. The other graphic papers, including major super calendered (SC) and light weight coated (LWC) paper grades for magazines, are still essentially produced from virgin fibres. A great potential exists for these grades to increase the use of deinked pulp, and consequently the overall paper and board-recycling rate, to further improve the resource efficiency of the sector.

The continuous development of paper recycling over the last decades has indeed strongly contributed to improve resource efficiency through the saving of wood resources. The European paper and related industries will continue on this sustainable path to reach a new target of 70% recycling rate by 2015, according to the last European Declaration on Paper Recycling [4].

Improving overall resource efficiency, including water and energy, was the objective of a large European project Ecotarget [5] "New and innovative processes for radical changes in the pulp & paper industry" (2004-2008) aiming at reducing energy, wood raw material and fresh water consumption as well as waste and emissions. To achieve these goals of "more from less", Ecotarget included 6 sub-projects among which SP2 Recycled fibre supply and SP3 Furnish solutions with main activities on deinking and fractionation and SP4 Papermaking solutions with focus on stratified paper forming.

Fractionation, i.e. the separation in different fractions of various pulp components, such as fibres with different morphological properties, cellulosic fines, minerals pigments and inks, showed potential to save energy in the field of deinking as the right treatments where limited to the right pulp fractions instead of the whole pulp in the conventional deinking process.

Innovation in stratified paper forming technology based on a new headbox design showed potential to reduce the sheet basis weight at given physical properties, leading to savings in fibre raw material and consequently in the directly related energy consumption at the pulp and paper production. The new headbox technology achieved significantly reduced layer mixing in order to enable the application of stratified forming to graphic paper grades. Together with fractionation, the new stratification technology offered then new perspectives to develop improved resource efficient papers by using the best pulp fractions in the right layers to achieve the best paper bulk and surface properties.

The European project BoostEff [6] "Boosting raw material and energy efficiency using advanced sheet structure design and fibre modifications" (2010-2013) aims at developing new manufacturing concepts for wood-fibre based products giving a significant reduction in environmental footprint. The objectives are to achieve at least: 20% energy efficiency increase, 20% CO_2 and other GHC emission reduction, 20% raw materials saving and 10% operating cost reduction or productivity increase.

Future manufacturing concepts meeting these goals will be developed within BoostEff for 3 products: SC paper made from virgin fibres (mainly mechanical pulp); LWC paper made from recycled fibres (deinked pulp) and fibre board for the construction and furnish sectors. The BoostEff research and demonstration programme established for the SC and LWC papers includes further development of the findings achieved in Ecotarget, namely the new sheet stratification technology and fractionation based on hydrocyclones, as well as a new fractionation technology based on micro-hole screening.

The work reported in this manuscript has been carried out in the framework of the BoostEff project. The research has been focused on "**fines fractionation**", i.e. the separation of fine elements towards the optimisation of the deinking process and the use of the pulp fractions in a layered paper sheet.

The main objectives were:

- To **separate the fine elements**, i.e. ligno-cellulosic fines, mineral fillers and pigments, inks and other small/colloidal deinking pulp contaminants, from the fibre fraction, for further treatment and use, including in stratified sheets,
- To **develop the characterisation** of fine elements in this respect, i.e. for the evaluation of the fractionation processes and the understanding of the role and effects of fines in the paper,

- To determine **the fractionation possibilities** of a new **micro-hole screening technology** and develop the understanding of the screening mechanisms, as no fundamental research has been reported before on such micro-hole fractionation technology,
- And finally to **evaluate first applications** of **fines fractionation** to the optimisation of deinking processes and the use of fibres and fines fractions in stratified SC and LWC papers.

Most of the experimental work, including the characterisation of fine elements, the investigations on fractionation processes, and the treatment and use of different fractions has been mainly performed on deinking pulp (DIP), as well as on stone ground wood (SGW) mechanical pulp according to the target stratified paper products, i.e. LWC and SC papers defined in BoostEff.

The manuscript has been composed of the following 3 sections:

Chapter 2 is devoted to the characterisation of fines in both laboratory pulped and industrial grade recycled fibre raw material composed of Old NewsPrint grade (ONP) and Old Magazine grade (OMG). A state of the art has been first established on fines which relates to their importance in papermaking operations. To have a better understanding of their 'weight' distribution and more importantly for microscopic observations, a new manual method to sub-fractionate fines in lower size categories was developed. Pulp classification by laboratory equipment - Bauer McNett and the new method provided a complete end-to-end picture of the fibre and the fine fractions. Ink occurrence in various sub-fractions and fine types were analysed with light microscopy. To possibly distinguish fine types, a new image analysis method was shown to separate particle types based on their grey-level intensity.

Chapter 3 concerns a detailed, in-depth study focussing on the phenomenon of fines fractionation with a micro-hole screen plate and solid core rotor. Separation has been analysed with respect to morphological properties of fractions and by developing flow models. The degree of fractionation/selectivity achieved with micro-hole has been assessed and compared with other aperture openings. To understand the hydrodynamics of micro-hole screening mechanisms, research has been centred on the measurement of the screen plate losses and rotor pressure pulsations. Possible reasons of capacity constraints have been provided with simple simulation methods.

Chapter 4 deals exclusively with the application of fines previously separated during pressure screening fractionation. Possible integration of such a screening system with the objective of deinking line simplification has been studied, with the concept of right treatment to right fraction. Separately, another approach has been put forth where the ability of fines in enhancing paper sheet properties has been illustrated by their further fractionation and incorporation.

Chapter 5 provides the concluding remarks and perspectives.

2. Characterization of fines

2.1. - State of the art

A paper sheet is mainly composed of naturally occurring cellulose fibre extracted from the wood and annual plants. Dimensional and shape characteristics of cellulose fibres making up the paper sheet vary in a wide range.

The cellulose fibres are liberated from the wood matrix by processes using chemicals or mechanical action. The process themselves are called as chemical pulping and mechanical pulping respectively.

The uniqueness of cellulose fibres from different origin provides different or specific paper properties. For example, to enhance optical properties of a paper sheet: fibres from mechanical pulping are desired as these assist in light scattering coefficient as compared to that of a chemical pulp fibre which increase the mechanical strength and related properties of a sheet of paper. The technical term for softwood fibres is tracheids, but in general paper industry parlance, they are also called as fibres.

The typical fibre dimensions (length and width) are reported in Table 1.

Table 1: Cellulosic elements characteristics, from Passas [7]

	Length mm	Width µm	Length/Width ratio
Fibres	**0.8 – 1.6**	**15 – 20**	**~150**
Softwood fibres	**2 - 4.5**	**20 - 75**	**100 - 200**
Tracheid fibres	**0.6 – 1.6**	**15 – 25**	**~100**
Vessels	**0.6 – 1.5**	**40 – 150**	**1 - 30**
Parenchyma cells	**0.08 - 0.015**	**10 – 15**	**8 – 10**
Shives	**0.4 - 0.5**	**60 – 400**	**1 – 50**

2.1.1. - Cellulosic fines

A cellulose fibre is not a single and solid entity but is composed of different layers (or sub-layers) of varying thickness as show in Figure 3 and the layers have different chemical compositions. The middle lamella (M) serves as a cementing matrix to hold the different fibres together as the tree grows. The S2 layer occupies the maximum volume of the fibre multi-layer structure and with the S3 layer contains the majority of the cellulose content of the fibre.

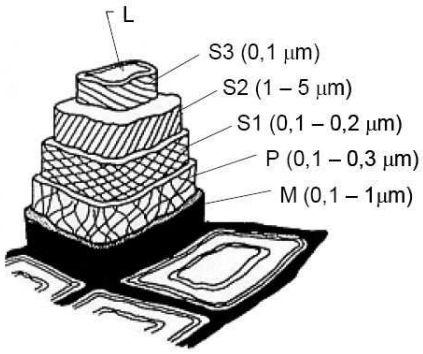

Figure 3: Fibre structure, from Forsström [8]

Fines as the name itself indicates refers to the finer material contained in the pulp suspension. The difference between the fines category and other components of the pulp suspensions is made on the basis of size. The term combines all particles in the fibrous suspensions (both organic and inorganic) not including dissolved and colloidal substances, which **p**ass (**P**) an opening of 75µm or a nominal 200 mesh screen. Mesh N° is equal to the number of open ing per linear inch, lower mesh numbers indicates large opening. The part of fibrous suspensions which does not pass the aperture and is retained/rejected on it is generally denoted by **R**. The Technical Association of Pulp and Paper Industry, TAPPI, standard T-261-00 recommends using this approach which is based on the review of the published articles. This differentiation has been generally agreed by numerous researchers. There are many other authors who have supported this definition either on account of TAPPI standard or on the basis of other authors who have used the P200 basis while defining fines [9][10][11][12] even if some authors mention the use of 100 mesh or 150µm opening [13][14][15]. Bauer McNett P200 mesh criteria have been followed while performing fines characterisation analysis in this thesis.

Mechanical pulp contains a considerable amount of fines, their quantity can be as high as 30-50% by mass [10][16][17] whereas in case of chemical pulps it is in the range of 10-15% by mass [10][17]. Kartovaara [18] mentioned “It is no exaggeration to say that the position of mechanical pulp as a raw material for printing paper production is due almost exclusively to its unique properties of fines components.” A major utilisation of mechanical pulp is in the manufacture of newsprint where sheet opacity and good printing properties are necessary. Since the middle of the last century, the mechanical pulp fines have been extensively studied [19][20].

Cellulosic fines are broadly classified into 2 categories according to their formation during the pulp manufacturing process.

Primary fines:

These fines are released during the pulping stage where the de-fiberation takes place to release individual fibres from the wood matrix. In other words the primary fines are present before the pulp is subjected to any mechanical treatment. They consist in majority of ray cells, pith, parenchyma cells [17] and also possibly fragmented vessels.

Secondary fines:

These fines are formed during the application of mechanical energy on fibres structure (e.g. refining operation for fibre characteristics development). Such fines result mostly from the fibre shortening and fibre fibrillation which gives rise to very thin, slender, long and linear ribbon-like particles and also thin lamellae (cf Figure 4).

However, all the fines particles of mechanically manufactured wood pulp cannot be termed as secondary fines. In such pulps, the ray and parenchyma cells still belong to the category of primary fines. The classification of fines into primary and secondary fines/particles derives from the research on chemical pulps in which there are primary fines (ray cells) liberated from wood structure during the chemical pulping. Secondary fines are generated when the pulps/fibres are beaten.

Fibrils and flakes

The first fundamental studies on fines characterization were performed in 1939 by Brecht & Holl [19] and later in 1953 Brecht & Klemm [20]. They divided the cellulosic fines (using 135 mesh) into two very distinct categories based on morphology (shape) and dimensional characteristics (size). And coined the terms: ‘flour stuff- *Mehlstoff*’ consisting of fibre pieces and ‘slime stuff- *Schleimstoff*’ which contained fine fibrils shown in Figure 5. The flour stuff or flakes are present either as primary fines- ray or parenchyma cells and fragmented vessels elements or as cell wall fragments / thick lamellae formed during mechanical action. Whereas the fibrils are thin band, ribbon like particles generated during refining action on fibres.

The flakes or the flour stuff consist of granular fibre pieces, fibre fragments, cell wall fragments, thick lamellae particles and ray cells; stiff and compact block/brick-like particles. The flake fines originate from primary fines or during mechanical action on fibre wall – lignin rich middle lamella/ primary wall [21]. The slime stuff consisted in majority of ribbon like fine fibrils and thin lamellae particles. Alince *et al.* [22] mentioned that the mechanical pulp fines contain fibrillar as well as flaky material whereas the chemical pulp contains mostly fibrillar fines. Fibrils are more flexible than flakes

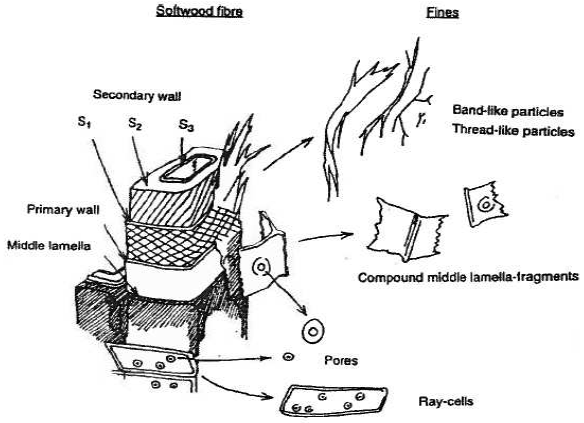

Figure 4: Formation of TMP fines, from Rundlöf [23]

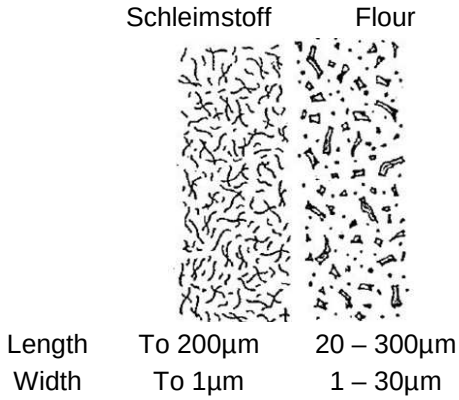

Figure 5: Schleimstoff (left) and Flakes (right), from Brecht & Klemm [20]

The idea of Brecht *et al.* [19][20] was later elaborated by Forgacs [16] in his study to understand the formation of the two types of fines particles, with the last fraction being the particle debris shown in Figure 6. Conformable, well separated fibres, ribbon like thin fibrils provide much better bonding potential in comparison to fibre bundles or type chunk fines.

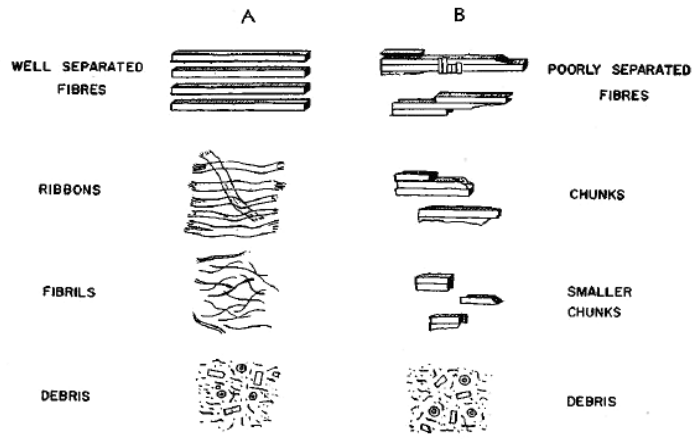

Figure 6: Formation of fibrils and chunk fines (or flakes) in mechanical pulp, from Forgacs [16]

Fines properties

Fines play a pivotal and defining role in control of sheet properties. Addition of specific fines can shift in considerable proportions the property evolution as shown by Retulainen *et al.* [17] in Figure 7. Chemical pulp fines (kraft pulp) had little impact on light scattering coefficient and a major impact on tensile index whereas the mechanical pulp fines (TMP) increased both light scattering and tensile strength but to a lower extent for this last property. Another important aspect even with a blend of different pulp, the final properties are being defined by fines.

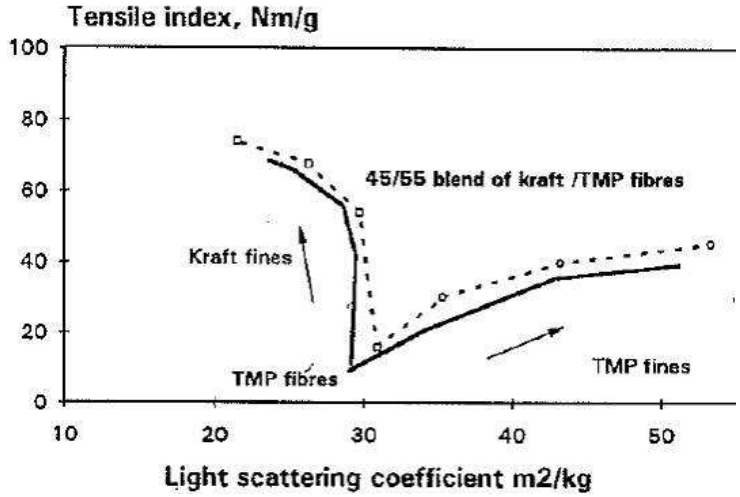

Figure 7: Chemical pulp (Kraft) and Mechanical pulp (TMP) fines effect on a blend ofKraft and TMP fibres, from Retulainen *et al.* [17]

Fines increase the sheet densification and sheet consolidation improves sheet mechanical properties notably the tensile index and also the surface smoothness. However, sheet densification lowers the light scattering coefficient, air permeability and sheet porosity as well as sheet bulk. Being small particles, fines fill in the voids between fibres and create additional bonding area, thereby increasing sheet mechanical properties. The evolution of the tear strength reaches an optimum increase with a certain amount of fines addition [11][15][20][24]. Apart from size difference between fibre and fines, one of the major differences is the specific surface area. Indeed due to their small size, fines offer a high filtration resistance to dewatering as compared to fibres as they possess a high specific surface per gram of matter [11][14][16]. Using the measure of permeability across a fibre pad, Forgacs [16] observed that for mechanical pulps the value of R28 fraction was 0.5-0.9m²/g, for P100 R200 was 2.5 – 4.0m²/g and it was highest for P200 fines 14-19m²/g. More finer is the material, higher will be its specific surface area and better will be the sheet properties.

Since the time of Brecht & Klemm [20], very extensive, elaborated and dedicated research has been done by numerous workers to better understand fines as such or the two distinct categories with respect to properties they provide to a cellulosic paper sheet. Majority of the studies have been focussed on mechanical pulp fines as their amount is of significant proportions in the pulp.

Flake fines possess poor bonding ability and constitute the non-fibrillar material. The flaky ray cells constitute the majority of primary fines in case of chemical pulps [25]. During the mechanical pulp manufacture, these ray cells, which are highly lignin rich, are liberated. These cells have low aspect ratio, poor bonding as well as swelling ability and cause sheet linting defect [25][26][27]. Wood contains 5% of ray cells and the fines fractions as much as 15-20% [27].

Fibrillar fines improve the sheet consolidation- sheet density, have a pronounced positive effect on the strength properties, improve printing pick speed, reduce sheet linting and sheet roughness [20] [26].

Luukko & Paulapuro [21] observed that the mechanical pulp fibrillar fines originating from the cellulose rich S2 layer of the fibre have a much larger specific surface area, indicated by specific volume in Figure 8, and swell more. These fibrillar fines are able to overcome the drying cycles of sheet making and hornification (cf. Figure 9). Laivins & Scallan [10] reported that fines swelling degree is double that of a fibre and hornification associated with chemical pulp fines could be negated by a beating treatment, which also leads to formation of high ability secondary fines. Krogerus [27], Bäckström *et al.* [28], Mancebo *et al.* [29] mentioned that the secondary fines swell more and provide better sheet properties than the primary fines.

Studying the fines produced during the secondary and reject refining stages of the mechanical pulp manufacture, Richardson *et al.* [30] and Luukko [31], noted that the later stages fines were more fibrillar with a higher specific surface area as compared to first stages. These fines gave better improvement to sheet characteristics.

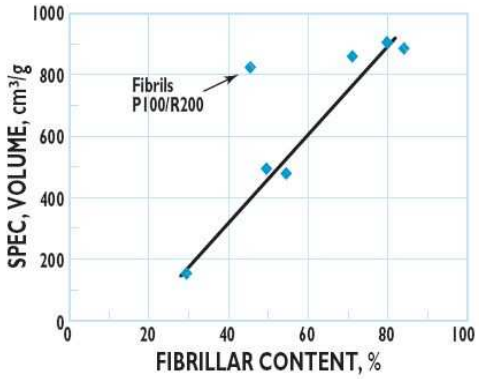

Figure 8: Fines specific volume and fibrillar content, from Luukko & Paulapuro [32]

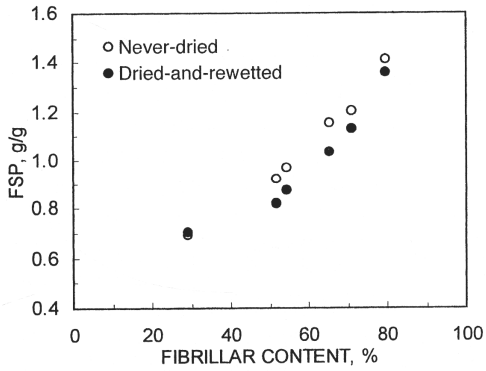

Figure 9: Fibre saturation point for mechanical pulp and fibrillar content, from Luukko & Maloney [21]

Researchers noted and emphasised that the fibrillar content of fines (produced either during chemical pulp beating- secondary fines or mechanical pulp manufacture) define the mechanical strength properties of the paper sheet in comparison to flakes, and this is specifically and principally related to their high specific surface area [20][28][32] as shown in Figure 10.

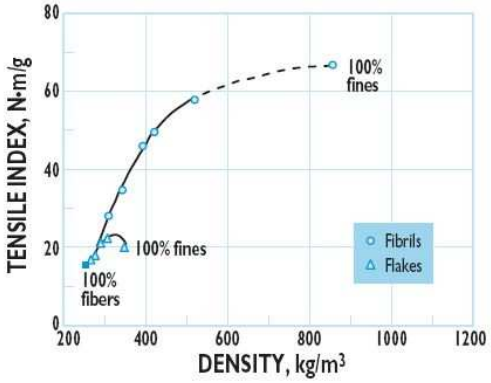

Figure 10: Effect of fibrillar and flakes fines content, from Luukko & Paulapuro [32]

Fines dimensions

One defining dimension comes from the initial definition – particles passing through a 200 mesh screen or 75µm square side/106 µm square diagonal. But the size range does not stop over here, indeed as mentioned by Rundlöf *et al.* [33][34], fines dimensions can be much smaller than a 635 Bauer McNett mesh or 20µm opening.

For a mechanical pulp Luukko *et al.* [35] mentioned 70% of fine particles (P200) are contained in the P400 mesh fraction (38µm opening) and fibrils are light weight – 80% fibril population could correspond to just 30% mass fraction. Retulainen *et al.* [12] while studying chemical pulp fines (P200) also observed that over 60% of such particles traverse a 400 Bauer McNett mesh.

Fines particle shape and the particle size are important criteria defining the paper sheet properties. The finest particles addition (P400) gave the best results for the tensile strength increase (cf. Figure 11 and Figure 12). It could be said that such category of fine particles provide excellent 'packaging'

between fibre layers. Rundlöf *et al*. [36] also observed that the smallest particle fraction passing the P400 mesh fraction gave the best properties.

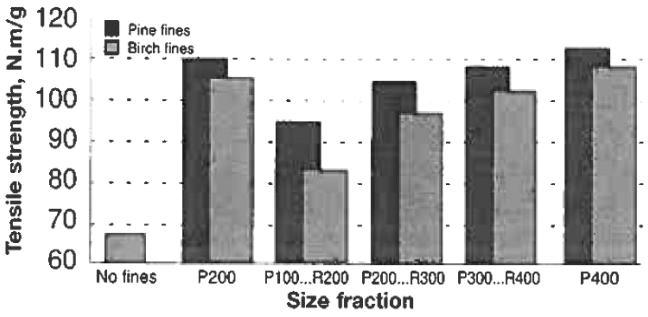

Figure 11: Effect of fine size on tensile strength, from Retulainen *et al.* [12]

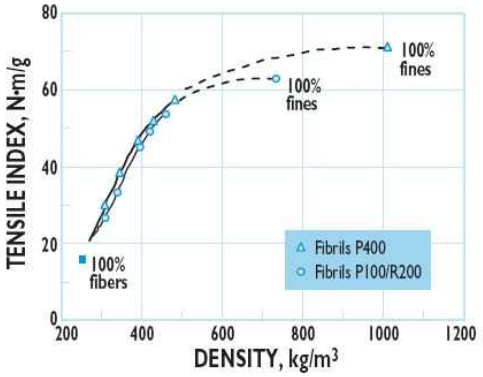

Figure 12: Fibril size effect, from Luuko & Paulapuro [32]

Luukko *et al.* [35] using image analysis techniques observed the fibril length of different mechanical pulps fines, which varied from 60µm to 119µm. Retulainen *et al.* [12] indicated the equivalent diameter (diameter of a circle having the same area as particle surface area) of fines particles between 5.5µm to 7.1µm. The length of the fibrils can be equal or shorter than the original fibre length. Ferreira *et al.* [37] observed that for a lab prepared kraft pulp secondary fines, most of the fine are less than 10µm equivalent volume diameter. A summary of fine particle dimensions by Krogerus *et al.* [26] is presented in Table 2.

Table 2: Fine dimensions, from Krogerus *et al.* [26]

Fines type	Origin	Morphology	Content %	Size
Mechanical fibre fines	**Mechanical pulp**	**Fibrils Flakes Ray-cells**	**10-40**	**Fibril length: <200 µm Width: 0.2-10 µm, Lamellas: <20 µm Flour stuff: 20-300 µm**
Primary fibre fines	**Unbeaten chemical pulp**	**Ray-cells Lignin flakes from middle lamella**	**2-10**	**Softwood ray cells length: 10-160 µm width: 2-50 µm**

Fines separation and characterization methods

Pulp fines elements contain a wide range of particle size as well as shape. Researchers have employed various fractionating equipment as well as 'modified' techniques to separate fines elements principally based on size characteristics or surface characteristics – specific surface area. The investigations focussed on the different types of fines elements present in the pulp suspension – cell wall elements or separation of fibrillar and non-fibrillar/flaky material.

One of the widely used fines separation method used in laboratory set up is the Bauer McNett classifier which consists of 4 or 5 series of agitated tanks fitted in series with decreasing mesh opening aperture. Water at constant flow rate is introduced in the first tank; where a fixed amount of pulp is also introduced. The overflow flows by gravity to the next tank, containing particles- organic or inorganic which have passed through the tank screen. This continuous process is repeated till the last tank and the final outlet or overflow from is drained off or collected for analysis. After a stipulated time, retained fibres on screens are collected, dried and weighed to calculate mass fraction retained on each mesh screen, while the difference between the starting pulp amount and the sum of all retained fractions gives the final passing fraction. The TAPPI standard T 233 cm-06 relates to fiber length of

pulp by classification and reports the use of Bauer McNett equipment for pulp fractionation. Opening size of Bauer McNett mesh used for pulp analysis is reported in Table 3.

Table 3: Bauer McNett mesh opening size

Bauer McNett mesh	Opening size
14	1180 µm
28	600 µm
48	300 µm
100	150 µm
150	105 µm
200	75 µm

Dynamic drainage jar is equipment, which consists of a single vertical cylindrical agitated jar with a single screen of 76µm opening. To have more information on smaller size particles, researchers worked on successive sieving and sedimentation methods. For example, Hardell & Westermark [38] developed a method to separate wood elements into fibres, fines, ray cells and vessels by the use of different wire openings as shown in Figure 13. This was further developed by Westermark [39] using nylon sieves to isolate and study the middle lamella fragments using a 30µm sieve opening as shown in Figure 14.

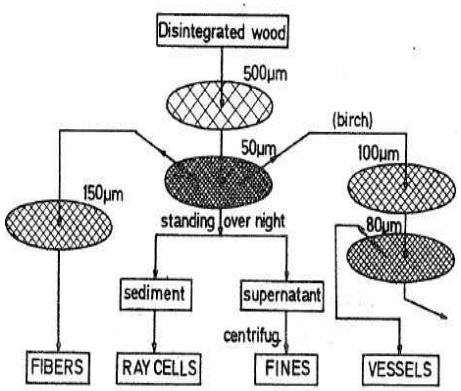

Figure 13: Separation technique of wood elements, from Hardell & Westermark [38]

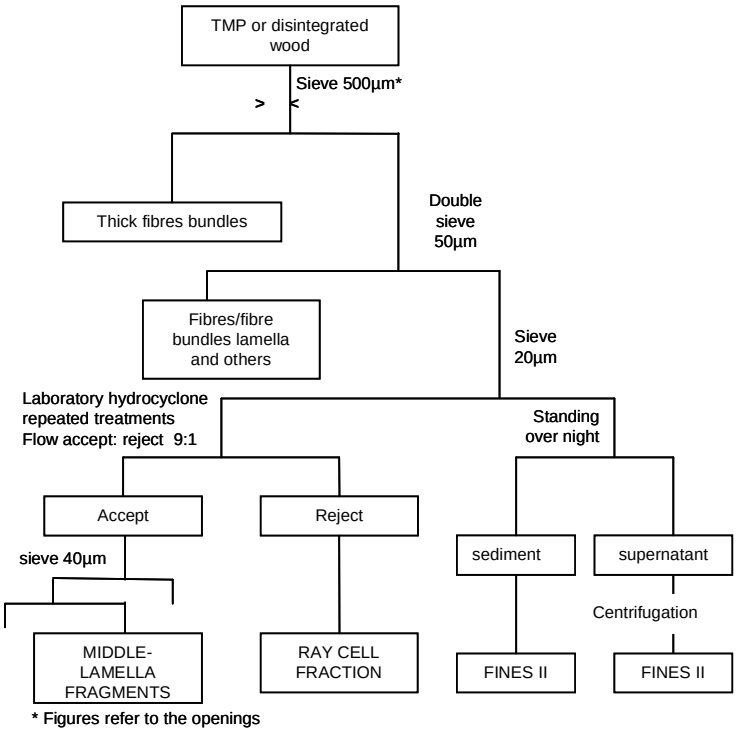

Figure 14: Separation technique for middle lamella fragments, from Westermark [39]

Other equipments to separate fines include Celleco washer as shown in Figure 15, with diluted slurry jet impingement on a small aperture screen with reject recirculation [26][40]. Represented in Figure 16 is a float wash fractionator – employing vacuum suction [40] and a tube-flow fractionator [41], which is other laboratory scale equipments for fines separation.

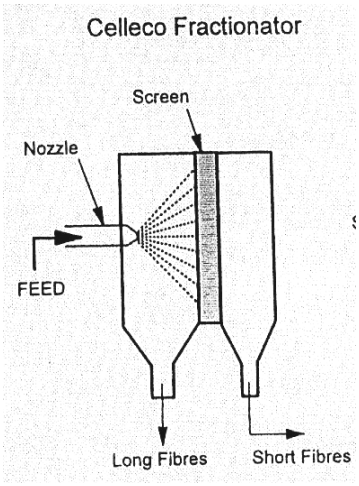

Celleco fractionator
from Karnis [40]

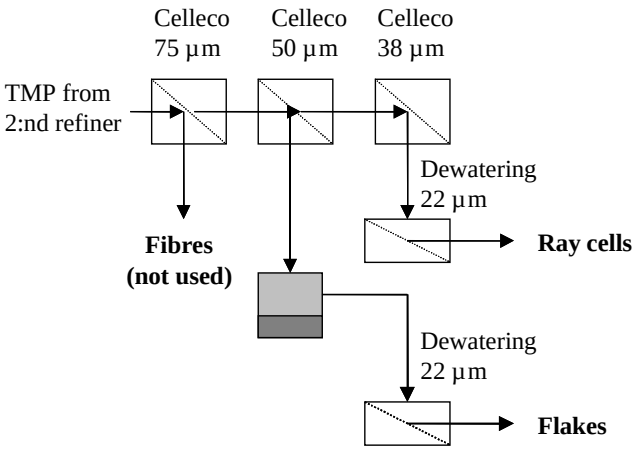

Series of celleco fractionator,
from Krogerus *et al.* [26]

Figure 15: Celleco washer (left) and a combination of washers with different opening sizes (right)

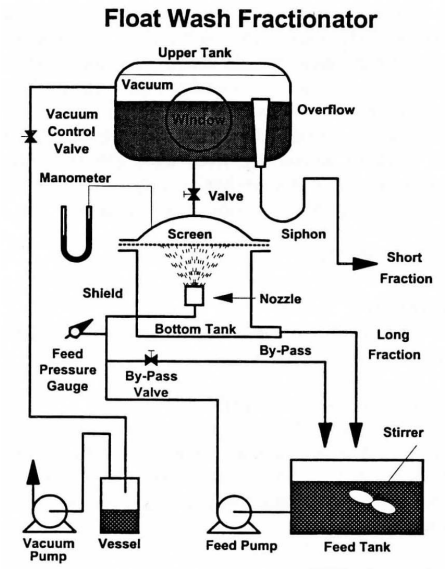

Float wash fractionator
from Lapierre *et al.* [42]

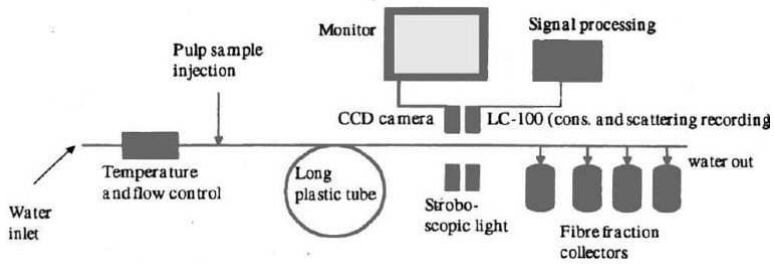

A tube-flow fractionator device outline,
from Laitinen *et al.* [41]

Figure 16: Laboratory fines separation equipments

Fractionating hydrocyclones have been adopted to separate fibre and fines based on specific surface area. The accept fraction contained high specific surface area elements or the fibrillar material while the rejects contained low specific area flakes [1][39][43]. More details have been provided in the chapter n°3. -Fractionation processes and separati on of fines.

Fine separation method usually requires large quantities of water, for example in case of Bauer McNett 11.35L/min for 20 minutes (TAPPI standard 233-cm-06). Overnight sedimentation is one of the techniques employed to concentrate and recover the diluted fines [24][26][31][35]. The process of settling and sedimentation techniques has also been proposed to separate inorganic fines from cellulosic fines in specially designed wedge-wire sedimentation cells [44].

Due to their small dimensions and heterogeneity of particles (especially in the case of deinking pulp) the fines measurement techniques are often based on image analysis (one of the first study done Pelton *et al.* [45]) on microscopic slides or flow of very dilute fines suspensions across a very narrow tube [35]. Developments in imaging and measurement technology have helped to advance their

understanding. It is generally agreed that a human eye can visualise particles with at least two dimensions larger than 40µm [46].

To measure the fibrillar and non-fibrillar (or flakes) Luukko *et al.* [35] developed a new system, the first of its kind based on image analysis and used it to quantify mechanical pulp fines (relative volume proportions). The basis of differentiation was the fact that the thin ribbon like fibrils are brighter or have a higher grey tone value as compared to thick and dark flakes, which have lower grey tone values. The image was treated with relative and joint entropy algorithms. An exponential function was observed between particle thickness measured using confocal laser scanning microscopy, and grey tone values of flakes and fibrils, shown in Figure 18. The first version of the equipment is shown in Figure 17, which measured the two different fines type stained with basic bright blue dye deposited on a glass slide. Manual microscopy is time consuming and laborious and does not lead to rapid analysis [47]; hence the system was further developed and improved consisting of image analysis of dilute fine suspension flowing through a flat rectangular glass cell with 200µm spacing and 5mm wide [26][47]. The image analysis program catered for and eliminated flocculated particles, which might be appearing as one large single particle. Rejection filter was created for only flakes when the size corresponded to 200 mesh size. However all fibrillar particles which might influence bonding properties were not accounted for in light microscopy as the lower limit was 1µm.

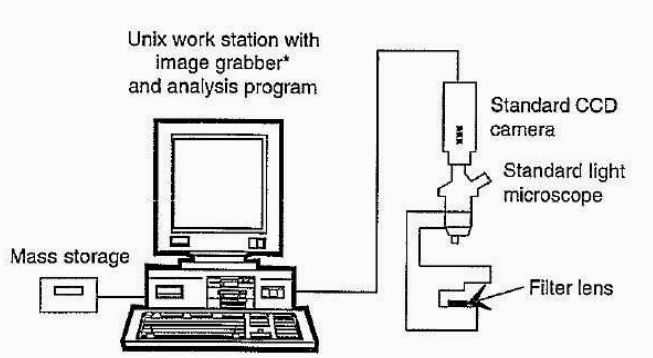

Figure 17: Image analysis method set-up 1st version, from Luukko *et al.* [35][47]

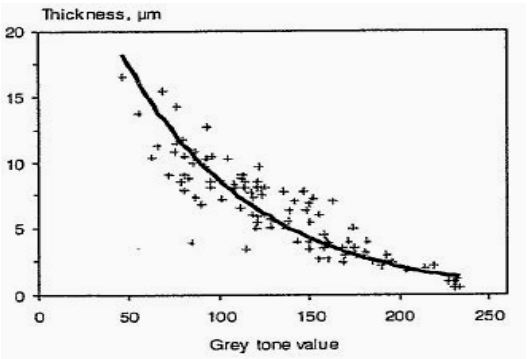

Figure 18: Exponential relation between fine particle thickness and grey tone values, from Luukko *et al.* [35][47]

The specific surface area of fines has also been correlated with turbidity measurements [26][43] [48][49]. As indicated in Figure 19, smaller is the particle; higher is the value of turbidity. At very low fines concentration, the turbidity value is low and the relationship to consistency is not linear. Fibrils, owing to their high specific surface area, leads to an increase of turbidity values while augmenting their amount, cf. Figure 20.

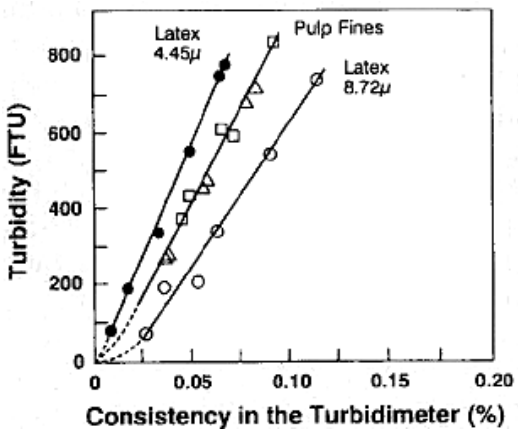

Figure 19: Comparison of turbidity of polystyrene latex spheres and mechanical pulp fines, from Wood & Karnis [49].

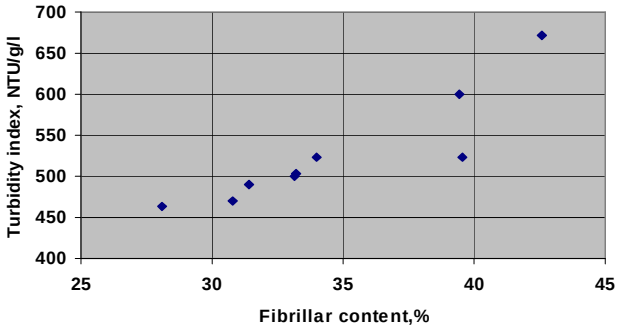

Figure 20: Turbidity index and fibrillar content, from Krogerus *et al.* [26]

A summary of the fines characteristics in general and their types is provided in Table 4.

Table 4: Fine typical characteristics summary

Classification by (ex.) Bauer McNett Dynamic drainage jar	Fines separation based on size (irrespective of fine type) – quantitative and not qualitative
Fines in general	High quantity – Mechanical pulp and deinking pulp Low quantity – Chemical pulp Highly important for sheet properties. Development of mechanical strength properties. Contribute to sheet surface structure. Provide optical properties enhancement. Ash (mineral content): negative effect on sheet strength properties, improvement of optical properties Homogeneous material - mechanical or chemical pulp fines; only organic cellulose fines Heterogeneous material – Deinking pulp Organic cellulose and inorganic mineral filler, ink particles, stickies
Cellulosic fibrillar fines	Long, slender, filaments, narrow, thin ribbon like structure, thin lamellae. Excellent bonding ability. Proportional to paper strength. High specific surface area/ drainage resistance. Lead to a high value of turbidity Cellulose rich, more swell-able, more flexible Brighter: higher grey tone value. Light in weight
Cellulosic flake fines	Chunky, block, thick, cell wall fragments, ray cells Poor bonding ability. Low specific surface area/ low drainage resistance. Lead to low value of turbidity. Cellulose deficient, lignin rich (ex. ray cells). Cause linting, extractive deposits Darker: lower grey tone

2.1.2. - Deinking fines and characterization

In a deinking line, one of the major pulp component falls in the category of fines. Depending on the raw material for paper manufacture, the amount could be in the range of 25-55% [41][50][51][52]. These fines are composed of the different types of cellulosic organic fines as described earlier and inorganic materials which are either introduced into the paper during its manufacture (mineral fillers) or either during its printing (mineral fillers in surface coatings and ink) and converting (adhesives). The cellulosic fines are however at least once dried before being recycled in the deinking operations.

2.1.2.1. - Mineral fillers

The microscopic mineral fillers lend different properties to the paper sheet, noticeably amongst them is the increase of opacity and the gain of brightness. The individual particle diameter of these fillers is less than 10µm, (cf. Table 5). In general paper industry jargon, the agglomerates of mineral fillers having their origin from paper coating are called coating flakes or mineral flakes with respect to their origin.

Table 5:Filler dimensions, from Katsura & Murakami [53]

Mineral filler type	Particle diameter (µm)
Talc	2.31
Clay	1.06
Ground calcium carbonate	0.94
Precipitated calcium carbonate	0.49

Mineral filler added in paper mass are coarser than fillers added during coating. However, when reslushed (for e.g. repulping of coated magazines in deinking operations) a part of filler from the coating layer is still strongly linked together leading to mineral filler flake. A part of the filler can be also found in individual form.

2.1.2.2. - Ink

One of the most ‘disturbing’ element, which leads to easily noticeable visual contamination, is the ink. It has to be efficiently removed to manufacture high quality paper. Individual ink particles (before being deposited on the paper sheet) are in the microscopic and sub-microscopic range and are composed of naturally occurring pigments or carbon black. Saari [55] indicated that the fragmentation level of ink covered cellulose fibre is different for different types of ink. Ferguson [54] mentioned the ink particle size after the initial defibering operations from various printing processes, Table 6, Most of the ink particles measured by image analysis techniques were lower than 30µm range, except for coated papers and non-impact xerographic toner particles.

Table 6: Ink particle size after pulping printed paper, from Ferguson [54]

Printing process	Letter press	Offset	Flexography	Gravure	Laser/ Xerographic
Uncoated paper µm	2-30	2-30	0.3-1	2-30	40-400
Coated paper µm	10-100	5-100	0.7-2	5-30	40-400

One of the widely used optical control parameter used in recycled fibre operations is **E**ffective **R**esidual **I**nk **C**oncentration or **ERIC** [56]. This value provides the qualitative aspect of the ink present in the pulp, but does not give the actual amount of ink in the pulp suspension. Measurement is made using infrared light spectrum at 950nm as it was shown that the ink only absorbs light at this wavelength spectrum. Small ink particle size leads to a high value of ERIC [57] and its removal or reduction leads to an increase of brightness levels across the ink removal unit operations [41][52][57].

In deinking operations, one of the first studies using an image analysis, a model was proposed by McCool & Silveri [46], where the removal efficiency of specks for different deinking unit operations was

described. Many researchers have mentioned that the small size ink particles are removed during the flotation operations, which is very selective [41][58][59] (cf. Figure 21 and Figure 22).

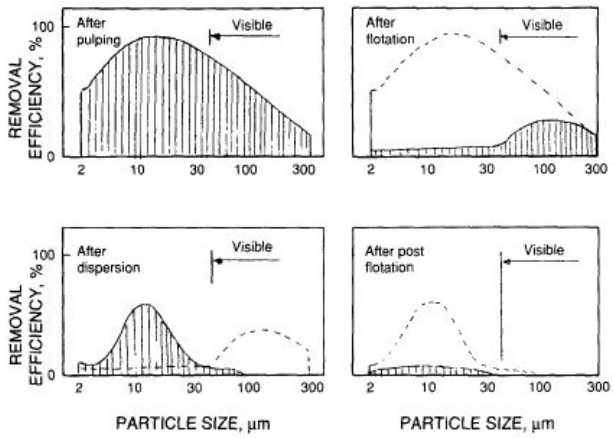

Figure 21: DIP unit operations particle size distribution and removal, from Rangamannar & Silveri [59]

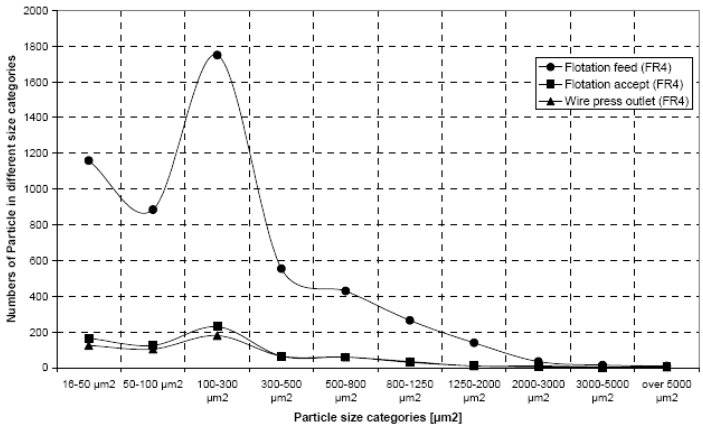

Figure 22: Ink size distribution, from Laitinen *et al.* [60]

In 1976, Galland *et al.* [61] developed the simple and fast method of 'Hyper-washing' to rapidly calculate the ink detachment efficiency during the defibering operation. The method included high-pressure water jet (400 – 600kPa) washing of a quantity of pulp on a 200 mesh wire till the filtrate was clear. Ink particles, mineral fillers, cellulosic fines, and short fibres followed the water phase and long fibres were retained on the wire mesh. Measure of brightness or ERIC on whole pulp and hyper-washed pulp gave the ink detachment efficiency. Measurement of the fibre amount retained on 200-mesh opening was termed as long fibre content.

Lapierre *et al.* [42] fractionated and bleached the ink containing fines fraction and mentioned that metal ions are preferentially present in the fines fraction and the ink particles seem to be strongly associated with the cellulosic fines. Using a modified method of fines separation by Britt jar, Ben *et al.* [50] mentioned rejects from process water cleaning units contained 45% of pulp in P400 fraction while a deinked pulp 10%. They also observed that the process water rejects from water cleaning unit and DIP pulp had similar amount of ink in the P100R400 fraction, while the P100 fraction contained more ink indicated by ERIC measurement, slightly lower for DIP (cf. Figure 23). This suggests that the ink in water rejects was much smaller than the P400 fraction.

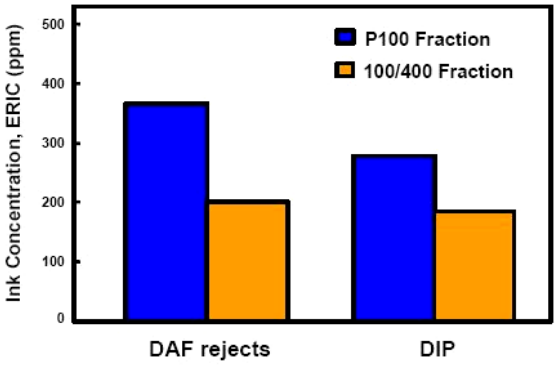

Figure 23: ERIC in different fractions, from Ben *et al.* [50]

Deinking sludge or flotation operations rejects are composed in majority of inorganic content and cellulosic fines. They contain very less or negligible amount of long fibres (cf. Figure 24)

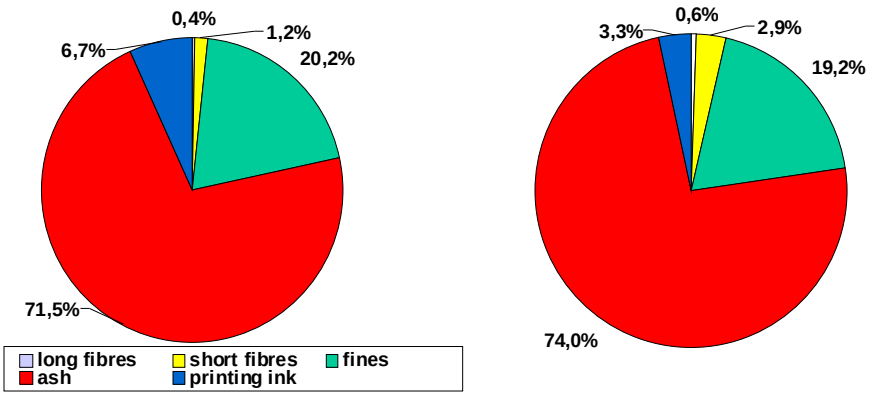

Figure 24: Deinking sludge composition in flotation operations, from Hanecker [62]

Ricard *et al.* [63] mentioned the flotation rejects (of process waters) contained majority of particles, which were less than10µm, the average particle size being 4µm.

The detachment or the release of ink from paper surface is a complex phenomenon. Rao & Stenius [64] put forward ink release approach. They mentioned that the dried ink is composed of 3 layers, while the tertiary uppermost layer is loosely bound and has no contact with the cellulose fibre, and a primary layer is attached to the paper surface. Disintegration of the tertiary layer will lead to free ink particles, which will not at all be associated with the cellulosic fibres or fines.

As in the case of cellulosic fines, image analysis methods principally involving a microscope associated with a camera [41][58][65][66][67] [68][69] have been extensively used to understand the ink particle dimensions and process unit operations efficiency in rejecting contamination. The 'darker' ink particles are 'captured' by proper segmentation from the bright background. Image analysis tool can then be applied to understand the ink particle dimension characteristics.

Emphasis has also been to understand the association of ink with the cellulosic fibres. That is to say 'free' ink particles detached from the surface of fibres. Ye & Vilenius [69] reported the use of two imaging channels having visible (polarised) and near infra red light source to distinguish ink from fibres. This was continued and worked upon by Kesti [66] using the same set-up but only in the visible spectrum (polarised) to measure the ink content; with the mean ink absorbance defined on the ratio of ink to background pixel intensity. However, more enhancements of the analysis/microscope setup procedure were required.

There are numerous ink compositions and each year new inks are introduced into the market for specific printing techniques and support papers. The formulations contain esters, alkyd resins (as ink binders), mineral and vegetable oils, synthetic resins (as ink vehicles), waxes and solvents (as ink modifiers) [70][71].

2.2. - Development of a laboratory fines fractionation technique

As reported in preceding sections of this chapter, deinking cellulosic fines are a very heterogeneous category of material with a wide range of particle sizes and shapes (– organic and inorganic). Image analysis methods have been used at the whole pulp scale and or the fines scale to get information on the ink particle size characteristics.

The losses from the deinking flotation stages are majority fines [52]; they could be as high as 98% [72]. Previous studies on ink particle characterization have not dealt with the approach of ink particle attachment to either the cellulosic fines fraction (fibrillar or flakes) or mineral filler or in complete free form. The removal of 'clean' cellulosic fines or mineral fillers with no ink association will lead to 'non-

justifiable' losses. Printed paper contains 2% in mass of the ink while the flotation losses could be as high as 10-30%. The approach and focus should be very selective removal of only ink particles and not the clean fines or fillers.

Observation of deinking pulp fines obtained from laboratory pulped recovered paper under a light microscope reveals all the 'complex' particles having a wide range of dimensions (from some micrometer to more than 100µm) and colour, as can be seen in Figure 25 for P200 fines from a deinking pulp or a 100% ONP pulp such as in Figure 26. To have a better understanding of such particles it becomes necessary to separate the fines according to dimensions or large fines from the smaller fines or in other words: divide the fines into smaller sub-fractions.

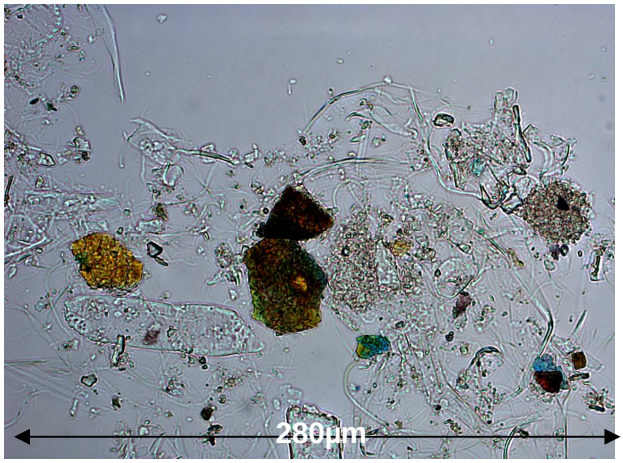

Figure 25: P200 fines from DIP rich in magazine

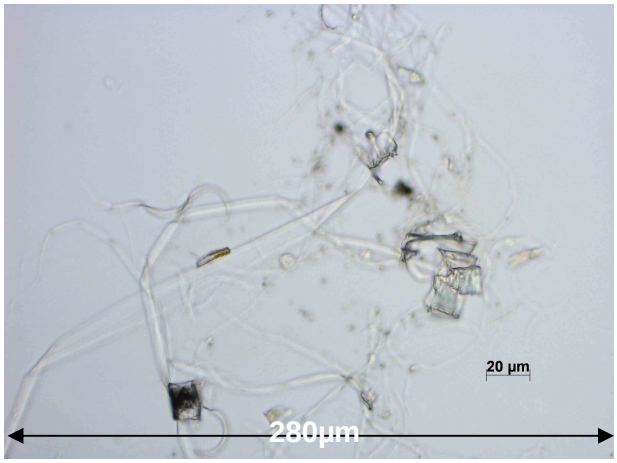

Figure 26: Whole pulp from a 100% ONP pulp

2.2.1. - Fines sub-fractions by soft-hyperwashing method

A new and simple method was developed [73] to separate deinking fines on different small aperture screens available in the laboratory as the finest mesh present was 200. The method is based on the concept of Hyperwashing [61] but involves light water pressure. Normal high pressure jet or spray hyperwashing is continued till the filtrate is clear or it involves visual control to stop the water flow. Fines fibrils are flexible cellulosic particles and have very small diameter. The basic idea of soft-hyperwashing is not to 'force' the fines across the aperture. This was done by employing a cylindrical water jet from a ~1mm diameter orifice at 70 ± 10kPa pressure. Low pressure also prevents spurting and loss of fines on lower size aperture. As fines are microscopic particles, the flow of a water jet is maintained till the filtrate turbidity drops below 15-18FNU or less. In fact, a Bauer McNett apparatus or a Sommerville equipment could be termed as a 'soft-hyperwasher' with respect to fines removal.

The principal steps in this method are as follows (a detailed description is given in the Annexe 1)

1. Collection of P200 fine particles using a Bauer McNett classifier. A large amount of initial pulp 30-40g oven dry is taken to collect considerable amount of fines. This was done to have the maximum probability of all types of fines. The fines were collected in large volume containers, allowed to settle overnight and decanted the next day.

2. A small quantity of the concentrated fines was taken on a hand held mesh and washed with low pressure cylindrical water jet. Care was taken to have the particles in a small area and not on all the surface of the sieve.

3. The filtrate turbidity was regularly checked and the process was stopped when the turbidity dropped below 15FNU.
4. The particles were then collected on a Millipore filter (or membrane filter) and weighed after drying overnight in an oven at 105℃.

Very small amounts of fine particles were taken to have a better control and 'produce' less amount of filtrate for subsequent sieves. Other fractionating equipments also use small quantity, for example the tube flow fractionator uses 150mg of initial pulp suspension [41].

2.2.2. - Deinking pulp characterization

The deinking pulp characterization are broadly grouped into two parts. Studies with laboratory pulped raw material and industrial samples.

Initial laboratory experiments were performed to understand the basic pulp characteristics especially with respect to ink presence in fractions and then secondly to perform fines fractionation.

Laboratory pulping method

Alkaline Hélico pulping conditions are reported in Table 7. Chemicals are applied on oven dry (O.D) fibre basis.

Table 7: Laboratory pulping conditions

NaOH	**0.7%**
Silicate	**2.0%**
Hydrogen Peroxide	**0.7%**
Soap	**0.7%**
Pulping time	**15 min**
Pulping temperature	**45℃**
Consistency	**~9%**
Water hardness (adjusted to)	**~150 mg Ca^{+2}/L**

Bauer McNett classification (TAPPI norm 233 cm-06)
2 different series of McNett mesh were used. Series 1 consisted of 14-28-48-150 configuration and series 2 consisted of 14-28-48-200 configuration.

Optical properties
Pulp pads for optical properties determination were adjusted to neutral pH by addition of Aluminium Sulphate solution. Technidyne spectrophotometer with a UV filter was used for brightness and ERIC measurement.

Hyperwashing
Performed with a high pressure water jet on a 90µm wire opening. Controlled by visual inspection till filtrate was clear. The pulp fibres retained on the wire (long fibres (LF) and while those passing are short fibres (SF), mineral filler and fines) were deposited on a 90mm diameter Whatman filter paper and dried and weighed as done for pulp concentration. Values used for calculations purposes are average of 2 pads.

Microscopy
Light microscopy was performed using Axio Imager M1m microscope (Zeiss). Images were taken in transmitted and reflected mode of illumination. The microscope is equipped with a motorised platform in X-Y-Z directions and allows taking images in mosaic mode after defining the image area. The slides were prepared in the dry state by firstly washing the particles with Milli-Q water (purified and deionised) and then depositing and drying the fine particles using a slide warmer.
To have information on the chemical composition of coloured particles, infra red microscopy coupled with a library search of the spectrum so obtained to identify components present was performed. This was done using Thermo Scientific Nicolet iN10 MX IR microscope with MCT detector (middle range FTIR: 500cm^{-1} – 4000cm^{-1}) with a surface area of 25µm x 25µm.

2.2.2.1. - Lab pulp characterization – raw material comparison

To understand the effect of raw material, two different recycled fibre combinations were analysed. The first set consisted of equal quantities of magazine grade material (7 month naturally aged) and newspaper (1 month naturally aged) and the second consisted of 100% ONP material (8 months naturally aged). 100% ONP was printed the first time on 1st generation virgin mechanical pulp and contained no mineral fillers. The basic idea behind working on the 1st generation was to understand the presence of ink particles in the absence of mineral fillers which are essentially associated while pulping old newsprint and old magazine grade papers.

McNett distribution is reported in Figure 27, combined for the 2 configurations and the raw material studied. The mass distribution indicates the presence of a large quantity, 41%, of suspended material in the P200 fraction for 50% ONP 50% OMG and less quantity, 32%, for 100% ONP. In both combinations the fibres in the fraction P48 R200 represents 16 – 17% of the whole pulp amount. Less than 3% of the matter is present in the P150 R200 fraction for both the materials. Hyperwashing value indicated 53% long fibre content for equal OMG ONP and 67% for 100% ONP material.

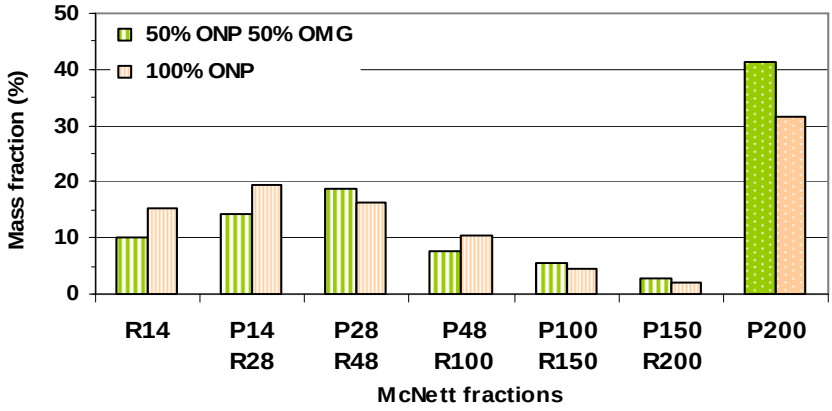

Figure 27: Mass fraction distribution – whole pulp

The distribution of the fine sub-fractions is reported in Figure 28. An important difference is observed between the fines sub-fraction distribution of recycled fibre fractions from ONP OMG raw material and 100% mechanical pulp fines. Approximately 42% of the mechanical pulp fines are contained in the P11µm fraction as compared to 70% in the deinking pulp. One of the major factors is the presence of mineral fillers in the finest fines fraction in case of pulp from recovered fibres and the presence of 'long' fibrillar material as well as 'rectangular', blocky ray cells flakes in case of 100% ONP mechanical pulp

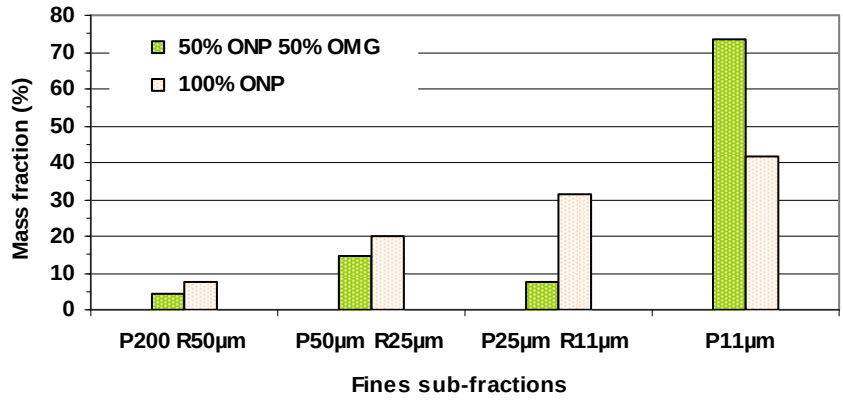

Figure 28: Mass fraction distribution – fine sub-fractions

Workers have reported that a Bauer McNett classifier releases fine particles which are smaller than a 20µm opening, [33][34] and 60 to 70% of the virgin pulp fines fraction is contained in the P400 mesh fraction, (38µm opening) [12][35].

The P11µm fraction contains the finest of the cellulosic fines and the mineral material. The presence of more than 70% of the deinking fines quantity in a smaller fraction (11µm) is mainly the result of mineral material coming into the raw material as a result of the coated magazines or incorporated into the paper manufacture, this was extensively observed during the microscopic analysis.

The fibre and fines fractions distribution in the whole pulp is reported in Figure 29. The P11µm fraction contains 30% of the whole pulp mass for 50% ONP 50% OMG (representing the single largest entity amongst all the fibre and fines fractions in the given McNett configuration) and less quantities for 100%ONP ~ 13.4%.

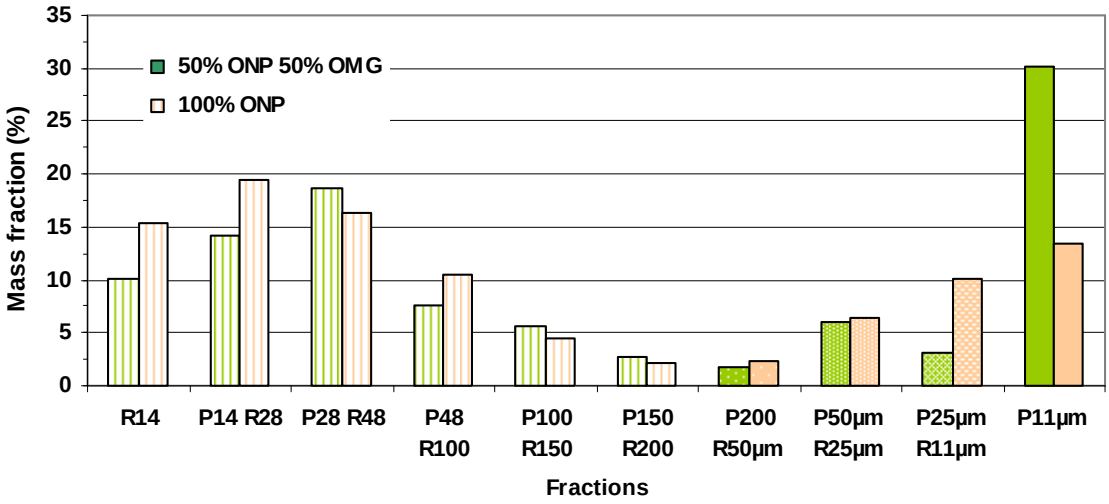

Figure 29: Mass fraction distribution – fibre and fines

Differences were also observed in the optical properties for the whole pulp and reported in Table 8. The values indicate higher whole pulp brightness for the magazine containing material, 46% ISO as compared to 34% ISO for all ONP. What is also interesting to note that after hyperwashing, the 100% ONP brightness value just reaches the whole pulp value for 50% ONP 50% OMG. The transfer of ink while printing a coated magazine takes place on the surface of the coating layer and does not reaches the fibre layer, while in case of 100% ONP, fibre surface is in direct contact with the ink.

Table 8: Optical properties

		50% ONP 50% OMG	100% ONP
Brightness ISO %	Whole pulp	46	34
	Hyper-washed	63	46
ERIC ppm	Whole pulp	1245	1784
	Hyper-washed	98	579

Figure 30 and Figure 31 represent the brightness and ERIC values of the McNett fractions respectively.

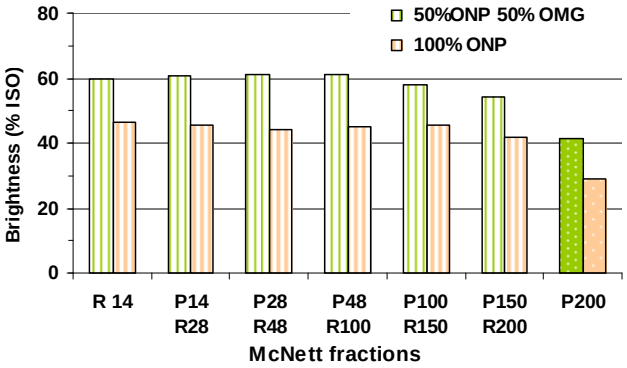

Figure 30: Brightness of McNett fractions

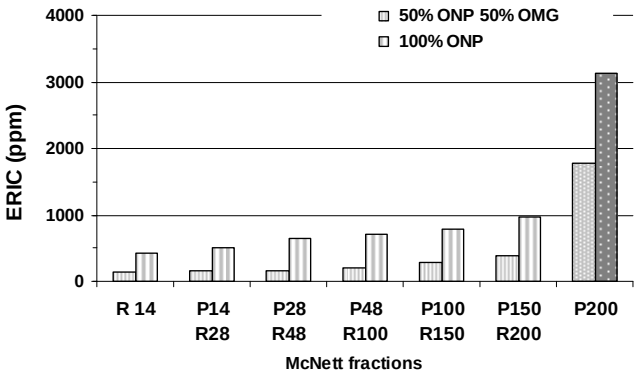

Figure 31: ERIC of McNett fractions

Maximum quantity of the ink particles are contained in the fines fraction, whereas the fibre fraction till R200 mesh contains very low level of ink. However, ERIC value increases in the lowermost fractions, P100 R150, P150 R200; this trend was also observed in the previous experiment.

In case of 100% ONP, the McNett fractions brightness value (retained) is lower for the fibre fractions (approximately 45% ISO) as compared to 50%ONP 50%OMG (approximately 60% ISO). The ERIC values are higher for lower fractions, indicating smaller particle fragments (or higher quantity) in the lower fractions which decrease the pulp brightness especially for P150 R200 fraction.

Figure 32 and Figure 33 reports the optical properties for the fines – sub fractions for 100%ONP. P200 R50µm and P50µm R25µm fractions have a brightness value slightly lower to McNett fibre fractions and a higher value of ERIC. Smaller ink particles have an important influence in the increase of ERIC value as compared to large ink particles or specks. The ERIC value for P25µm R11µm is almost 3 times the P200 R50µm and twice of P50µm R25µm fraction, with a significant lowering of brightness. But the fraction P25µm R11µm still has a higher brightness and lower ERIC value as compared to the whole P200 fraction. This indicates that the maximum ink presence is not in these fractions but in the P11µm fraction. While studying process water fractions, Ben *et al.* [50] also observed presence of ink in the P400 McNett fraction, more than the P200 fraction.

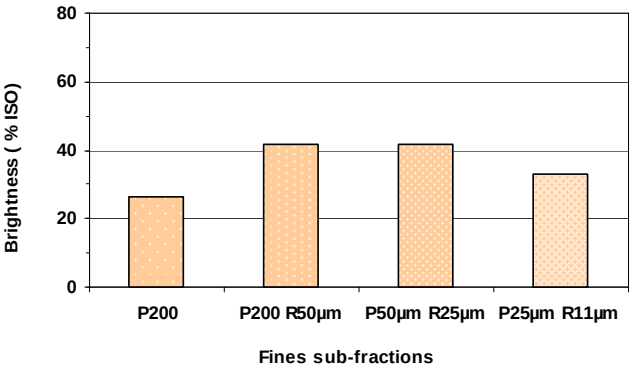

Figure 32: Brightness of fines sub-fractions, 100%ONP

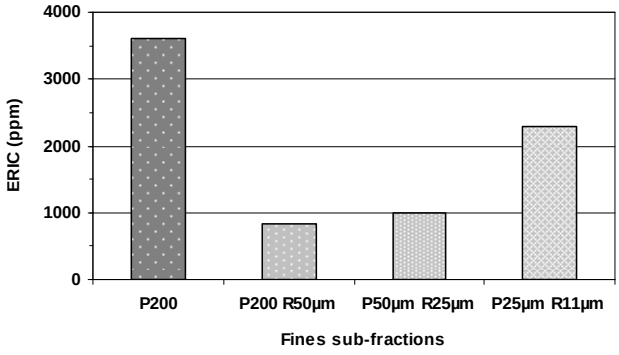

Figure 33: ERIC of fines sub-fractions, 100%ONP

Optical microscopy images of the different fractions are reported in Figure 34 for 50% ONP 50% OMG. The slides have been prepared in dry state.

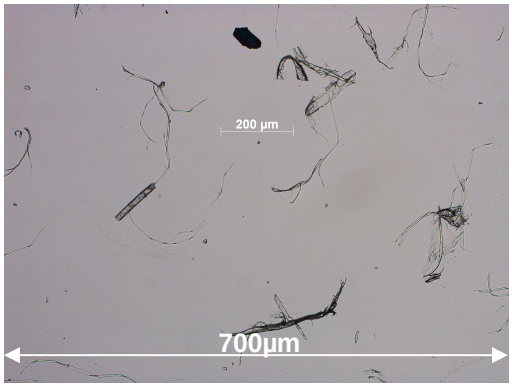

a) P200 R50µm

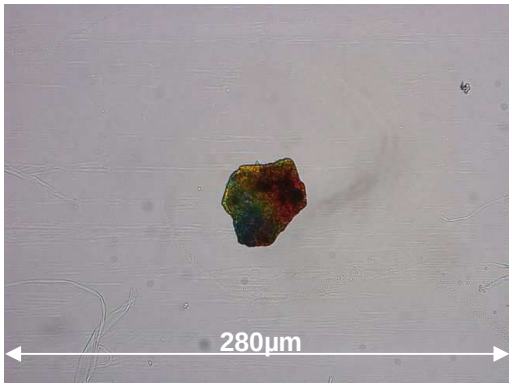

b) P50µm R25µm

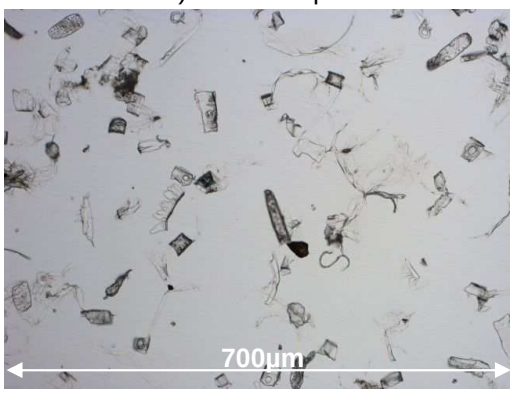

c) P25µm R11µm

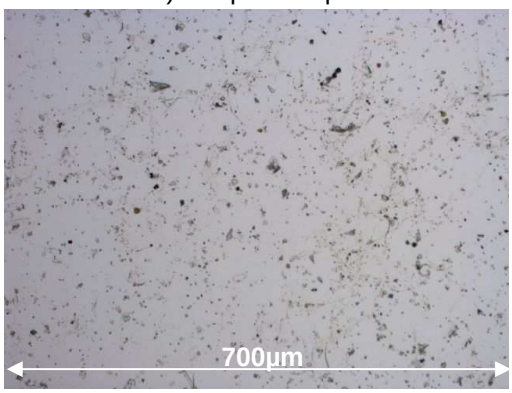

d) P11µm

Figure 34: Fine sub-fractions images

The fines sub-fractions contain essentially 3 types of particles: cellulosic thin ribbon like linear fibrils, cellulosic 'non-linear' flakes, which consist of cell wall fragments, broken ray cells, thick lamellae and lastly coloured coating flakes. The finest, thinnest fibrils and shortest flakes are present in the P11µm fraction, which also contains very small (lowest microscopic scale) coloured particles. The mineral fillers are in majority free state and seem not associated with cellulosic fibrils or flakes. The P11µm fraction has the smallest microscopic particles and such particles are difficult to disperse and observe in individual separated images shown in Figure 35 for particles deposited on a glass slide. In fact this particular category of particles could be termed as debris as mentioned by Forgacs [16], but could contain very high specific surface cellulosic fine particles which provide the best mechanical sheet properties. However, this will depend upon the type of recycled fibre raw material, especially the amount of inorganic mineral fillers which hinder sheet strength properties. P11µm particles deposited on a 0.8µm opening Millipore and observed under the optical microscope, revealed the presence of important quantities of mineral fillers and the smallest coloured particles as shown in Figure 36.

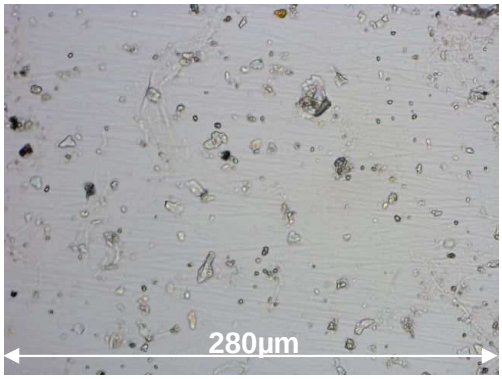

Figure 35: P11µm fraction images

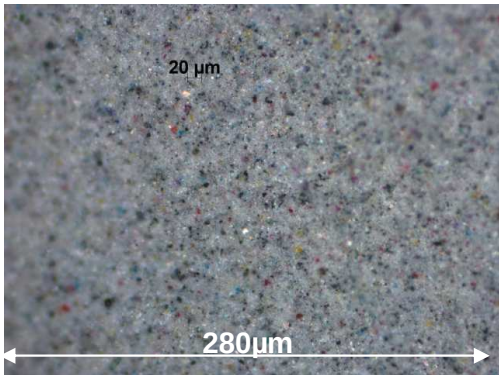

Figure 36. Millipore pad of P11µm particles

The results for a coloured particle (for example as in Figure 34b) IR analysis are reported in Figure 37.

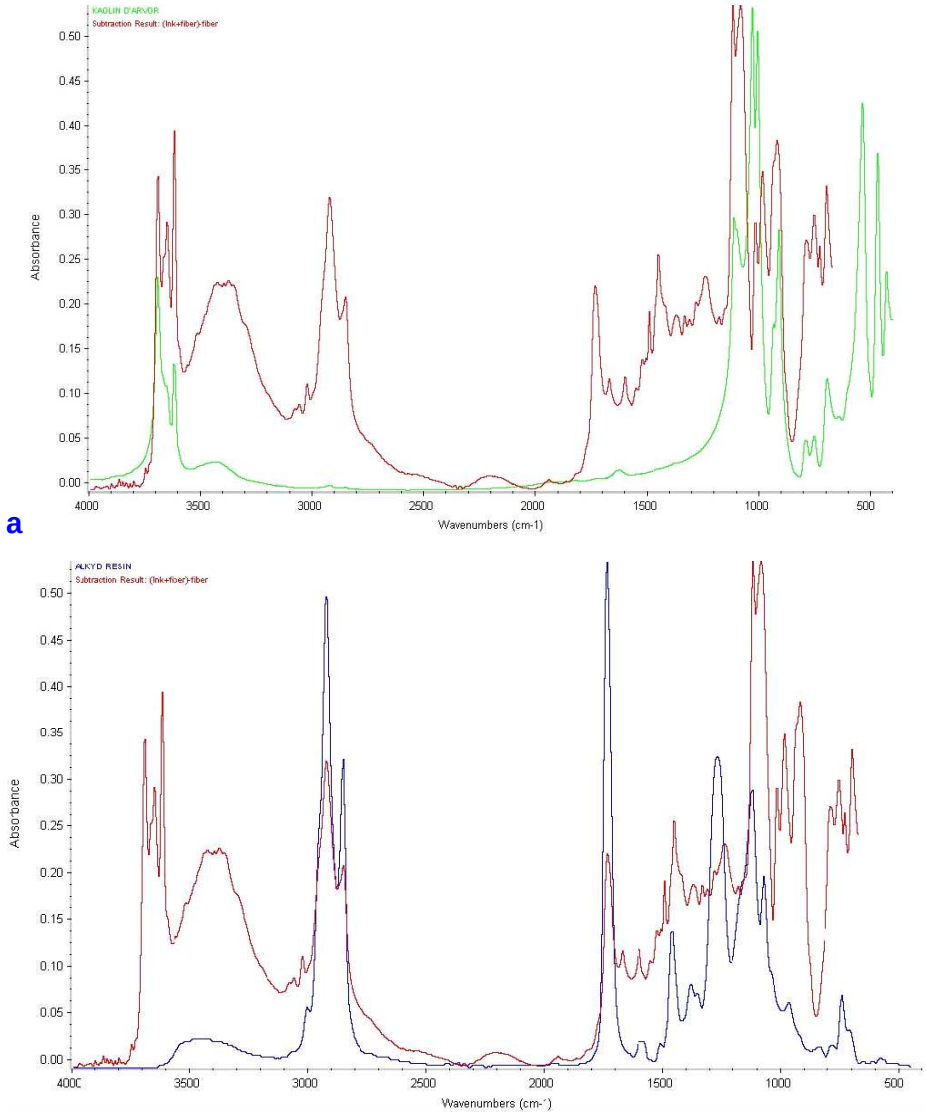

Figure 37: IR spectrum a) Particle spectrum (red graphic) and kaolin spectrum (green graphic) b) Particle spectrum and alkyd resin spectrum (blue graphic)

The spectrum so obtained was compared with the microscope library after subtracting the spectrum for cellulose to avoid interference. One part of the spectrum matched with kaolin Figure 37a, and the second part resembled to that of an alkyd resin Figure 37b, a component of ink formulations. This analysis shows that the particle is a coating flake covered with ink on the top surface.

An important difference is observed between the fines sub-fraction distribution of recycled fibre fractions from ONP OMG raw material, Figure 28, and 100% mechanical pulp fines. Approximately 42% of the mechanical pulp fines are contained in the P11µm fraction as compared to 70% in the deinking pulp. One of the major factors is the presence of mineral fillers in the finest fines fraction in case of pulp from recovered fibres and the presence of 'long' fibrillar material as well as 'rectangular', blocky ray cells flakes in case of 100% ONP mechanical pulp. This is illustrated in Figure 38. It was also observed in this case that the fibrils are free of ink at least till the R11µm fraction. Ink presence was on flakes which provided a higher 'contact' area. The presence of dark spots in the P11µm fraction indicates to ink occurrence which is observed as very fine small dots.

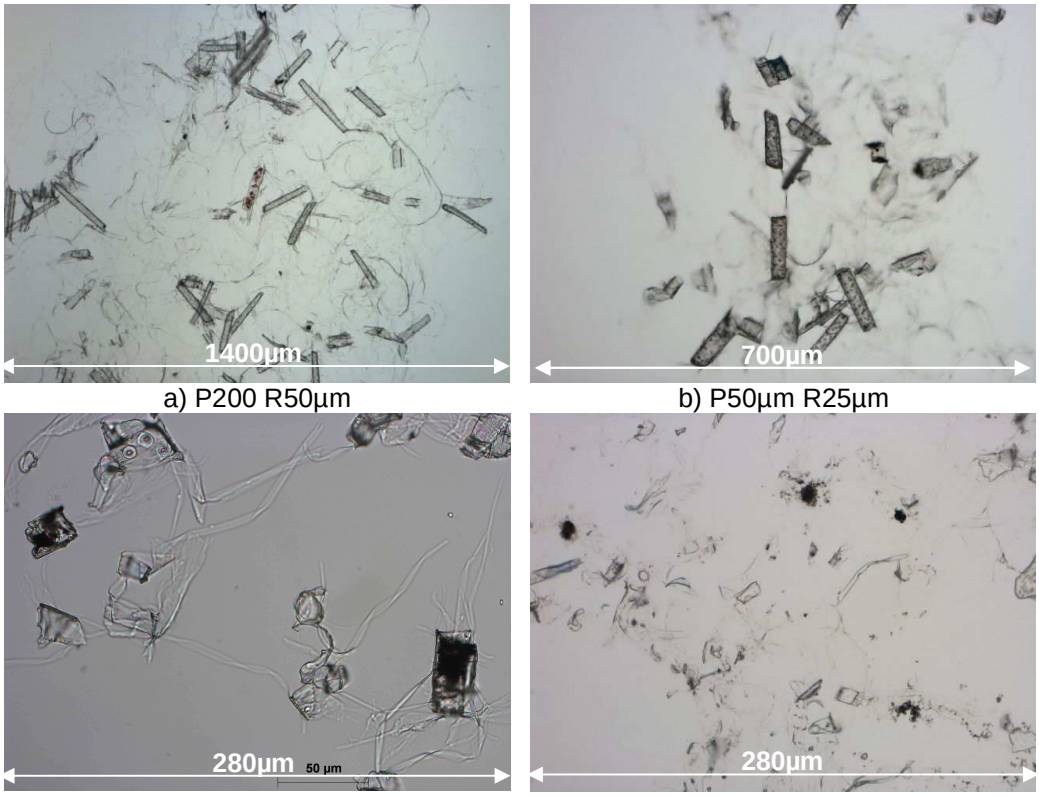

a) P200 R50µm b) P50µm R25µm

c) P25µm R11µm d) P11µm

Figure 38: Fine sub-fractions images, 100% ONP

The finest fraction as expected contains the smallest cellulosic as well as non-cellulosic ink particles. The fibrils seem to be free of ink in higher fines sub-fractions. However it is difficult to comment on the P11µm fraction, due to the very small size of particles as well as their tendency to flocculate and form a bunch. The fibrils appear to 'hold' them together.

Fibrils are very thin fine particles which are flexible and possess more swelling ability. Their thickness is in the range of less than 1µm [35]. Such fine particles offer a very less surface area for ink particles to remain attached as compared to thick flakes which provide a larger area for ink particle attachment and are stiff. However, the ink attachment will depends upon numerous other factors too, like type of ink, ink attachment forces, mechanical action applied during ink detachment process.

2.2.2.2. - Industrial deinking lines analysis

The methodology of fines sub-fractionation was applied to industrial line samples. The mill situated in Western Europe produces improved newsprint grade of paper using a raw material rich in magazines. The pulp manufacturing process involves classical 2 deinking loops with a drum pulper and intermediate high speed dispersion; with low consistency fine screening.

Representative samples all along the deinking line were sampled from the process start to the final pulp. McNett distribution of the different unit operations are reported in Figure 39.

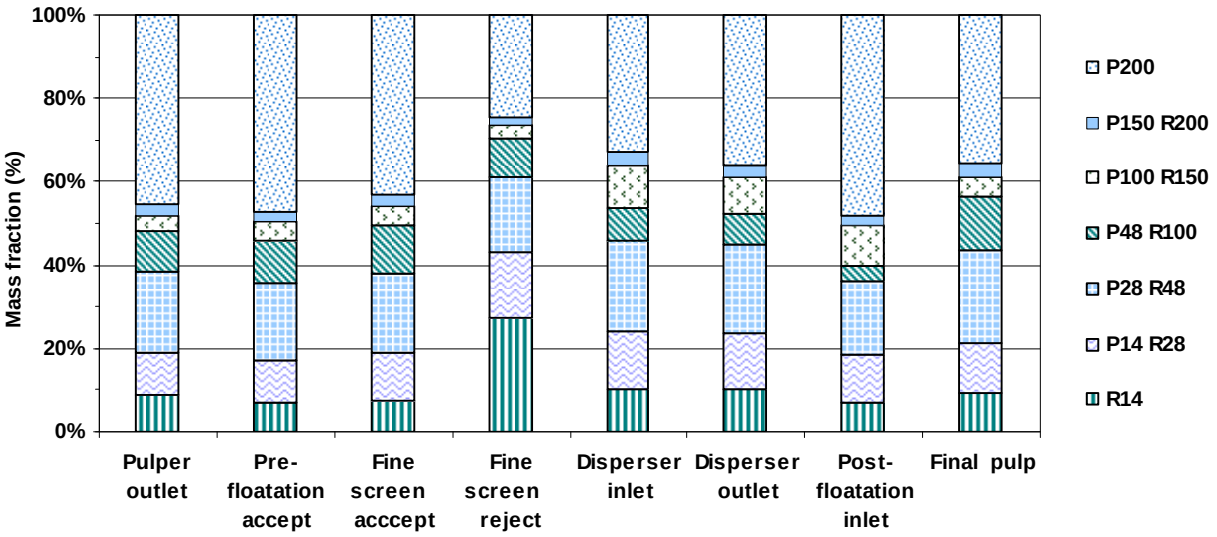

Figure 39: Industrial DIP line Bauer McNett fractions

Approximately 40% of fibres are present till the R48 fraction at the process start and in the final pulp, with the maximum fraction being P28 R48. The fractions P100 R150 and P150 R200 have much less amount of material. However a major change occurs in the fines content which drops to 36% in the final pulp from 45% in the process start. The fine sub-fractions of some unit operations are reported in Figure 40, while Figure 41 reports the flotation reject fractions (from secondary cells). The results for pulp indicate presence of 73% fines particles in the P11µm fraction in the initial pulper outlet pulp, which drops to 63% in the final pulp. The loss of P11µm fines occurs in the flotation stage, which removes the ink. Flotation rejects analysis reveals presence of 85-93% of particles present in the P11µm fraction.

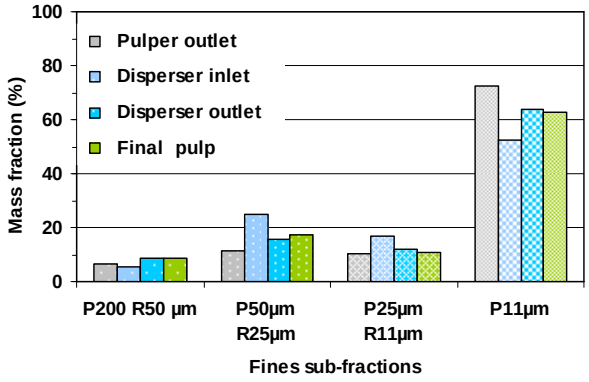

Figure 40: Pulp fine sub-fractions

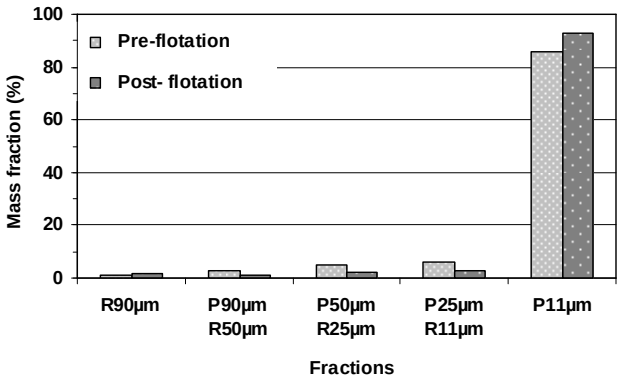

Figure 41: Flotation rejects secondary cell fractions

More results related to whole pulp ash content at 425℃, whole pulp and two McNett series optical properties are reported in Annexe 3. The flotation rejects have the lowest brightness, 31-33% ISO, highest ERIC value, 2600-3000ppm, and the highest value of ash content, 80% amongst the different samples all along the deinking line. P11µm particles concentrated by centrifugation for 10 minutes at 3000g on a millipore indicated an ERIC value of 3000 ppm. This high value of ERIC, which is also equal to the whole pulp reject sample, is expected as the maximum of the flotation rejects particle are present in this particular fraction. The microscopic images of the flotation rejects fractions on millipore pads are reported in Figure 42, which shows a massive presence of coloured mineral particles. The smallest size mineral fillers are present in the P11µm fraction. The mineral fillers are either partially, wholly or in a non-inked state.

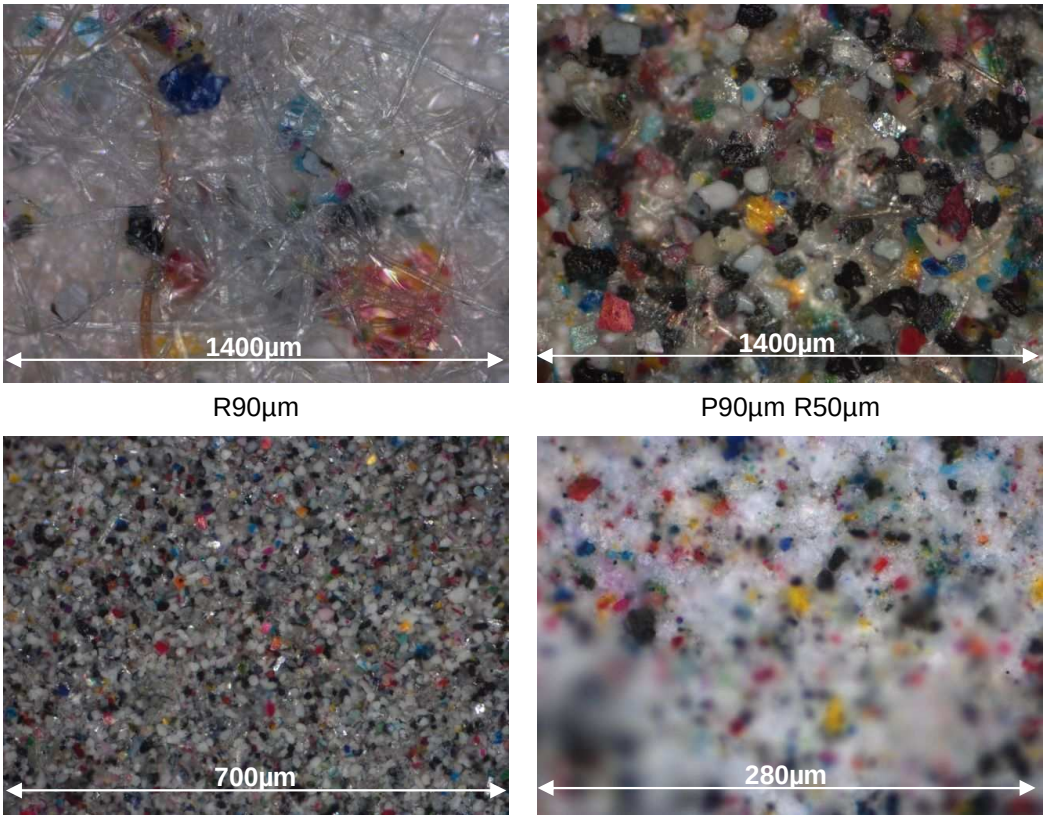

R90µm P90µm R50µm

P25µm R11µm P11µm

Figure 42: Flotation rejects fractions images

Analysis by scanning electron microscope of the P11µm Millipore pad revealed important quantity of aluminium, calcium and silica, coming from mineral fillers. The element analysis graph is shown in Figure 43.

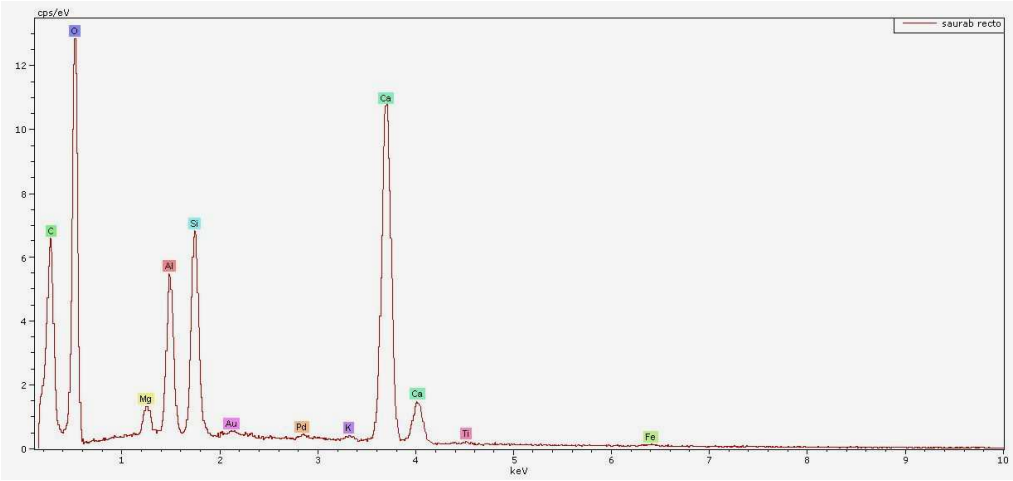

Figure 43: SEM analysis of the P11µm Millipore pad

The results reported in Figure 41 show that the flotation systems for ink removal are very selective in removing the smallest of the particles, with very few fibre losses as retained on the 90µm sieve and majority of the particles concentrated in the smallest fraction containing all the ink. The formation of these small particles could be explained by the fragmentation and breakup of large coating flakes (or to the relase of mineral particles added during paper manufacture). This is illustrated in Figure 44. Application of light pressure manually by a needle fragments them into much smaller particles as shown in Figure 45 to Figure 46.

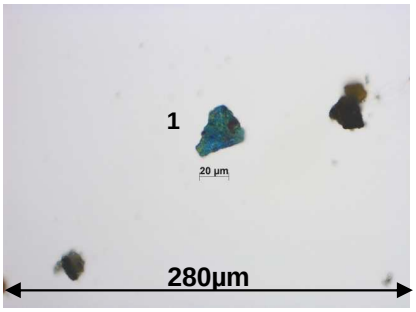

Figure 44: Original particles

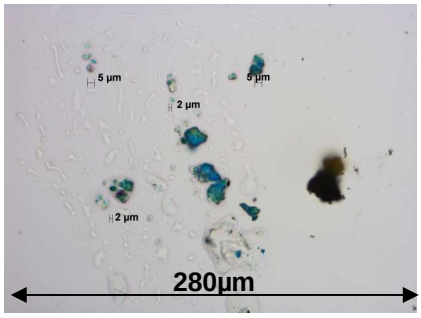

Figure 45: Coating flake 1

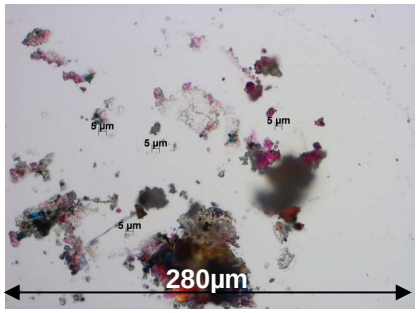

Figure 46: another coating flake

'Uninked' mineral fillers could arise from 4 situations. Firstly they could have their origin from mineral fillers added during the paper manufacture (to enhance sheet opacity and brightness) and if such filler particles remain completely embedded inside the sheet thickness, between the surface layers, hence do not come in contact with the printing ink. Secondly, they could be related to the part of coating layer where no ink has been applied. This has been explained in Figure 47 which shows the microscopic view of a coated magazine from the top surface, patches of uninked coated surface are clearly visible and Figure 48 which is the image of the sheet in Z direction taken after the sheet has been 'torn' manually. This image shows that the coloured and non-coloured broken coating flakes which are clinging on to the fibre layers, as found in Figure 42.

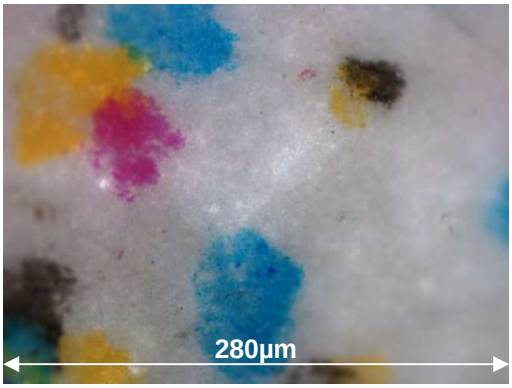

Figure 47: Coated magazine view from top

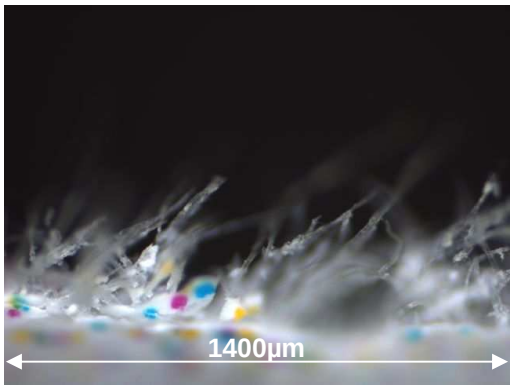

Figure 48: Coated magazine view in Z direction

Thirdly, break up of 'clean' sub-layers of a coating flake exposed after the top ink covered layer has chipped off; will lead to formation of uninked mineral fillers. For example, in Figure 49 a partial ink covered coating flake is shown. Chipping of a part of top ink covered layer reveals the white uninked portion. The chipped inked portion will lead to the formation of much smaller free ink particle, not attached to a cellulosic fibre or fine. The fragmentation and possible break up of the exposed part will lead to the formation of uninked mineral filler.

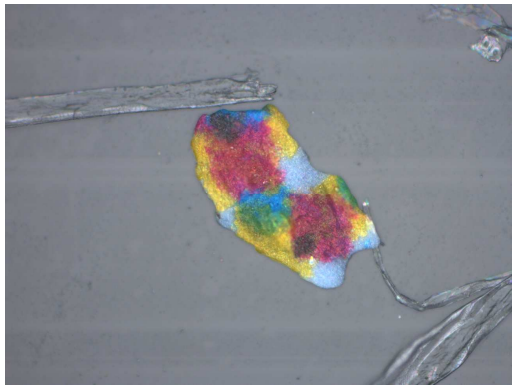

Figure 49: Coated flake with partial ink coverage

The fourth reason is more related to the slide preparation for microscopic analysis. The position or the manner how the coating flakes gets placed on the glass slide surface will also decide whether the mineral filler has ink on it or not. This is illustrated in Figure 50 which shows an uninked mineral filler image taken in reflected illumination and the same mineral filler in transmitted illumination in Figure 51, which indicates ink presence on the other side. This also indicates that the ink layer remains on the surface of the coating layer. However, the penetration of ink solution inside the coating layer will depend upon other factors also, for example- the layer thickness.

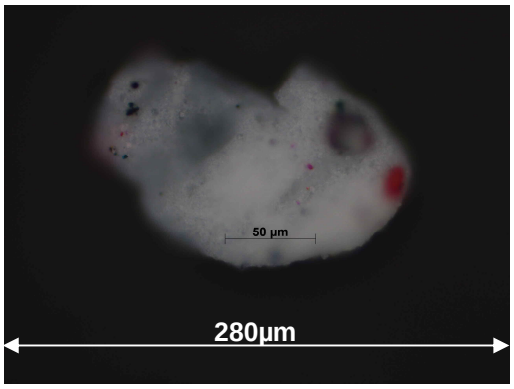

Figure 50: Coating flake in reflected illumination

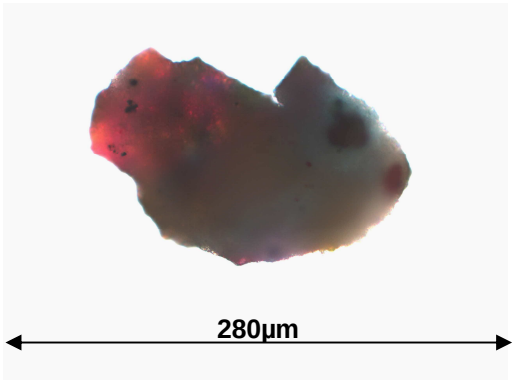

Figure 51: Coating flake in transmitted illumination

Indeed, the loss of P11µm fraction in the flotation rejects can be observed in the final pulp fraction distribution in Figure 52. The initial P11µm content of 33% drops to 21% in the final pulp.

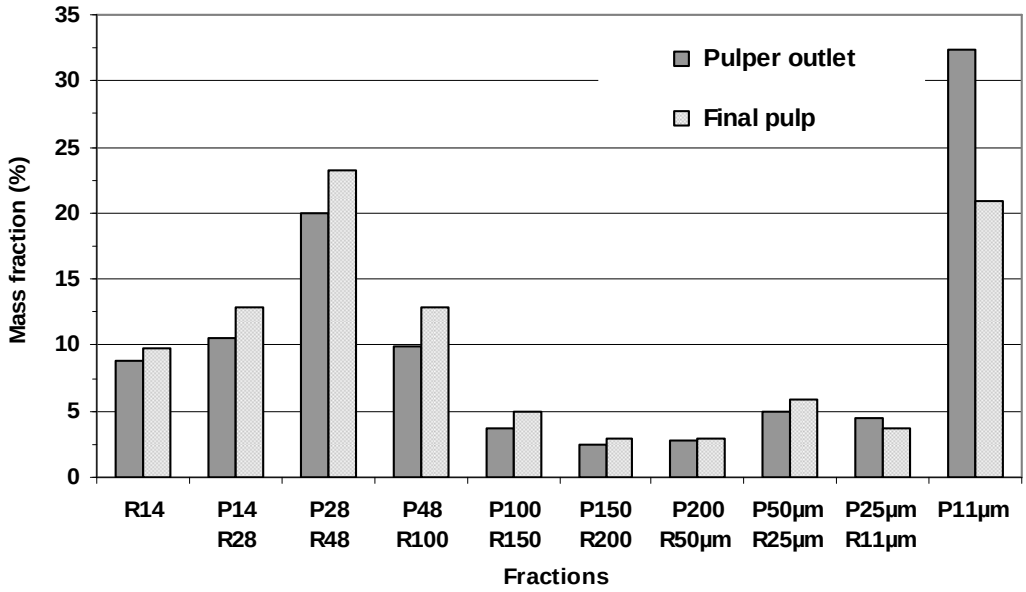

Figure 52: Industrial DIP line 1 fractions- pulper outlet and final pulp

Flotation rejects essentially involve the loss of the fine particles. This loss also includes the cellulosic fibrillar fines which do not have ink association with them and as could be observed from the images, mineral particles which have ink to various degree. One way to reduce the flotation losses is the selective rejection of only the fine flakes, inked mineral particles, free ink particles and conserving with the accepted pulp the clean fraction. The clean fractions which do not have ink on them are found in each fine sub-fractions. The higher fines sub-fractions are much 'cleaner' with respect to the P11µm fraction.

Figure 53 reports the images of fines sub-fractions from pulper outlet and the final pulp deposited on a Millipore. From amongst these images is clear that smallest and highest number of coloured particles

are found in P25µm R11µm fraction and such coloured particles are removed from each fraction, rendering the pulp clean (the majority of ink is in the P11µm fraction). These images also highlight the fact that cellulosic material in these fractions is clean in a large majority even if there are some ‘specks’ of colour, which can be said to be insignificant as compared to the dark particles.

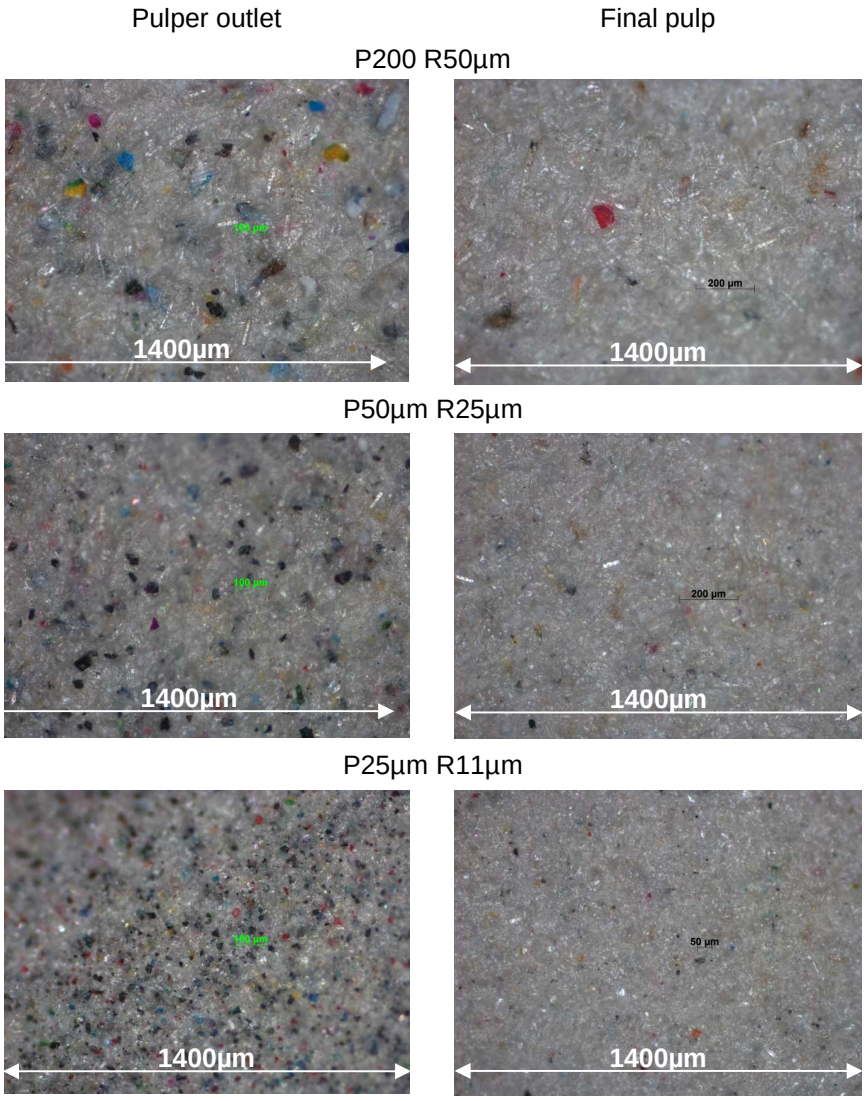

Figure 53: Fines sub-fractions millipore pad images

Pulp samples from two other deinking lines were also analysed consisting of final pulp and flotation rejects. The results indicated the presence of 30% of the total pulp amount in the P11µm fraction as shown in Figure 54 and 84% of the flotation rejects again in the P11µm fraction as indicated in Figure 55. These results were very similar to those measured on samples of the first deinking line studied as well as on the laboratory prepared samples.

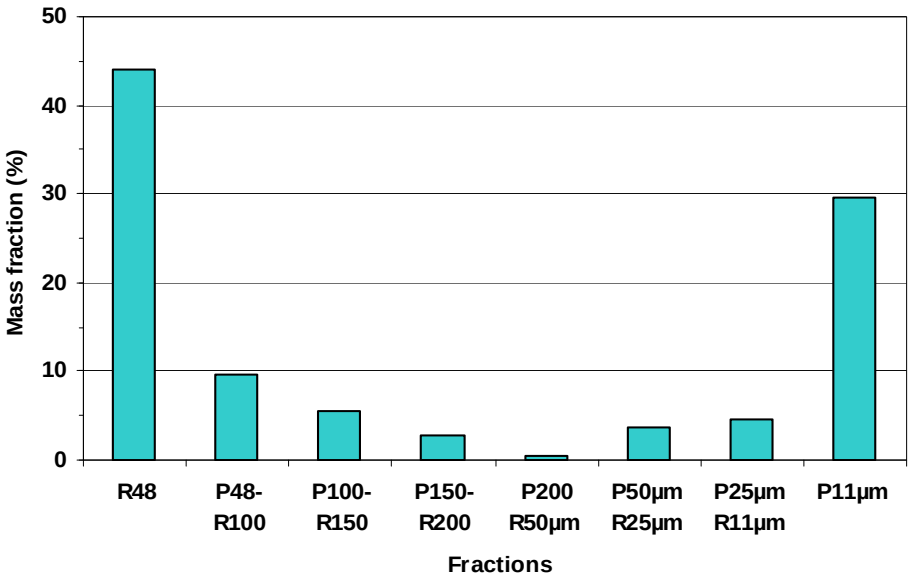

Figure 54: Deinking line 2 - final pulp fractions

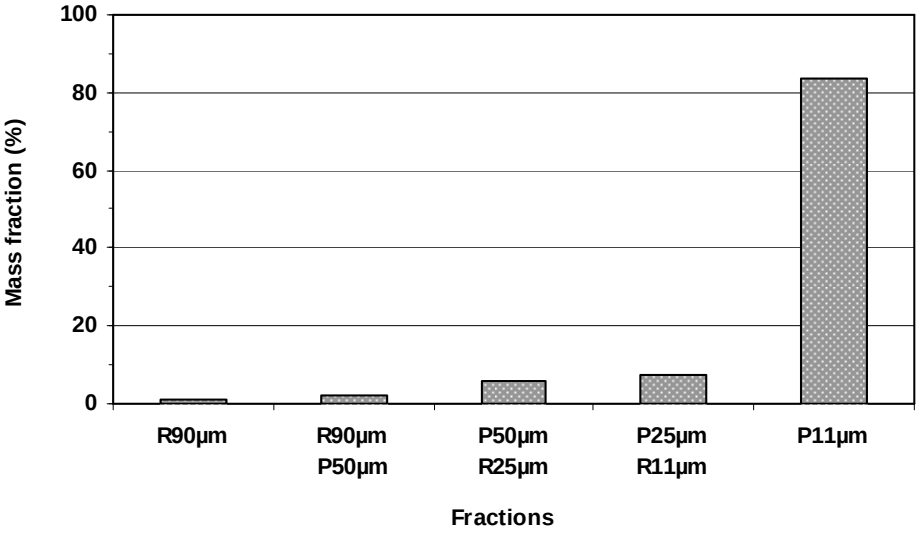

Figure 55: Deinking line 3 - flotation rejects fractions

The analysis of the deinking lines as well as laboratory pulp samples indicated the presence of large amount of particles in the P11µm fraction either in the pulp samples or in the flotation rejects.

The results obtained during either the deinking pulp analysis or the rejects analysis were in agreement with the work reported in the literature. Most of the pulp fines are composed of very fine particles and the best efficiency for flotation is related to the smallest of the particles. More importantly flotation operations lead to the removal of the very small particles, mainly constituted of ink, the finest mineral fillers and the cellulosic fines composed of flakes and fibrils.

2.3. - Development of image analysis module

Fines, either in virgin pulp or contained in the deinking pulp play a vital role in sheet properties. With respect to their different types, it becomes important to acquiring information on their amounts, even if in relative proportions in a sample.

Apart from long, thin, slender fibrils and chunky flakes, deinking pulp contains mineral fillers, either inked or non-inked. To better understand the different types of fines present in the pulp from recovered paper, image analysis is one of the potent method to characterize such particles.

As reported by Luukko *et al.* [35][47], fibrils are bright and hence, have a higher grey tone on the grey scale. The difference of grey tones between fibrils and other particles is more pronounced in transmitted illumination than in reflected light.

Images taken in transmitted and reflected light in visible spectrum were treated with VISILOG 6.7 image analysis software to separate three categories of particles: long and slender fibrils, flakes and mineral particles. This software also provides details of particles pixel grey level intensity values.

The program (in development) treated the transmitted image, generate information on cellulosic flakes and mineral flakes. The first process was to obtain the grey scale image (range of 0-255) of the RGB colour image (green channel). Binarisation of this image was performed using entropy algorithm. 'Most' part of the thin and bright fibrils dissolves into the background and or their remaining 'parts' are eroded or thinned out (Luukko [47]) leaving the cellulosic and mineral flakes.

In a transmitted image (visible spectrum) thin cellulosic fibrils lead to higher mean grey level intensity compared to cellulosic and mineral flakes; which appear opaque hence lowest value of grey level intensity. Table 9 resumes the particles observed with respect to image type, i.e., reflected and transmitted illumination.

Table 9: Appearance of particles under a light microscope

Illumination type	Cellulosic Flakes	Cellulosic Fibrils	Mineral flakes
Transmitted light	**'Dark' edges, darker body surface (partial or full)**	**Very bright**	**Dark shade**
Reflected light	**Dark**	**Dark edges, bright interior surface**	**Bright (if no ink coverage) or dark –depending upon ink coverage**

However, it must be noted that the appearance of any particle will depend on the light intensity as well as objective magnification.

Figure 56 depicts the mean intensity values of particles (~800 particles detected) obtained in transmitted light after performing operations to 'remove' the visible fibrils. The sample was taken from the pulper outlet P50µm R25µm fraction of the industrial grade pulp. The dotted blue square represents the particles which are in the 'very' low grey level mean intensity range.

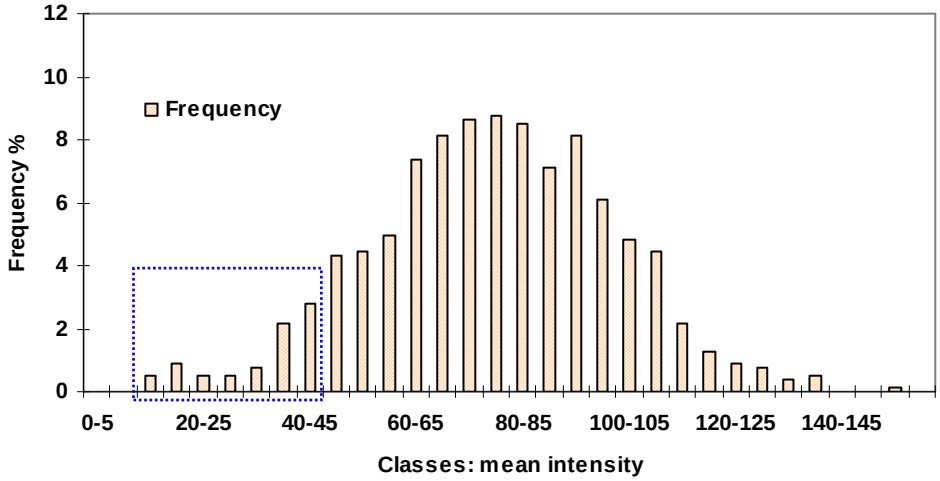

Figure 56: Mean intensity distribution of particles in transmitted light

While the Figure 57 shows less difference between the particles maximum and mean grey level intensity values, where the difference is much less remarked.

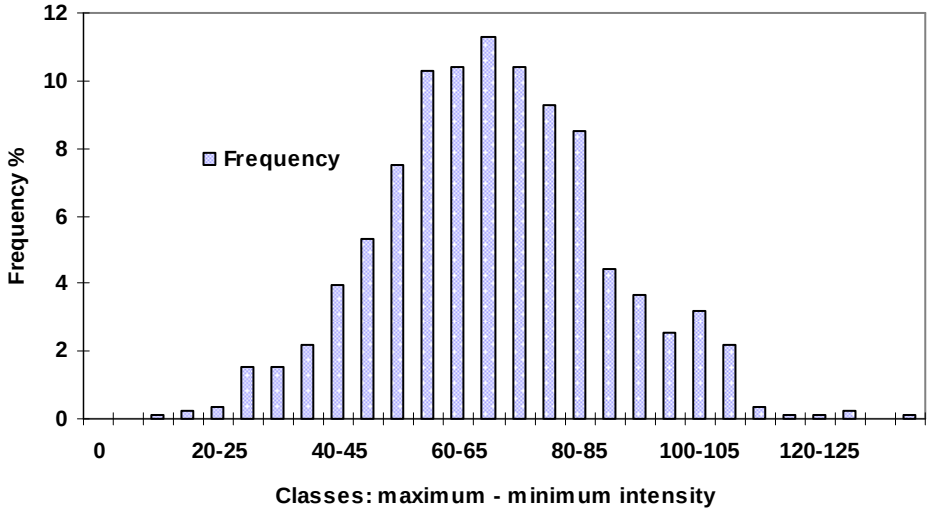

Figure 57: Difference of Maximum-Mean intensity distribution of particles in transmitted light

It is difficult to separate out the mineral flakes from cellulosic flakes based on mean intensity alone or using the difference of particles maximum and minimum intensities. Hence **Intensity Factor, IF**, Eq. 1, was defined to separate cellulosic flakes and mineral flakes based on grey level intensity,

Eq. 1 : **Intensity factor**

$$IF = \frac{(I_{max} - I_{min})}{I_{mean}}$$

I_{max}: Particle maximum intensity
I_{min}: Particle minimum intensity
I_{mean}: Particle mean intensity

The value of the intensity factor as defined was then used to filter out the mineral particles from cellulosic flakes, above a certain value (however, during the image analysis of various samples of the microscope images, it was observed that this value is close to 3, hence this value was fixed *manually* in the filter created in the image analysis program to separate the mineral particles and cellulosic flakes), the particles were defined as mineral particles and the rest as cellulosic flakes. One question could be pointed out: why a manual input and why not a 'totally' automated program. In fact, the issue arises when in a large batch of images to be treated contains very few mineral particles and a large amount of cellulosic flakes. When analysing and calculating the mean intensity distribution, these

mineral particles will be masked and it will appear that there are no inorganic particles, which would then not be true. While observing different pulp fines sub-fractions (till R11µm) images it was observed that the amount (in number) of mineral particles was always 'much' inferior (cf. Figure 34) to the cellulosic flakes except in case of flotation rejects where the situation was the opposite (cf. Figure 42). This would correspond to a situational artefact where much 'less' fillers do not allow to put forward the low mean intensity values. Hence, it could be beneficial to fix a given value of the **IF**, to have information on the few mineral particles, rather than not counting them at all. This value could be fixed for all images, if they are taken with the same illumination conditions of microscope.

While performing a Gaussian approximation of the intensity factor values of the particles calculated from Eq. 1, the mid value of the intensity factor class size was 2.8 as reported in the green curve in Figure 58, very close to the value of 3 put manually.

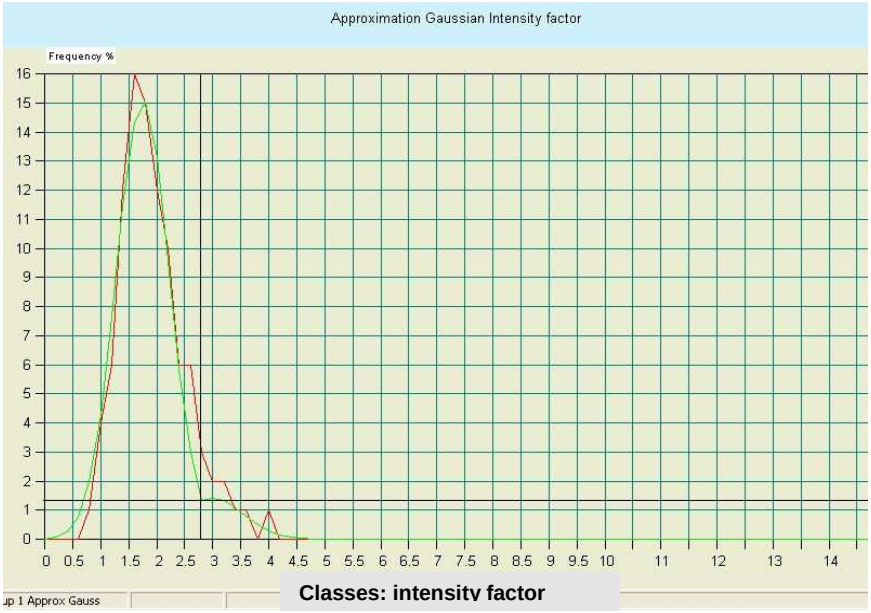

Figure 58: Intensity factor Gaussian distribution for cellulosic flakes and mineral flakes

While plotting the values of IF obtained for cellulosic flakes and mineral particles after their separation it was observed as reported in Figure 59 high peak values for mineral particles centred mostly in the class 3-4, while for cellulosic flakes they were centred around 1.6 – 1.8.

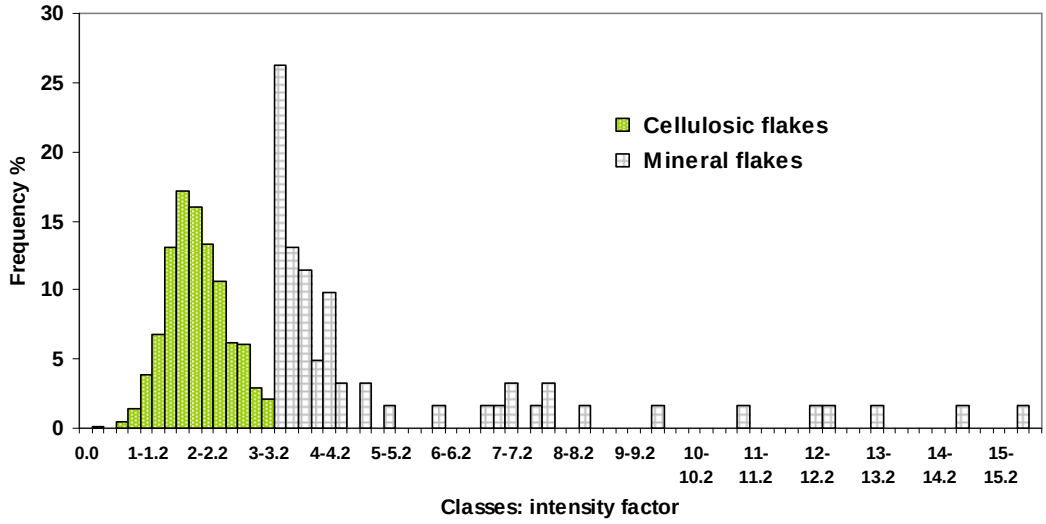

Figure 59: Intensity factor values for flakes and mineral flakes

Figure 60 shows the mean intensities values of the particles (individual category) identified after separation. This gives more information on the low values for mineral particles as compared to flakes and more importantly some ‘overlapping’ with cellulosic flakes. The mean intensity distribution shown by cellulosic flakes corresponds to a classical distribution normally associated with cellulosic parenchyma cells.

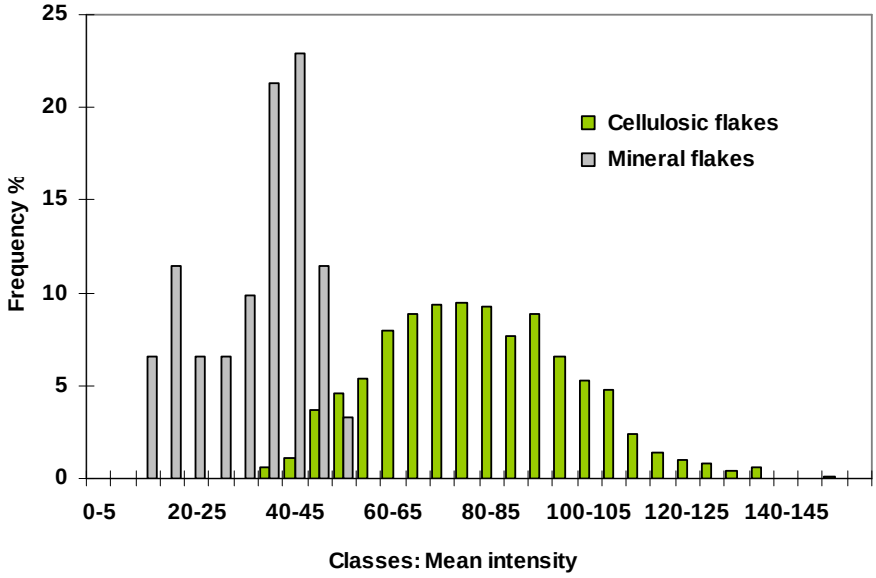

Figure 60: Mean grey level intensitiy values for flakes and mineral flakes after identification

Figure 61 shows the evolution of difference of maximum and minimum intensity values, showing similar values for certain particles for certain classes and more ‘overlapping’ hence less possibility of separation with this criteria or particle mean intensity alone.

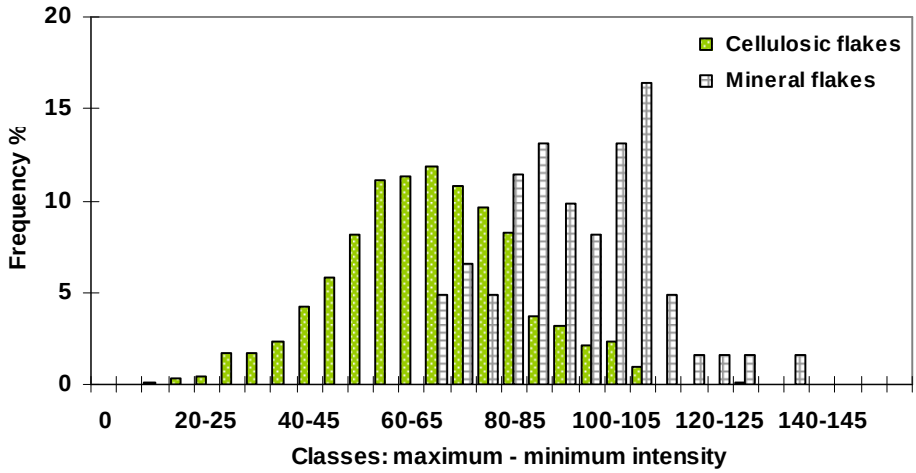

Figure 61: Maximum-minimum grey level intensitiy values for cellulosic and mineral flakes after identification

Having identified the cellulosic and mineral flakes, the image in the reflected mode of illumination was then treated to recover all the particles. The cellulosic and mineral flakes previously determined by the image in transmitted light were then subtracted to have information on fibrillar fines. The complete schematic of the analysis is represented in Figure 62 and also illustrated in Figure 63.

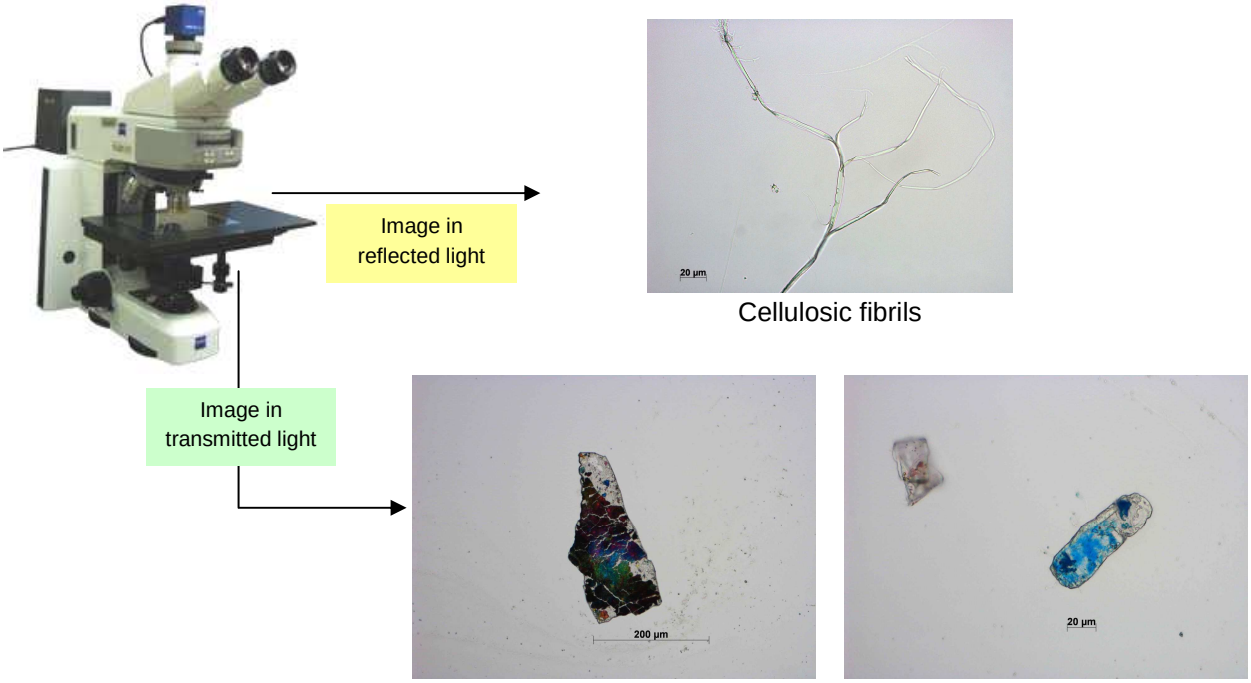

Cellulosic fibrils

Mineral flakes

Cellulosic flakes

Figure 62: Image analysis schematic to obtain 3 categories of the fine particles.

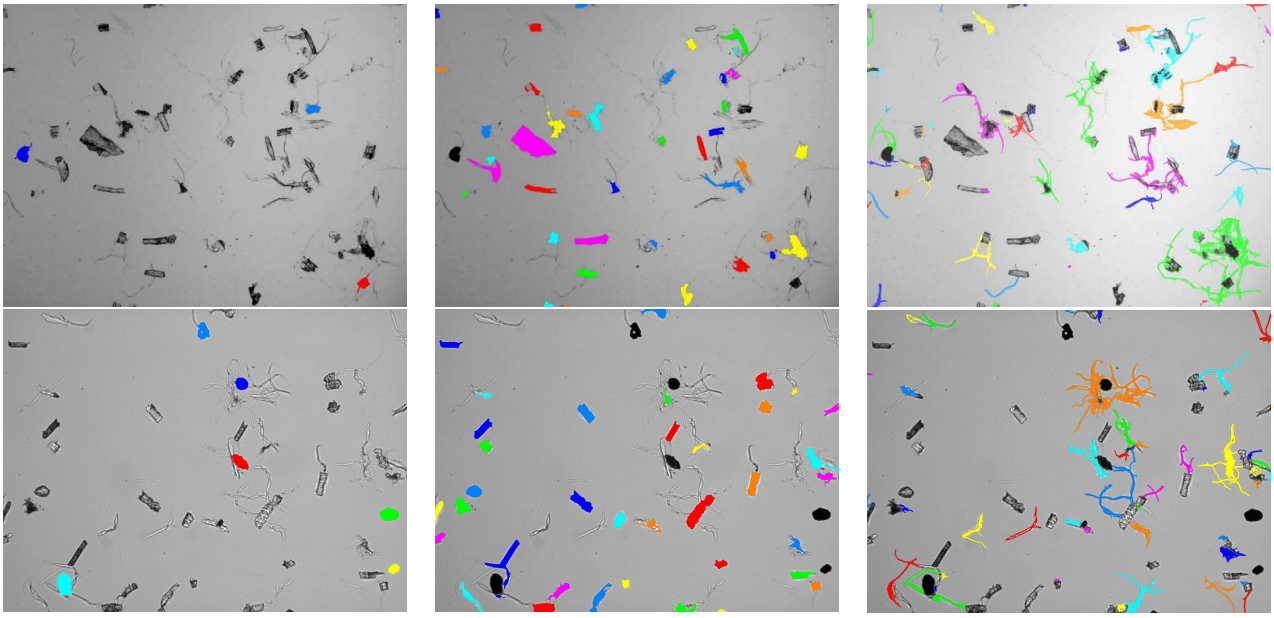

Mineral flakes **Cellulosic flakes** **Cellulosic fines**

Figure 63: Differentiation of particles with image analysis technique

The examples showed that fine sub-fractionation coupled with image analysis process could reveal information about the particle type found in the fractions, especially with respect to the deinked pulp. However, the present image analysis module would consider an impurity as a mineral flake if it has a very low grey scale level, for example a fragment of plastic or other impurities which are opaque in transmitted light, will give rise to a 'high' value of intensity factor and will be classed as mineral flake.

Deinking pulp is a multi-component system (with respect to fibre origin, their pulping conditions and contamination) where different types of pulps are present, hence different categories of fines. Moreover, the age of the particles, the recycling conditions, number of recycling cycles and the treatments they have undergone will affect their grey level intensity; hence their division into fibrils and flakes categories. Fines dyeing with a stain were not performed as it would have affected the grey tone values of fibrils and flakes. The adsorption/absorption of the stains on recycled pulp flakes and fibrillar fines is not known. Luukko [47] while working with pure 1st generation (produced the first time) mechanical pulp fines indicated that the stain absorption on cellulosic fines might be irregular. He stated that the error could be related to fines chemical composition, pH, and the bleaching process they have undergone. Imaging and illumination conditions while performing microscopic analysis vary and will define the values obtained by image analysis [47] and the intensity factor will need to be adjusted according to the particles visually observed with the human eye. For example Ferreira *et al*. [9] used area filters to reject particles which resulted from impurities or image thresholding. No system could be termed as 100% perfect and it is very likely that fibrils are counted as flakes and vice-versa as it is intensity based classification/calculation. Errors could also arise from the dry water lines as the slides were prepared in dry mode by thoroughly washing the collected particles with MilliQ water and also by fines overlapping which would lead to detection of a large particle.

2.4. - Conclusions

Deinking fines contain the majority of the ink amount, while the long fibres are relatively clean with respect to ink contamination (ERIC measurement). The lower fibre fractions (or higher Bauer McNett mesh) however have a slightly increased ink amount as compared to higher fibre fractions (or lower Bauer McNett mesh). The brightness value for the McNett fractions is very near to that of the hyperwashed fraction. While the fines fractions are heavily contaminated with ink particles.

A simple laboratory scale method was developed to obtain fines sub-fractions on different sieve openings down to 11µm. The 'soft – hyperwashing' of fines (P200 Bauer McNett) revealed the presence of majority of the fines with the finest fibrils and flakes fraction as well as the maximum amount of ink particles in the P11µm fraction.

The slender, swell-able, thin, flexible fibrils were mostly free of ink, while ink was associated with flakes fines. Mineral fillers were either partially or fully or not-coloured at all, but they were in majority present in the P11µm fraction.

The smallest and the finest of the particles float in a deinking flotation unit. Flotation rejects from a deinking line were composed of maximum particles 85-90% in the P11µm fraction.

A new module of image analysis program was attempted to treat the deinking pulp fines sub-fractions. Simultaneous treatment of images in transmitted light and reflected light was made to separate mineral flakes, cellulosic flakes and cellulosic fines. This method however does not take into account fines contamination arising from opaque impurities other than mineral flakes.

The analysis performed gave a minute insight into the fines fraction and provided useful information on their characteristics. The new method of soft-hyperwashing could be applied to different pulps to ascertain particle characteristics. The image analysis featuring a new module showed encouraging results and indeed can also be applied to virgin fibre fines having no mineral flakes. Having established the study background, the next steps will be experimental trials with industrial level equipment which can selectively separate fines fractions. An all-encompassing and comprehensive study of a pressure screening system dealing specifically with fines separation and application is provided in the next two chapters.

3. - Fractionation processes and separation of fines

3.1. - State of the art

3.1.1. - Fractionation processes

Fractionation essentially involves division or separation of a pulp suspension into two separate streams which possess different pulp characteristics in terms of pulp morphological characteristics or sheet properties. The difference between screening and fractionation arises from the fact that the former is devoted to pulp cleaning or removal of contaminants associated with the pulp (shives, plastic films, adhesives stickies, etc.), while the latter is dedicated to fibre type processing. Screening leads to rejections of contaminants with the 'objective' of minimum fibre loss and cleaner pulp while a fractionation process produces 2 fractions which can be used or treated accordingly to reduce process costs and/or provide value addition and enhancement of the paper sheet properties.

Classification of fibres based on their length and understanding the evolution of sheet properties as well as in-depth study of the fractions has been performed by many researchers since the first quarter of the last century [74]. For example Lindholm [11], Forgacs [16], and Mohlin [75] found differences in sheet properties of the different fibre fractions obtained using a Bauer McNett classifier. The fundamental idea was to assess the properties of fractions best suited for paper manufacture and later for the final usage of the final product, namely the printing properties. Fractionating the flux of fibres offers the possibility to fine-tune the paper manufacture and optimise the usage of fibres for a better manufacturing efficiency and also provides a means to innovate how paper is manufactured.

For example as suggested by Felsvang *et al.* [76] fibre fractionation could be applied in a variety of ways as represented in Figure 64 (PM referring to Paper Machine).

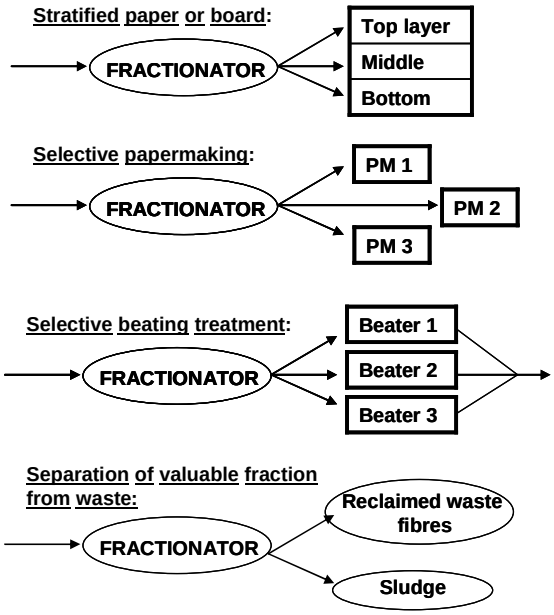

Figure 64: Fractionation applications, from Felsvang *et al.* [76]

At an industrial scale, pressure screens represented in Figure 65 and cleaners or hydrocyclones shown in Figure 66 are the two systems, which are efficiently utilised for performing fractionation of pulp streams.

Fractionation by pressure screening

In case of a pressure screening, fractionation occurs when the pulp suspension flows across (and between) a screen plate (or also called screen cylinder, basket) and a pulsating element called rotor. While centrifugal and hydrodynamic drag forces in relation to particle density and surface characteristics are responsible for fractionation in a hydrocyclone. The basket in pressure screening either is perforated (for example holes of dimensions 1.0 mm - 2.0 mm) or has narrow slots (for example 0.10mm- 0.15 mm).

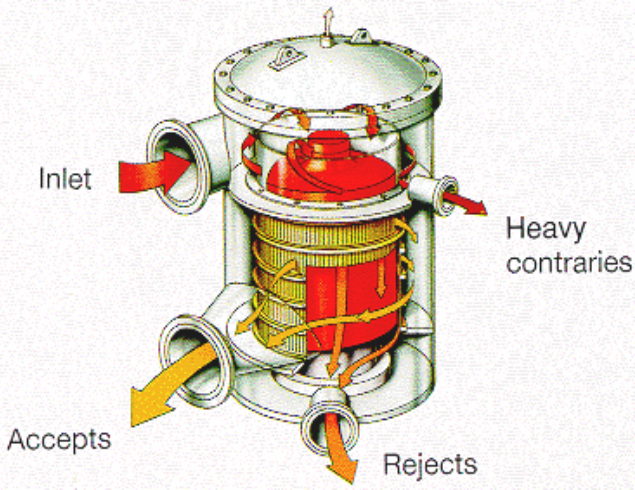

The solid red colour central part is the pulsating element or **rotor** surrounded by a cylindrical slotted screen plate or slot **screen**

Figure 65: VOITH / ESCHER-WYSS- Omnisorter (trade name -technical Notice)

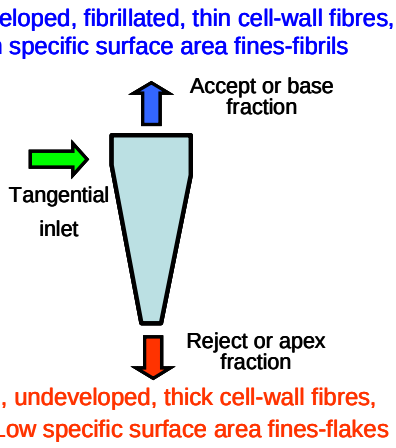

Figure 66: Representation of a fractionation hydrocyclone with fractions characteristics

In the manufacture of high-yield/ mechanical pulps, fractionation by employing pressure screens has found widespread usage. Research has been focussed on fractionating the pulp stream in order to selectively treat the non-fibrillated, coarse fibres which lead to poor bonding ability [77]. This is performed by directing the 'non-optimum' fibres and shives to reject refiners leading to an improvement in their bonding characteristics [78] and a reduction of sheet defects. Such an approach leads to reduced quantity of fibres to the reject refining systems (hence it could also lead to energy reduction as only a part 35-40% of the total pulp flow is treated). Fractionation the pulp flow also allows applying different levels of energy intensity on fractionated streams [79][80][81] and chemical treatment [82] for added benefits.

Workers also reported fractionation applied on the chemical pulp to enhance end product properties [83] and as done for mechanical pulp, the fractionation strategy has also been to perform selective refining of fractions [84][85][86].

Fundamental work by many authors to understand of how fibre fractionate across the screen surface has led to the conclusion that pressure screen fractionate primarily on the basis of fibre length, while flexibility/ stiffness are secondary factors [40][87][88][89][90][91]. Longer fibres are removed in the rejects while shorter fibres and fines, pass into the accept side of the screen plate.

A representation of a screening system is shown in Figure 67. Water associated with the pulp suspension encounters the least resistance to traverse the apertures followed by mineral fillers, cellulosic fines and short-length fibres. Due to this principal reason, accepts get diluted and the rejects thickened, orchestrating an effect very well known in the paper industry known as **reject thickening**.

The increase in reject concentration also signifies that the screen is fractionating. Hence, the concentration order for the whole pulp is:

Reject concentration (C_r) > Inlet concentration (C_i) > Accept concentration (C_a)

The passage of particles across the apertures or their rejection is governed by many factors and complex hydrodynamic conditions prevailing on the screen plate surface. Fractionation effects are more pronounced for a softwood pulp with a wider range of fibre length dimensions as compared to a hardwood pulp.

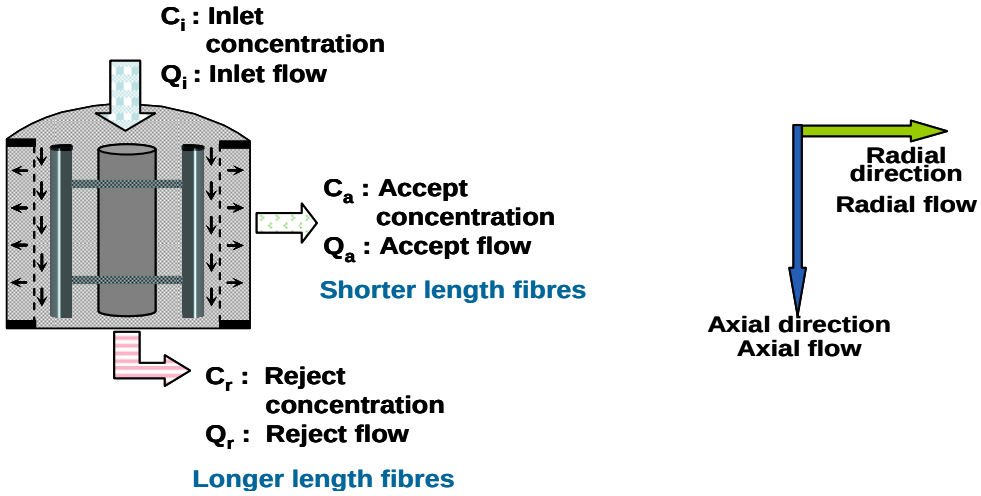

Figure 67: Screening system representation with different flows

Fibre and contaminant dimensions as well as their 'elastic' properties (to get deformed, for example flexibility in case of cellulose fibres and deformable characteristic of adhesive contaminant stickies) are the key factors governing their flow behaviour inside the screening system.

Fractionation and screening across basket openings are based on two very different principles. **Barrier** mechanism where all particle dimensions are larger than the aperture size, hence the entity is effectively stopped and flows out in the rejects. This is valid for stiff particles, since soft deformable particles like for example macro-stickies from pressure sentitive adhesives can be pressure extruded through the slots. The second and more complex mechanism is **Probability** screening where at least one dimension of the particle is smaller than the aperture opening. In any screening system, both mechanisms work in tandem. Screening by probability involves the situation where the particle to get accepted has first to get located just over the aperture surface and get captured in the upstream boundary flow and additionally get itself 'aligned' in the flow towards the screen opening. By modifying the screen plate design (aperture dimensions, geometry and type) the generation of turbulence just upstream of the aperture can be modified to continuously disturb the formation of flocs and 'increase' the boundary layer thickness to improve the particle capture probability.

Fractionation by cleaner or hydrocyclone

Cleaners, represented in Figure 66 are effectively used to remove high-density contaminants like for example sand, metal, glass, grit particles as well as low-density contaminants essentially consisting of hot-melt glues and plastic films [92].

A fractionation hydrocyclone is a cleaner which is used for fractionating. Such hydrocyclones differ from cleaners mainly through the dimensioning of apex and base outlets, which are designed in such a way to achieve a more balanced flow split between the two fractions as compared to high or low density cleaners, where respectively the base and accept flows are reduced to minimise the rejection of fibres.

In case of hydrocyclones, density and specific surface area are the main criteria for fractionation, with accepts getting enriched in higher specific surface area fibres and fines. Indeed, hydrocyclones separate fibres on the basis of cell wall thickness and surface characteristics, which is another important criterion for sheet properties development, together with fibre length.

Flexible springwood or early-wood fibres during the growth season have narrow or thin cell wall in comparison to summerwood or latewood fibres, which have thicker cell wall dimensions, are stiff and possess higher coarseness. The first patent to separate such fibres was granted in 1963 [93]. Thin cell wall fibre have a better collapsibility potential, thereby increasing the fibre bonding area and providing better sheet strength as well as printing properties. Many workers have studied the fractionation potential of hydrocyclones [43][94][95][96][97][98][99][100].

Alince *et al.* [22]fractionated only fines (P100 mesh) of a mechanical pulp (TMP) using a hydrocyclone and studied the sheet properties by incorporating various amounts of apex and base fractions. They reported the addition of high specific surface area, fibrillar fines (the accept fraction) to the fibre fraction increased mechanical and optical properties.

Comparison between pressure screening and hydrocyclone fractionation

Niinimäki *et al.* [101] reported findings from different authors about pulp/fibre morphological and sheet properties in pressure screen and hydrocyclone fractions. Table 10 reports the trends for accept fraction morphological properties and Table 11 sheet properties (the trends for reject fractions are opposite).

Table 10: Accept pulp fraction morphological properties, from Niinimäki *et al.* [101]

	Pressure screen	Hydrocyclone
Property	**Trend**	**Trend**
Fibre length	**Lower**	**Higher/Lower**
Freeness	**Lower**	**Lower**
Coarseness	**Lower**	**Lower**
Cell wall thickness	**Lower**	**Lower**
Fibril content of fines	**Lower**	**Higher**
Fibre fibrillation	**No difference/slightly lower**	**More**
Ray cell concentration	**-**	**Lower**

Table 11: Accept pulp fraction sheet properties, from Niinimäki *et al.* [101]

	Pressure screen	Hydrocyclone
Property	**Trend**	**Trend**
Apparent density	**Higher**	**Higher**
Tensile strength	**Higher**	**Higher**
Tear strength	**Higher/lower**	**Lower/higher**
Light scattering	**Higher**	**Higher**
Light absorption	**Higher**	**-**
Air resistance	**Higher**	**Higher**
Opacity	**Higher**	**Lower**
Surface roughness	**Lower**	**Lower**

The overview of the fractions characteristics for the two fractionating technologies is illustrated in the Figure 68 by Sandberg & Shagaev [102]. Indeed as the name indicates, the short fraction (accepts) of pressure screening contains short length fibres, irrespective of cell wall thickness. Whereas in case of hydrocyclone, the base fraction (or accepts) contains thin cell wall fibres irrespective of fibre length.

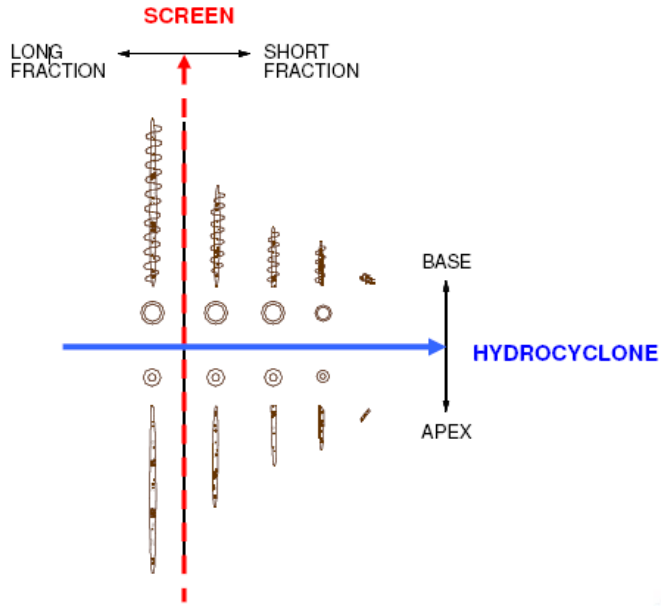

Figure 68: Illustration of fibre morphological characteristics resulting from pressure screening and hydrocyclone fractionation, from Sandberg & Shagaev [102]

Fractionation in deinking operations

The manufacture of paper from deinking operations using a fractionation step is currently limited to simplification of a deinking line and selective treatment of fractions obtained. This strategy differs from the application of fractionation to high-yield mechanical pulps or multilayer board manufacture, where fibre up-gradation is focussed to enhance pulp characteristics or the final product.

In other words, fractionation process applied in a deinking operation essentially relates to right treatment to the right fibre type as the whole pulp flux is not treated in the different unit operations. These unit operations either treat the fibrous suspension for ink removal (flotation or washing) or work upon the fibres to detach ink (high speed disperser or low speed kneader treatment) or fragment the specks.

In the 90's, this concept was studied by Floccia [103] and Eul e*t al* [104]. Fines fractions (containing majority of microscopic ink particles) selectively removed by washing fractionation were further treated in flotation operations (50% capacity requirement only- fractionation benefit) followed by bleaching. The benefits of such configurations in comparison to conventional systems are illustrated in Figure 69.

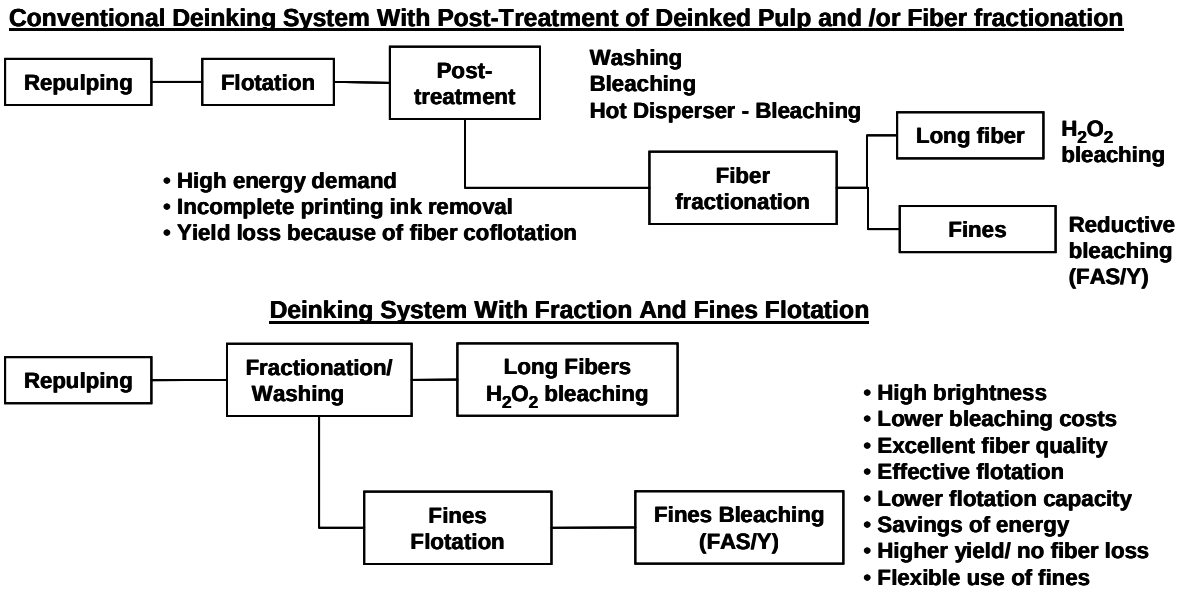

Figure 69: Benefit of fractionation in a deinking line, from Eul *et al.* [104]

In the last years, researchers have studied the deinking pulp stream fractionation and fractions selective treatments. Deinking lines are designed and traditionally are 'single' line configuration, where all the recycled fibre entering the defibering stage is treated in each and every unit operations. But increased energy costs and poor input quality of recycled fibre have led to parallel processing of fractionated streams while maintaining the normal final paper quality, with the focus on reduced equipment size and loops; or a lean [105] / compact design [106] ink splitting approach [107]. This is achieved by using screens with narrow aperture dimensions: micro slots or holes [106][107][108]. The concept of deinking fractionation has also been applied to a full-scale industrial plant in 2005 producing newsprint [109] and reporting annual savings as well as improved operational stability.

It has to be understood whether the deinking line will still be configured with a 2-loop system, a fractionating system positioned between the loops and only the long fibre being treated for ink detachment in a disperser with final bleaching of the total stock [109]. For example in [109] a 0.15mm slot fractionating pressure screen has been adopted after pre-flotation. Note that in this approach, it was mainly to apply dispersing stage on only a part of the stream, no dedicated treatment was proposed for the fine fraction that is recombined to long fibre fraction before post-flotation.

The positioning of the fractionation system in a deinking line could be said to be critical with respect to the end gains to be achieved. As mentioned by Fabry & Carré [110] the perfect process running situation will be when mechanical energy is applied on only the fibrous fraction and specks, while the 'free' ink by-passes this step, thereby splitting the flow to allow reduced pulp mass for mechanical energy application, and avoiding detrimental fragmentation of the already detached ink.

Fractionation immediately after defibering and initial contaminant removal step and before ink removal steps could also be envisaged [107][108][110], while performing ink removal operations only on ink containing fraction (or fines) and mechanical action on long fibre fraction and re-blending later [108] [107]. This is the most ideal scenario with no flotation capacity increase and leading to a compact one loop process design.

To supplement the removal of the detached ink after dispersing operations, a washing step/thickening step could be thought of or a final washing step for de-ashing in case of tissue paper manufacture [107]. Fabry & Carré [110] studied dispersing application of fractionated long fibre treatment before flotation operations and re-blending with non-treated short fibre followed by laboratory flotation. Their

approach led to an increase of the final pulp ERIC content after 1-deinking loop due ink fragmentation in dispersing operations.

Some simplified different scenarios are represented in Figure 70.

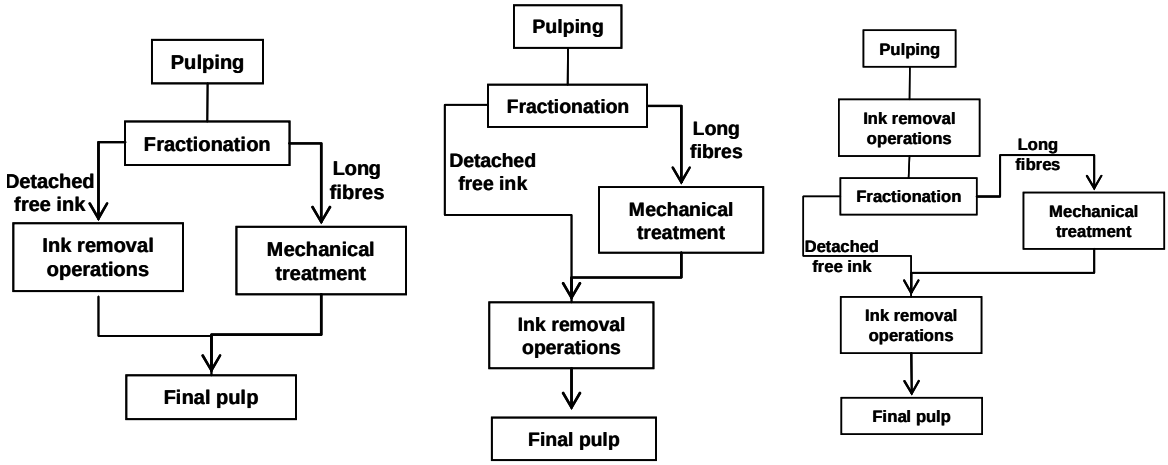

Figure 70: Fractionation configurations in the manufacture of paper in deinking lines.

It must be noted that fractionation using pressure screens (holes and slots) in the field of recycling has been used to manufacture brown grades and in multilayer paperboard from old corrugated containers (OCC) since a long time. The ‘high-grade’ long fibre fraction and a ‘low-grade’ short fibre fraction could be used to produce a range of products ranging from linerboard to lower quality products [111][112]. Long fibres selectively refined after fractionation provide strength to the top layers whereas short fibres are used as filler material in the middle layer. The removal of short fibres and fines increases the pulp freeness, with some workers considering the removal of ‘dead‘ fines associated with the OCC furnish as beneficial to improve bonding and freeness [113].

3.1.1.1. - Fractionation by size – screening/ washing

The presence of any physical barrier (for example a screen) with narrow opening will lead to fractionation by size. For example with a mesh screen Brissaud et al. [114] illustrated the notion of fibre flexibility and the possible fibre lengths that could be retained on the mesh screen with a square opening of dimensions 'd' as reported in Table 12. Or with a pressure screening system, equipped with different sizes of narrow apertures (slot width) results in fractionation by length as represented in the Figure 71, and the distribution of fibres changes by varying the running parameters (passing velocity), (more details are provided in later sections of this chapter)

Table 12: Bauer McNett fibre length distribution range, from Brissaud *et al.* [114]

Minimum length	$L_{minimum}$	2.26 d
Mean length	L_{mean}	3.19 d
Maximum length	$L_{maximum}$	4.12 d

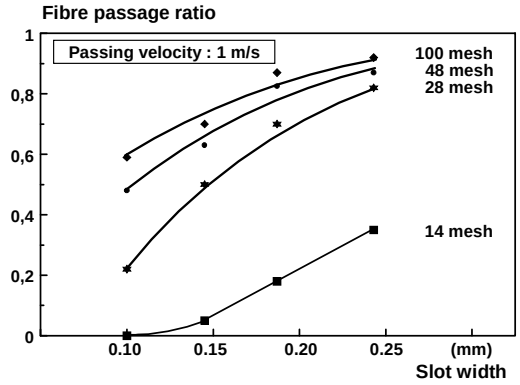

Figure 71: Effect of fibre length (Bauer McNett fractions) on fibre passage ratio and slot width, Julien Saint Amand & Perrin [88]

Washing is a unit operation, which involves barrier separation and thickening effect. This happens when the liquid pulp suspension gets thickened over a mesh screen and the filtrate gets enriched in mineral fillers, ink particles and cellulosic fines. Thereby the retained 'thickened' fibres on the wire surface get cleaned of ink particles and deinking occurs. The coarse particles are not removed as they are preferentially retained in the pulp mat formed, while the smallest of the ink particles as well as the mineral fillers are preferentially removed or washed away in the filtrate. It is for this particular reason that this technology is employed during the manufacture of tissue paper essentially involving removal of mineral particles or the pulp 'deashing'. In an ideal scenario if the fibre network formed during the thickening operation does not acts as a filter, then all the fine particles follow the flow split.

3.1.1.2. - Fractionation by density – cleaning

Fractionation in case of cleaners is based on particle density and size, leading to differences in radial particle slip velocity towards the wall, in the centrifugal flow field:

- Coarse and dense particles, including shives and latewood fibres, with low specific surface area have high centrifugal slip velocity and concentrate in the cleaner rejects, i.e. in the heavy or coarse fraction. Large coated flakes concentrate in the reject stream as well as specks.

- Fine particles with high specific surface area, including fines and early-wood fibres as well as fibrillated fibres, have lower centrifugal slip velocity because of their smaller size and/or apparent density in the case of early-wood fibres, and/or because of their increased drag coefficient in the case collapsed and/or surface fibrillated fibres. These particles also tend to concentrate in the cleaner rejects, but much slower, so that the cleaner accepts, i.e. the "light" or fine fraction, becomes enriched in these pulp components. Very fines particles, have extremely low radial slip velocity and tend to follow the cleaner "flow split".

- High consistency and long fibres content affects negatively the separation process, as effective de-flocculation will be hindered. For good efficiency, individual elements should have free movement with minimum interaction between the elements in an ideal scenario. Low reject diameter will lead to long fibres bouncing back into the central core and being carried into the accepts, hence deteriorating the removal efficiency.

3.1.1.3. - Fractionation by surface physico-chemical properties - flotation

Flotation systems employed widely for ink removal in the deinking industry work on surface property modification of the ink particle surface (hydrophobicity) and their removal in aerated cells. The small ink particles get attached to the upward moving air bubbles and are removed in the rejects. Indeed, flotation systems are highly effective in the removal of fines and small dimension particles and their selectivity towards such particles is very high.

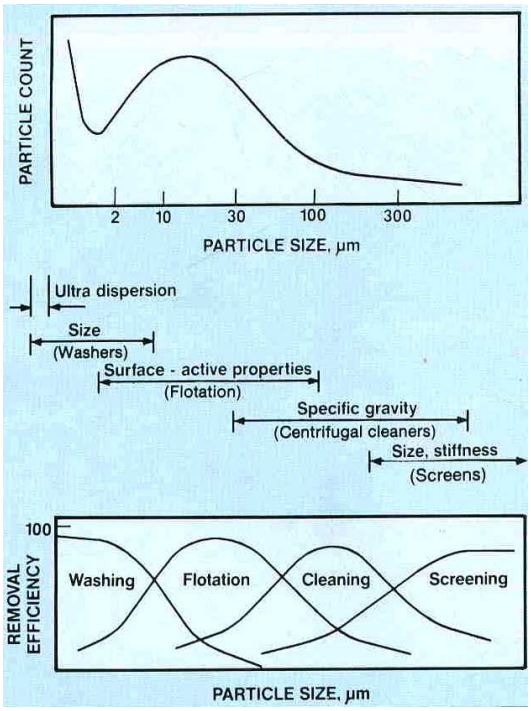

Figure 72: Particle size distribution and removal efficiencies, from McCool & Silveri [46]

The particle size and fragmentation level at the pulper level defines its exit from the process. Figure 72 shows the model of specks distribution at the exit of the pulper stage. Screening and washing are ineffective in removing specks, whereas flotation is most effective in 2 – 100µm particle size range. Specks are generally considered as particles with average size of more than 50µm.

3.1.2. - Screening parameters

In the beginning of the 20th century, screening systems worked under open atmospheric conditions. Unwanted debris not required for paper manufacture were removed using a vibrating screen plate, using gravity filtration, for example the Lamort Super-Type Screen, era 1910. Then around 5 decades later, saw the advent of pressurised screens and the development of rotor foils as well as advancement of the screening system as a whole.

Any screening system has two main design parts, which define the ensemble of the equipment, its efficiency with respect to throughput or the pulp production and operational characteristics.

Acting as 'flow barriers', the **screen plates** remove the contraries and undesirable components from the pulp suspension which would degrade the final pulp quality. The cylindrical screens or baskets have apertures: either smooth holes or smooth /profiled slots to screen out the contaminants or to perform fractionation. There are various types of screens on the market, which cater to the needs of various pulp segments: from mechanical pulp to chemical pulps and to different fibre characteristics.

Rotors function as a hydrodynamic directional element to the incoming flow of the pulp suspension and more importantly to control or improve the ever changing, complex hydrodynamic conditions on the surface of the screens apertures. They impart tangential velocity to the pulp suspension, having a much higher magnitude than the axial velocity resulting from the continuous reject removal. They are equipped or have elements, which create pressure pulsations. More details have been provided in the coming sections.

3.1.2.1. - Rotor

A screening system normally is based on a centrifugal configuration where the rotor is located on the feed side (cf. Figure 65) and the pulp suspension flows outward. However, centripetal flow configuration screens (cf. Figure 73) also exist in the commercial market where the rotor is either at the feed side or situated on the downstream. In this 'inward' flow configuration, either the screen is rotating and rotor is stationary (a stator) or the inverse. The biggest advantage of a rotor situated on the feed side in centripetal flow configuration is the minimization of the accept side pulsation.

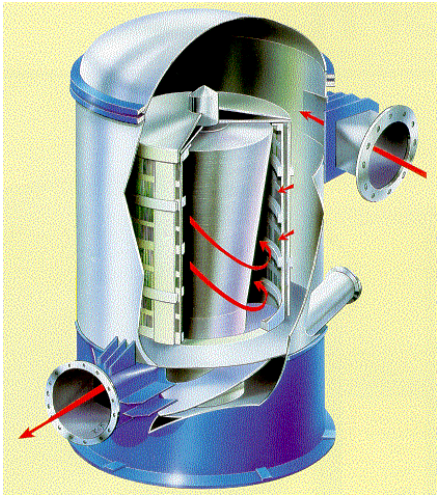

Figure 73: KADANT LAMORT SP Screen (Technical Notice)

Rotors are divided into 2 different and specific categories based on the radial flow thickness available between the rotor central axis and the basket (in a centrifugal flow configuration). **Open** or **foil** rotors typically have a large pulp flow thickness and the fibrous suspension is able to flow around this type of rotor, used essentially for low consistency operations. Whereas **closed** or a **solid core** rotor design provides a very narrow pulp flow thickness. The foil rotors by origin design have hydrodynamic elements, however in case of a closed rotor type, hydrodynamic elements are embedded or welded/attached or carved out onto a solid cylinder core. The two types have been represented in Figure 74 to Figure 76.

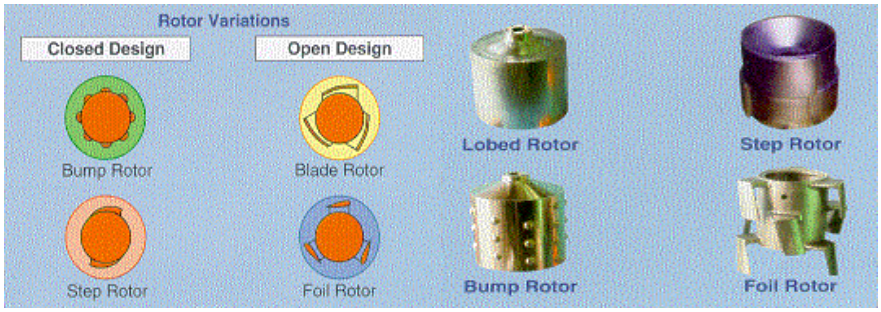

Figure 74: From Rienecker [115]

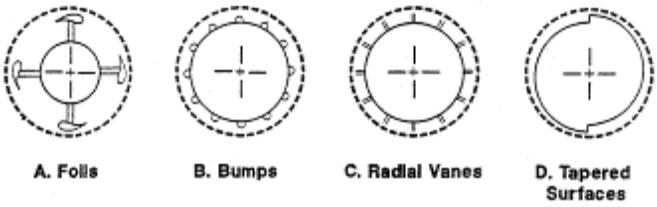

Figure 75: From Bride Mac [116]

Figure 76: Foil rotor, from Olson *et al.* [117]

The type of screens (more details described later) defines the screening or fractionating efficiency together with the running parameters, but for their efficient and smooth operations, the function of the rotor is an indispensable part. Rotor acts in two different ways, firstly the pulp or the fluid flux entering the screening system is rapidly ‘entrained’ by the rotor and taken aboard inside the screening zone. Revolving around a central axis, the rotor fluidises, deflocculates and homogenises the pulp suspension for its even distribution across the screening area. This happens as soon as the pulp comes into contact with the rotor and continues along the axis from the point of entry. A centrifugal screen configuration, with rotor on the feed side, is much better suited to control the continuous and rapid hydrodynamic interactions and changes taking place between the rotor and screen surface.

Another important function of the rotor is to keep the screen surface free of debris accumulation including the pulp layer formed and deposited during the screening phase. This pulp layer formed has to be continuously removed for efficient operation. The surface cleaning or de-plugging is achieved by back-flushing or reverse flow process where the accept pulp suspension in the downstream flow is re-pumped through the apertures across the screen in the upstream flow, a phenomenon happening due to the formation of pressure pulses by the rotor, having a positive and negative component. The backflushing action is associated with the negative pressure pulse. This is illustrated in a very simplified way in Figure 77. The concept of a rotor design shows similarities to an aerofoil with its various design parameters as shown in Figure 78. However, contrary to relative wind (atmospheric conditions), the rotating foil is inside a pressurised system with narrow clearance between the rotor tip and screen cylinder surrounded by a liquid pulp suspension.

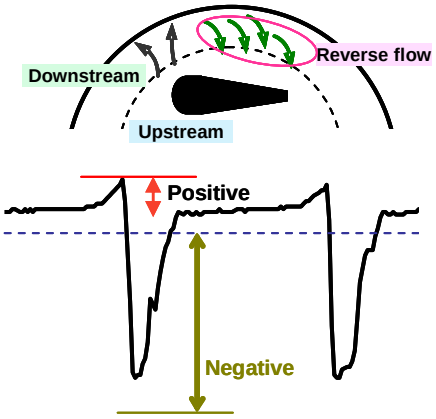

Figure 77: Simplified illustration of reverse flow or back flushing action and relation to pressure pulse

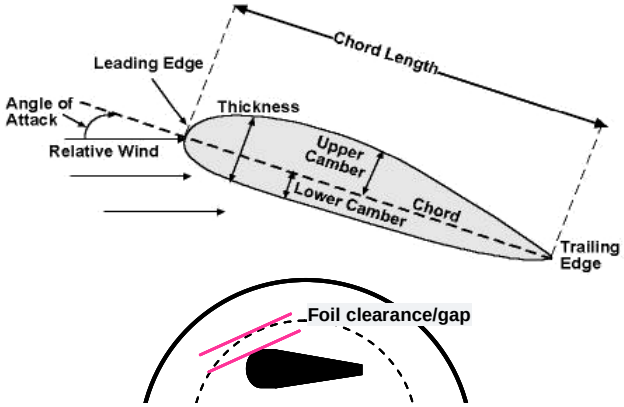

Figure 78: Aerofoil geometry details [118]

Generally, the passing velocity across the screen plate is calculated by the accept flow rate to the open surface area available. This gives an average passing velocity. The volume of the backflushed suspension added to the continuous pumped (or injected) suspension increases the total or effective volume to be treated across the screen plate during the positive pulse (screening phase) duration. Hence, the 'effective' passing velocity, Ve, during the screening phase could be considerably higher depending upon the re-pumped volume.

The pressure pulses generated by the rotor define the smooth working, handling capacity and efficiency of the screening system. These pressure pulses are in turn dependant upon either the rotor design parameters, for example angle of attack, camber and on its operating parameters, for example tip speed (or linked to rotations per minute- RPM), clearance between rotor tip and screen. The pressure pulses magnitude could also be altered by the pulp consistency.

Using advanced methods of simulations of the movement of the fluid flow over the foil and also experimental measurement techniques, different workers have assessed the effects of rotor geometry parameters and operating variables on the shape and magnitude of the pressure pulses. It could be however mentioned that different rotors in combination with different screens give a characteristic pressure pulse profile which could be unique to the rotor and screen type combination [119].

Figure 79 reports two different pressure pulse measurements done on an industrial size screen using foil and blade type rotor by Julien-Saint-Amand & Perrin [89]. Extended duration negative pulse of a long-blade rotor will lead to a higher volume of pulp suspension flushed back into the accept side, resulting in a much higher effective slot velocity or Ve as compared to a short duration negative pulp of foil rotor. The negative pressure pulse magnitude was approximately 200kPa for foil rotor and 150kPa for blade rotor.

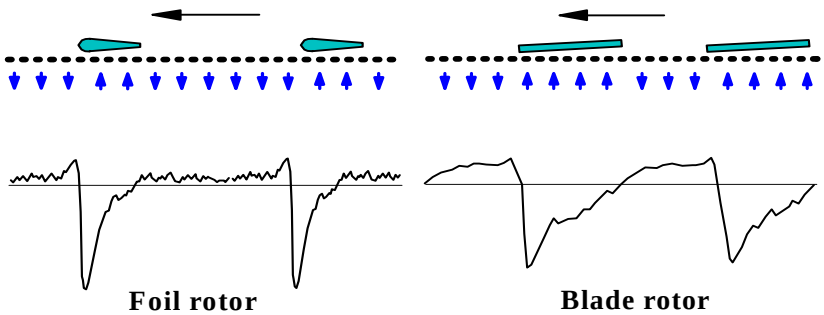

Figure 79: Effect of rotor design on pressure pulse shape, from Julien Saint Amand & Perrin [89]

In one of the first studies on pressure pulsation produced by a foil, Karvinen & Halonen [119] studied turbulent flow field in the clearance using firstly numerical and then experimental methods. They mentioned foil shape influences the pressure pulse profile (cf. Figure 80) and an increase in the pressure pulsation magnitude with increase in rotation speed (or rotor tip velocity). They also numerically deduced that clearance distance has a pronounced effect on pressure pulsation, its decrease results in an increase in the pulse magnitude or the pressure difference. Since then a number of studies have been performed to understand the importance and factors affecting generation of pressure pulses.

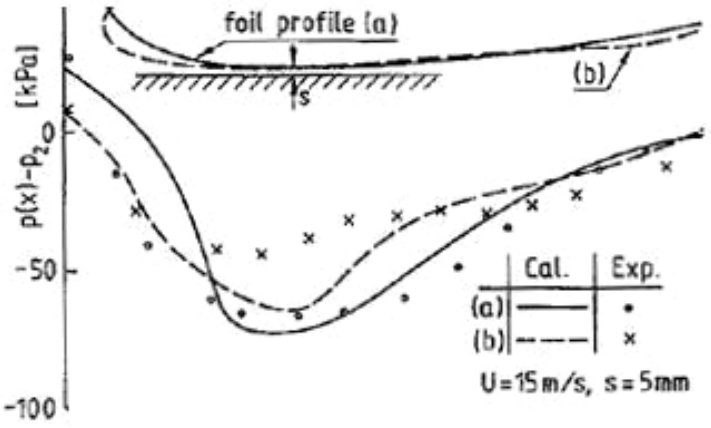

Figure 80: Pressure distribution, from Karvinen & Halonen [119]

Levis [120] in 1991 gave a relation between the augmentation of the rotor tip velocity or a reduction in clearance and the pressure pulse magnitude. The author indicated that the increase of the pressure pulse magnitude is a function of the square of the rotor tip velocity change, (cf. Figure 81) and is directly proportional to change in clearance (cf. Figure 82). Increase of the cleaning pulse will increase in pulp handling capacity of the screening system. However if such an increase is related to an increase of tip speed (or in other words pulse frequency), the rotor power consumption increases to 2.5 power of the speed change. Also, the capacity increase reaches a stagnation point at a particular maximum rotor speed after which no further increase occurs. From his data, it could be observed that the pulse magnitude is in the order of 207kPa. Increase in rotational speed also increases the positive pulse magnitude.

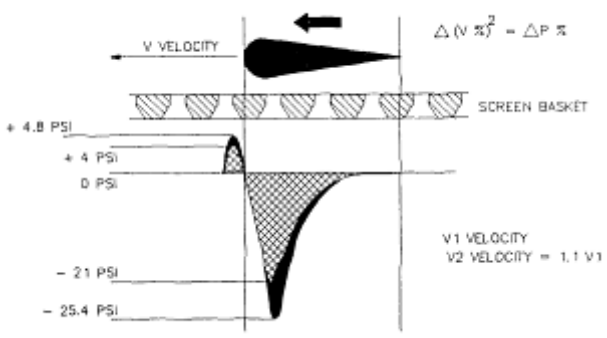

Figure 81: Relation between tip speed and pulse magnitude, from Levis [120]

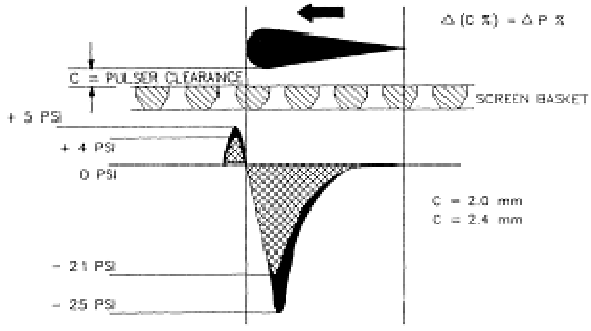

Figure 82: Relation between foil clearance and pulse magnitude, from Levis [120]

Yu [121] measured the pressure pulsation of a S shaped rotor along the axis of a pressure screen configured with a perforated wavy basket with bleached kraft pulp at 2% consistency. Reporting data for one revolution of rotor, the author mentioned different pulse profiles along the axis of the screen varies and at a particular section they are the strongest, higher by 35 to 138kPa. However they are not affected by a change in the accept flow rate. Higher rotational speed is associated with a higher

positive pressure pulse, and the shape and magnitude of the pulse also changes, as reported in Figure 83. Too long negative pressure pulse will blind the screen.

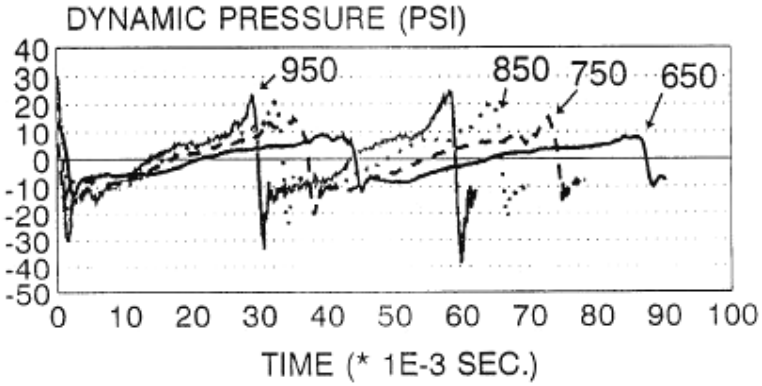

Figure 83: Pressure pulse and rotational speed, from Yu [121]

It has been also suggested that during the reverse phase, a fibre mat formed on the accept side allows only water to filter through and move into the feed side, thus diluting the suspension at the inlet [122][123]. Higher pulsation magnitude will decrease the screening efficiency at the same time increasing the capacity of the system. The efficiency decrease is related to the positive pressure pulse which forces the debris mat through the apertures before the negative pulse disturbs the mat and remixes the fibres back into the turbulent flow upstream.

Pinon *et al.* [124] studied the pressure pulses produced and their position with respect to cord length in a laboratory cross sectional screen by solid core rotor element against a smooth wall. The authors defined a non-dimensional pressure coefficient, Cp, based on rotor velocity, represented in Eq. 2.

Eq. 2 :

$$Cp = \frac{P_r}{\frac{1}{2}\rho V_t^{\,2}}$$

P_r: Pressure at screen plate surface, Pa
ρ: Fluid density, kg/m^3
V_t: Rotor tip velocity, m/s

They varied the rotor tip speed, rotor and basket clearance, while using water and pulp at various concentrations. They deduced that although the magnitude of the pressure pulse changes to a large extent with respect to rotor tip velocity, the shape remains however the same (cf. Figure 84 a). This trend was similar for gap change: lower gap induces a higher pulse magnitude. The positive pressure pulse starts much before the leading edge of the foils. More importantly the pressure coefficient remains approximately constant for all the range of tip speeds (cf. Figure 84 b). There is no effect of concentration on the positive pressure pulse magnitude, while it decreases at higher pulp concentrations for the suction cleaning pulse (cf. Figure 84 c).

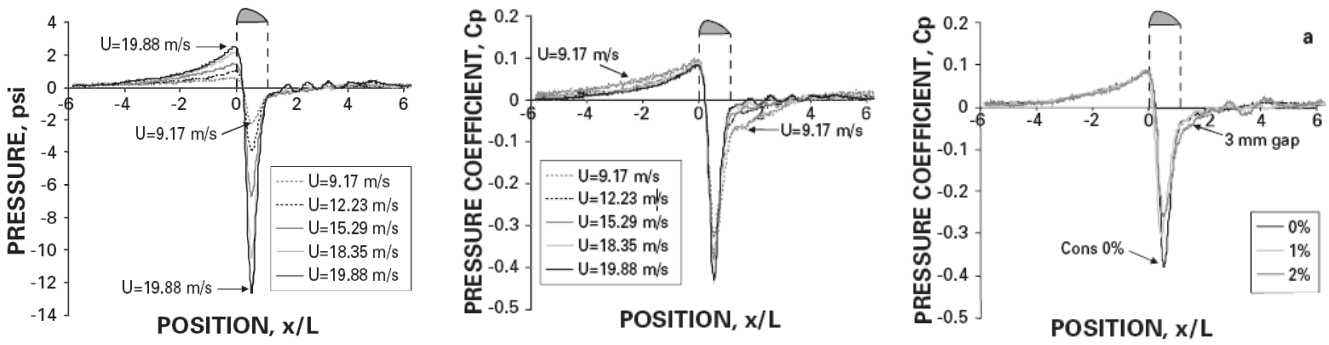

a) Rotor tip velocity b) Pressure coefficient c) Concentration

Figure 84: Effect of various parameters on pressure pulse magnitude for a solid core rotor, from Pinon *et al.*[124]

Feng *et al.* [125] using computational fluid dynamics (CFD) simulated the design as well as operational parameters of a foil rotor: angle of attack, camber, tip speed, clearance, and performed experimental analysis on the set up as of Pinon *et al.* [124] with water as test fluid. The experimental results indicated a 40% underestimation for simulated values of pressure coefficients. The pulse magnitude had a linear increase with square of tip speed for any angle of attack. The results showed that a 5° angle of attack gave the highest magnitude of suction pulse with no positive pulse at leading or trailing edge, with a decrease of the pressure coefficient at higher angles of attack (cf. Figure 85 a). This could drastically improve the contaminant removal as well as fractionation efficiency. The shape of the pulsation curves changed for different angles of attack. Increasing foil camber increased both the pressure coefficient as well as width of the negative pressure pulse (cf. Figure 85 b).

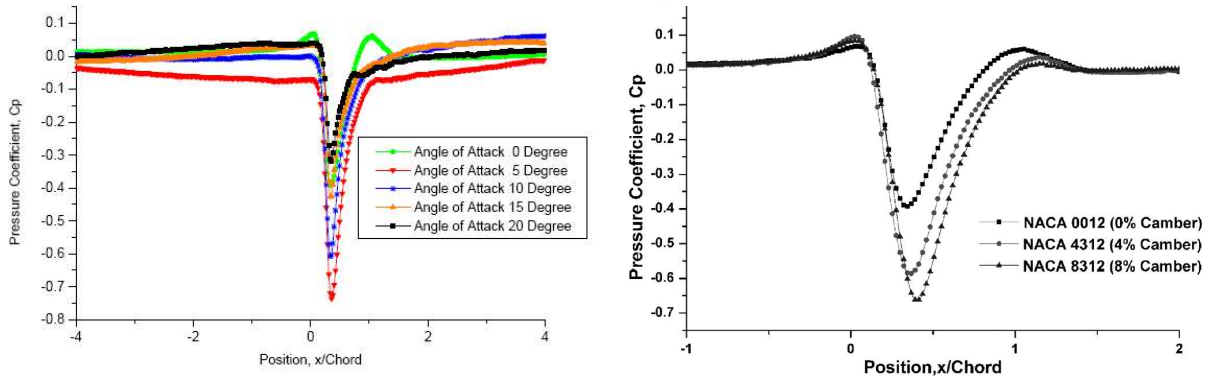

a) Angle of attack at constant clearance b) Foil camber

Figure 85: Experimental values of pressure pulse magnitude of a foil rotor, from Feng *et al.* [125]

The importance of a pressure coefficient with respect to pressure screen throughput is highlighted in the work of Feng *et al.* [125] for a foil rotor and reported in Figure 86. Higher negative pressure results in increased production for a 0.20 mm slot with 0.9mm profile height at a constant foil rotational speed and foil-screen clearance.

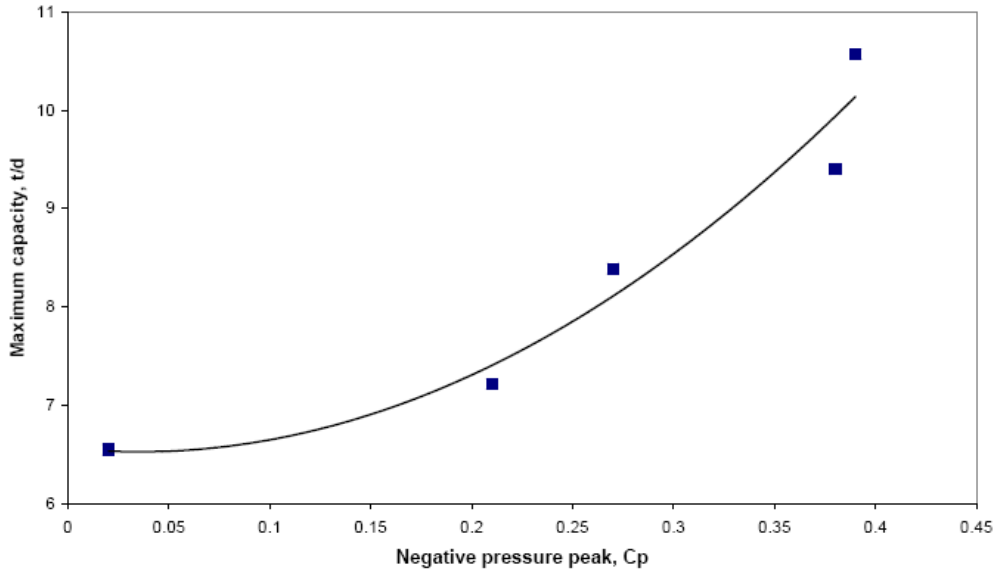

Figure 86: 'Maximum mass flow rate through the screen plate (0.20mm wide slots) as a function of increasing negative pulse magnitude', from Feng *et al.* [126]

While the pressure pulse magnitude varies with the square of the rotor tip speed, the power required varies with the cube and the capacity coefficient linearly. The non-dimensional power coefficient Cp_w is defined in Eq. 3 and the capacity coefficient *Cq* in the Eq. 4. [127]

Eq. 3 :

$$Cp_w = \frac{Pw}{\rho V_t^{\,3} \mathrm{D_t}^{\,2}}$$

P_w: Total rotor power consumed, w
ρ: Fluid density, kg/m^3
V_t: Rotor tip velocity, m/s
$\mathrm{D_t}$: Rotor diameter at tip, m

Eq. 4 :

$$Cq = \frac{Q_i}{V_t \mathrm{D_t}^{\,2}}$$

Q_i: Inlet flow, m^3/s

Increasing the rotor tip speed will lead to linear increase of capacity but the power consumption will be cubed.

3.1.2.2. - Screen plate

Screens are the critical design element defining the pressure screen systems capacity or throughput, contaminant removal and fractionation efficiency. Dotted with apertures in the form of holes or slots, screen plate design has evolved and is being continuously improved by advanced design and manufacturing techniques to improve process efficiency to reduce pressure screen running costs and to provide flexible operation.

At the beginning, the screen plates were equipped with large holes (cf. example Figure 87 a.) which were either punched or drilled. The size of the holes decreased under the constant demand to provide a more cleaner pulp, especially dedicated to the manufacture of high yield mechanical pulps where the removal of shives was of heavy importance. The entry as well as exit shape of holes was varied/evolved in shapes of divergent and convergent angles to decrease the pressure drop across the plate, improve efficiency and production or the 'smooth' passage of fibres.

The advent of slotted (milled slots with sharp edges or wedge wire design with rounded edges) screen changed the whole scenario (cf. example Figure 87b, c) which provided a vastly improved screening efficiency but unfortunately a reduced capacity. This was encountered by the development of contoured slots, which have almost outfitted most of the screening systems.

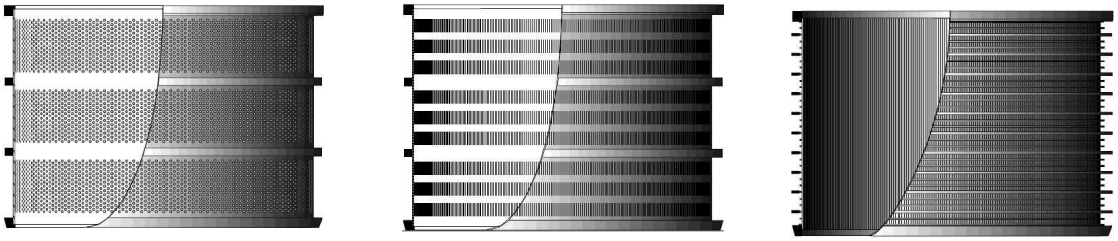

a. Hole screen | b. Milled slots | c. Wedge wire slots (full length of screen)

Figure 87: Screen basket types, [128]

The terms associated with the pulp suspension across the screen plate and the design parameters have been reported in Figure 88 and Figure 89. The rotor tip velocity, V_t, is related to rotor diameter at the hydrodynamic diameter extreme position as well as rotations per minute, whereas the global passing velocity, V_s or V_p, is calculated on the basis of accept flow rate and open area (OA) available or Q_a/OA. Increasing the passing velocity would in general increase production or in other words increase hydraulic loading.

Contours also known as profiles or surface roughness create 'micro-turbulence' vortices at the screen surface to direct the flow into the slots and create fibre non-alignment as well as de-flocculation. Contour height, slot and wire width have a pronounced effect on the fractionation or probability mechanism as well as reject removal efficiency of the pressure screening system.

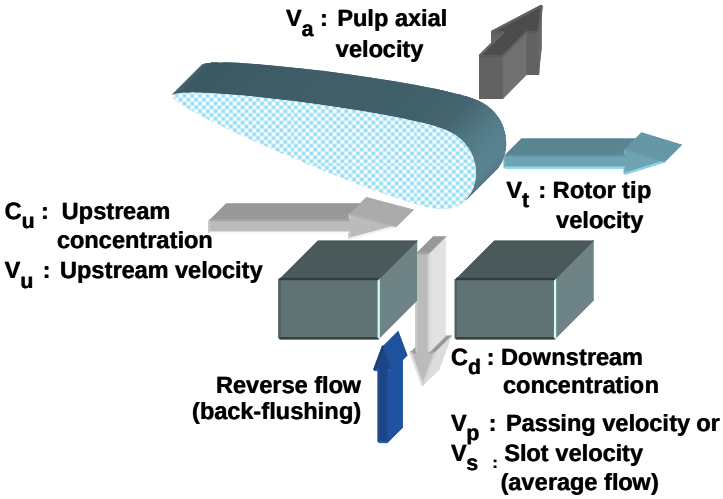

Figure 88: Smooth slot and terminology

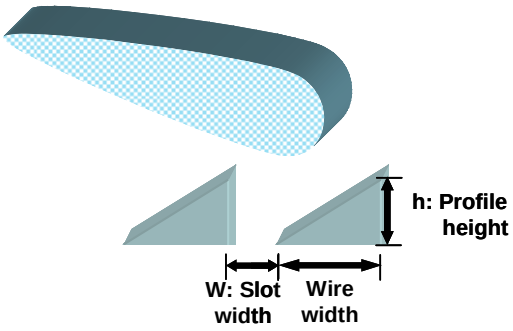

Figure 89: Contour slot representation

It has been observed that increasing the contour height (low profile height varies from 0.5 to 0.6mm whereas high profile are situated between 1.2 to 1.5mm) increases the long fibre passage into the accepts, increasing capacity [123][129], but degrades the contaminant removal. The best screening efficiency (accept pulp cleanliness at a given reject rate) is provided by low profile screen plates [130] [131]. It has been reported that a low profile height slotted screen consumed less rotor power at same slot velocity as compared to high profile slots [132].

Increase of profile height increases the kinetic turbulence intensity / energy just above the aperture, (cf. Figure 91) and the vortices generated become bigger (cf. Figure 90), these vortices act as 'defined' paths for a fibre to follow. The entry of a fibre into the accept stream through a slot will depend upon its exit probability into accept; which comprises of the probability to be captured in the boundary layer above the slot and the probability of exit through the slot. The boundary layer thickness above the aperture has a higher thickness for high profile slots. Contouring either a slotted basket or a smooth hole screen increases the fibre passage, reducing selectivity or fractionation efficiency [83].

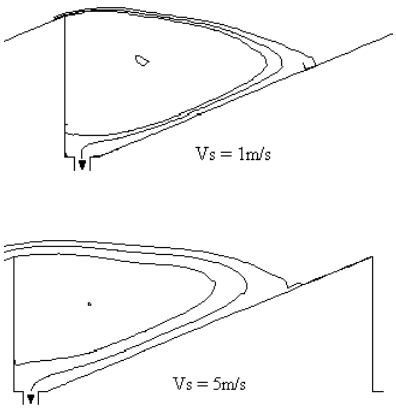

Figure 90*:* Numerical simulation of the fluid lines on a machined screen plate with 0.10mm slots for a surface flow velocity of 10m/s and slot velocities of 1 and 5m/s, from Grégoire *et al.* [133]

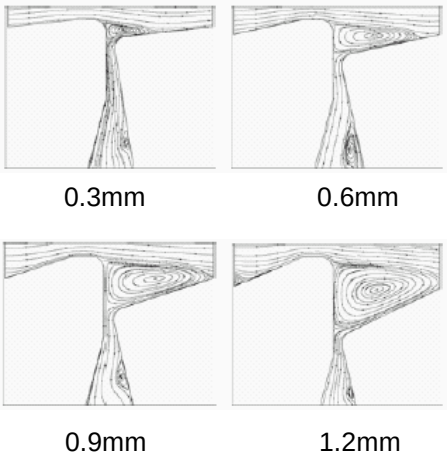

Figure 91*:* Streamline plots of flow approaching a slot for 1m/s slot velocity and 15m/s upstream velocity and for different contour heights of 0.3, 0.6, 0.9 and 1.2mm from Mokamati *et al.* [134]

Increasing the size of aperture opening increases the capacity of the screening system but decreases the screening efficiency [88][89][123][129].

The wedge wire slot structure (cf. Figure 91) has normally a convergent inlet flow and a divergent outlet flow. This design parameter reduces the pressure drop, hence in turn increasing the effective slot velocity. Studies have shown that the pressure drop increased slightly for a low profile height screen and it was twice in reverse flow in comparison to forward flow [129]. The profile height change did not affect the amount of pulp suspension in the reverse flow related to rotor pulsation [123].

Absence of profiles on smooth plates generates high surface upstream tangential velocities and these can match up to the rotor tip speed (20 to 25m/s). A smooth surface or a low profile height slot generates low turbulence hence low hindrance to fibre flow/ course. A fibre can thus be easily removed and finds itself in the reject part.

The motion of fibres near an aperture opening, either smooth or various profiles has been studied by many workers [87][95][135][136][137]. The possibility of a rigid fibre to come in contact, rebound in the bulk flow above the boundary layer and not follow the fluid lines entering an aperture is much higher than a flexible fibre. A rigid fibre if it does not flow through the aperture can remain stuck inside the aperture, making other fibres to staple over it and form a bundle, effectively blocking the aperture or reducing the open area. Fibres across smooth apertures or low profile slots experience the slipping phenomenon where the long fibres (rigid fibres), shives or other contaminants hit the profile edges and are swept away. In case of smooth holes, it can be said that the long fibres are in a continuous sliding mode. These reasons dictated the decrease in applicability of smooth slots. However, small dimension smooth hole screen or slot opening with low profiles are used for fractionation purposes.

Wire width relates to the open surface area of a screen basket as well as to the basket mechanical strength. It more importantly also relates to fibre stapling which can occur if the wire width is smaller than the fibre length [138]. Jokinen *et al.* [129] reported that increasing bar width (leading to reduction of screen open area) led to an increase of capacity, whereas Mokamati *et al.* [134] reported an increase of turbulence intensity at the wire surface while decreasing the wire width.

The development of very small aperture technology (less than conventional 1mm hole or 0.10mm slot screen) started in the 90's (Beloit Dynamic washer, Black-Clawson / Kadant Liquid filter and later Fiedler / Andritz Pressure filter). This development was mainly for washing and the recovery of fibres from process waters.

Small aperture (micro-meter holes and slots) screening as a means of pressure filtration of process waters (low total and fibre concentration) was studied by Hamann & Cordier [139] with various micro-meter aperture sizes. They mentioned that for all the different types of opening studied, filler and micro-stickies followed the flow split while the bigger size macro-stickies had high removal efficiency. Fibres are more difficult to pass through the holes than slots, where the fibre thickness is defining the passage and not fibre length.

Workers have observed that micro-hole or micro-slot screening concentrates or enriches the accept pulp with the fines fraction [79]. This fine fraction also contains higher amounts of ray cells and vessels elements, metals (Copper, Iron Magnesium, Manganese) and extractive content (for example with bleached never dried birch Kraft pulp [140] and unbleached softwood Kraft pulp [97]). There was no selective separation of earlywood and latewood fibres [97]. Sheet properties made from the unrefined accept fine fractions [140] showed a higher value for mechanical strength properties than the initial pulp or the coarser fraction.

Jokinen *et al.* [141] studied the behaviour and separation of fine elements during fractionation with a pressure screen (0.09mm slots) and small head-diameter cleaners. They reported results for pulps and process waters from virgin fibre (TMP for newsprint & chemical pulp for coated fine paper manufacture) and recycled fibre (deinking pulp for super-calendered paper grade) mills. Pressure screening trials of TMP pulp showed higher fibril content in the rejects. The fillers in white water followed the flow split. The cleaner accepts contained more fillers (except for wire water) but there was

less selectivity for ink separation. Approximately 60% of the fines (defined on 100µm sieve) were smaller than 25µm. The ink and filler particle size was less then 10µm for different cleaner fractions.

Fibre passage into the accept side, or fibre stapling will depend not only on the design configuration of the screen as well as the rotor but also and more importantly on fibre length distribution and fibre flexibility.

3.1.2.3. - Operating parameters

A noticeable and pronounced effect of pressure screening is consistency changes occurring in accept and reject side. As water can easily pass through the slots, consistency in accept side decreases due to which, the consistency in reject side increases, feed consistency remaining constant. This is called as **reject thickening**, which is calculated as the ratio of the reject versus the feed consistency and is termed as **reject thickening factor or simply thickening factor - T**. From Figure 67 this factor could be written as in Eq. 5:

Eq. 5 : $$T = \frac{C_r}{C_i}$$

C_r: Reject concentration
C_i: Inlet concentration

Sometimes the thickening can be so pronounced that it can lead to screen failures as the reject line gets plugged due to high consistency, resulting in flooding of feed zone and blocking the slot opening of the screen which leads to failure. One important aspect of the reject thickening is that it indicates that the screen is fractionating. Ammälä *et al.* [142] reported that the consistency changes occurring in both axial and radial directions of an axially fed screening basket (cf. Figure 67) were more pronounced at the beginning of the screen.

Another term associated with the screen functioning is the volumetric reject ratio or R_v. It is defined as the fraction of the feed volume getting rejected as represented in Eq. 6. The industrial screening systems are operated in the range of 15 – 30%.

Eq. 6 : $$R_v = \frac{Q_r}{Q_i}$$

Q_i: Inlet flow rate
Q_r: Reject flow rate

The mass reject ratio or R_m, represents the mass fraction of the inlet pulp amount getting rejected and is represented in Eq. 7 in terms of concentration and flow rate of inlet and reject streams respectively.

Eq. 7: $$R_m = \left(\frac{C_r}{C_i}\right)\left(\frac{Q_r}{Q_i}\right)$$

As $\frac{C_r}{C_i}$ is the thickening factor, T, and $\frac{Q_r}{Q_i}$ is R_v, hence R_m can also be written as in Eq. 8.

Eq. 8: $$R_m = T.R_v$$

Studies have shown that operating a screening system at low R_v (10% or below) has a much pronounced effect on reject thickening and hence increase of the thickening factor and very slight drop on the accept pulp consistency as shown in Figure 92. The difference between inlet (or feed) consistency will depend upon the aperture opening. Smaller apertures will lead to a higher difference.

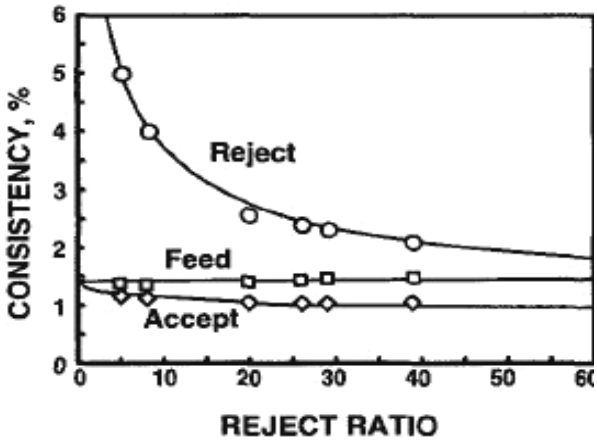

Figure 92: Effect of screening on streams concentrations, from Gooding & Kerekes [143]

In a screening system, effort is made to have the best possible efficiency and the least rejection of good fibres. There are various expressions to describe the screening efficiency in terms of debris (weight, number or area) in different streams. The reject efficiency, E_R and cleanliness efficiency E_C are defined in Eq. 9 and Eq. 10 respectively.

Eq. 9 :

$$E_R = R_m \cdot \frac{S_R}{S_F}$$

S_R : Debris in rejects
S_F : Debris in inlet

Eq. 10 :

$$E_C = 1 - \frac{S_A}{S_F}$$

S_A : Debris in Accepts

A host of parameters are involved which govern the changes in consistency occurring at the upstream of the screen aperture. There are numerous factors which play at the same instant to make the fibres pass or not to pass through the apertures. Noticeably amongst them are the fibre to fibre interactions, fibre morphological properties themselves, the trajectory of the fibre, their alignment/orientation just above the aperture, fluid flow, rotor pulsation, and the level of turbulence, etc. To sum up, very complex and very fast occurring hydrodynamic phenomenona dictate the terms of fibre passage through the apertures.

Researchers have worked on reduced scale models of single apertures to understand the fibre passage phenomenon, deriving relations which can predict their passage.

Reject thickening is an important phenomenon occurring during the operation of a pressure screening system and is higher for a smooth hole screen surface than for a slotted screen surface at similar operating conditions. A higher thickening relates to a higher selectivity for the passage of very short fibres and fines as compared to long fibres [143].

Increasing the aperture velocity will lead to a decrease of reject thickening. Small apertures provide a high value of reject thickening at the same passing velocity. A higher thickening factor value could indicate to a lower ‘pulp’ passage ratio but a high index of fractionation and selectivity, (cf. Figure 93). Different rotors behave differently with respect to reject thickening. At same slot velocity a lower value of reject thickening will indicate a higher capacity, (cf Figure 94). Sloane [83] reported that for a constant value of R_v and V_s, the thickening factor for different rotor types does not change while increasing the rotor tip speed. Fibre reject thickening is always greater for long fibres as compared to short fibres and fines and is more pronounced at low values of R_v

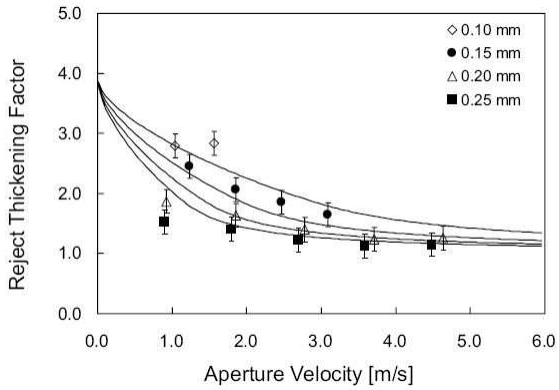

Figure 93: Thickening factor and slot velocity for different slot width, from Olson [148]

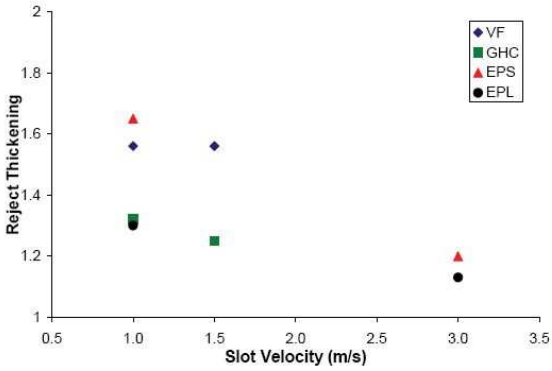

Figure 94: Thickening factor and slot velocity, for different rotor types, from Pflueger *et al.* [144]

As described earlier, for a given pulp characteristic, thickening is essentially related to the type of screen plate. This is further illustrated in Figure 95 for a screening system with wedge-wire slot screen and foil rotor. The pulp furnish consisted of 50% hardwood 50% softwood pulp (fibre length 1.36mm) at 10 g/L. The thickening factor varied between 1.3 and 1.45 at 10% (very low) volumetric reject rate (though peculiarly the high profile slots gave high thickening, the hypothesis could be high surface upstream velocity sweeping away the long fibres)

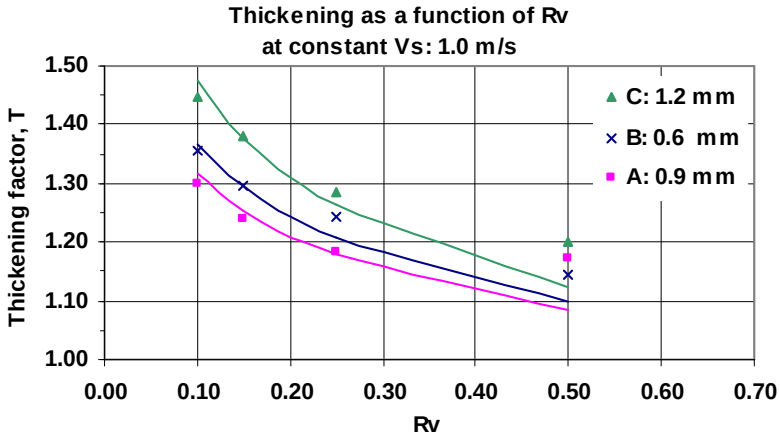

Figure 95: Thickening factor as a function of R_V for different slot profile heights at constant slot width (0.15mm) & wire width (3.2mm), from Kumar [131]

Another example is shown in Figure 96 for 1.8mm smooth hole screen plate and a solid core rotor pressure screen. Higher thickening values at similar volumetric reject rates with a bleached kraft pulp (fibre length 2.37mm) at ≅ 1.4% concentration. Longer fibres also contribute to a higher thickening factor.

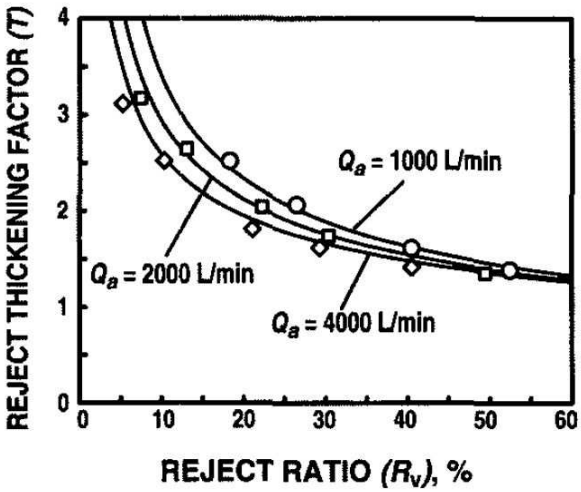

Figure 96: Thickening factor as a function of R_v for 1.8 mm smooth hole plate , from Gooding & Kerekes [143] (1000L/min ≅ 0.5m/s V_p, 2000 ≅ 1.0 m/s, 4000 ≅ 2.0m/s)

The examples described signify the importance of screen plate aperture size and design. Thickening factor are a typical characteristic of a screen plate and eventually define the working capacity (or hydraulic loading). Experiencing higher thickening at low pasing velocity or higher volumetric reject rates would lead to decrease in capacity.

3.1.3. - Screen fractionation theory

Length based fractionation across narrow apertures involves selective or preferential enrichment of a certain size category of fibres in one stream (for example long fibres in rejects) and there depletion in another stream (hence decrease in the long fibre content in the accepts).It signifies, understanding the fibre ability to pass into the accept stream at the operating conditions of the pressure screening system.

As described in section 3.1.1. -Fractionation process, the probability of passage in case of barrier screening is 0, whereas in case of probability screening it lies between 0 and 1. At the value of 1, the particle (whether organic or inorganic) faces no resistance to pass into the accept side.

Effective removal of contaminants, i.e., high removal efficiency are the very desired results from a screening system.

Karnis [40] defined a fractionating index, FI, to ascertain the fractionation efficiency of various devices. This index was related to the average values of a particular fibre property in two different fractions, Eq. 11.

Eq. 11 :

$$FI = 1 - \frac{X_I}{X_{II}}$$

X_I X_{II}: average value of fibre property X in fraction flow I and II respectively, from Karnis [40]

3.1.3.1. - Passage ratio

The earliest study in 1955, Kubat & Steenberg [145] studied the screen performance and defined a screen permeability index, which varied between 0 and 1.

The reject thickening was modelled in 1989 by Gooding and Kerekes [143][146] giving rise to a mathematical relationship defining the Passage ratio, P, for the bulk state or homogenous category of particles. From Figure 88, passage ratio is defined as the ratio of downstream to upstream concentration or as in Eq. 12.

Eq. 12 :

$$P = \frac{C_d}{C_u}$$

C_d: Downstream concentration
C_u: Upstream concentration, from Gooding and Kerekes [143][146]

This relationship has been extensively studied by numerous workers to better understand the fibre passing ability through apertures. Passage ratio is dependant upon numerous variables, both operating parameters as well as design parameters. Work has been always focussed to find a sort of compromise to increase the passage ratio of fibres and decrease for contaminants to improve the reject removal efficiency.

A dimensionless parameter called Penetration number, Pe was defined by Kumar [90][136], represented in Eq. 13, which relates the fibre passage to the slot dimensions- width, flow conditions- fluid velocities and fibre length. The results were achieved by working with very low concentration of synthetic fibres through single slot and in absence of rotor pulses. Indeed, the fibre length (l) plays an important role in the fibre passage and also the part of fibre length which goes inside the aperture opening (w). A higher fraction of fibre inside the aperture opening will result in a high probability of passage in comparison to a smaller portion which might result in the fibre being swept away in the upstream bulk flow. The author mentioned that the l/w ratio is a critical parameter in fibre passage. A value of less than 2 for this ratio indicates similar passage ratio for flexible and rigid fibre and ‘simple

dependence' on slot and upstream velocity. Fibre flexibility becomes the dominant factor in fibre passage, above this value.

Eq. 13 :

$$Pe = \frac{V_s}{V_u}\frac{w}{l}$$

V_s: Downstream slot velocity
V_u: Upstream slot velocity
l: Fibre length
w : Slot width
from Kumar [136]

In 1998 Olson *et al.* [147] showed that the fibre passage ratio was approximately characterized by a single function of penetration number as defined in Eq. 14. They mentioned that if P < ½ then P is proportional to Pe_t and if P ≥ ½ then (1-P) is inversely proportional to Pe_t. Here Pe_t is based on the rotor tip velocity, V_t in place of velocity in the upstream flow, V_u. The single constant 'mk' is the product of two constants of proportionality determined experimentally.

Eq. 14 :

$$P = \frac{1}{2}\frac{Pe_t}{mk} \qquad \text{If } P < ½$$

$$P = 1 - \frac{mk}{2Pe_t} \qquad \text{If } P \geq ½$$

From Olson *et al.* [147]

The dependence of fibre length on passage ratio was first reported in public domain by Olson [148]. The passage ratio function for fibre length was demonstrated to be a negative exponential function mentioned in Eq. 15

Eq. 15 :

$$P(l) = e^{-(\frac{l}{\lambda})^{\beta}}$$

λ: size constant
β: shape constant
from Olson [148]

The value of λ is related to the aperture size, operating conditions and pulp type, whereas β is related to the degree or quality of fractionation. The author reported a value of 1.0 for β for smooth hole screen plate and 0.5 for slotted screens, with the hole screen plate providing a higher degree of fractionation efficiency. This is illustrated in Figure 97, which shows that for a smooth hole screen plate as opposed to the slotted screen plate the passage ratio is higher for short fibres and lower for long fibres, indicating the hole screen curve is 'nearer' to the ideal step curve. However, the passage of long fibres, especially for slotted screens will also depend upon their alignment and orientation vis-à-vis to the slot opening.

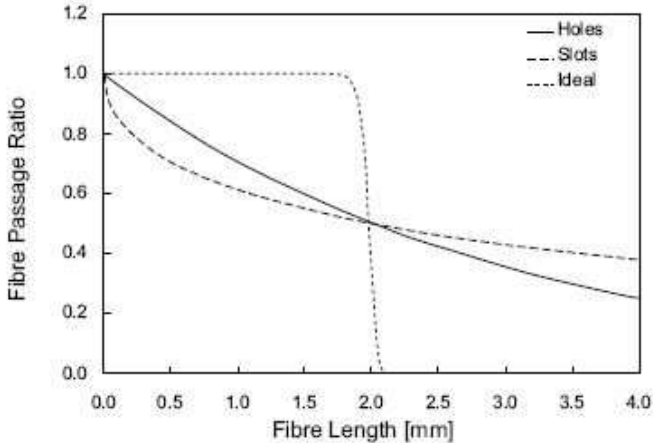

Figure 97: Passage ratio for different fibre length and aperture type, from Olson [148]

Gooding *et al.* [149] reported the analysis of the fibre length passage ratio curves, with varying degree of λ (which relates to the position of the curve) and β (which relates to the shape of the curve), illustrated in Figure 98. A very high value of β translates to the ideal step curves and provides a high degree of fractionation efficiency, signifying that at a particular value of λ, all the short fibres follow the fluid and long fibres are rejected. Increasing the value of λ increases the overall passage ratio. Higher level of thickening and lower passage ratio is essentially related to a high degree of fractionation efficiency.

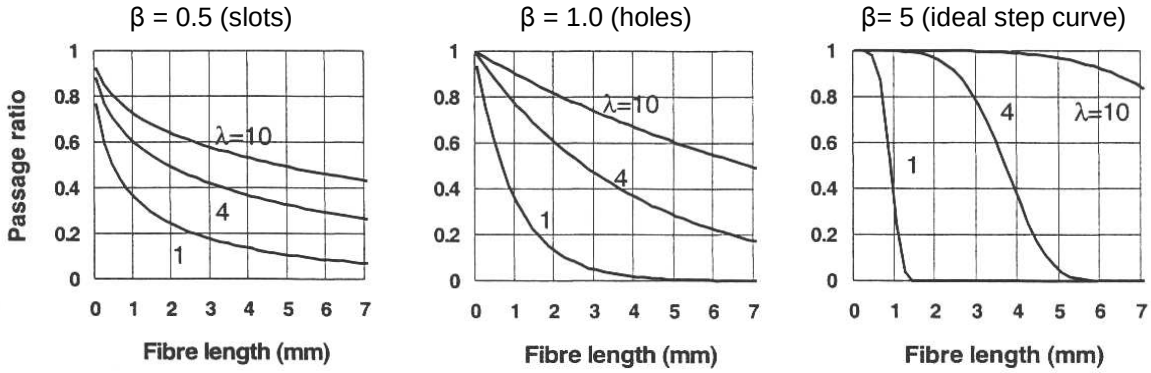

Figure 98: Influence of λ and β on fractionation efficiency and selectivity, from Gooding *et al.* [149]

Increasing the slot profile height, decreases the fractionation efficiency. For low profile height screen plates, Julien Saint Amand & Perrin [95] reported a value of 0.5 - 0.6 for β and slightly lower for high profile screen plates, indicating a diminution of fractionation efficiency. This is mirrored in another study where Julien-Saint-Amand *et al.* [150] reported a high value of λ (9) for high profile slots (hence lower reject thickening) in comparison to 5.4 for low profile at similar values for β. Olson *et al.* [151] reported a value of λ of 0.95 for a small aperture 0.88mm smooth hole screen and 5 for a 2.10mm hole screen. They mentioned that the effect of an increase of fluid velocity through the smooth hole apertures is negligible in comparison to slotted screens, which show a high dependence. Also, the increase in passage ratio with an increase in aperture diameter was linear. The range of passing velocity tested could have an impact on the passage ratio, with a lower velocity range showing no appreciable effects on passage ratio.

It has been extensively studied and reported that increasing the passing velocity lead to an increase of passage ratio and a decrease of screening efficiency as the contaminants are also *squeezed* out into the accepts [89][148][149]. This is illustrated in Figure 99, which shows a higher passage ratio for fibres and contaminants for larger width slots and an increase of passage with an increase of slot velocity. However, it has also been reported for smooth hole plates that the passage ratio does not vary with an increase of passing velocity (in a limited range of values experimented).

Consistency increase within the screen operating range, generally does not affect the passage ratio except at low rotor tip speed where the mat formation leads to a reduction of passage ratio [152]. Increasing the rotor tip speed for a given feed concentration and passing speed increases the passage ratio [153]. However, other researchers indicated a decrease in passage ratio with an increase of rotor tip speed, with no difference of passage ratio or fractionation index with respect to the rotor types (bump or blade) at different tip speeds [149]. The reduction in passage ratio with an increase of tip speed could be attributed to higher surface velocity leading to 'sweeping' away of fibres upstream into the bulk flow towards the rejects. On the other hand, increasing V_t leads to increase of negative pressure pulses, with higher amounts of reverse flow, leading to a higher effective passing velocity, hence passage ratio.

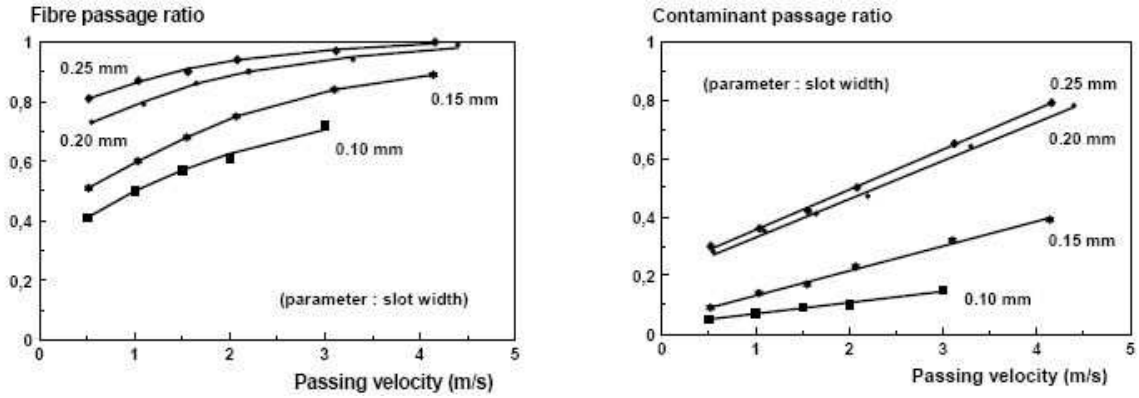

Figure 99: Influence of passing velocity on fibre and contaminant passage, from Julien-Saint-Amand & Perrin [88]

3.1.3.2. - Flow Models

Gooding and Kerekes [143] defined flow models to derive expression relating the thickening factor and reject rates on the basis of fibre passage ratio.

Mixed flow model

This model assumes perfect mixing in radial and axial directions of the screen. The concentration all along the axis is constant and the upstream concentration, C_u is equal to the final reject concentration, C_r. Each section of the screen has the same concentration on the upstream and treats the same pulp. Open foil rotor or very short length screens tend to follow a mixed flow model [89][154], where there is a high turbulence and mixing in the larger pulp layer thickness between the screen and rotor body. The dependence of passage ratio on the thickening factor is represented by the Eq. 16.

Eq. 16 : $$T = \frac{1}{P - P.R_v + R_v} \quad \text{or} \quad P = (\frac{1}{T} - R_v)(\frac{1}{1 - R_v})$$

Plug flow model

This model assumes no axial mixing of pulp suspension, but a perfect interactions and homogenous pulp concentration in the radial direction. The expression for the thickening factor and hence the passage ratio is reported in

Eq. 17 : $$T = R_v^{(P-1)} \quad \text{or} \quad P = \frac{Ln(T)}{Ln(R_v)} + 1$$

The concentration of pulp along the length of the pulp screen increases from the inlet side to the reject exit and becomes equal to the reject concentration in the final screening length. Hence in a plug flow as the pulp moves in the axial direction towards the reject exit, the concentration presented at the upstream screen section changes for each forward movement. The pulp passage ratio decreases along the screen length. The solid core rotors have non-significant probability of mixing in the axial directions as the pulp flow through a narrow opening between the core and screen. Screens equipped with closed rotor body mostly follow the plug flow behaviour as the passage ratio curves for fibre length distribution were independent of R_v [89][143][146][148][154]. An example is illustrated in Figure 100 for a bumped type rotor showing constant passage ratio with varying R_v for a given length of fibre. It could be assumed that the plug flow model is made up of infinitesimal small mixed flow model in series.

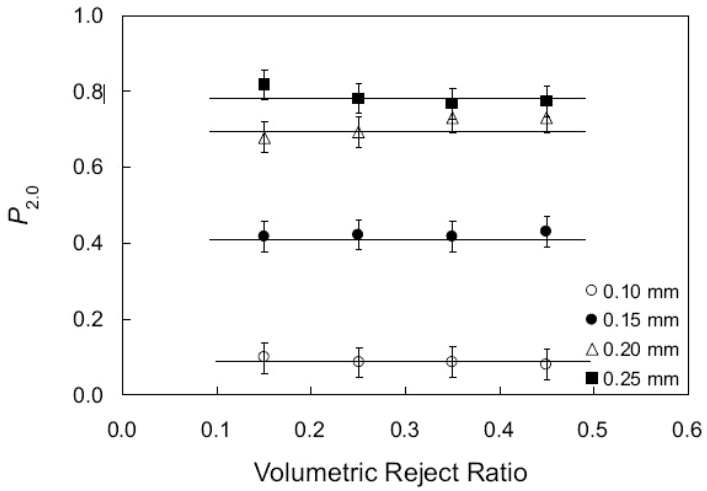

Figure 100: Passage ratio for 2.0 mm length fibre at constant Vp
for different slot widths, from Olson [148]

The thickening factor evolution with respect to volumetric reject rate, R_v, provided by a plug flow model is higher as compared to a mixed flow model.

Screening efficiencies E_R and E_C can also be represented for the two models described above. If the passage ratio of 'homogenous' class of fibres is P_F and of contaminants is P_K then the screening efficiency of the plug flow model could be represented by Eq. 18 and mixed flow model by Eq. 19

Eq. 18 :

$$E_R = R_m^{\zeta}$$

where $\zeta = \frac{P_K}{P_F}$

Plug flow model

Eq. 19 :

$$E_R = \frac{Rm}{R_m + \zeta - \zeta . R_m}$$

Mixed flow model

3.2. - Study of micro hole screen fractionation

The selectivity and better the degree of fractionation with respect to fines and very short fibres offered by hole screening is much more than profile slots. Selective removal of fines which contain the majority of ink could be achieved by small aperture size or in other words micro-holes (termed as such because the hole size is very small in comparison to the classical 1.0 mm hole size). Because of these reasons, the fractionation trials were performed with small size smooth hole screen.

3.2.1. - Pilot fractionation trials

Pulp fractionation by pressure screening were performed at the screening/fractionation unit of the CTP recycled fibres pilot plant. Image 1 shows the general view of the facility.

Image 1: General view of the pilot plant screening facility

3.2.1.1. - Equipment, material and methods

The configuration of the pressure screen consisted of a 0.25mm smooth hole screen basket and a solid core rotor with 3 hydrodynamic pulsation elements. The rotor elements were not parallel to the rotor axis. Image 2 shows the rotor details. The screen with 10% open nominal area had an internal diameter of 353mm, an effective screening length of 257mm and screen plate thickness of 2mm.

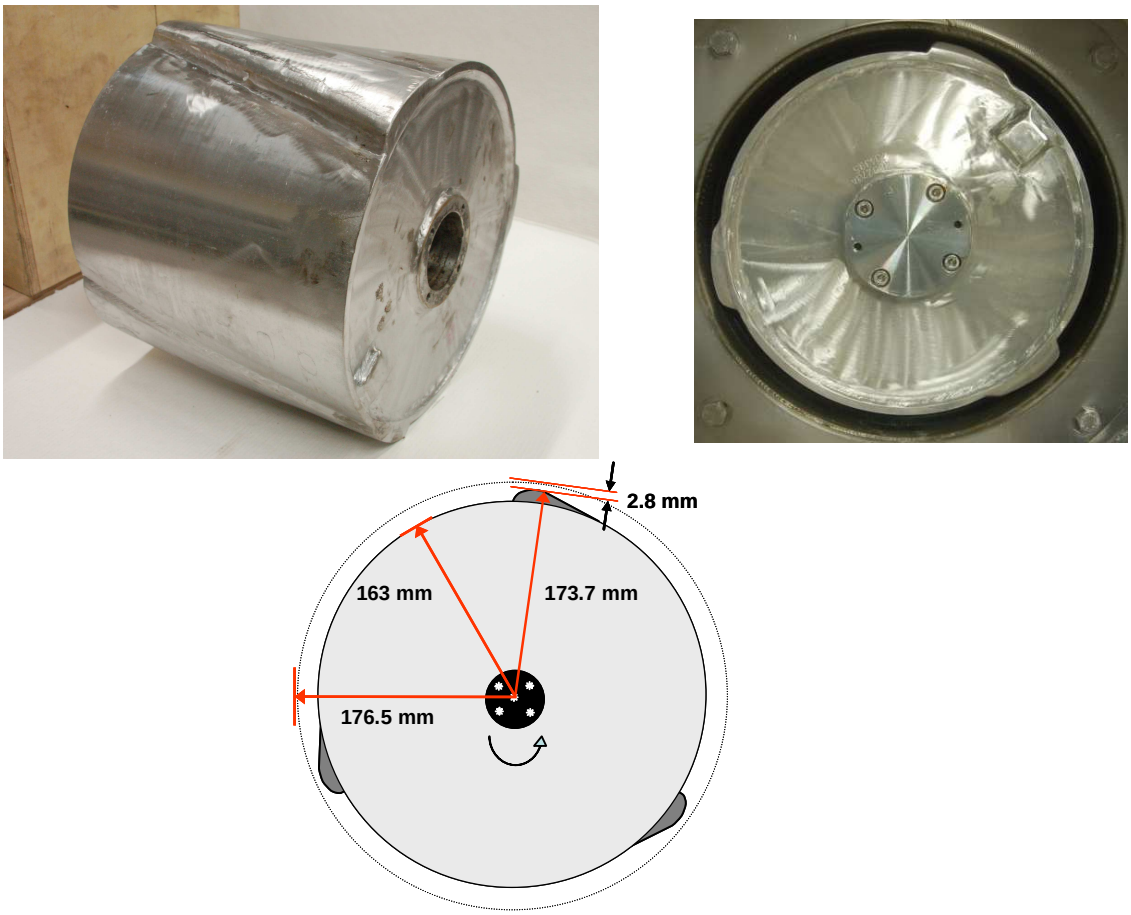

Image 2: Closed/solid core rotor and its dimensions at inlet section

The rotor speed were fixed (no variable frequency drive) with a tip speed, V_t, of 25 m/s. The clearance between the rotor tip and screen plate was of the order of 2.8 mm (measured at the inlet section).

The flow schematic of the different streams is shown in Figure 101. The screen was fed from a $3m^3$ agitated tank. Pressure gauges (PG) were present on the inlet (P_i) and accept lines (P_a), while inlet and reject lines were equipped with flow transmitter (FT) (the difference gave the flow in the accept line). Manual throttling of the valves resulted in flow change to obtain the desired operating parameters. Samples were taken from lines (full opening) that re-circulated back the accepts and rejects into the feed tank.

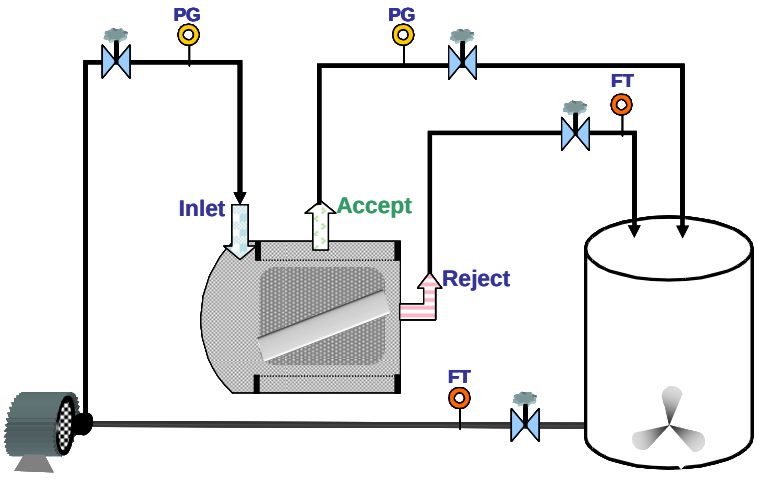

Figure 101: Schematic of pilot plant screening system.
PG: pressure gauge, FT: flow transmitter

Three different pulps were fractionated as reported in Table 13.

Table 13: Pulps studied

Pulp	Remarks
Stone groundwood mechanical pulp (SGW)	Pulp from a Scandinavian mill.
Chemical pulp	Prepared at CTP pilot plant by refining a 65% softwood pulp and 35% hardwood pulp mixture. ❖ After refining, the pulp was thickened in a screw press and dried at 60℃ for 2 days to simulate recycled fibre as it they least once dried before being recycled ❖ 23% kaolin mineral filler added.
Deinking pulp (ONP/OMG)	A mixture of 75% old magazine grade and 25% old newsprint grade. The re-slushing was done in a pilot Hélico pulper in neutral conditions at 45℃.

Table 14 reports the studied pulp average length-weighted-fibre length, lw and width at the inlet, indicating SGW pulp has the lowest fibre length and ONP/OMG 2nd stage the highest.

Table 14: Inlet pulp morphological properties

	SGW pulp	Chemical pulp	ONP/OMG 1st stage	ONP/OMG 2nd stage
Fibre length, lw, mm	0.66	1.10	1.15	1.26
Fibre width, µm	23.0	21.0	25.60	27.10

The morphological characteristic (fibre length) reported for different pulps is consistent with Bauer McNett distributions as reported in Figure 102. SGW pulp is a short fibre pulp, with higher amounts in the lower mesh fractions (P48-R200), while the ONPOMG pulp (1st stage) contains highest amount of P200 fraction mainly due to the presence of mineral fillers (Figure 104), which are absent in case of SGW pulp.

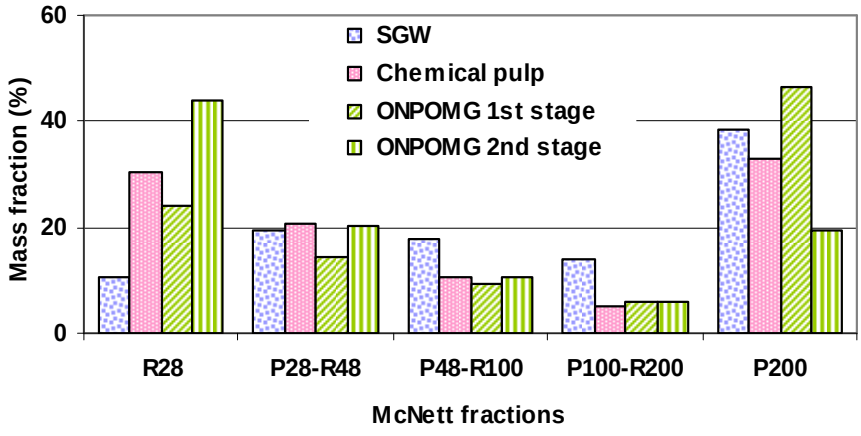

Figure 102: Inlet pulp Bauer McNett distributions

Figure 103 representing inlet pulp fibre length distributions also shows the same trends as for Bauer McNett classification with SGW pulp having a higher amount of short fibres.

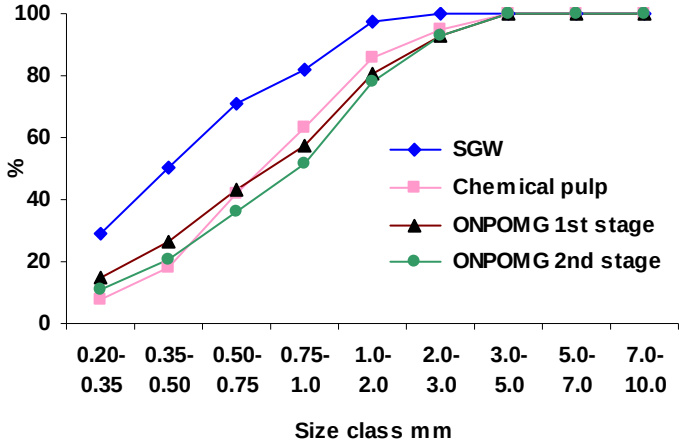

Figure 103: Cumulative inlet stream distributions

The mineral content of the pulp in terms of ash content is reported in Figure 104. Removal of mineral particles during the 1st stage fractionation results in a less amount for the 2nd stage ONP/OMG inlet pulp. More information is provided during the result discussion.

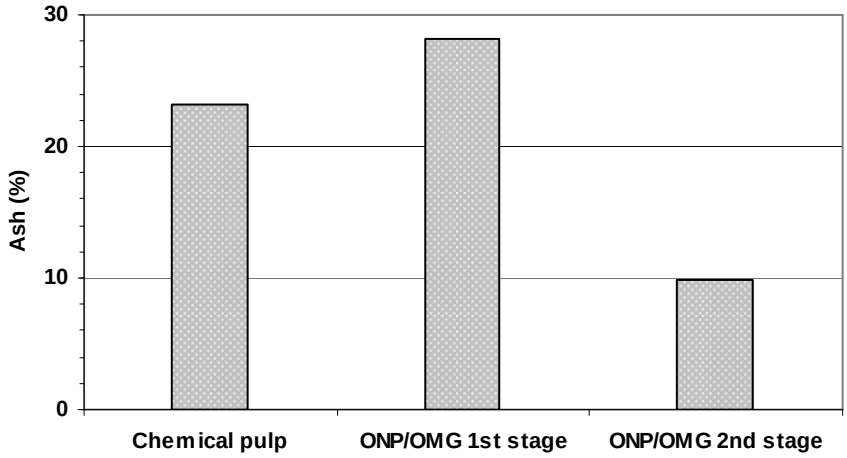

Figure 104: Inlet pulp ash content

❖ Fractionation parameters

The fractionation conditions for both the stone groundwood mechanical pulp and chemical pulp are reported in Table 15.

Table 15: Fractionation conditions for both SGW pulp and chemical pulp

Consistency g/L	Passing velocity V_p m/s	Volumetric reject ratio R_v %
11	0.3	20, 30, 40
05	0.3, 0.7	20, 30, 40

In the case of chemical pulp fractionation, 23% by weight of kaolin filler was added as a tracer. The slurry of this filler was laboratory prepared and added to the fibrous pulp suspension after pulping of the dried pulp.

For SGW and deinking pulp additional treatment of the accept fraction was made, which is reported in the chapter 4. -Application of fractionation to deinking and paper layering.

For the deinking pulp a different strategy was adopted with 2-stage fractionation. The 2nd stage fractionation was done on the rejects obtained at 20% R_v of the 1st stage. The pulp concentration for the two stages was lower than for the virgin fibre pulps. The operating parameters are reported in Table 16.

Table 16: Fractionation parameters for ONP/OMG pulp

Stage	Consistency g/L	Passing velocity V_p m/s	Volumetric reject ratio R_v %
1st stage	06	0.6	20, 30, 40
2nd stage	05	0.5	30, 40

The screening system was run in recirculation mode (cf. Figure 101) during the 1st stage fractionation trial to sample the rejects and accepts. At 20% volumetric reject rate, accept and reject streams were directed into separate tanks. The rejects were then diluted with hot water to a concentration of 5g/L for the 2nd stage fractionation. Only two values of volumetric reject ratio were tested for this stage.

- **Analysis performed**

1). **Pulp concentration**: A fixed quantity of pulp was taken to have 3 to 8g of dry matter on a Whatman filter paper of 90mm (accepts) or 125mm (rejects) diameter. The pulp suspension was vacuum filtered and dried on a hot plate heated to 105℃ and weighed on a balance reading to 3 decimal places. The pulp pH was adjusted to neutral pH by addition of aluminium sulphate solution in case of deinking pulp only. However, 5-6mL of flocculating agent was added for all the pulps. (values used for calculations purposes are average of 2 pads)

2). **Hyperwashing**: Performed with a high pressure water jet on a 90µm wire opening. Controlled by visual inspection till filtrate was clear. The pulp fibres retained on the wire are termed as long fibres (LF) while those passing are short fibres (SF), mineral filler and fines. The LF were deposited on a 90mm diameter Whatman filter paper and dried and weighed as done for pulp concentration. (values used for calculations purposes are average of 2 pads)

3). **Bauer McNett classification**: TAPPI norm 233 cm-06. Only one mesh combination was used: 28-48-100-200. The idea behind was to measure the amount of fibres in the lower series category or in other words, short fibres which could pass into the accepts. (analysis performed twice: one for mass fraction and the second time for MorFi analysis on McNett fractions)

4). **Optical properties**: Pulp pads made for pulp concentration were used to measure the optical properties brightness and ERIC (Effective Residual Ink Concentration) on a Technidyne spectrophotometer with a UV filter. (values used for calculations purposes are average of 8 readings made on two pulp pads both sides)

5). **Fibre morphological properties**: MorFi fibre analyser [155] was used to characterise whole pulp as well as pulp retained on 100 and 200 mesh Bauer McNett fractions. The fibre length in this manuscript refers to length-weighted fibre length. (Values used for calculations purposes are average of measurements)

6). **Ash content**: An oven dried weighed sample concentration pad sample was subject to 425℃ in a furnace for 8 hours. (values used for calculations purposes is based on one measurement)

7). **Specks content:** For only the deinking pulps, the specks content was measured by making handsheets of hyperwashed pulp 1.2g in weight on Rapid Köthen sheet former. The sheets were then analysed for specks content using the SIMPATIC image analyser. (values used for calculations purposes are average of 3 handsheets, with measurements made on both sides)

During the discussion of results, WP refers to whole pulp, indicating to all pulp entities, which include the organic and inorganic components.

3.2.1.2. - Fractionation results

Reject thickening is one of the important phenomenons occurring during the pulp screening. The evolution of the thickening factor with volumetric reject rate and passing velocity will have an impact on the separation efficiency of fibres and fines. Indeed, reject thickening behaviour could be said to be a 'characteristic' of a given screen plate and rotor combination.

❖ **Thickening factor**

1). Whole pulp

The thickening factor and mass reject ratio at various R_v values (obtained during pilot trials) are represented for SGW and chemical pulp in the Figure 105. The values were calculated on the basis of recalculated inlet concentration (C_{ir}) by performing a mass balance for each R_v value, reported in Eq. 20.

Eq. 20 : Recalculated inlet concentration C_{ir}= $C_a(1-R_v)+C_r.R_v$

This was done as during the screening phase, long fibres are concentrated in the reject line and short fibres and fines in the accept line, hence to avoid any discrepancies that might occur due to improper mixing in the pulp feed tank, thickening factor were represented by recalculation.

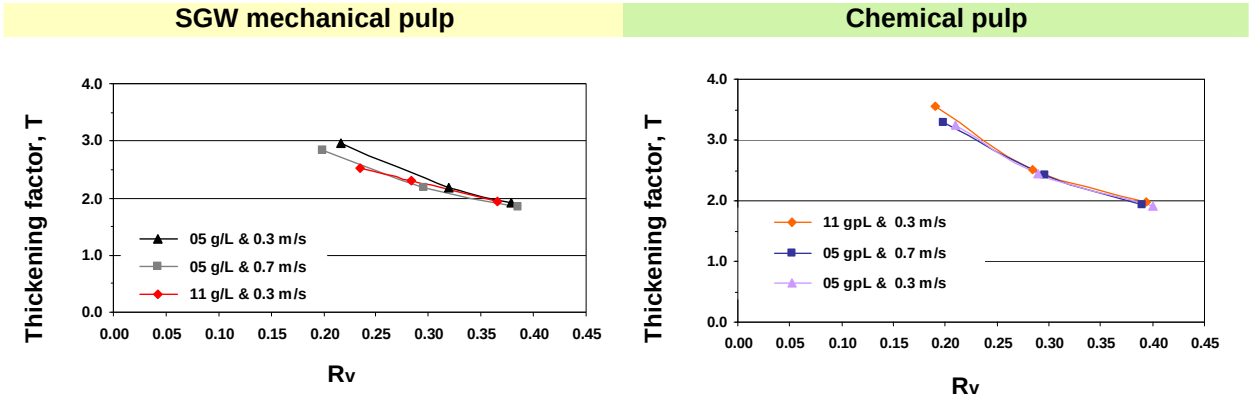

Figure 105: Thickening factor for SGW and chemical pulp

Thickening increased and was more pronounced at low R_v. It was possible to thicken both the mechanical as well as chemical pulp even at 20% R_v. The effect of passing velocity is slightly evident at low R_v, where a lower thickening is achieved at high passing velocity of 0.7m/s.

The thickening factor values obtained with a higher SGW pulp concentration had a tendency to follow the thickening profile at high passing velocity and low pulp concentration. It might indicate to screen surface plugging at higher value of concentration, hence non-passing of any elements – cellulosic and *water* thorough this mat, hence concentrating the rejects and decreasing the thickening factor.

The effect of either the concentration or passing velocity of chemical pulp on thickening is very limited. The reason is related essentially to the low amount of very short fibres (lower mesh fraction -100 & 200) which would have a higher probability of passing through the screen plate. Hence the fractionation is limited to the fines in this case.

Another information that can be observed from the results is the low (SGW pulp) or negligible (for chemical pulp) difference of hydraulic loading on the 0.25mm hole screen. Higher passing velocity

would result in a lower thickening factor. Indeed at whatever concentration and passing velocity, the evolution of the thickening factor remains the same for the conditions tested.

For ONPOMG pulp the thickening factor evolution with respect to R_v is reported in Figure 106. As longer fibres thicken more, the 2nd stage fractionation showed a higher value of thickening factor for the whole pulp at almost same operating conditions as for the 1st stage fractionation.

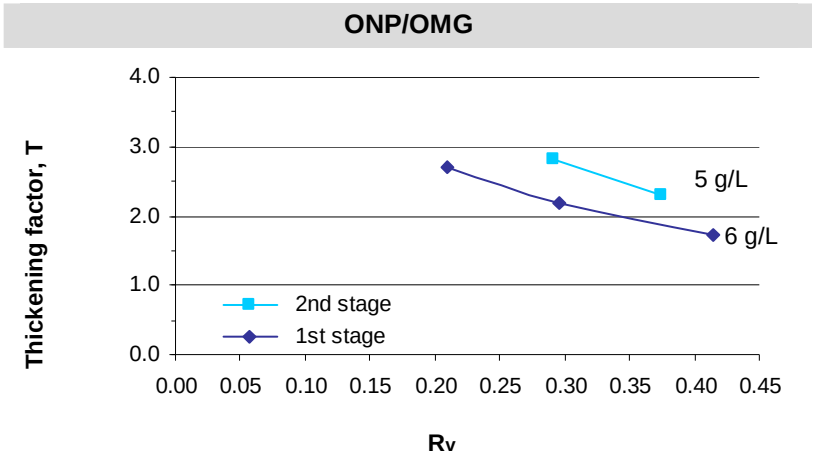

Figure 106: Thickening factor for deinking pulp

As it could be expected, the thickening evolution of the micro-hole screen plate is very different in comparison with a slot screen plate shown in Figure 95 or a smooth-hole screen represented in Figure 96 [143]. Indeed, higher thickening factor values were achieved with 'lower' average length fibres in comparing a 1.8mm hole screen. Analysing further the passage ratio for fibre length classes would illustrate how high reject thickening is impacting the fibre passage ratio. (This has been developed in 3.2.2.2. -Pressure screen fractionation: separation of fibres and fines)

2). Fibre and filler fractions

In case of chemical pulp, thanks to the addition of kaolin as a trace material, thickening factor and mass reject ratios were also calculated for only cellulosic fibre (referred to as fibre) and mineral filler content (referred to as filler) and reported in Figure 107.

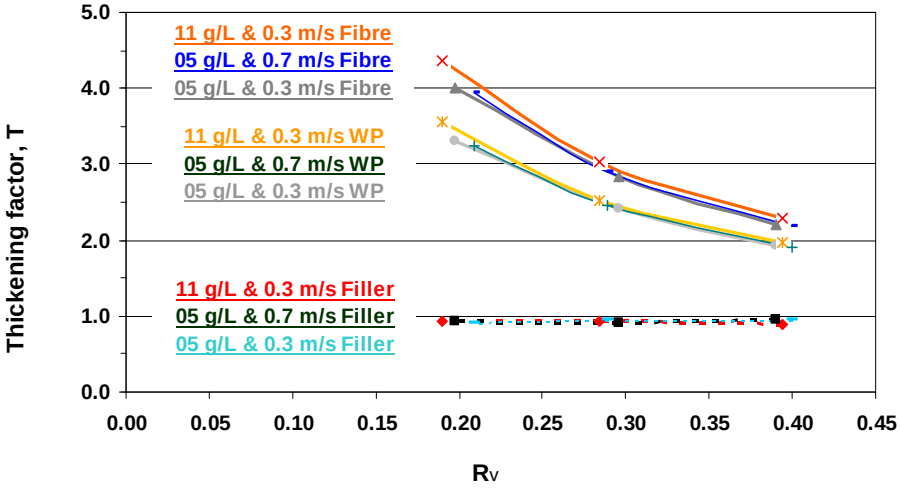

Figure 107: Chemical pulp constituents thickening factor

The results show the fillers follow the volumetric flow split as the thickening factor is 1.0, meaning their mass reject ratio is equal to the volumetric reject ratio. The cellulosic fibres have a very high thickening factor and hence they will have a high mass reject ratio also, even at low R_v.

As done with the case of chemical pulp, individual thickening factors for mineral filler, cellulosic fibre were also calculated for the ONP/OMG pulp and are reported in Figure 108.

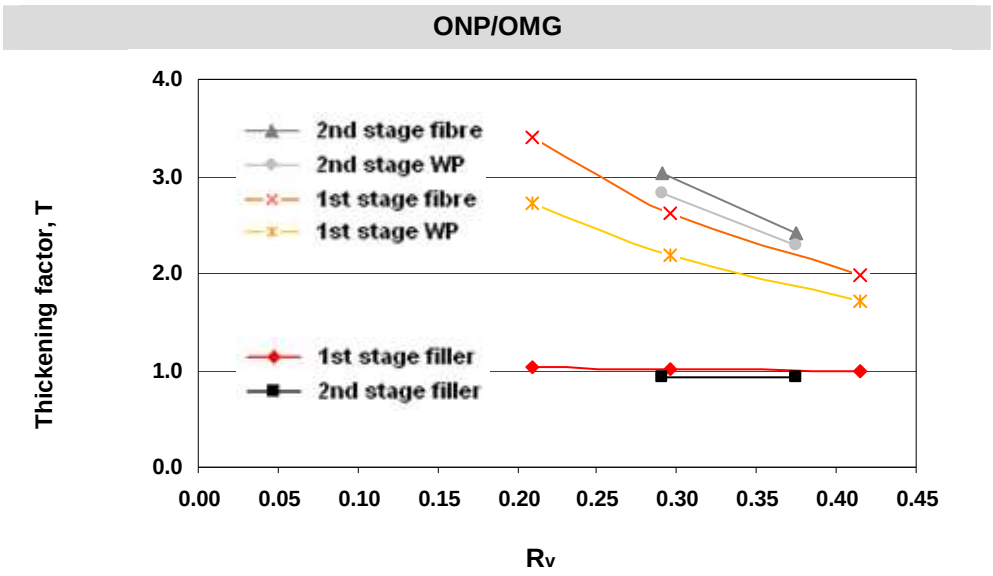

Figure 108: Thickening factor for individual components for deinking pulp

The results again confirm (as observed for chemical pulp) that the mineral fillers follow the flow split. The removal of fines during the 1st stage fractionation results in higher value of the thickening factor for the 2nd stage cellulosic fibre and whole pulp. Indeed, the 'narrow' difference of the thickening factor evolution for the 2nd stage is a result of effective separation of fines in the 1st stage.

3). Long fibre and short fibre/fines/filler fractions

From the values of hyperwashing ratios, the thickening factor for long fibre (LF) and short fibre (SF) was calculated for SGW pulp and chemical pulp and reported in Figure 109.

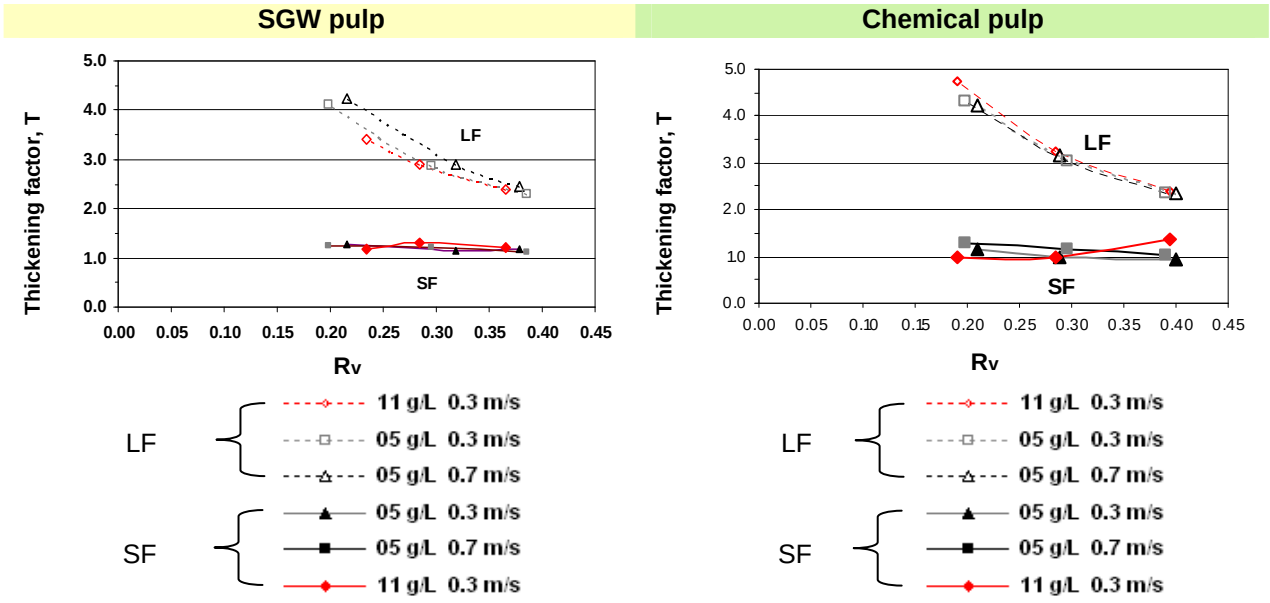

Figure 109: Thickening factor of long and short fibres

The long fibres in both the type of pulps have a much higher thickening factor as compared to short fibres. From these results, it is also evident that the chemical pulp long fibres thicken slightly more at low R_v than the SGW pulp, with a factor close to a value of 4.5-4.8.

The amount of long fibres in accepts and rejects (calculated by hyperwashing method) in the 2 fractionation stages for ONPOMG pulp are reported in Figure 110. It must be noted that the fibres in the accepts are shorter in length in comparison to rejects. This will be illustrated further in the morphological characteristics section.

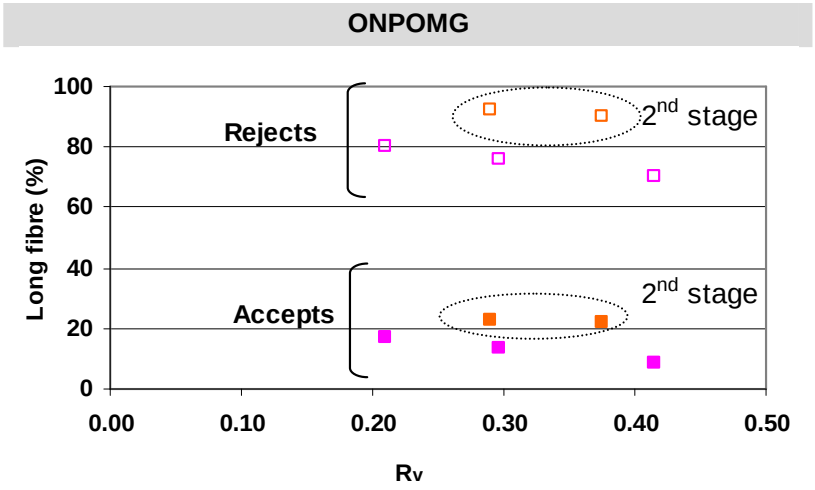

Figure 110: % long fibres in accepts and rejects

From the values of the amount of long and short fibres, their respective thickening factors were calculated on the basis of recalculated inlet concentration and reported in Figure 111.

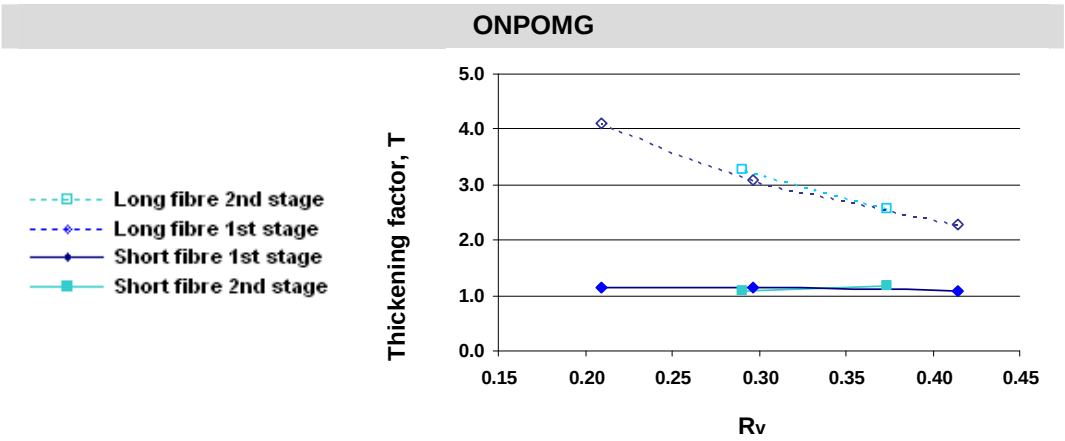

Figure 111: Thickening factor for long and short fibres of the deinking pulp

The evolution firstly indicates higher thickening at low volumetric reject ratio and then more importantly almost the same values of reject thickening for both the stages, similar (slightly higher for the 2nd stage) mass reject ratios. This indicates that at similar operating conditions for different stages, for a 0.25 mm hole screen the thickening and mass reject values for long and short fibres remain the same. The reason lies in the results for fibre fractions analysis with Bauer McNett, and as it could be observed that almost all the long fibres are rejected, hence under similar pressure screen operating conditions the mass reject ratios are same.

Short fibres having a higher probability to pass through the apertures of the screen plate enrich the accept stream of the pressure screening system. This phenomenon is illustrated by studying the Bauer McNett distributions, which more importantly provide information according to fibre length passage.

❖ Bauer McNett results

Figure 112 and Figure 113 show the SGW pulp Bauer McNett distributions for the accept and reject pulps at different operating conditions respectively.

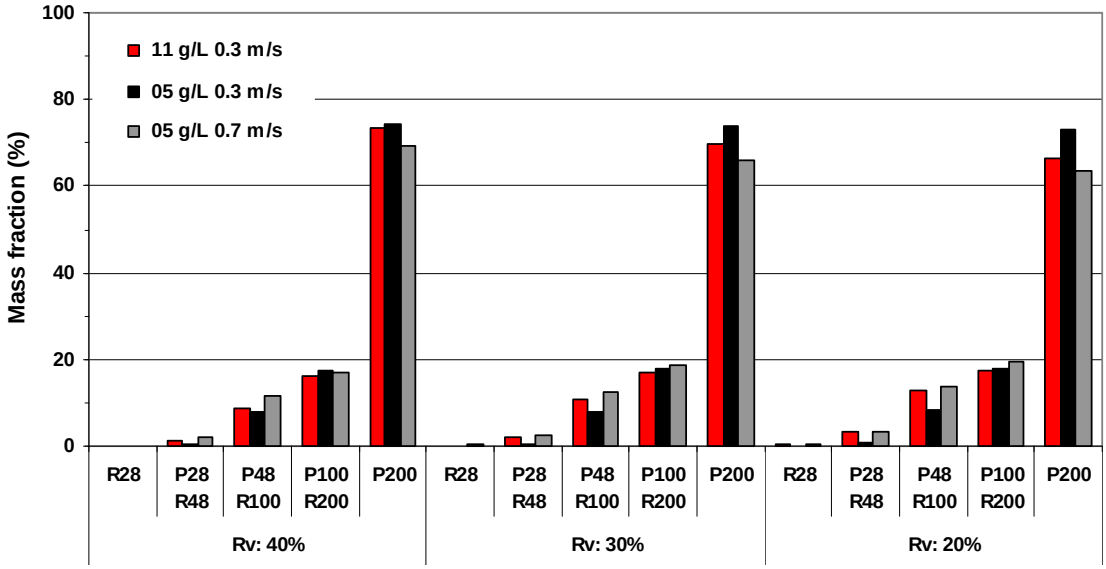

Figure 112: SGW pulp accept Bauer McNett distributions

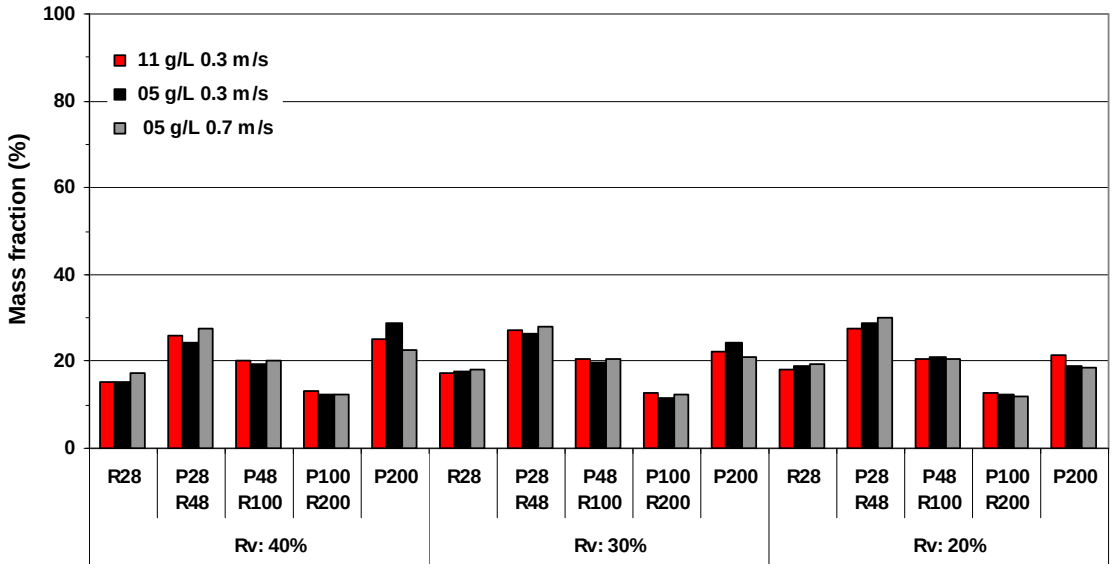

Figure 113: SGW pulp rejects Bauer McNett distributions

As it could be expected, the results indicate the enrichment of fines fraction in the accept stream, and enrichment of long fibres in the reject fraction. The accumulation of fibres (till R200) in the reject is slightly higher at low values of volumetric rejects, hence lower amount of fines. However, the effect of passing velocity and concentration is not explicitly observed.

Chemical pulp fractionation results indicated in the Annexe 4 (Figure 238 for accepts and Figure 239 for rejects) shows the same trend as for SGW pulp. The short fibre and fines enrichment tendency was also confirmed during the ONPOMG 2 stage fractionation, results also indicated in Annexe 5 (Figure 240 for 1st stage streams and Figure 241 for 2nd stage streams). The 2nd stage fractionation reduces the fines content in the rejects. A 3rd stage or the 2nd stage at lower R_v would reduce further the residual fines in the rejects, hence the ink content.

❖ Morphological properties

Whole pulp

The fibre length and width distributions for the whole pulp are presented for different values of R_V averaged for concentration and passing velocities.

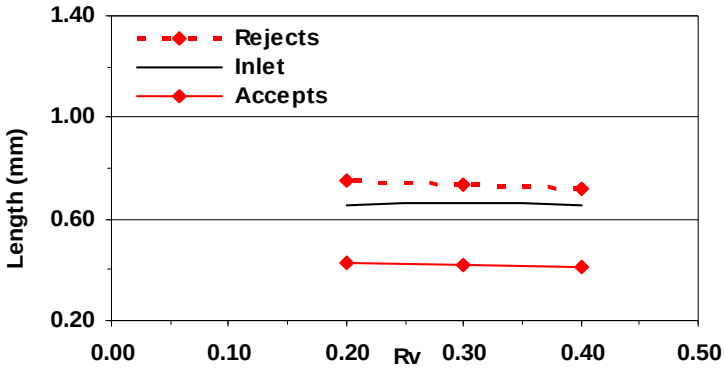

Figure 114: Fibre length for SGW pulp

Figure 114 shows fibre length values for SGW pulp fractions. As also observed in the Bauer McNett fractions, rejects have a higher fibre length.

Annexe 6 contains the results for chemical pulp (Figure 242) and ONPOMG (Figure 243- 1st stage & Figure 244- 2nd stage). The fractions follow identical trends as seen in SGW pulp scenario, with rejects containing higher fibre length as compared to accepts, while the 2nd stage ONPOMG reject pulp fibre length is the highest.

- **Distributions whole pulp**

The fibre length distributions for all the studied fractionation parameters (pulp inlet concentration, passing velocity, and volumetric reject rates) are shown in Figure 115 for SGW pulp. As observed before in Bauer McNett distributions and whole pulp values, accepts fraction has short length fibres.

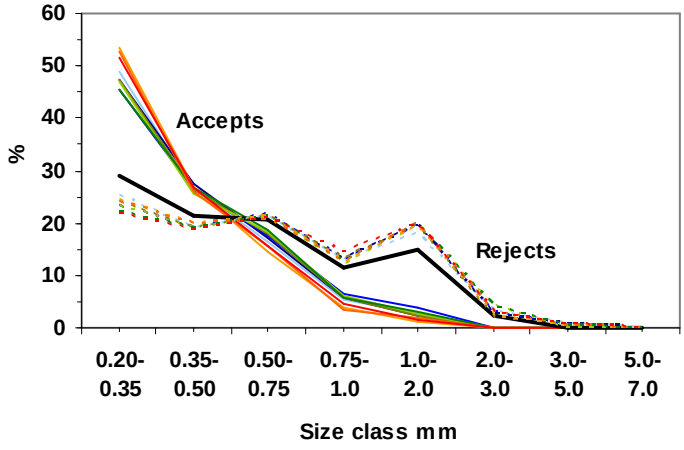

Figure 115: Fibre length distribution for SGW pulp for all fractionation parameters (solid black line is inlet pulp distribution)

The effect of parameters (operating -passing velocity, R_v and pulp concentration) is very low, at least for the rejects length distributions. Hence, for other fibre length distribution observations, the average values are shown.

The fibre cumulative length distributions for the whole pulp are presented as an average for different values of R_v, inlet concentration and passing velocities. Figure 116 illustrates the fibre length distribution for SGW pulp.

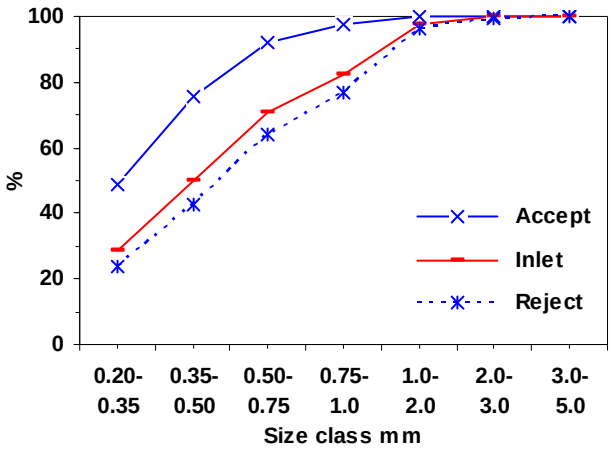

Figure 116: Cumulative fibre length distribution for SGW pulp

Fibres with shorter length having a higher probability to pass the fine holes and get preferentially accepted, with the SGW having the highest fraction of the shortest fibres in the accept stream as shown in Figure 117. But this does not signify that SGW pulp would have a higher passage ratio in comparison to chemical or ONPOMG pulp, as mechanical pulp fibres have a higher rigidity.

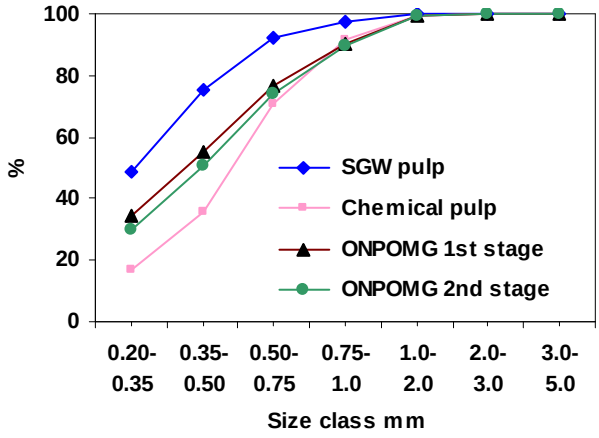

Figure 117: Cumulative accept stream distributions

- **Distributions Bauer McNett**

As observed from the Bauer McNett distributions reported earlier, negligible or almost zero amount of fibres is retained on R28 and P28-R48 fractions. Short length fibres have a higher probability of passing into the accept fraction. Hence, only the fractions retained between P48-R100 and P100-R200 on the Bauer McNett mesh were analysed for morphological characteristics. This was done for the inlet, accept and reject streams.

The mesh screen analysis for inlet, accept and reject streams analysis reveals similar distributions for the different size classes, for fibre length as it can be observed in case of SGW pulp fractions, from Figure 118 and Figure 119. Hence, in the different mesh screen distributions; there is not preferential acceptance or rejection of a particular class size of fibre.

The distributions also illustrate another fact that there is no perfect separation according to fibre length in a Bauer McNett as similar size class length fibres could be found in P48-R100 and P100-R200 mesh fractions, however their amount vary, with P100-R200 fraction containing more of smaller length fibres

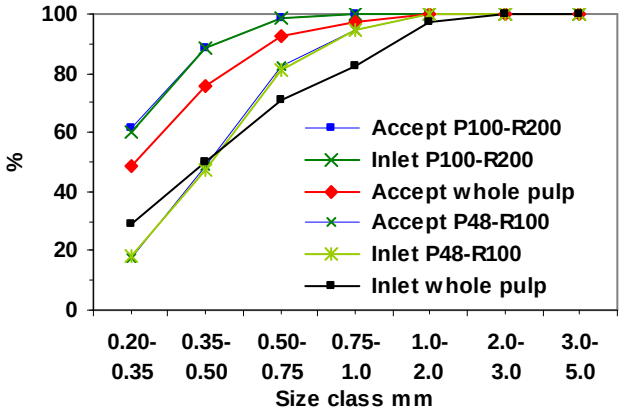

Figure 118: Fibre length for SGW pulp Reject – R100 & R200

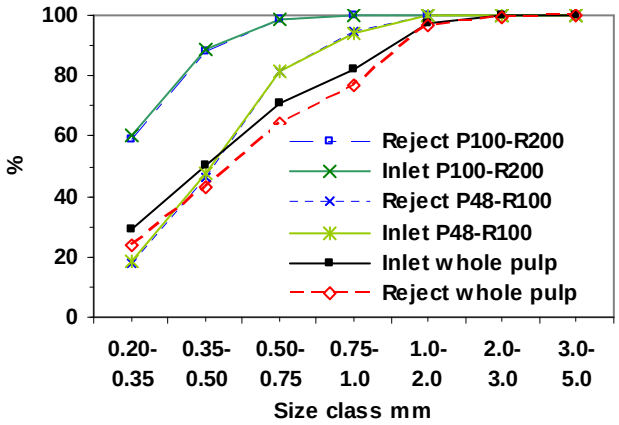

Figure 119: Fibre length for SGW pulp Accept – R100 & R200

Results for chemical pulp are given in Figure 247, Annexe 8. The fibre length distributions are quite different as seen for SGW pulp, with more amount of fibres in size range of 0.5.to 1.0 for P48-R100 fraction.

The rejects and accepts fibre length distributions for ONPOMG 1st and 2nd stage pulp streams are given in Figure 249 to Figure 252, Annexe 8. Here again we observe no difference between the reject and accept pulp distributions for the different Bauer McNett fractions for both the stages.

3.2.2. - Analysis of micro hole fractionation process

The separation of fibres and fines in the micro-hole screen fractionation process can be characterized by the passage ratio of the different fibres and fine element length/size classes through the screen, which determine the efficiency of the system as a function of the reject flow rate, the objective being to remove selectively the fine elements from the fibre fraction. The characterisation of the fractionation mechanisms on/through the screen plate in terms of particle passage ratio distribution requires the identification of a model describing the upstream flow conditions.

Special attention has been paid to the behaviour of fines in the fractionation process. Fines represent an important quantity of material in a deinking pulp, which includes the ink and filler fractions. Fundamentally understanding their probability of passage across an aperture will help to determine their maximum removal or traversing capacity. Ämmälä [156] studied the hypothesis of whether the fines follow freely the water phase across a screen and later concluded that mechanical pulp fines in a pressure screen follow the flow split in a loose fibre network, however their free flow is obstructed by the formation of a fibre layer as a result of reject thickening and their perfect passage drops.

Investigations were first performed on a laboratory wire screen, the Bauer Mac-Nett classifier, working in very dilute conditions under low-pressure steady-flow screening conditions. The objective was to study the behaviour of fines (the fine elements defined as the fraction passing the Bauer Mac-Nett 200 mesh screen) when passing wires of different mesh sizes under the Bauer Mac-Nett fractionation conditions, i.e. without interactions with fibres. The flow conditions in the classifier allow using the mixed-flow model to determine the passage ratios as a function of the aperture size.

The analysis of the micro-hole fractionation process has then been developed through the analysis of particle passage ratios of both Bauer Mac-Nett size classes and fibres length classes. The mixed flow and the plug flow models were used, which gave indications on the average flow conditions between the rotor and the screen cylinder.

3.2.2.1. - Laboratory fractionation: behaviour of fines

The passage ratio of only fines with respect to their own defining aperture size was studied using a Bauer McNett classifier. Three different raw materials – 50% ONP 50% OMG, 100% ONP and 100% OMG were pulped in a laboratory helico pulper for 15 minutes at 45℃. No chemicals were used for 100% ONP and 100% OMG, while 50% ONP/50% OMG pulping was performed in standard alkaline conditions. Fines were first collected in large quantities using a Bauer McNett classifier. The material passing the 200 mesh screen was recovered and allowed to settle overnight and then concentrated by sedimentation.

To understand the passage ratio of only ‘pure’ P200 fines (in absence of other fibre classes), a new method was used. This method involved re-circulation of previously collected P200 fines across a 200 and larger mesh size screen as shown in Figure 120 and measuring the upstream as well as downstream concentration to calculate the passage ratio values. A variable frequency drive pump controlled the flow rate of fines suspension in the 1st tank and was equal to 11.35L/min, similar to TAPPI norm 233 cm-06 (fiber length of pulp by classification). To have a stable level in the 2nd tank and to avoid overflow, the outlet flow in the 2nd tank was controlled by a manual valve and was re-circulated back to the container to which the pump was connected feeding the 1st tank.

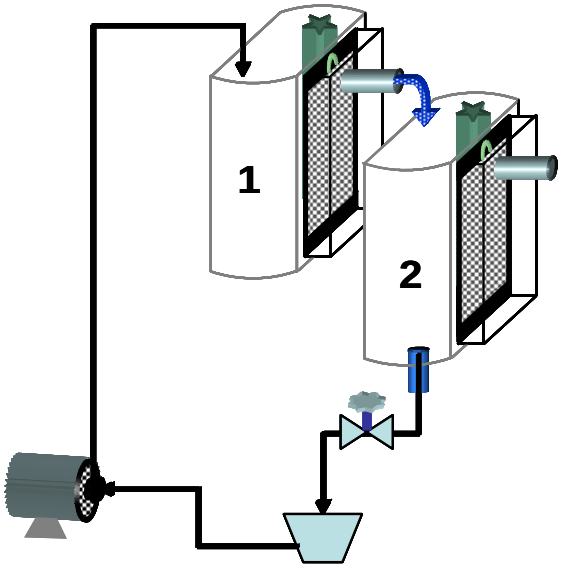

Figure 120: Fines recirculation schematic

5 samples of upstream (in front of the mesh screen) and downstream (outlet of 1st tank) were taken simultaneously containing approximately 175-180g of suspension. After sampling, the 200 mesh screen in the 1st tank was then replaced by a larger aperture mesh to calculate the passage ratio of P200 fines with respect to larger mesh openings. This particular set-up provided the flexibility to calculate the passage ratio of a particular category of fines using different mesh sizes by just changing the mesh size in the 1st tank. Concentration was measured on 0.8µm opening Millipore filter. After concentration measurements, the thin pulp pads were then carefully removed to analyse the combined ash content at 425℃. This was done to calculate th e passage ratio of the inorganic mineral fillers.

The contents in a Bauer McNett classifier are agitated continuously and the pulp entities are mixed all over the tank volume (or in other words, the tank depth and tank width, which corresponds to 'axial' and 'radial' mixing case). Under this situation a mixed flow model better relates to the fractionation phenomenon and the passage ratio could be calculated as a ratio of the downstream to upstream consistency.

As the fines were recirculated across mesh screens of increasing aperture size, it was more pertinent in this case to report the results in terms of aperture opening ratio. This ratio has been calculated on the basis of mesh size to 200 mesh size and reported in Table 17. P200/200 means passage ratio of P200 fines across 200 mesh screen whereas P200/150 indicates passage ratio of P200 fines across a 150 mesh screen or larger aperture size.

Table 17 : Aperture opening ratio

Passage ratio reference	Aperture openings (mesh size/200 mesh size)	Aperture opening ratio
P200/200	75µm/75µm	1.0
P200/150	100µm/75µm	1.4
P200/100	150µm/75µm	2.0

Figure 121 and Figure 122 report the results for 100%OMG and 100%ONP raw material. The results indicate that the cellulosic fines (or only fines as indicated in the graphic) have a lower passage ratio across a 200 mesh screen (aperture opening ratio 1) in comparison to mineral fillers which have higher passage ratio nearly equal to a value of 1.0. In case of 100% ONP the passage ratio of cellulosic fines is much lower across the 200 mesh screen as well as the passage ratio of whole fines due to lower ash content.

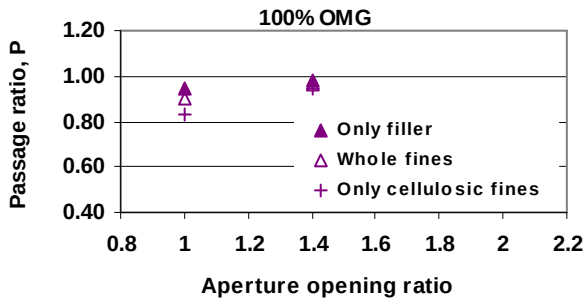

Figure 121: Passage ratio for 100% OMG

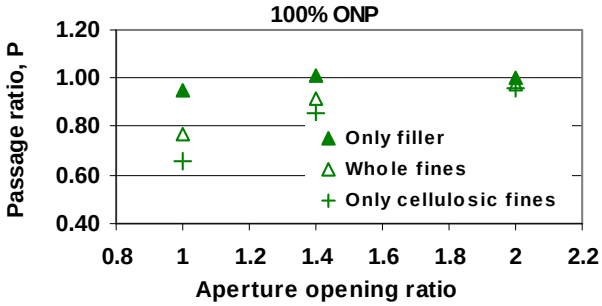

Figure 122: Passage ratio for 100% ONP

At 1.4 times aperture opening ratio for 100% OMG, the passage ratios for different pulp entities- only cellulosic fines and only mineral fillers reach a value of 1.0, but for 100% ONP an aperture opening ratio of 2.0 is required to attain a passage ratio of 1.0. The presence of mineral fillers has a pronounced effect on the overall passage ratio. The value of the average ash content in fines for 100% OMG is 67.3% whereas for 100% ONP is 44%. However the nature of fines particles will also lead to a difference in passage ratios. It has been observed that fibrillar fines during screening are concentrated in the rejects and exit the screening system [27][47]. The lower passage ratio value for 100% ONP fines at across 200 mesh screen (aperture opening ratio of 1) could be a result of more fibrillar content of fines present in the pulp coming from mechanical pulp, as compared to 100% OMG fines containing chemical pulp. Figure 123 represents passage ratio for 50% ONP and 50% OMG. The passage ratio for the cellulosic fines is achieved at an aperture opening ratio of 2, similar to the case of 100% ONP. However the passage ratio values are slightly higher at aperture opening ratio of 1; the average ash content being 51%

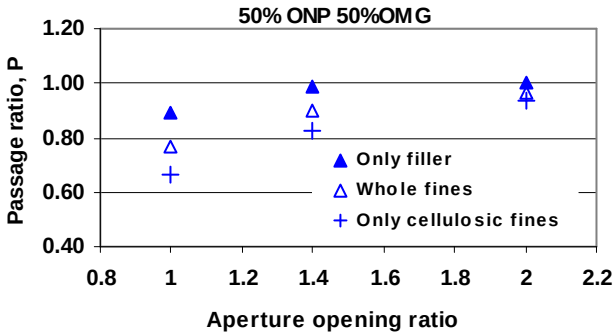

Figure 123: Passage ratio for 50% ONP 50% OMG

Defined as material passing through a 200 mesh, the cellulosic fines do not freely traverse the same aperture opening. However, their capability of passage increases at a higher aperture opening ratio. It has been also found out by different workers that during the screening phase, the amount of fibrils in the rejects was more than that in the accepts. Fibrils tend to entangle and get associated with the fibrillar fibres as compared to relatively stiff and 'straight' and block like flakes, which might pass the apertures like narrow discs. As the aperture ratio is increased the passage ratio increases almost linearly for the whole fines. This is in agreement with Olson *et al.* [151], where they observed a linear relationship with increasing aperture size.

3.2.2.2. - Pressure screen fractionation: separation of fibres and fines

The rejection of fibres and fines in a micro-hole pressure screen has been analysed in terms of particle passage ratios for different classes of as far as possible homogenous particle, i.e., the mineral fraction of fillers and pigments, Bauer McNett fractions, and fibre length classes, as required for correct theoretical analysis.

The evolution of particle passage ratio also requires identifying a model of the average flow pattern along the upstream side of the screen cylinder, with at the limits the perfect mixed flow and plug flow models, which are both used in the calculations.

- **Mineral fillers**

The inorganic fraction measured by the ash content, represents essentially the free mineral fillers and pigment in coat particles of the deinking pulp, which are essentially much smaller than the micro-holes openings.

Figure 124 shows the passage ratio of the mineral fraction with the chemical pulp where kaolin was added, and Figure 125 for ONP/OMG pulp.

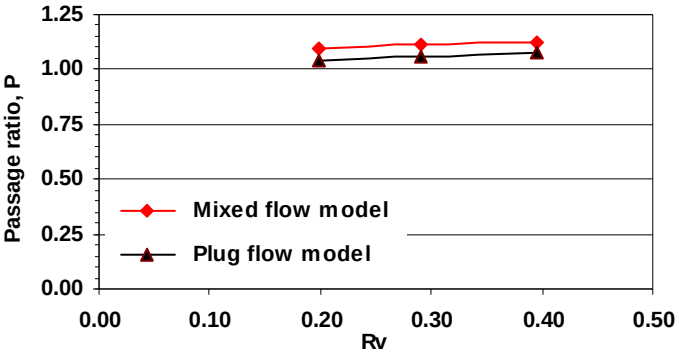

Figure 124: Mineral filler passage ratio for chemical pulp

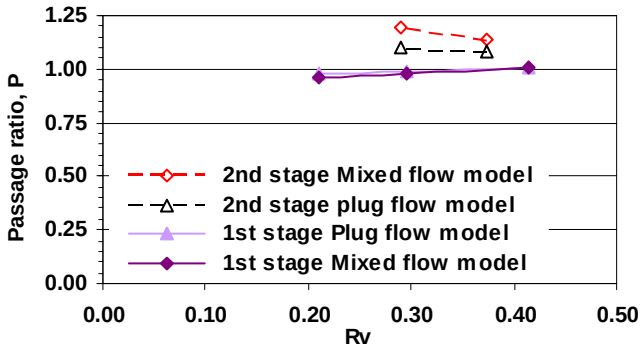

Figure 125: Mineral filler passage ratio for ONPOMG pulp

The results showing a passage ratio closer to 1 with the plug flow compared to the mixed flow model suggest that the plug flow model is more relevant for both the pulps. The 2nd stage of ONPOMG fractionation contains fewer amounts of mineral filler in the rejects (~3%). A part of this ash content is of fibre origin (fibre intrinsic content), which amounts to 1% (measured on hyperwashed pulp). Low ash content measured in the rejects could lead to a slightly higher passage ratio (more than 1.0) with the plug flow model for the 2nd stage ONPOMG pulp as thickening would be less than 1.0. Nevertheless, the values are lower than those observed with the mixed flow model. The model can be further validated by observing the influence of R_v on fibre length dependant passage ratio, which has been described in Figure 132.

- **Bauer McNett fractions**

The passage ratios for the Bauer McNett fractions are reported for mixed flow model and plug flow model in Figure 126 and Figure 127 respectively for SGW pulp and in Figure 128 and Figure 129 for chemical pulp. For both pulps, the values are reported for 5g/L and 0.3m/s. The inlet McNett distribution was recalculated based on accept and reject distributions, hence the graphics are based on recalculated thickening factor.

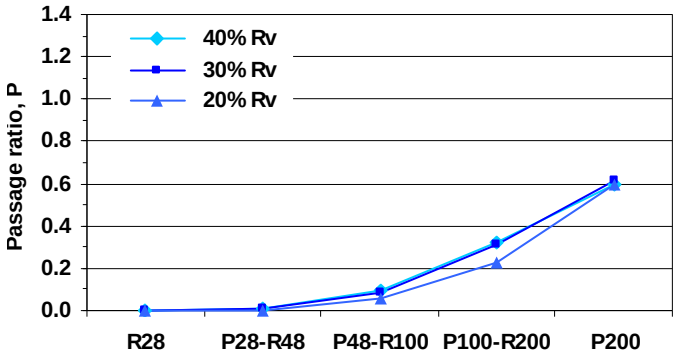

Figure 126: SGW pulp- mixed flow model

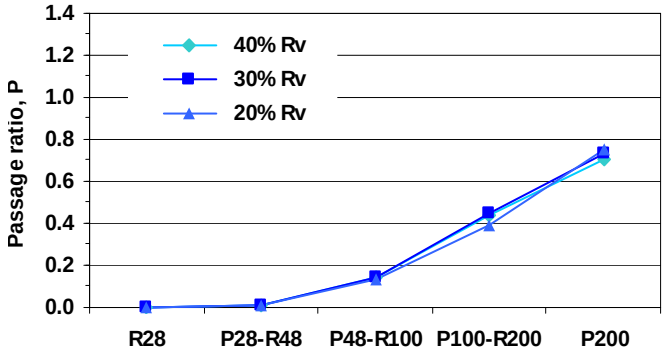

Figure 127: SGW pulp- plug flow model

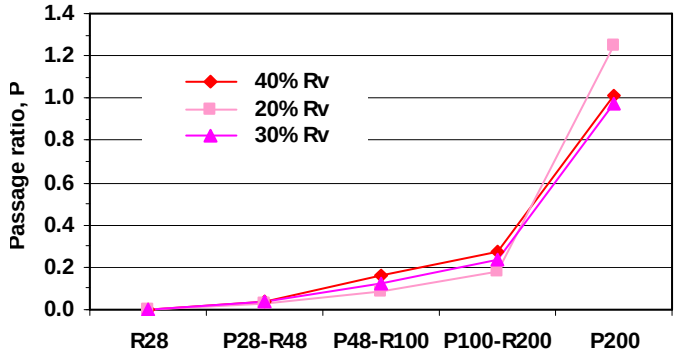

Figure 128: Chemical pulp- mixed flow model

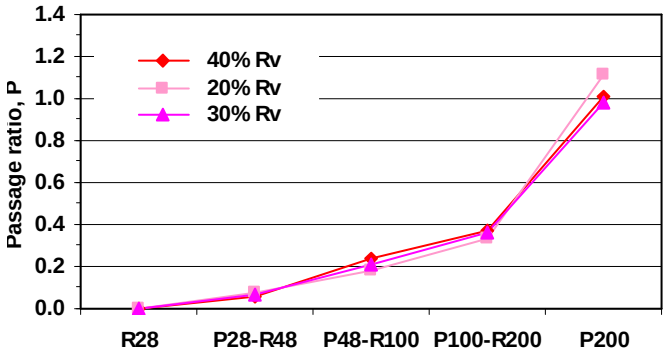

Figure 129: Chemical pulp- plug flow model

The results for both pulps show a high value for the P200 fraction. However, the value of cellulosic pulp fine fraction given by SGW pulp is not 1.0 (perfect passage) and lower than chemical pulp. The mineral filler contained in the chemical pulp 'increase' the passage ratio associated with the P200 fraction. The fibre fractions have a very low passage ratio, especially for long fibres.

The very low influence of R_v on passage ratio distribution of the different fractions with the plug flow model compared to the mixed flow model suggests again that the plug flow simulates better the flow conditions in the pressure screen.

Figure 130 shows the Bauer McNett fractions plug flow model passage ratio distribution for both fractionation stages with the ONPOMG pulp. The 2nd stage coarse fibres in lower mesh screen fractions have a slightly lower passage ratio in comparison to the corresponding screen fraction of the 1st stage.

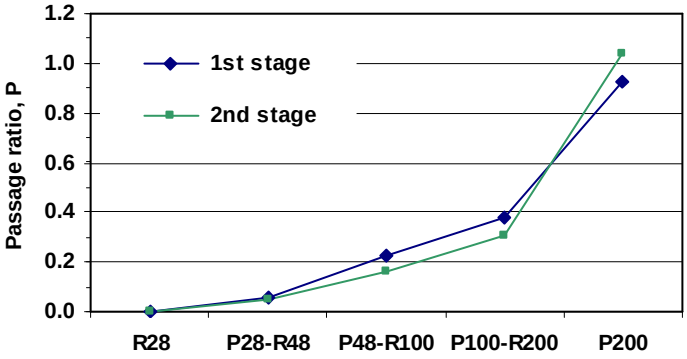

Figure 130: ONP/OMG plug flow model

- **Fibre length classes**

The analysis of passage ratio distribution as a function of fibre length enables a more detailed analysis of the fractionation efficiency with respect to the fundamental studies developed by Gooding *et al.* [149], who characterised the fibre length dependant passage ratio curves in terms of the 'size' and 'shape/fractionation efficiency' constant λ and β respectively. Passage ratio for different fibre length classes based on mixed flow and plug flow were calculated. This gave the measured passage ratios for both models. Using regression analysis the measured passage ratios were recalculated for the negative exponential function (cf. Eq. 15), to determine λ and β. An example of the calculation is given in Annexe 9.

As an example, the thickening factors for fibre length classes at different values of R_v are reported in Figure 131. Long fibres have higher thickening factor. This value increases at low R_v. The graphic illustrates the fact that thickening behaviour is a fibre length dependant; hence the passage ratio analysis should be performed for fibre classes of homogenous length. Broader fibre length classes were used for the longer fibres in order to get more accurate, statistically sound results, as there are much less long fibres than short fibres counted by MorFi.

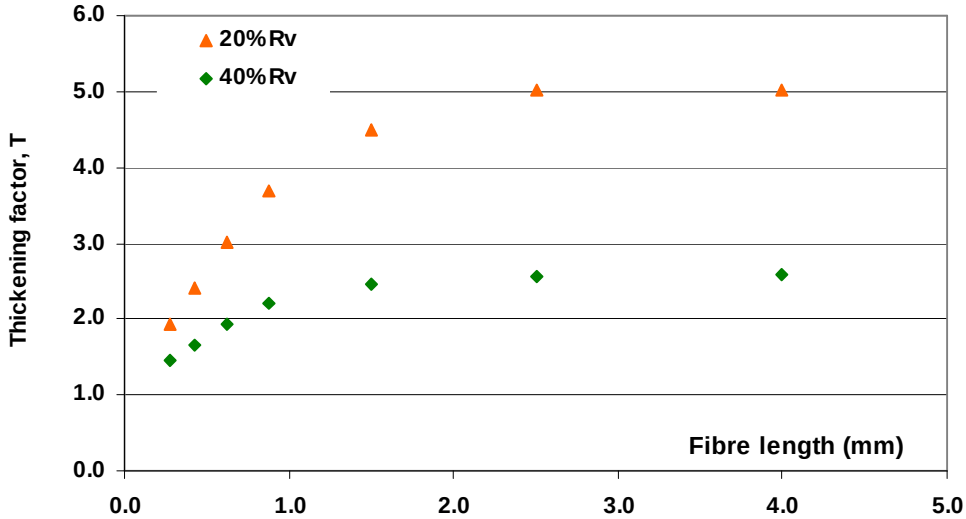

Figure 131: Thickening factor SGW pulp, 05g/L, 0.7m/s

Figure 132 represents passage ratio for different fibre lengths for the two flow models for SGW pulp and Figure 133 for chemical pulp. The results indicate the screening system functioning is based on plug flow model as the passage ratio distributions are independent of R_v. The observations here are in agreement with the passage ratio values observed for Bauer McNett fractions.

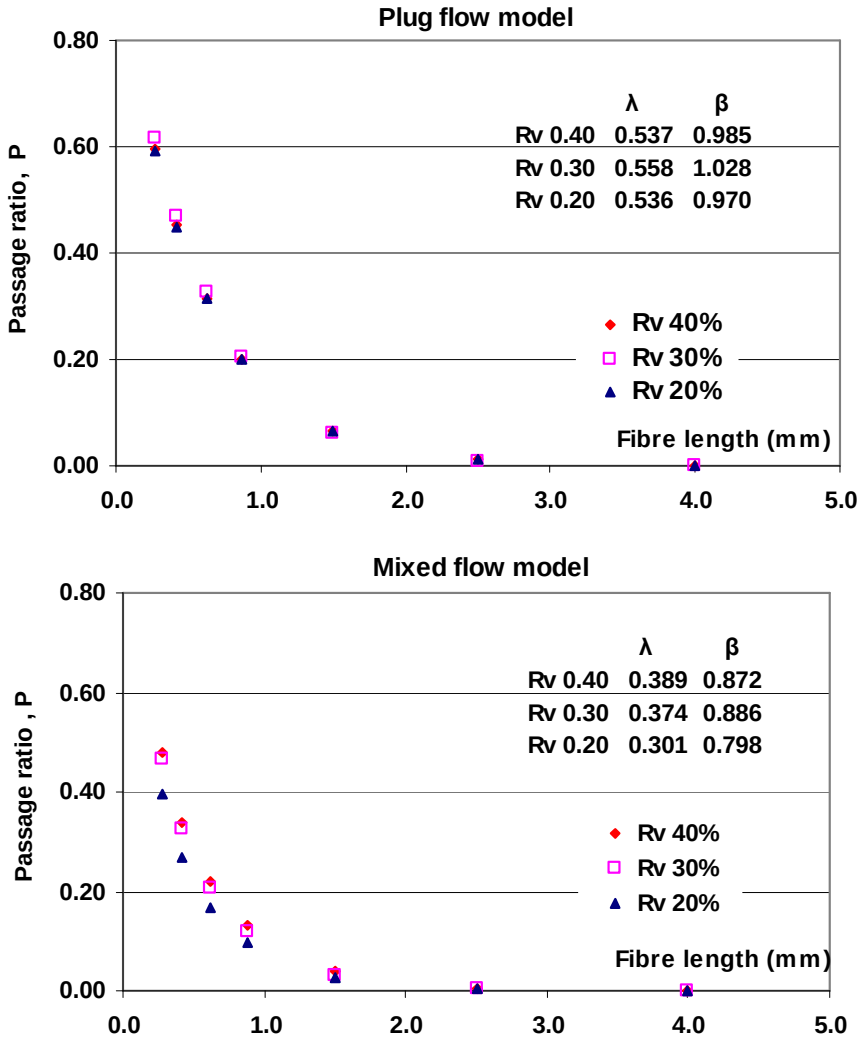

Figure 132: SGW pulp, 05g/L, 0.7m/s

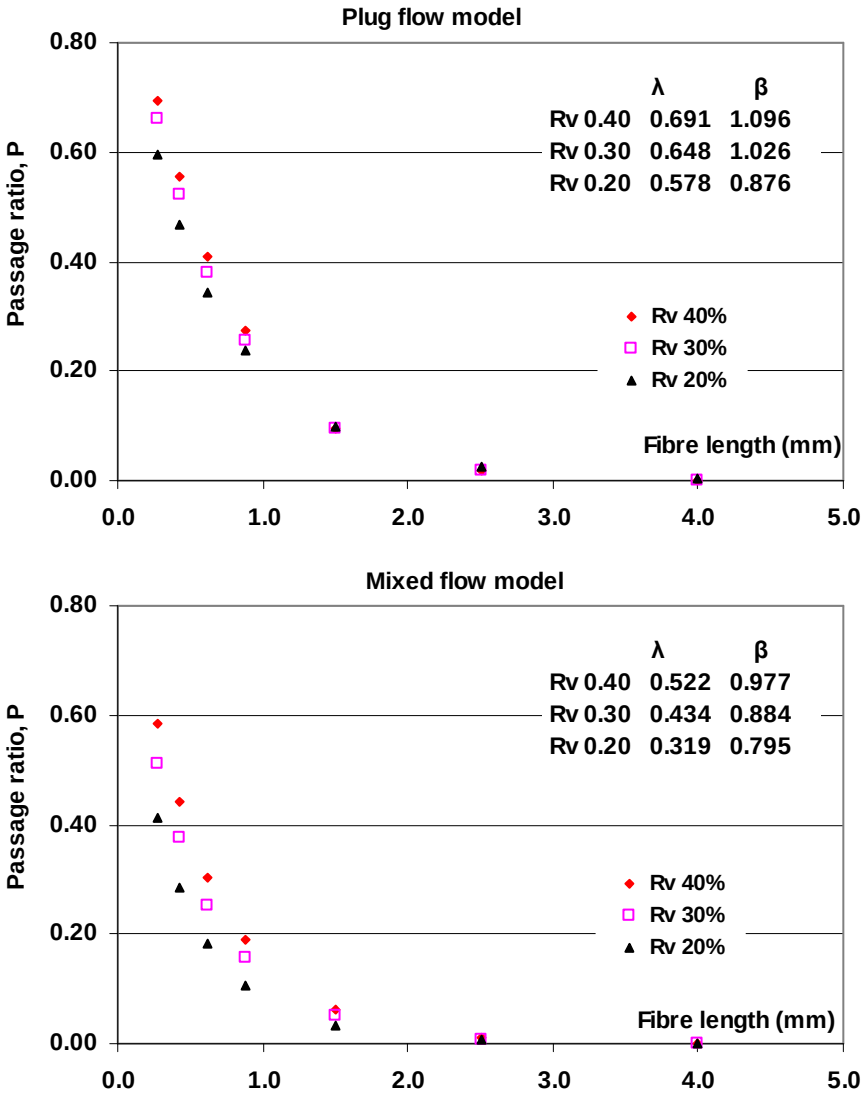

Figure 133: Chemical pulp, 05g/L, 0.7m/s

For SGW pulp the average value of λ is 0.54 with a β close to 1.0 (0.99) and for chemical pulp respectively 0.6 and 1.0. The value of λ, the size factor, is dependant on pulp, the chemical pulp with longer fibres than the SGW leading to the higher λ value, i.e., the average fibre length (with respect to given screen openings) is higher for a given passage ratio. The high value of β signifies a better degree of fractionation efficiency.

Figure 134 gives a comparison of the passage ratio distributions for the different pulps. For the same value of fibre length, the chemical pulp shows a higher passage ratio in comparison to SGW pulp, as expected since chemical pulp fibres being more flexible pass easier through the micro-hole screen plate.

The results obtained when comparing the passage ratio distribution at the first and second screening stage with the ONP/OMG, are also as expected, with lower passage ratio observed with coarse/ stiffer fibres at the second stage. In other words, it is not surprising to observe that the fibres which in a given length class are concentrated in the rejects, i.e., have lower passage ratio, effectively show lower passage ratio when screened in a second stage. This behaviour also confirms the observation of the Bauer McNett fractions passage ratio (cf. Figure 130), where the difference between 1st and 2nd stage passage ratios were however lower, due to the fact that the Bauer McNett itself also fractionates by fibre stiffness.

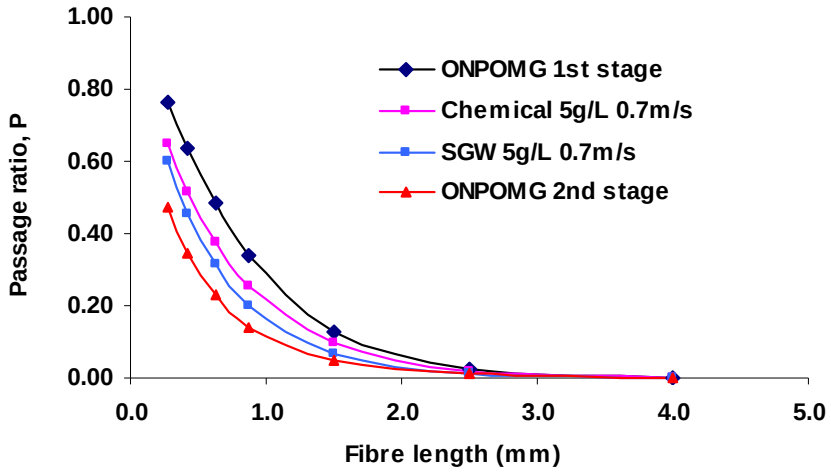

Figure 134: Passage ratio comparison plug flow model (0.25mm smooth hole screen plate)

Concluding remarks

The results obtained while analysing the passage ratio distributions as a function of fibre length showed firstly that the screening system configuration follows a plug flow model. This was expected with a closed rotor and had been observed in the previous works of different workers [89][143][148][154].

Further, the pulps studied do not have the same behaviour for the passage ratio, the flexible chemical pulp fibres having a higher passage ratio in comparison to stiffer SGW mechanical pulp fibres, as expected, confirming the results of previous papers [89][90]

The micro holes provide a higher degree of separation efficiency and selectivity for very short fibres and fines as compared to the fine low profile slots. This can be observed while comparing Figure 134 with Figure 135. For the 0.25mm smooth hole screen plate used in the experimental trials, the passage ratio values are higher for low fibre length, close to 0 for fibres with length greater than 2.5mm and very low between 1.5mm and 2.5mm fibre length. However, the 60µm low profile slots allow fibres with length between 2.5 and 3.5mm to pass through and lead to a lower passage ratio values for low fibre length. The passage ratios obtained for Bauer McNett fractions also indicate high separation efficiency of micro-hole screen plate compared to the slot screen (cf. Figure 71 and for example Figure 129).

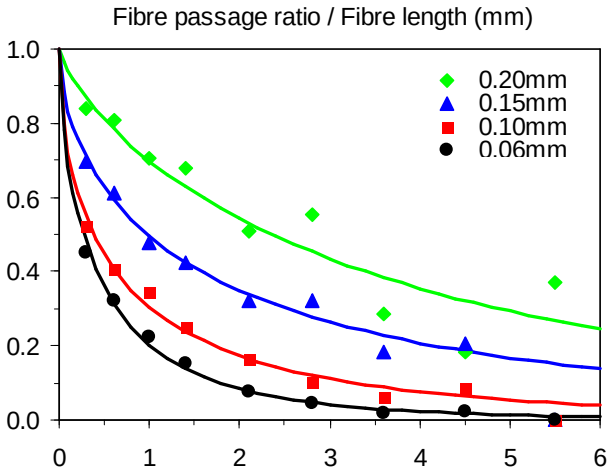

Figure 135: Fibre passage ratio and fibre length, low profile slot, Vp 1m/s, mechanical pulp, from Julien Saint Amand & Perrin [95]

Smooth hole screen plates fractionate more efficiently than slotted and profiled screen plates. This is evident by a value of 1 found for β and as reported and in agreement with other workers [148][149].

The authors also showed that the effect of passing velocity or concentration on reject thickening was minimal in the range of values tested. Indeed, it has been reported that passing velocity does not affects the passage ratio for smooth hole apertures [148] (in a 'lower' range of values). However, it could be possible to have an effect of passing velocity if it can be increased to a higher level of 2m/s or 3m/s. The inability to increase the passing velocity, which directly relates to hydraulic loading of screen plate needs to be understood with respect to the ability of the rotor to de-plug the screen surface and maintain a high 'effective' passing velocity. To understand the rotor (cf. Image 2) hydrodynamics, pressure pulsation measurements were studied with a special sensor, analysis on these aspects will be developed in the section 3.2.3. -Hydrodynamics of micro-hole screening mechanisms

3.2.3. - Hydrodynamics of micro-hole screening mechanisms

3.2.3.1. - Pressure drop and pressure pulse analysis

Rotor pressure pulsation measurement

The pressure pulsations were measured with a miniature piezoelectric quartz sensor: KISTLER type 601A, of less than 5 mm diameter. The output charge signals from the sensor in the order of pico-coulombs were amplified by a 5011 KISTLER charge amplifier to volts. The data acquisition was made at 5000 kHz with the charge amplifier set at a short time constant and connected to a data acquisition device. The co-axial sensor cable, KISTLER 1651C, protected the data from external noise disturbance and the sensor was company calibrated.

The image of the sensor with its dimensions in mm is shown in Image 3.

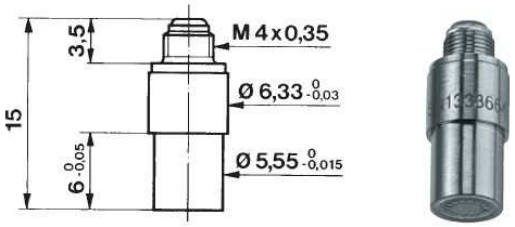

Image 3: Piezoelectric sensor and its dimensions in mm

The pressure pulsation was measured at three different positions of the 0.25 mm micro-hole basket along the rotor axis in a straight line, shown in Image 4. The positions were chosen to have information on the pulse magnitude and shape; approximately at the inlet side, in the middle and in the reject sections of the screen. The sensor was screwed on a block welded to basket as shown in Image 5.

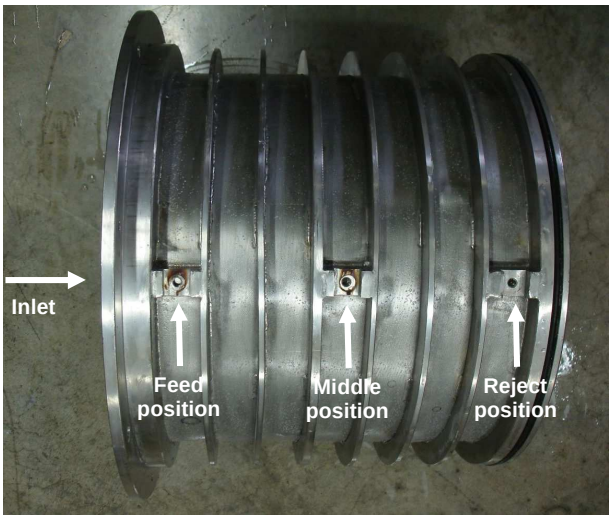

Image 4: Basket and the 3 measuring positions

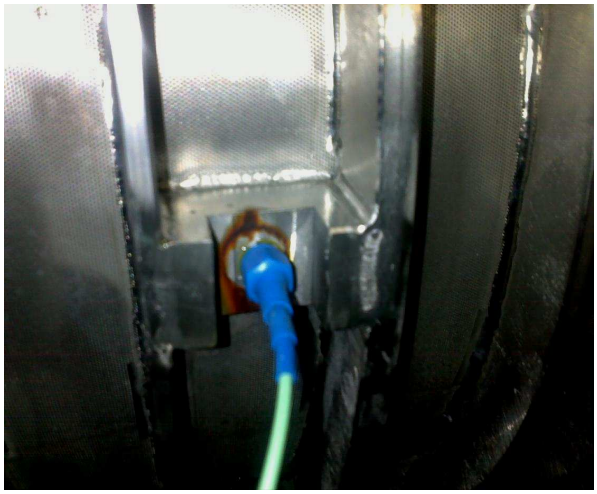

Image 5: Wired sensor mounted on the basket

The raw signals from the sensor were recorded for durations of 20 seconds which corresponded to 100,000 measurements at 5000 Hz. The pressure pulse data were then averaged for 13 seconds by a CTP software which automatically calculated the matching positions for the 3 hydrodynamic elements (cf. Image 2) for the 13 seconds duration, which related to approximately 310 rotations. Apart from the

mean values, the software gave information on the maximum, minimum values as well as 95% and 5% confidence interval graphs. These raw data were then converted to absolute values with the calibration factor and adding the inlet absolute feed pressure.

The measurement of pressure pulsation was performed with water and with deinking pulp at two concentrations of 4g/L and 7g/L.

The holes on the screen each of nominal diameter 0.25mm are arranged in a staggered triangular configuration as shown in Image 6.

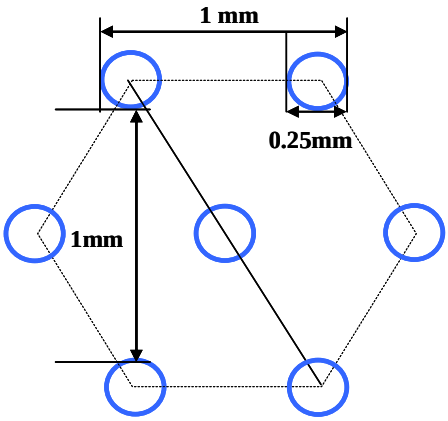

Image 6: Holes arrangement

Imprints of the micro-holes were taken in order to determine precisely their dimensions with respect to their nominal diameter.

Image 7 shows the convergent entry design of the 0.25mm hole. The downstream hole design is similar to the upstream design, i.e., a divergent entry. Image 8 shows the hole internal diameter and wall characteristics with respect to smoothness. Indeed, the microscopic measurements of the hole imprints allowed to indentify that the holes diameter varied between 0.25mm and 0.30mm.

Image 7: Upstream hole internal imprint showing convergent entry

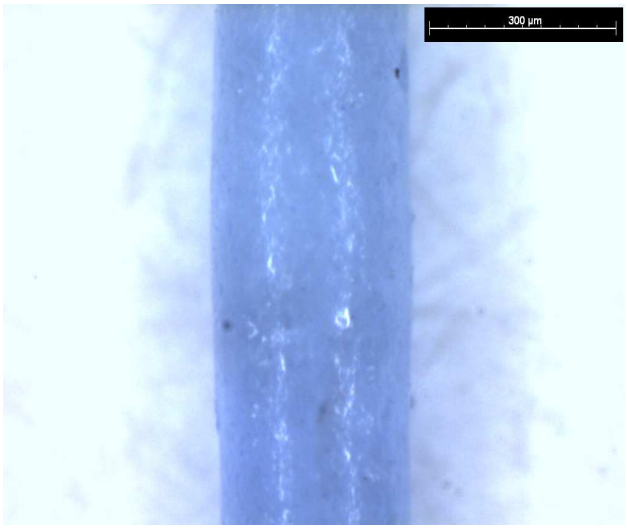

Image 8: Hole internal imprint

Screen plate pressure drop measurement

Analysis of effective velocity (Ve) required understanding the pressure drop across the micro-hole screen plate for calculation purposes (this pressure drop is the energy loss happening at the immediate surface). With the given capacity of the feed pump and the screen basket with the high open-area, the possibilities to attain high average passing velocity (V_p) were limited.

In this case it was necessary to reducing the screen open area. The first trials by temporarily plugging the apertures with foam sheet and high-strength scotch tape did not yielded desired results. As after some minutes of operation, the scotch tape and foam gave away and were found floating in the feed tank. Hence, a different approach was used to calculate the pressure drop across the screen plate at high passing velocities. This was done by submerging the screen basket in a large water filled container and recording the pressure gauge reading attached to a 8mm flexible pipe (internal diameter) firmly held (manually) against the screen basket. The flow in the pipe was maintained and altered through a pump having a variable frequency drive and a flow meter. Different flow rates were obtained to allow for pressure drop calculation at high passing velocities. The number of micro-holes receiving the flow through the pipe was visualised through a hand lens and corresponded to 112. The pressure drop readings were made at 2 axial positions, in both radial directions, i.e., 'upstream' from inside to outside of the screen basket in the screening flow direction and 'downstream' from outside to inside of the basket in the reverse flow direction.

Theoretical pressure drop calculations were made using the hypothesis that the total pressure drop across the screen plate consisted of:

1. The pressure drop/ frictional losses resulting from the flow of water across a 2mm long cylindrical pipe (this is the screen plate thickness) of 0.25mm internal diameter (neglecting the losses at the entry to the micro-hole)

2. The total dissipation of the energy at the exit of the water jet from the micro-hole. If all the energy is lost, this could be defined as:

Energy lost by dissipation: $\frac{1}{2}\rho V_P^2$

ρ: water density, 1000kg/m^3
V_p: passing velocity, m/s

The pressure drop occurring due to fluid flow in the cylindrical section was calculated in different flow regimes (laminar and turbulent) identified using the Reynolds number Re, defined as:

$$\mathrm{Re} = \frac{V_P D \rho}{\mu}$$

μ: water dynamic viscosity, 1mPa.s (20℃)
ρ: water density, 1000kg/m^3
D: cylinder internal diameter, m

In the laminar flow region (Reynolds number < 2100), Eq. 21 derived from Power Law (for water) [157] was used

Eq. 21 :
$$V_P = \left(\frac{n}{3n+1}\right)\left(\frac{-\Delta p.r}{2mL}\right)^{1/n}.r$$

L: cylinder length, m
r: cylinder internal radius, m
m: power law consistency coefficient, Pa.s^n
n: power law flow behaviour index

For water n = 1 and m is the water dynamic viscosity. Eq. 22 results on simplifying Eq. 21 in terms of Δp

Eq. 22 :

$$-\Delta p = \frac{8\mu L V_P}{r^2}$$

In the transitional and turbulent flow regions (Reynolds number > 2100), Darcy–Weisbach equation represented in Eq. 23 was used.

Eq. 23 :

$$-\Delta p = \frac{fL\rho V_P^2}{2D_h}$$

f: Darcy friction factor

D_h: cylinder (hole) internal diameter, m

The friction factor value was read from the Moody diagram at a relative pipe roughness of 0.01m/m (assumed value, corresponding to a roughness of 2.5 – 3µm, consistent with visual observation of micro-hole internal imprints) for different values of Reynolds number.

For given flow rates, while calculating the experimental passing velocity, different diameters of micro-hole were assumed: 0.25mm, 0.28mm and 0.30mm. The experimental pressure drop values (upstream and downstream) were plotted against the passing velocities and also the theoretical pressure drop by assuming a micro-hole diameter of 0.28mm as represented in Figure 136. Indeed, the experimental and theoretical readings corresponded well with a micro-hole diameter of 0.28mm (this value was also nearer to microscopic observations).

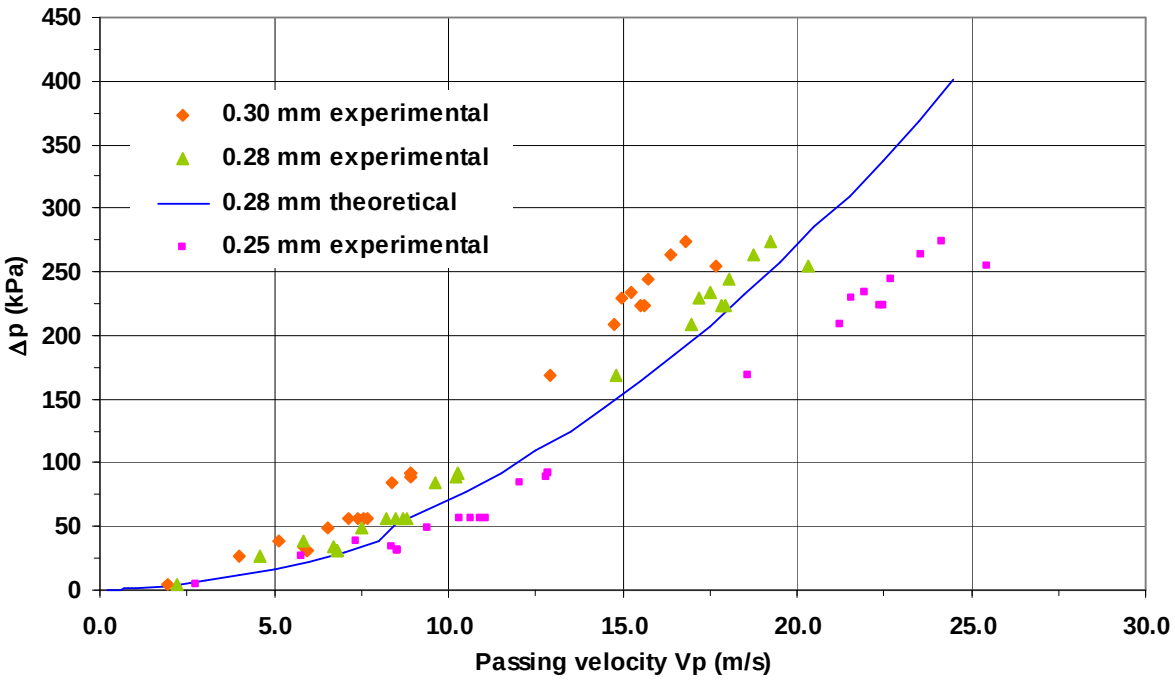

Figure 136: Experimental and theoretical pressure drop across the screen plate

For the micro-hole screen, the pressure drop followed a non-linear relationship, with considerable losses at higher passing velocities. The negative pressure pulse generated by the rotor movement to produce the required reverse flow has to overcome this pressure drop; hence the rotor “efficiency” associated with the negative pulse could decrease if the pressure drop across the plate is high.

Pressure drop values attained at higher velocities help to estimate the effective passing velocity (Ve). As reported by Julien-Saint-Amand & Perrin [89], this velocity could be much higher than the simplified ‘global’ average velocity calculated using the accept flow to the open area of the screen plate.

Indeed the total volume of suspension to pass though the screen plate increases considerably taking into account the volume re-pumped back to the upstream during the negative pulse phase (in case of micro-hole screen plate this would be essentially a fines suspension behaving like water dilution from accepts) added with the incoming suspension from the inlet. The re-pumped volume will largely depend on the negative pulse magnitude and its duration.

In order to calculate the total effective volume and Ve, the reverse passing velocity was calculated using Figure 136 corresponding to the negative pulse magnitude. With the average duration of the pulse and rotor tip speed, the open area swapped by the rotor was calculated, considering 13.4% screen plate open area, according to the micro-hole average diameter estimated to 280µm. These two elements gave the volume re-pumped. This was added to the incoming inlet flow leading to total effective volume. The effective passing velocity was then calculated with respect to the total volume and the open area.

Pressure pulse shape analysis

The significance of the pressure pulses generated has been described in the bibliographical section of this chapter. Before the description of the pressure pulse analysis, a short recall is made in for the various components of the pulses. The example shown in Figure 137 describes for a S-shaped rotor the 'effective' negative and the positive pressure pulses. The average feed side and accept side pressures represent time-average pressures at the upstream and downstream side of given screen cylinder section, and so the average pressure drop across this screen cylinder section, which is a time-average of the pressure drops generated in both directions during the positive and negative pressure pulses. The graph also illustrates that a too high average pressure drop across the screen cylinder, which may occur if the screen plate gets plugged, would lead to reduce the effective negative pressure pulse and this its de-plugging efficiency. The observation is *consistent* with experience when operating a pressure screen, showing that once screen plugging starts complete blinding occurs very quickly, and feed flow rate have to be strongly decreased to recover screen operation in order to *restart* the reverse pulse to enable effective de-plugging.

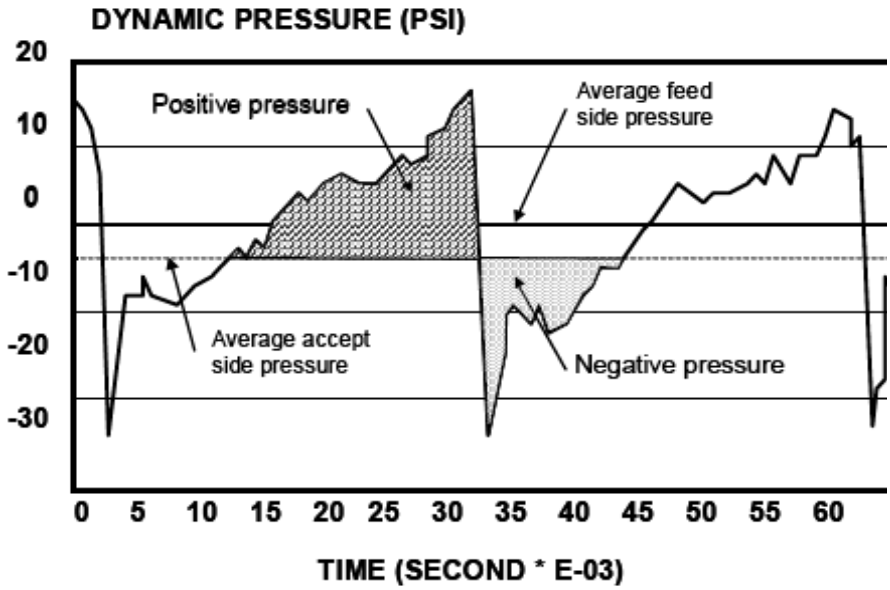

Figure 137: Pressure pulse generated by S-shaped rotor [153][121]

The pressure pulses observed in the feed, middle and reject sections of the screen cylinder showed to be different.

- Feed section of the screen cylinder

Typical pressure pulsation graphs (absolute pressure values) are reported in Figure 138.

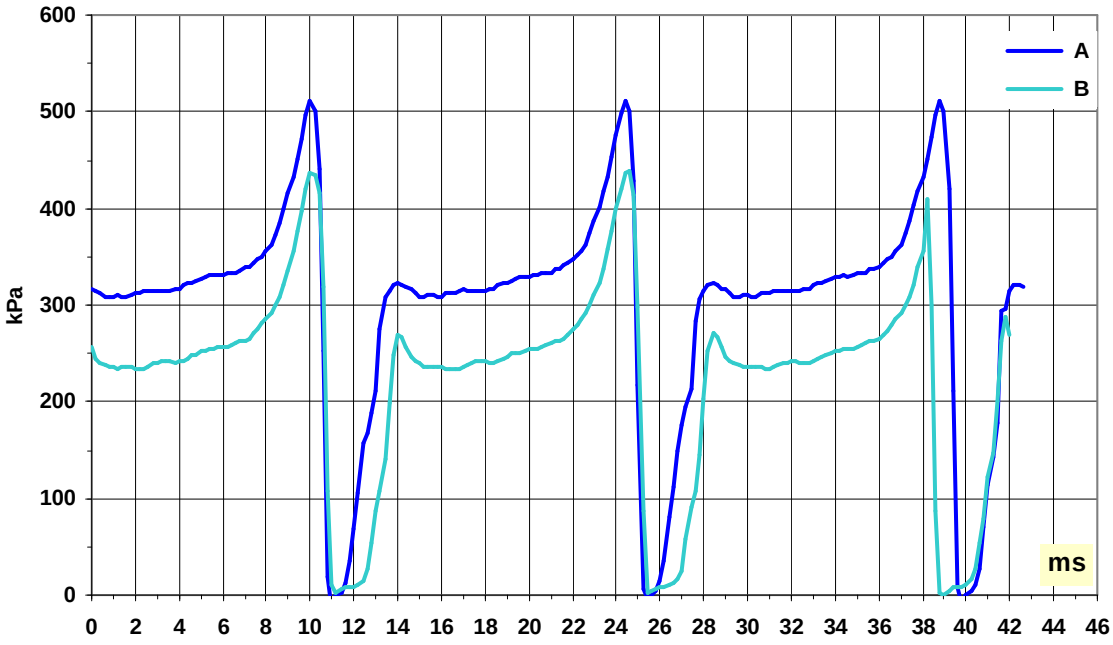

Figure 138: Feed section average pressure pulsation graphs (water)

With:

A graph conditions: R_v 20%, V_p 0.97m/s (Q_a 100m^3/h), P_i[1] 300kPa (abs), Δp 30kPa (global[2])

B graph conditions: R_v 21%, V_p 1.21m/s (Q_a 124m^3/h) P_i 230kPa (abs), Δp 40kPa (global)

The graph indicates firstly a high magnitude of peak to peak pressure pulse ~500kPa with the negative pulse magnitude varying between 250kPa to 300kPa. The possible explanation for such a high magnitude is firstly the high tip velocity of the rotor, 25m/s and secondly the clearance between the rotor tip and the screen plate being of the order of 2.0mm. The measured gap on the feed section (feed position of the pressure sensor) was 2.0mm. This clearance value differs from the 2.8mm due to a slight protrusion of the local area which occurred due to the metallic block welding on which the sensor was mounted.

Water (or a pulp suspension) when entering the feed chamber is not immediately entrained by the fast moving rotor, so that there is a higher speed difference between the axially fed water and the rotor. This result in a higher magnitude of the pressure pulse, in the feed section compared to the downstream sections as the fluid is progressively entrained by the rotor tip to stabilizing value.

The main difference in the two pressure pulses illustrated in Figure 138 is the truncated shape of the negative pulse B, which is due to the fact that, as feed pressure was lower, the negative pressure could not fully develop being limited to the absolute zero pressure. This means that consequently less flow was re-pumped, leading to a larger (wider) negative pressure pulse compared to negative pulse A, where the higher amount of re-pumped flow should 'fill in' more quickly the volume behind the rotor tip and the screen basket, and thus reduce the duration (width) of the negative pulse. Further consequence of the truncated shape of the negative peaks, i.e. a prolonged time at close to zero pressure, were observed in the middle section of the screen basket.

The effective velocities for A and B were 5.30m/s and 4.70m/s respectively.

[1] Inlet absolute pressure to the screening system.

[2] Here global signifies overall, inlet to accept pressure drop across the screening system and not across the screen plate.

- Middle section of the screen cylinder:

The pressure pulsations observed in the middle section of the screen plate were characterised by very different graphs reported in Figure 139 in comparison to those observed in the feed section

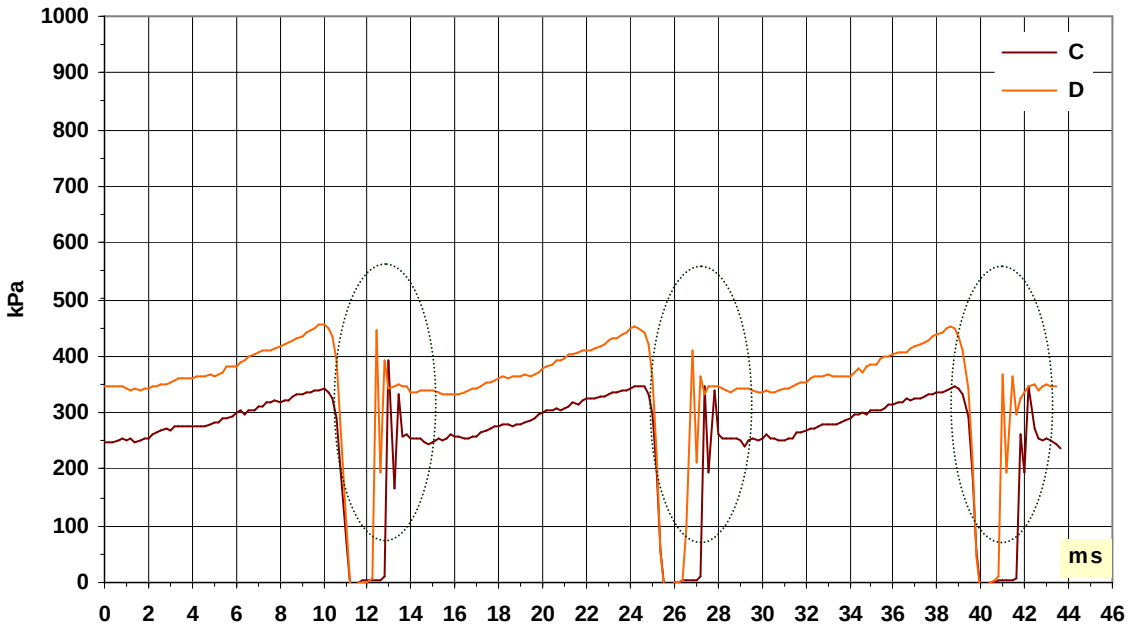

Figure 139: Middle-section average pressure pulsation graphs (water)

With:

C graph conditions: R_v 20%, V_p 1.22m/s (Q_a 125m^3/h), P_i 250kPa, Δp 30kPa (global)
D graph conditions: R_v 33%, V_p 0.74m/s (Q_a 76m^3/h), P_i 340kPa, Δp 30kPa (global)

In general, the graphs had truncated bottom sections and in some cases the absolute 0 pressure was not reached. Another characteristic feature of the pressure pulse at this particular screen plate position was the presence of heavily accentuated short burst of positive peaks at the end of the reverse pulse. This is illustrated by the maximum pressure pulse graph in Figure 140. The presence of such sharp peaks and several of such 'disturbances' (indicated in dotted ellipses in Figure 139 for average values), together with the truncated bottom sections strongly suggests cavitation phenomena occurring at this positions, with several disturbances indicating to several cavitations bubble formation. Indeed, the magnitude of the negative pressure pulse reaches below the vapour pressure of the liquid leading to the formation of several cavitation bubbles. Lying in the middle of the screen plate, this particular position on the screen plate does not allows axial flow of pressure increase to kill or disrupt the formation of one or several cavitation bubbles. At the end of negative pressure pulse, due to an increase of pressure of the surrounding medium these bubbles implode (in 100th of millisecond) creating a peak pressure of several hundred kPa (for example 900kPa in Figure 140)

The effective velocities for C and D were 5.6m/s and 3.60m/s respectively.

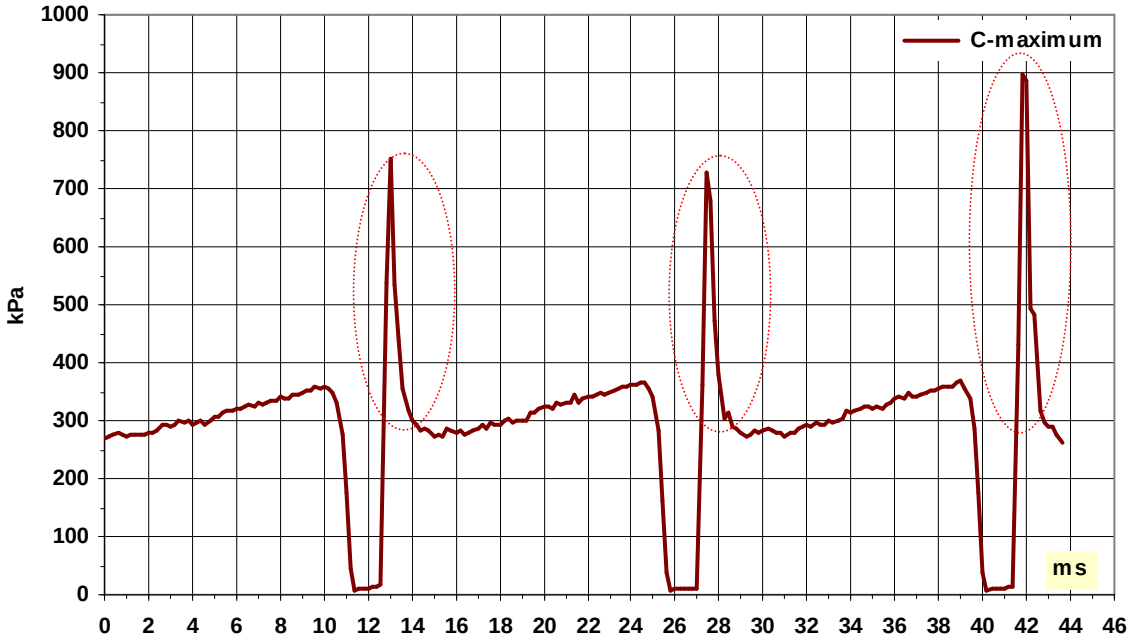

Figure 140: Mid-section maximum pressure pulsation graph for condition C (water)

- Reject section of the screen cylinder

The evolution of reject section pulsation graphs was similar to the middle section graphs as represented in Figure 141.

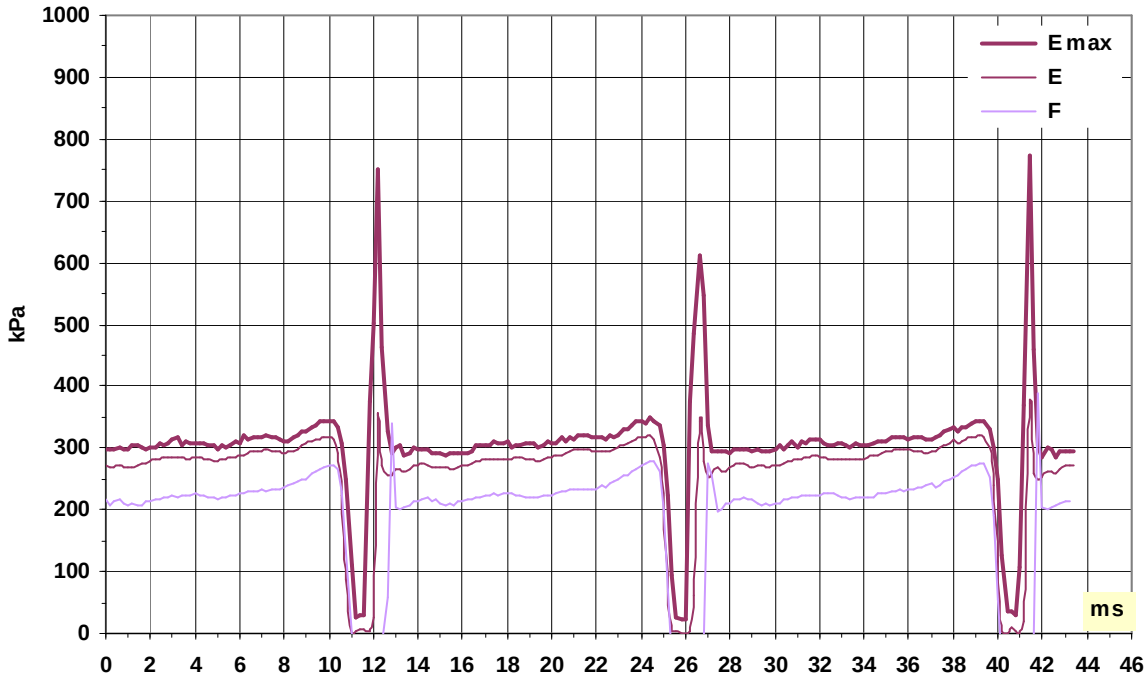

Figure 141: Reject-section maximum pressure pulsation graph for condition C (water)

With:

E graph conditions: R_v 33%, V_p 0.97m/s (Q_a 100m^3/h), P_i 260kPa, Δp 45kPa (global)
F graph conditions: R_v 21%, V_p 0.48m/s (Q_a 50m^3/h), P_i 200 kPa, Δp 05kPa (global)

The presence of flat negative pulse peak graphs was observed with sharp high pressure peaks (graph E max) after the end of negative pulse, this again indicates to the cavitation probability occurring at the surface of the rotor hydrodynamic tip. The effective velocity for E and F were 4.0m/s and 3.8m/s respectively.

A particular feature in the reject section could be due to the pumping effect generated by the rotor in the reject chamber (due to the rotation of the fluid, i.e. the radial pressure gradient) and axially towards the reject outlet since the rotor pressure pulse elements are not parallel to the central axis (cf. Image 2). Their non-linear axial arrangement could lead to a 'pump' effect and acting as a 'propeller' could lead to a higher suction/depression at the reject side, hence a higher probability of cavitation.

This additional suction effect, dP_r, induced by the rotor was evaluated considering the radial pressure gradient the basket surface and the rotor core, assuming a 'solid body' rotation of the flow at an angular velocity ω_f as given in Eq. 24. On the basis of the work by Grégoire [158], showing that the flow entrainment could attain a value of 60-66% with an axial flow rotor (according to respectively numerical simulation and experimental results) it is expected that the flow entrainment ratio should be at least 70% with closed rotor.

Eq. 24 :

$$dP_r = \frac{1}{2}\rho\left(x.\omega_r\right)^2\left(R^2{}_s - R^2{}_r\right)$$

ω_r: Rotor angular velocity, 148rd/s
ρ: Water density, 1000kg/m^3
R_s: Screen basket radius, 0.353m
R_r: Rotor solid core radius, 0.326m
$x = \omega_f/\omega_r$: flow entrainment ratio

The results obtained are indicated in Figure 142 and show that at a level of entrainment of e.g. 70%, the depression values relate to approximately to 25kPa. The values so obtained correspond to the 'missing' pressure in truncated flat graphs at position N°3 to reach absolute 0 values.

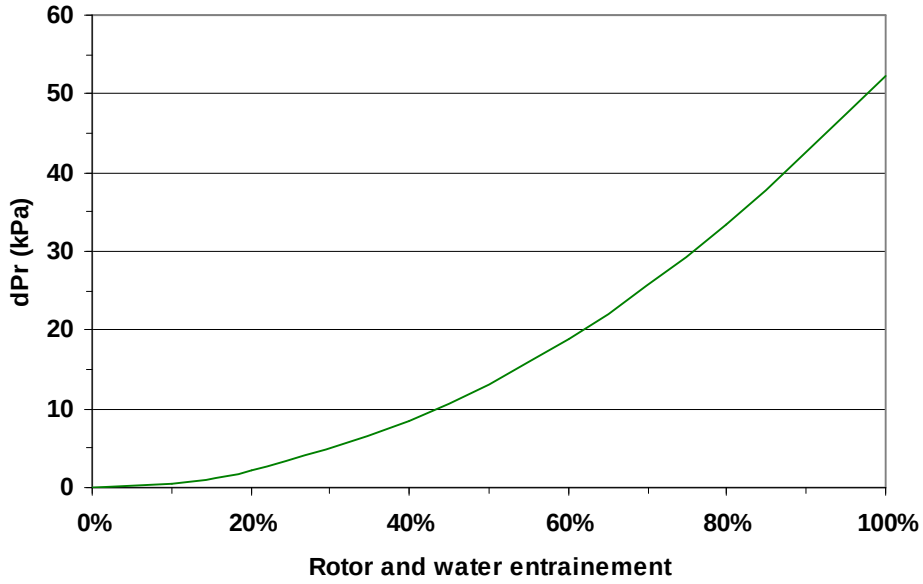

Figure 142: Rotor suction pressure due to foil arrangement

For the case of 4g/L DIP pulp, similar trends were observed as reported in the Figure 143, with truncated bottom sections at position 2 and 3, confirming the evolution as found in case with water.

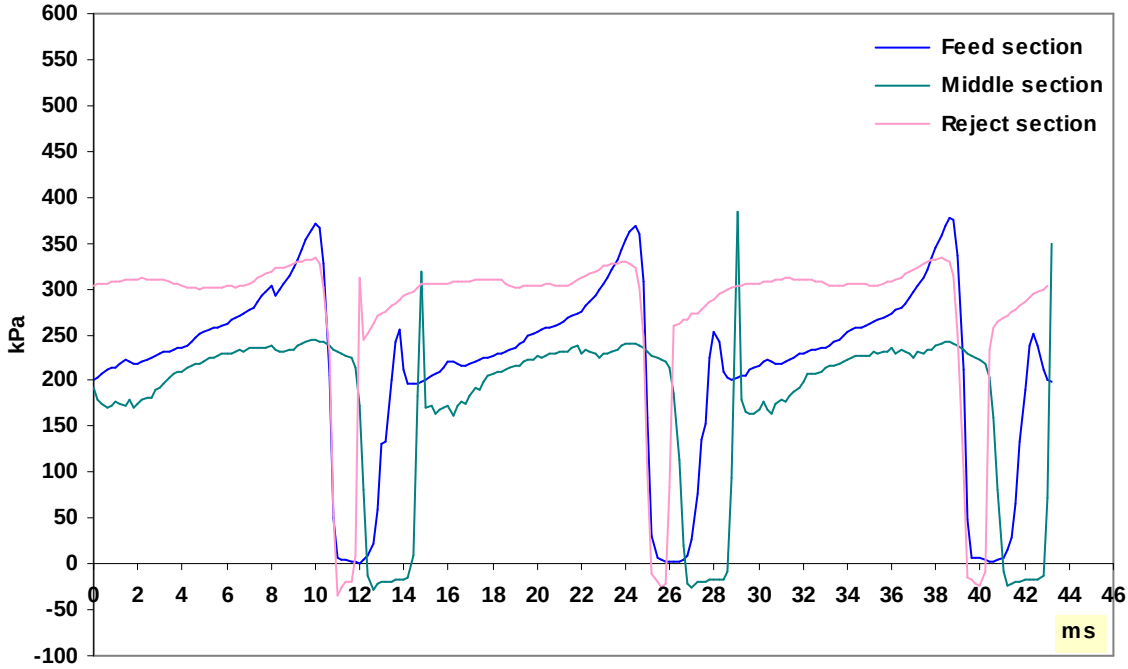

Figure 143: 4 g/L DIP pulp pressure pulsation graph for all sections (pulp)

Feed section conditions: R_v 39%, V_p 0.50m/s (Q_a 52m^3/h), P_i 215kPa, Δp 40kPa (global), Ve 4.50m/s
Middle section conditions: R_v 40% V_p 0.49m/s (Q_a 50m^3/h), P_i 180kPa, Δp 35 kPa (global), Ve 2.98m/s
Reject section conditions: R_v 09% V_p 0.50m/s (Q_a 52m^3/h), P_i 280kPa, Δp 60kPa (global), Ve 2.63m/s

Figure 144 groups together the passing velocities tested at the 3 positions (different operating conditions) and the effective passing velocity, V_e. The graph also shows the theoretical depiction of the conditions where effective and global passing velocities are the same.

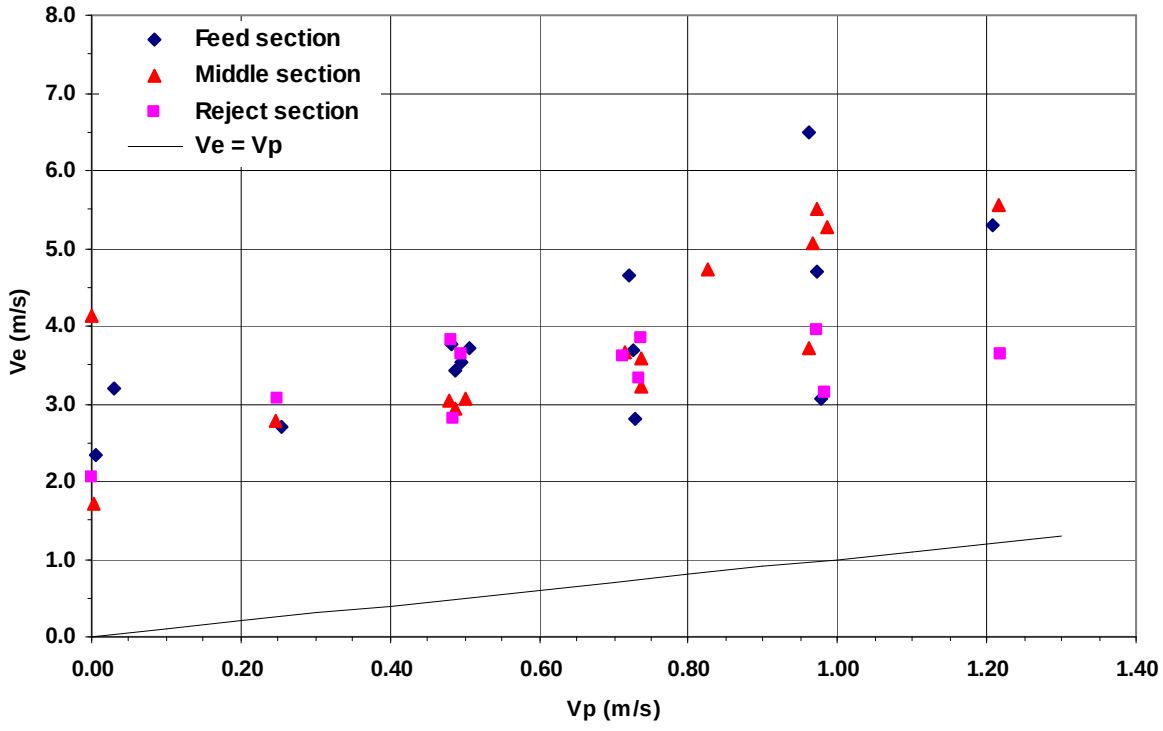

Figure 144: Effective passing velocity variation with respect to passing velocity with water

Indeed, there is a large dispersion of the data points due to the different screen operating conditions, but some general conclusions can be drawn from the graph.

The first observation is that the effective passing velocity is significantly higher than the average passing velocity, adding 3 to 4m/s passing velocity due to the reverse flow, to the average passing velocity given by the accept flow rate.

Secondly, the effective passing velocities estimated for the reject section are lower than those obtained at the feed and middle sections of the screen plate. This could be explained by the lower magnitude of the negative pressure pulse and thus the lower reverse flow generated at these sections.

On average for the whole screen cylinder the main conclusion is that at a given average passing velocity, i.e. at a given accept flow rate, changing other parameters like feed pressure (with an impact on negative pressure pulse, which can be truncated if Pi is too low) and reject flow rate, can significantly change Ve while the effect of changing Vp is relatively lower.

The latter observation gives a strong conclusion why the passing velocity did not have a clear significant effect on fractionation during the experimental trials. Indeed as it can be observed from Figure 144, for the average passing velocity values tested (0.3m/s and 0.7m/s), there was no huge effective velocity change and more importantly it did not double with an increase of average velocity from 0.3m/s to 0.7m/s: at lower range of average velocity (~0.3m/s) the effective velocity ranges between 3and 4m/s, while at double the average velocity (0.7m/s), the effective velocity remains at 4m/s and does not double to 6 or 8m/s.

The pressure coefficient, Cp (Eq. 2) calculated for the positive pressure pulse and the ‘complete’ (non-truncated) negative pressure pulse gave the following average values for the feed section:

Cp (-): 1.15
Cp (+): 0.64

The CFD simulations established by Grégoire [158] indicated the possibility of a pressure coefficient exceeding the value of 1.0, with consequently the probability that the fluid motion is reversed in the screen plate rotor gap with respect to rotor direction. Experimental measurements with a large range of rotor types gave a coefficient of ~1.0 demonstrated with a foil type rotor for 4mm clearance and with a ‘wing’ type rotor a Cp of ~0.75 for 3mm clearance.

The experimental suction pressure coefficient obtained on an average for a given rotor was compared with other results obtained with different rotor at different gaps by Pinon *et al*. [124], Feng *et al*. [125], Grégoire [158] (data plotted from the results) and is reported in Figure 145.

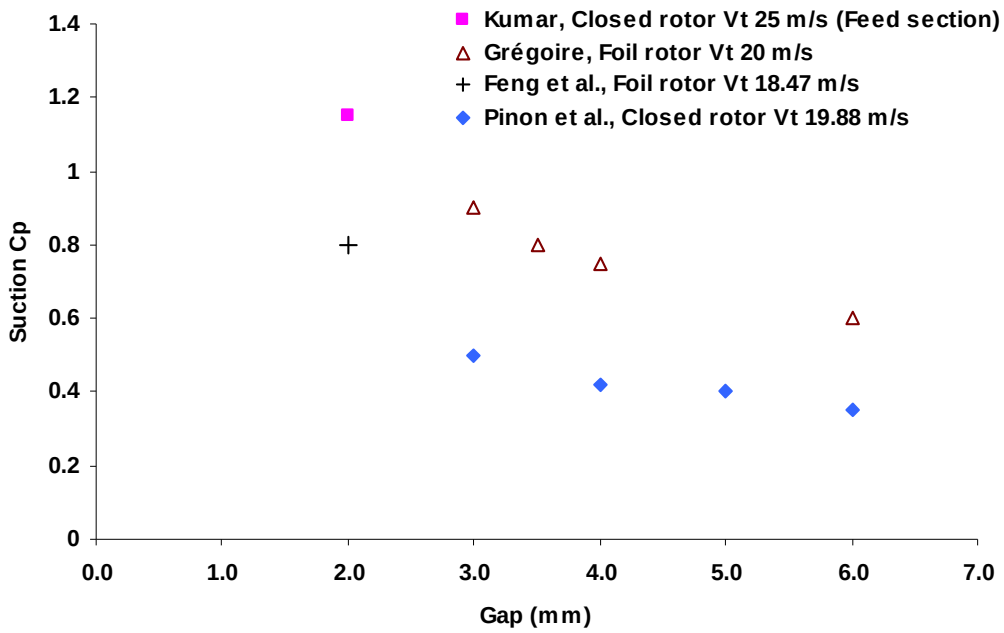

Figure 145: Suction pressure coefficient vs basket and rotor gap

The results show the strong influence of rotor tip to screen plate clearance on the suction pressure coefficient and are in line with the trend observed by Grégoire [158] but overestimated in comparison to Feng *et al*. [125] and Pinon *et al*. [124]. One possible reasons of this overestimation could relate to the measurement method, where for Feng *et al*. [125] and Pinon *et al.* [124] the measurements were performed on a smooth wall slice screen of 5cm width. This does not take into consideration the reverse flow and the wall effects that could arise thereof.

It has been well documented that increasing the suction pulse increases the screening system capacity and especially at higher pulp concentrations. However, during the experimental trials it was not possible to increase the average passing velocity at higher concentrations and low volumetric reject rates. Analysis has been made to understand the possible reasons and is reported in the section 3.2.3.2. -Fibre accumulation and screen capacity.

3.2.3.2. - Fibre accumulation and screen capacity

During the screening phase (duration of the positive pressure pulse) suspended matter of the pulp suspension accumulates on the screen surface. The 'retained ratio' of the different pulp components could lead to a significant amount of fibres being deposited on the apertures, hence leading to the possibility of progressive screen plugging during the screening phase and more importantly the inability to increase the hydraulic loading, i.e. the 'average' passing velocity.

In the duration of the positive pulse phase, quantity accumulated on the screen surface was evaluated as a grammage (g/m²) of fibre. The first mathematical model of fibre accumulation was proposed by Julien Saint Amand, where the author considered a host of variables and the duration of the positive pressure pulse [159]. The present calculation was based on the hypothesis that the suspended matter associated with the total effective volume (re-pumped + injected) gets deposited 'uniformly' on the screen surface with a retained ratio of (1-P) where P values are obtained with the plug flow model in the analysis of fibre passage ratio for different fibre lengths. A passage ratio of 0 will indicate 100% retention of this class of fibre on the screen surface.

Analysis was also made in terms of the resulting pulp concentration of the pulp that has to 'pass' or 'squeeze' through the clearance between the screen basket and the rotor tip. The calculations were made on the basis of the 'average' clearance of 2.8 mm.

A too high value of the concentration reached at the end of the screening phase in this pulp layer is expected to impair the fractionation process and limit the screen capacity. A too thick pulp may not pass the clearance and/or lead to pressing and squeezing of large particles into the micro-holes. The fibres and other particles (or contaminants) accumulated on the surface experience intermittently large forces during the positive pressure pulse. Being continuously pressed against the openings, the pulp entities try to force themselves into the micro-holes, resulting in their partial or complete blockage. Indeed, this was observed with another set of experimental trials (not reported in the manuscript) with mechanical pulp (TMP), where the fibre bundles or shives as can be observed in Figure 146, blinded the apertures. Their 'width' was approximately equal or slightly more than the micro-hole diameter. Indicating once in, they get blocked in the micro-hole, effectively blinding the aperture.

Figure 146: TMP shives blocked the screen apertures

The average variation of Ve is represented in Figure 147. The evolution has been obtained by averaging the Ve values for similar V_p values from the Figure 144. This shows that Ve varies between 2 and 5m/s. This has been done to understand the phenomena of fibre mat deposition and quantification at various values of passing velocities.

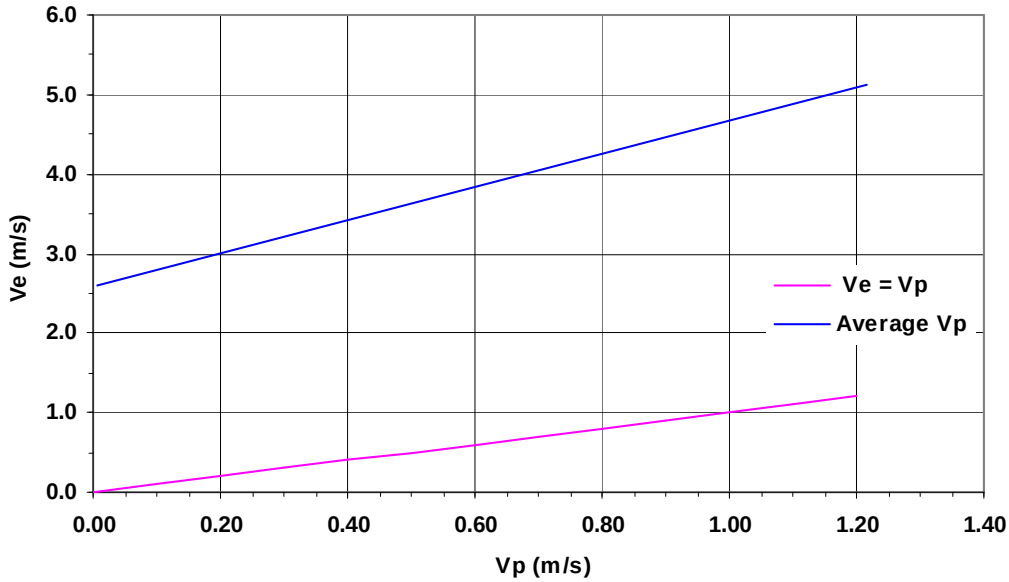

Figure 147: Average and effective passing velocity variations (water)

The results for fibre amount (grammage) deposited and the equivalent concentrations were calculated for SGW pulp at two inlet concentrations of 5g/L and 11g/L, at similar value of R_v (20%) and average passing velocity 0.3m/s V_p. The product of the effective velocity (m/s), screen open area (m^2/m^2) and positive pulse duration (s) gave the total 'effective' suspension volume (m^3) that is projected per unit screen surface (m^2). The fibre concentration (g/L) in different fibre length classes that was retained with a factor of (1-P) and the effective volume gave the grammage deposited on the screen surface. The estimations have been made for feed side taking into account the inlet concentration and reject side taking into consideration the thickening factor.

The results for pulp deposition are reported in Figure 148. Reject side experience higher fibre deposition and the severity increases with an increase of inlet concentration (as higher reject concentration occurs) and an increase of Ve. It could be indicated that for a Ve of 4m/s at the two inlet concentrations, a value of ~70-100g/m^2 deposited fibre on reject side could lead to a 'complete' aperture 'coverage' and disruption of screen running. Whereas on the feed side, even at the two inlet concentrations, the deposited fibre amount is comparatively less, ~20-35g/m^2 (for a Ve of 4m/s) and will not hinder screen operations.

Figure 149 shows the effective concentration in the rotor tip and screen cylinder gap. The situation is similar as seen for fibre deposition. Higher Ve and inlet concentration induce higher effective pulp concentration at the reject side. Low effective concentration can be 'handled' by the screening system at the feed side. A further increase leads to a critical limit where it results in screen plugging.

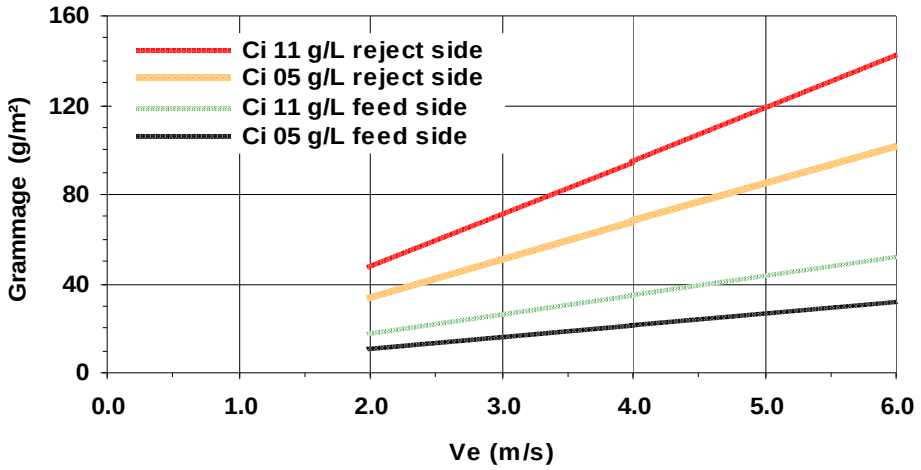

Figure 148: Effective velocity and pulp grammage deposited on screen cylinder surface

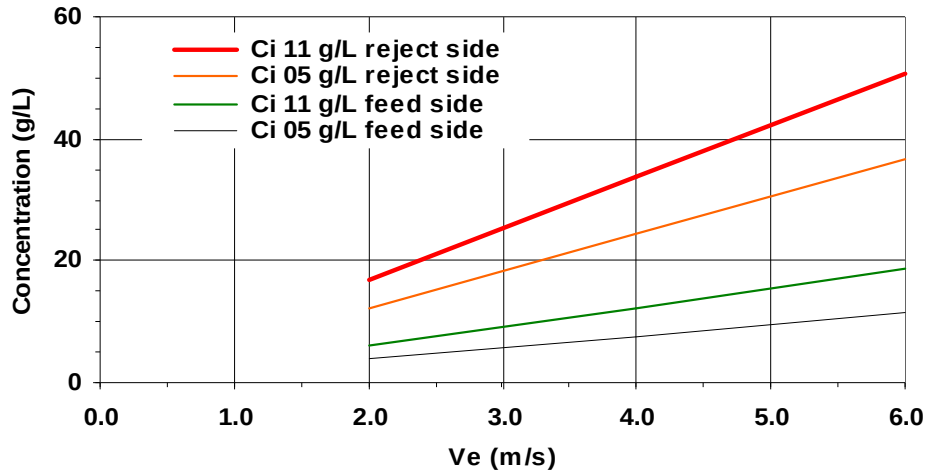

Figure 149: Effective velocity and concentration in the rotor-screen cylinder clearance

This was also experimentally observed when measuring the screening system pressure drop for different pulps. The experiments were made keeping accept and feed valves 100% open and throttling the reject valve to increase the accept flow, hence passing velocity (this could be termed as an uncontrolled state). The evolution of the pressure difference between inlet, Pi, and accepts, Pa, is reported in Figure 150.

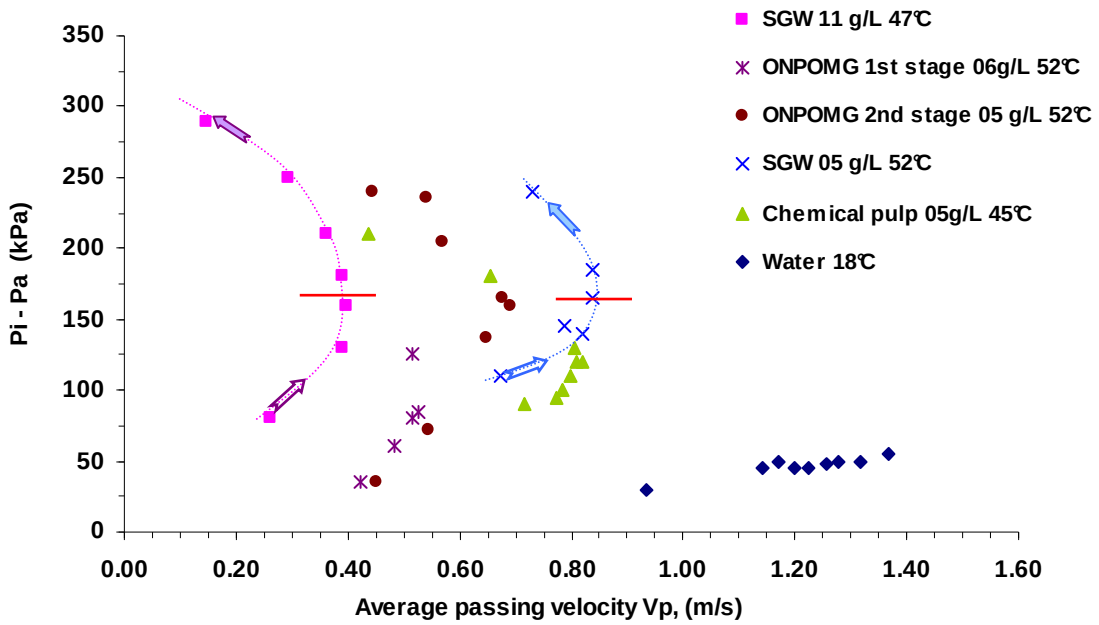

Figure 150: Screening system pressure drop with different pulps and water

Typical evolution of pressure drop was observed for the different pulp studied. Except for the case of water, the curves had a *mirror* 'C' shape. As an example, the case of SGW pulp is elaborated for the two pulp concentrations studied. In the first half of the curves, the pressure drop increased with an increase of passing velocity -indicated by a hollow arrow. In the second half, pressure drop increased but any further increase of passing velocity was not possible as indicated by a solid arrow.

In the conditions studied, the 'maximum' average passing velocity, V_p, achieved at 11g/L and 05g/L was 0.4m/s and 0.9m/s respectively. At these V_p, the effective velocity, Ve and hence the amount (grammage) of fibres deposited on the screen surface reject side can be calculated using the Figure 147 and the Figure 148 respectively.

Table 18: Fibre accumulation for SGW pulp at two concentrations

	Vp m/s	Ve m/s	Fibre accumulation (reject side) g/m²
SGW 05 g/L	0.9	4.5	~80
SGW 11 g/L	0.4	3.5	~80

Table 18 indicates that the critical value of ~80g/m² fibre accumulation initiated the decrease of accept flow. During the initial increase of passing velocity, the fibre accumulation is not severe and moreover the feed section of the screen basket is 'more' available/open/clear of fibre accumulation than the reject side. On further closing the reject valve (or to increase the accept flow), the 'network' of fibres deposited between the passages of rotor hydrodynamic elements made it difficult for the passage of fibres and fines. A deposit of ~80g/m² is non-negligible considering the fact that the 'long' fibres which have 0 fibre passage ratio are 'stacked' over one-another, completely covering the screen hole-openings. The first accumulated fibres act as a seed for the others, which then rapidly deposit. As the holes are themselves less than 500µm apart, it can be hypothesised that a ~2mm long fibre gets stuck/ stapled in adjacent holes. This situation then deteriorates more and the pressure drop increases while the flow across the screen plate decreases.

This phenomenon of fibre accumulation and pressure drop is explained further in analysing the pump pressure-flow characteristic curve with the pulp, which is the curve of the flow developed, Q_i, by the pump against the pressure head, Pi.

In analysing the pressure drop, normally the difference between the inlet pressure-Pi and accept pressure-Pa is taken into account. This pressure drop is a function of the accept flow, Q_a. However, it should be noted that at the feed (up-stream) side of the screen in the axial direction, the inlet pressure 'reduces' to reject pressure. Hence the pressure drop at the inlet section of the screen basket is between inlet pressure and accept pressure whereas on the reject side between the reject, Pr, and accept pressure.

Or in a simplified expression, the pressure drop could be represented as in Eq. 25, which is also a function of Q_a.

Eq. 25 :

$$\Delta p = \left(\frac{Pi + \mathrm{Pr}}{2} \right) - Pa$$

An example is given for SGW pulp in Figure 151. The graphic shows the measured pressure difference and the pump characteristic curve and the curve 'approximate' extension. As an indication, the estimated pressure drop curve is also represented.

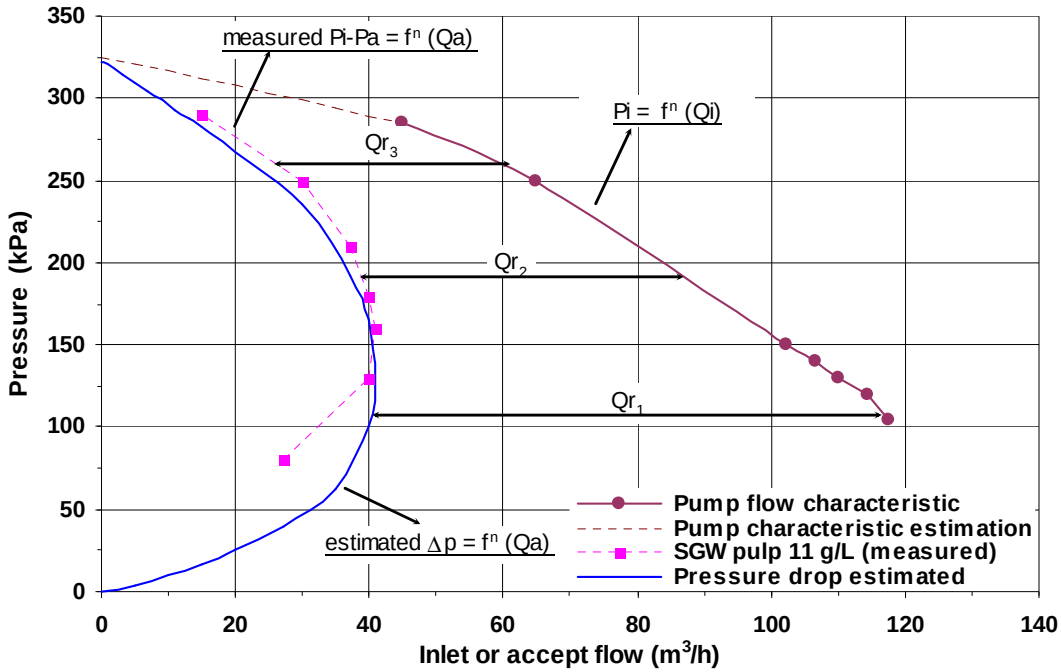

Figure 151: SGW pulp flows and pressure evolution

After the initial increase, the accept flow (or the passing velocity) and measured pressure drop aligns itself with the inlet flow and tends to follow the pump characteristic curve as the reject flow rate is reduced.

The estimated pressure drop curve can be explained taking into consideration the rejects flows (valve open -Qr_1, valve closed/throttled- Qr_3) and the corresponding reject pressure which is of the order of:

$$Qr_1 > Qr_2 > Qr_3$$
$$Pr_1 < Pr_2 < Pr_3$$

When the reject valve is fully open (Qr_1) the reject pressure, Pr_1 is very low, the estimated pressure drop is less severe and approximates to: $(P_i - P_a)/2$. Hence, a large difference is observed between estimated and measured pressure difference curves.

But when the reject valve is closed, the reject pressure increases. When the reject flow is zero, the reject pressure approaches the inlet pressure, P_i. The estimated pressure drop in this situation becomes similar to measured or: $P_i - P_a$. Hence less difference is observed between estimated and measured curves.

It must be noted that accept flow does not drops to zero which indicates that part of the screen, mainly at the feed side is still 'active'. Fibre accumulation (and non-'removal' from the screen surface) which results in flow reduction should be clearly differentiated from screen aperture blinding/clogging where no accept flow is possible.

The above analysis conclusively shows the reasons why it was not possible to increase the average passing velocity at higher concentrations when using a micro-hole screen basket.

3.3. - Conclusions

Pulp screening with small apertures baskets provides an effective means of fractionation primarily based on fibre length, while fibre rigidity is a secondary factor.

Laboratory understanding of fines passage ratio reveals cellulosic fines do not have a perfect passage ratio of 1.0 across their defining aperture while the small mineral fillers attain a value of 1.0.

The operating and pulp conditions tested during the pilot trials with the micro-hole screen and a solid-core rotor pressure screening configuration showed that the operating parameters of passing speed and pulp concentration have a very low or negligible effect on fractionation quality. Micro-hole screen baskets preferentially separate fines into accepts, additional screening stages on the reject treatment leading to reduction of residual fines in the rejects.

Analysis of the passage ratio based on fibre length shows that the fractionation system consisting of the solid core rotor and micro-hole basket follows the plug flow model with a degree of fractionation, β, approaching 1.0.

Pressure pulses produced by the solid core rotor show a high magnitude of negative pressure pulse with a cavitation phenomenon occurring at the middle and reject sections of the screen basket. The high magnitude of the negative pressure pulse, does not translate into a higher capacity. The effective passing velocity does not increase in the same ratio as the average passing velocity, hence diminishing considerably its effect on fractionation. The inability to increase the average passing velocity at higher concentrations is tied to the fibre amount deposited on the screen surface. This problem accentuates at the reject end at higher inlet concentrations.

Fractionation by micro-holes leads to better fractionation than a micro-slot basket. Micro-hole screening provides excellent industrial equipment to preferentially separate cellulosic fines, which can then be used to control specific sheet properties.

4. - Application of fractionation to deinking and paper layering

4.1. - Paper layering optimisation

4.1.1. - Context

Traditionally paper is a single layer structure. Controlled dewatering of a suspension of fibres, fines, additives and inorganic fillers results in a 'single' layer paper sheet structure, where all the entities which are present in the final sheet are mixed. This differs from a stratified formation, which leads to a multi-layered structure. The concept of multi-layer forming is not new; as an example Felsvang *et al.* [76] (cf. Figure 64) mentioned the usage of fractions in different layers of a paper structure. It must also be noted that some paperboards and tissue paper are in fact multi-layer products. In case of board, the layers can also be manufactured in individual headboxes and joined together at a later stage once they have been formed.

Stratified forming with different pulp and /or pulp fractions (Figure 152) has been investigated in the framework of the EcoTarget project considering a more environmental friendly approach for production of paper using less raw material with similar (reference) or better strength and sheet properties.

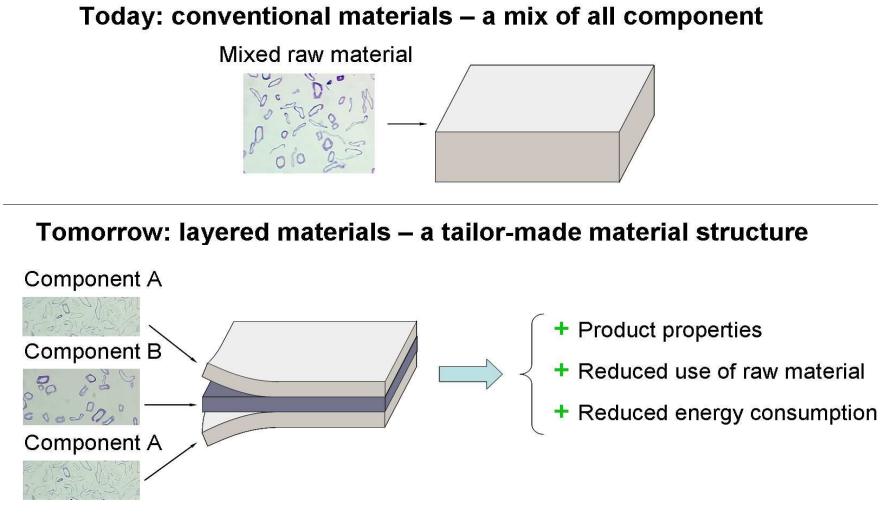

Figure 152: Single and multi-layer sheet structure concept [6]

A new patented headbox design [160] of multi-layer forming was evaluated and showed that stratified sheets using less amount of fibres provided similar or better properties as mono-layer sheet structure. This provided large economical potential in terms of energy and raw material reduction. Higher amount of mineral filler in stratified format could be loaded in the final paper while maintaining the desired sheet strength, hence leading to the replacement of the expensive cellulosic fibre [161]. The headbox design consisted of a new method of layer separation by a 'passive' liquid layer known as 'Aqua – vanes' [161], which enabled to reduce layer mixing as illustrated in Figure 153.

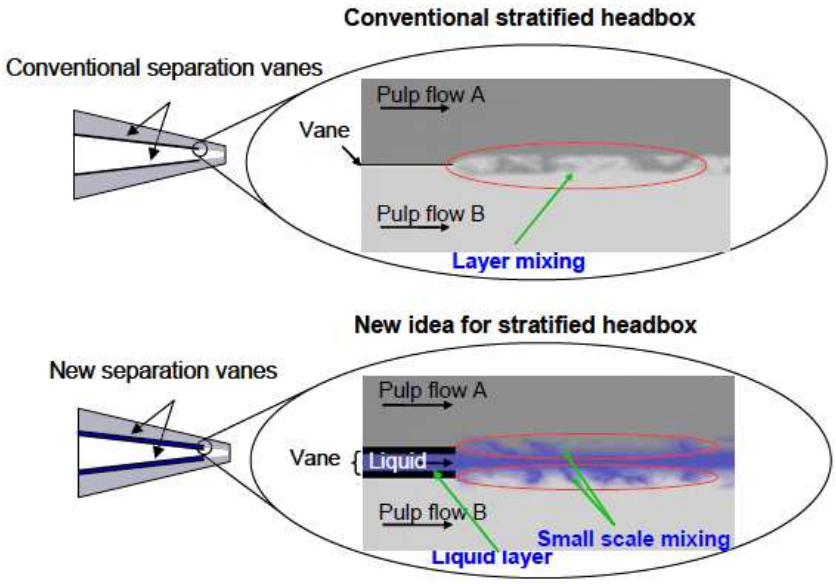

Figure 153: Pulp layer separation by Aqua-Vanes, from Soderberg [161]

The multi-layer headbox provides flexibility to layer different pulps or direct different fibre fractions to different positions in a stratified sheet structure, thereby optimizing it. This means, well developed, fibrillated, flexible, thin cell wall fibres and fibrillar fines can be placed on the surface layers, whereas coarse, bulky, thick cell wall fibres, flake type fines and 'contaminants' (for example shives and specks concentrated in a specific fraction in case of deinking pulp) can be 'hidden' in the middle layer, resulting in a 'tailor-made' structure. Indeed, these fractions are 'separated' components of a pulp suspensions obtained after fractionation.

It has been described and illustrated in the Chapter N°2 devoted to Fines and Their Characterization that fibrillar fines define paper sheet strength properties. Similarly fibre cell wall thickness has a pronounced effect on sheet strength properties. Thin cell wall fibres give better strength properties as they are more collapsible providing a higher bonding area. The thick non-conformable cell wall fibres have inferior strength properties. The influence of cell wall thickness has been studied by many authors. For example Panula-Ontto [97] studied the effect of cell-wall thickness of a hydrocyclone fractionated bleached softwood kraft pulp after laboratory refining (PFI). Decreasing cell wall thickness improved substantially the relative bonded area (RBA) and sheet strength properties (cf. Figure 154)

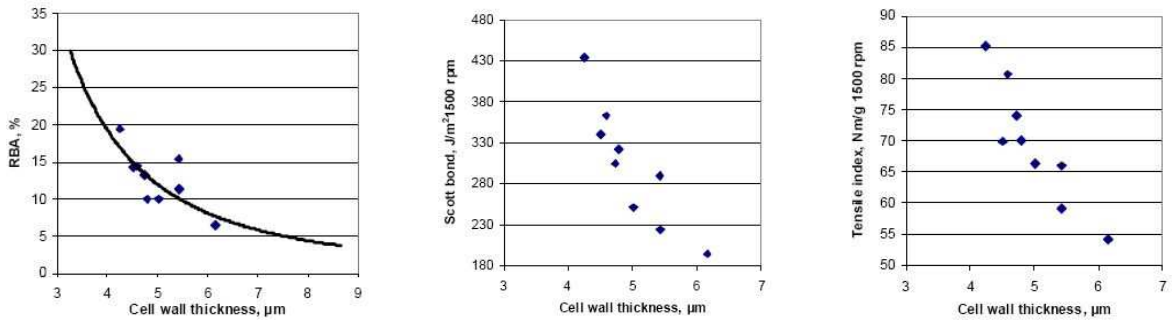

Figure 154: Effect of cell wall thickness (obtained by hydrocyclone fractionation) and sheet properties, from Panula-Ontto [97]

Similar findings of the effect of fibre cell wall thickness have been reported by other authors, Paavilainen [96], Reyier [98], Vomhoff [100] and Pande & Gratton [162].

Since fines play a pivotal role in defining sheet properties, the first part in this chapter deals with fines fractionation and their effect on sheet properties in the case of virgin fibre mechanical pulp.

4.1.1.1. - SGW micro-hole fractionation and fine fraction hydrocyclone fractionation

SGW pulp fines obtained from micro-hole screening (3.2.1.2. -Fractionation results) were fractionated using a small diameter – 65mm hydrocyclone. The approach was similar to deinking pulp fines fractionation with the objective of the fines separation according to their properties. The set-up is shown in Figure 155. Fines from micro-hole screening were obtained at 5g/L, 0.7m/s Vp and 20% R_v. The inlet concentration to the hydrocyclone was 3.2 g/L.

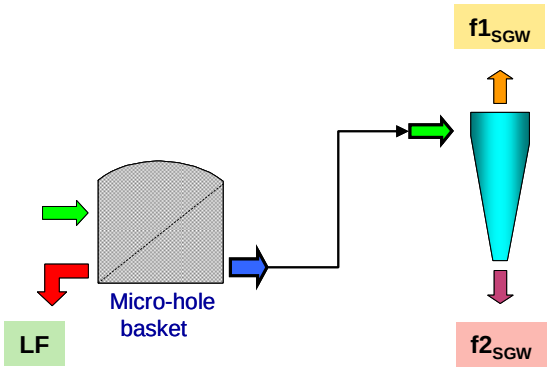

Figure 155: Fines fractionation set-up

Hydrocyclone was first calibrated by varying R_v in recirculation mode in order to determine the operating conditions to get equal proportions of the 2 fine fractions. The fines suspension was at 51°C and the pressure difference was kept constant at 150kPa.

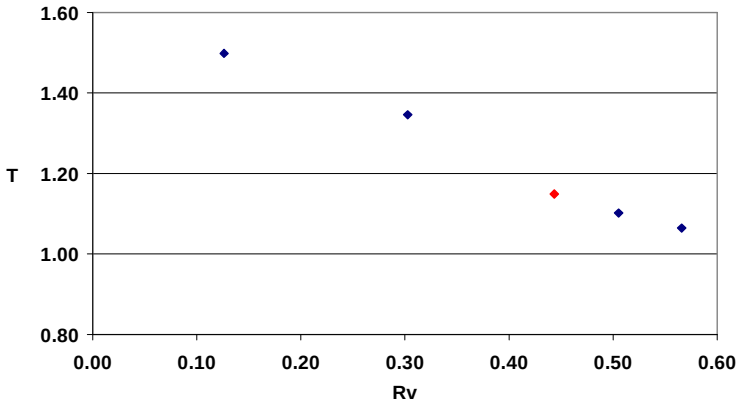

Figure 156: Thickening factor and R_v for SGW pulp hydrocyclone fractionation

The results are illustrated in Figure 156 (the red mark indicating the operating conditions for 50% Rm).

4.1.1.2. - Microscopic and morphological properties of the produced fine fraction

Microscopic analysis was performed on screening accepts sub-fractions obtained after soft-hyperwashing (described in 2.2.1. -Fines sub-fractions by soft-hyperwashing method), illustrated in Figure 157.

As evident, the images show presence of very small cellulosic particles, long and thin fibrils. There is also presence of fibre bundles in R50µm fraction.

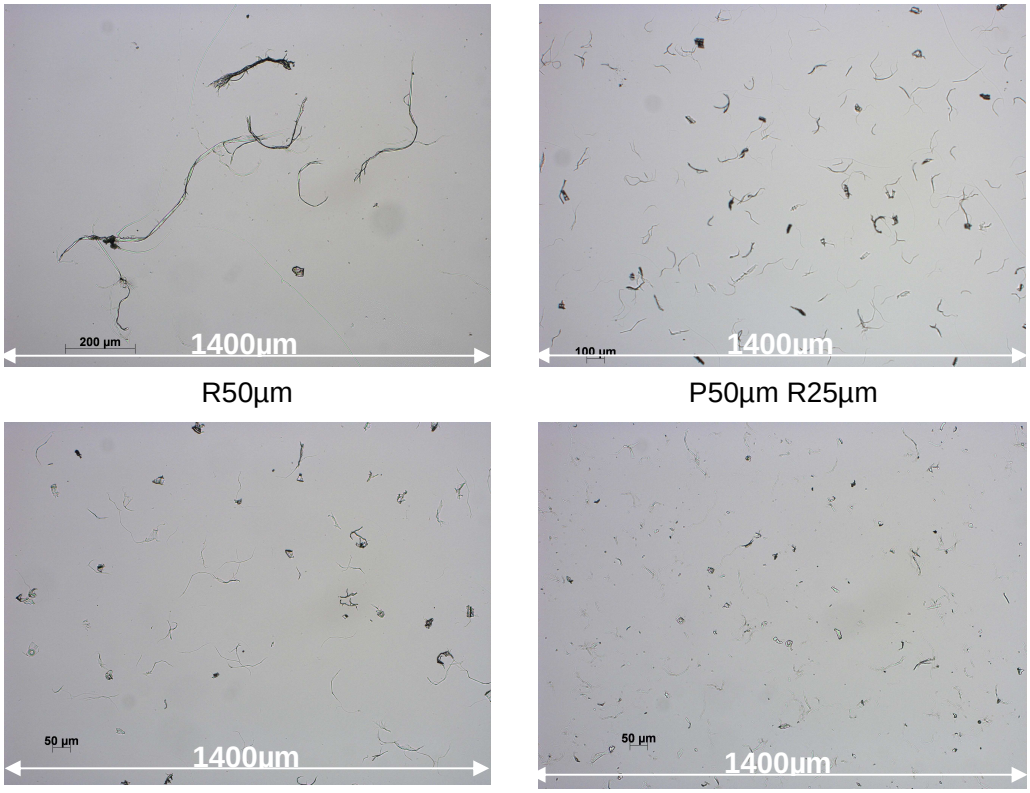

Figure 157: SGW pulp micro-hole accepts sub-fractions

The two hydrocyclone fractions microscopic images are shown in Figure 158. $f1_{SGW}$ type of fines seemed to be more fibrillar in comparison to $f2_{SGW,}$ which contained large fibre 'bundles'.

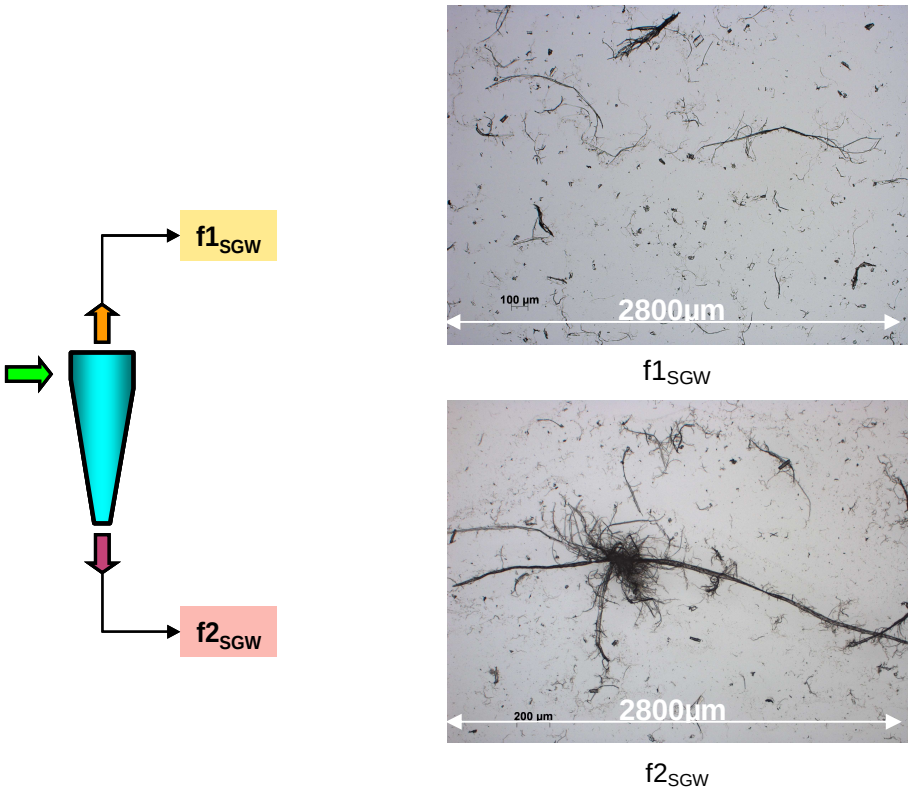

Figure 158: SGW pulp hydrocyclone fractions

Fibre length distributions for accept and rejects were almost identical as illustrated in Figure 159. This shows that Hydrocyclones do not fractionate on the basis of fibre length. Hydrocyclone accepts, have higher proportion of smaller width (as well as higher specific surface area fibres and fines) in comparison to rejects as reported in the Figure 160.

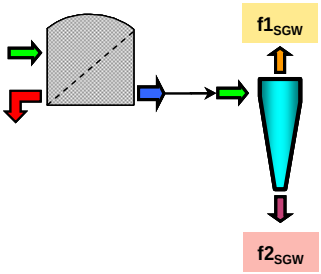

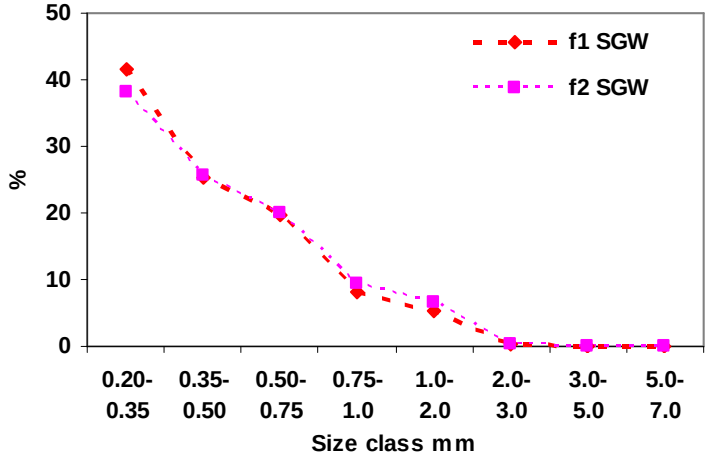

Figure 159: SGW pulp hydrocyclone fractions fibre length distributions

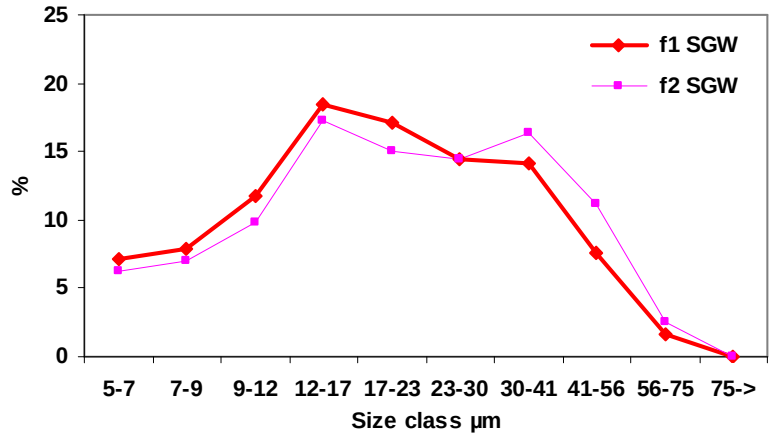

Figure 160: SGW pulp hydrocyclone fractions fibre width distributions

4.1.1.3. - Optimisation of fines distribution in layered paper structure

Once separated, the fines fractions could then be used to optimize sheet properties, especially in case of multi-layer sheet making. High specific surface area fines will lead to better strength and surface properties development. Less fibrillar and flake type fines fractions could then be put in the middle, sandwiched between the better layers.

SGW f1 and f2 fines fractionated by hydrocyclone and long fibre fraction (LF) from micro-hole screening (cf. Figure 155) were used to manufacture 60 g/m² handsheets using water re-circulation (Norm ISO 5269-3:2008 2008-05), by varying their quantity as reported in Table 19.

Table 19: Handsheets long fibre and fines content ratio

1	100 % LF (or 0% f1 & f2)
2	60% LF + 40% f1
3	60% LF + 40% f2
4	80% LF + 20% f1
5	80% LF + 20% f2
6	60% LF + 20% f1+ 20% f2

Manufactured handsheets were tested for mechanical and optical properties as reported in Table 20

Table 20: Norms followed for handsheet property testing

Property	Norm
Sheet thickness, Density	NF EN ISO 534
Air permeance Bendtsen	ISO 5636-3
Bendtsen surface roughness	ISO 8791-2
Light-scattering/absorption	ISO 9416
Opacity	NF ISO 2471
Tensile test	NF EN ISO 1924-2
Z-directional tensile strength (Scott Bond)	T569 om -09
Tearing resistance	NF EN 1974

Addition of fines results in reduction of sheet bulk, with the addition of higher specific area fibrillar $f1_{SGW}$ fines decreasing bulk more than $f2_{SGW}$ fines, Figure 161. As expected, the denser sheets are more closed with $f1_{SGW}$ fines showing higher degree of compactness. This could be observed in Figure 162 which shows that air permeance decrease is less by the $f2_{SGW}$ fines.

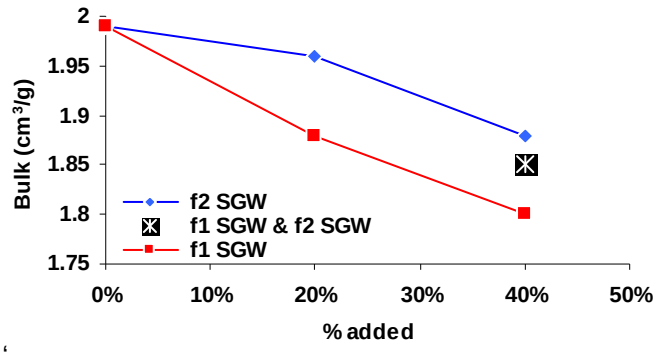

Figure 161: Bulk evolution according to fines type addition

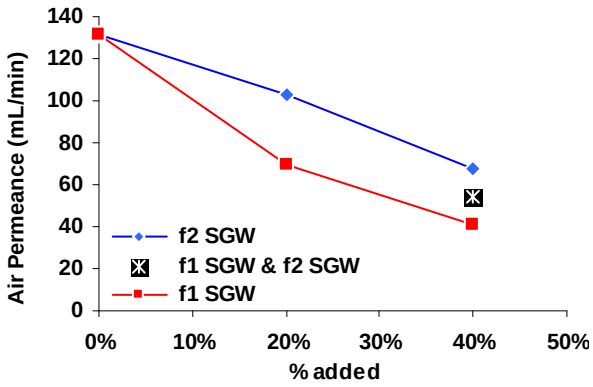

Figure 162: Air permeance (average of wire & felt side) evolution according to fines type addition

Figure 163 shows the increased tensile index value obtained with $f1_{SGW}$ fines whereas the $f2_{SGW}$ fines do not show much influence and even decrease the strength property at their higher concentration. Fibrillar fines impart and enhance strength properties of the sheet structure by improving the inter-fibre bonding. The flake-type fines are incapable of improving sheet structure strength. The results are in agreement with Alince *et al.* [22] as shown in Figure 164. The authors reported the effect of High Specific surface area fines (HSF) and Low Specific surface area fines (LSF) obtained from

fractionation by a small hydrocyclone of TMP pulp fines. The fines in their work were collected by employing a float-wash fractionator equipped with a 100 mesh screen. The authors also showed the comparison of model fibrillar and flake type particles by incorporating micro-fibrillated cellulose (MFC) and micro-crystalline cellulose (MCC) respectively. MFC being fibrillar contributes to increased tensile strength whereas the model MCC negatively affects the fibre bonding.

The $f1_{SGW}$ pulp fines are as effective in increasing the sheet tensile index properties as the model MFC fines reported by Alince *et al.* [22].

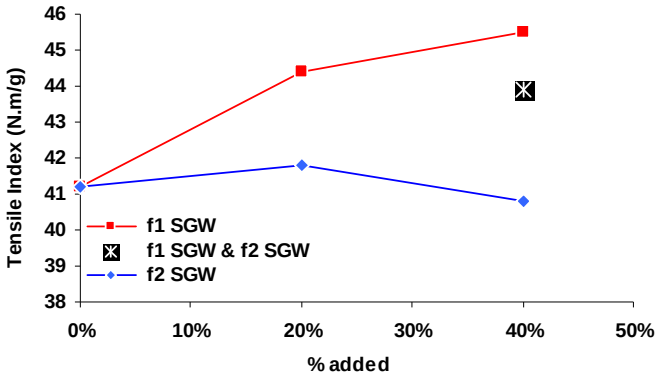

Figure 163: Tensile index evolution

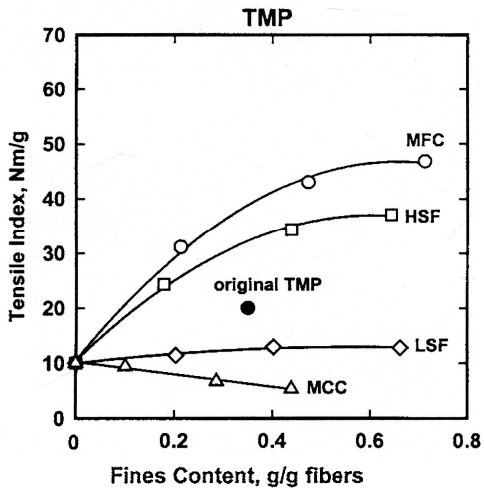

Figure 164: Tensile strength as a function of different types of fines, from Alince *et al.* [22]

The high specific surface area of the $f1_{SGW}$ fines is also highlighted by their higher light scattering coefficient values as reported in Figure 165. Similar trend was also found by Alince *et al.* [22] (High specific area fraction, HSF and low specific area fraction, LSF) and reported in Figure 166.

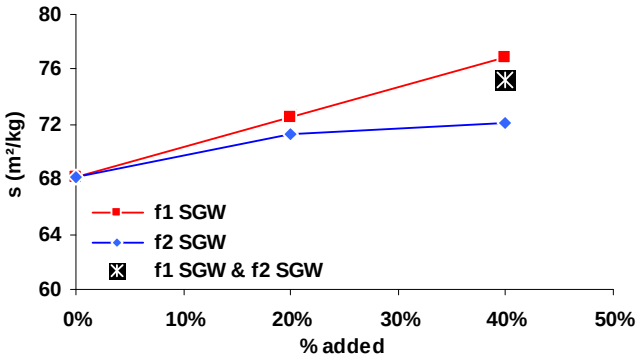

Figure 165: Light scattering coefficient evolution

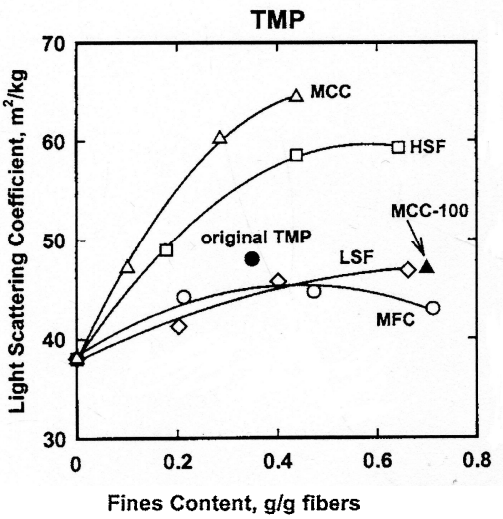

Figure 166: Light scattering as a function of different types of fines, from Alince *et al.* [22]

Figure 167 shows the relation between tensile index and scattering coefficient for the different fines. The fibrillar $f1_{SGW}$ fines are able to improve simultaneously the strength and optical characteristics. But the second category of fines, with lower specific surface, only affect the light scattering, with negligible or negative impact on sheet strength. This is also in agreement with Alince *et al.* [22] and indicated in

Figure 168, where the authors mentioned that the introduction of low specific area fines shows less improvement in light scattering property.

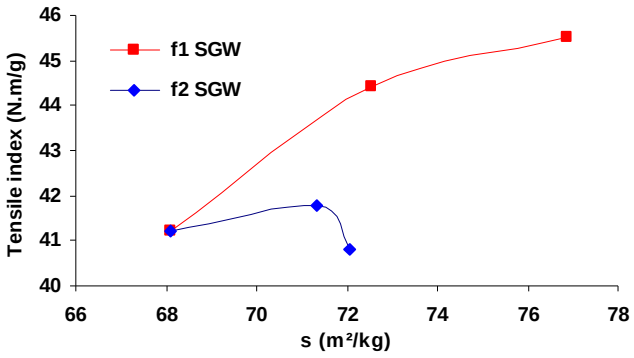

Figure 167: Tensile index and light scattering coefficient evolution

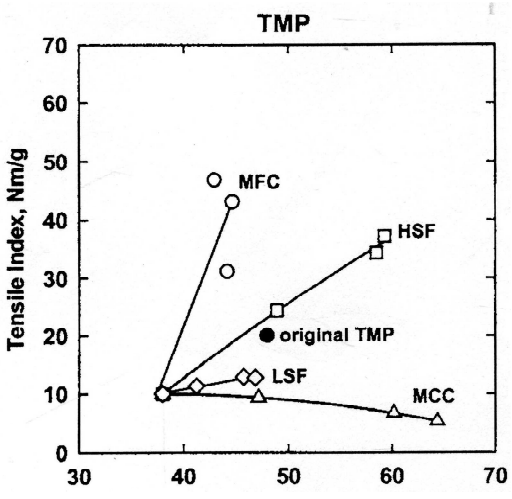

Figure 168: Tensile index and light scattering as a function of different types of fines, from Alince *et al.* [22]

Tear index is adversely affected at higher fines concentrations as reported in Figure 169. This has been previously observed for whole pulp fines and is in agreement with Lindholm [11].

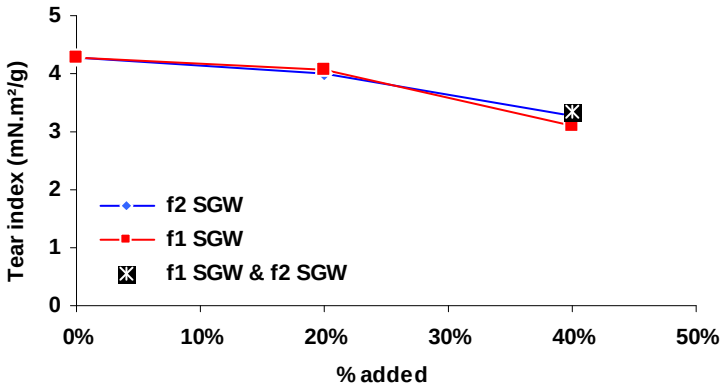

Figure 169: Tear index evolution

Other properties evolutions according to the fines type addition have been reported in the Annexe 10.

4.1.2. - Summarising fractionation of fines by hydrocyclone and sheet properties

Fractionation of SGW pulp micro-hole accepts containing majority of fines with a hydrocyclone results in two distinct fractions: low width, fibrillar, high specific area fines in accepts and high width, low specific area fines in rejects. Fibre length distribution in both fractions remains the same.

Handsheets made on Rapid Köthen laboratory sheet former with varying amounts of the two fractions highlight the positive effect of $f1_{SGW}$ fines (hydrocyclone accepts) on the sheet properties. This is illustrated in the Table 21. For some properties, as indicated in green colour filled boxes, only 20% $f1_{SGW}$ addition was equivalent to 40% $f2_{SGW}$ in terms of different properties.

Table 21: Summary of handsheet properties and fines types

Property / Fines fraction	Bulk (cm^3/g)	Breaking length (m)/ young modulus (MPa)	Tear ($mN.m^2/g$)	Opacity (%)	Light scattering coefficient (m^2/kg)	Air permeance ($cm^3/m^2.Pa.s$)	Scott bond (J/m^2)
f1	↘↘	↗	↘	↗↗	↗↗	↘↘	↗
f2	↘	No effect	↘	↗	↗	↘	No effect

The results indicate that addition of fibrillar fine fraction ($f1_{SGW}$) has a positive effect on mechanical strength properties (example breaking length and Z direction Scott bond), optical properties, as well as sheet surface properties-decrease of roughness. The strategy illustrates that managing fines could produce pulp fractions that can be directed in the right layer of the multi-layer head box, conforming to tailor made multi-layer paper product.

4.2. - Deinking process optimisation

4.2.1. - Context

Increase in energy efficiency and process yield have been the focus area since a very long time and it is still valid especially in today's scenario where energy reduction is of huge concern. A possible and industrial proven way [109] to achieve such targets is application of fractionation. Indeed, deinking process offers vast opportunity for rationalization especially with respect to right treatment to the right fraction.

Being a contamination removal and fibre up-gradation process, separation of defibered pulp into ink rich and ink depleted fractions would rationalise the process operations down the deinking line. Possible energy savings in capacity/equipment design could be achieved as the unitary operations handle the fractions and not the whole pulp.

This concept is illustrated in chapter N°3.1.1. -F ractionation processes, where the early developments and some scenarios are described.

In the last collaborative European Union research project- EcoTarget, research was conducted to provide process solutions to increase the usage of recovered fibre utilisation in European countries. One of the studied areas was related to the application of fractionation to simplify the deinking lines - from two loops to one loop process structure, as illustrated in Figure 170. The analysis was made at laboratory scale for a newsprint grade paper. As shown in Figure 171, application of fractionation after defibering (pulping) operations resulted in two fractions, where dedicated treatment can be implemented.

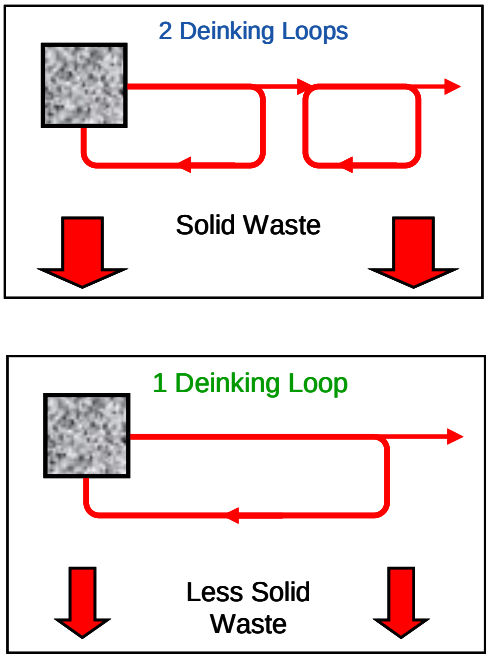

Figure 170: From 2 loop to 1 loop deinking line structure

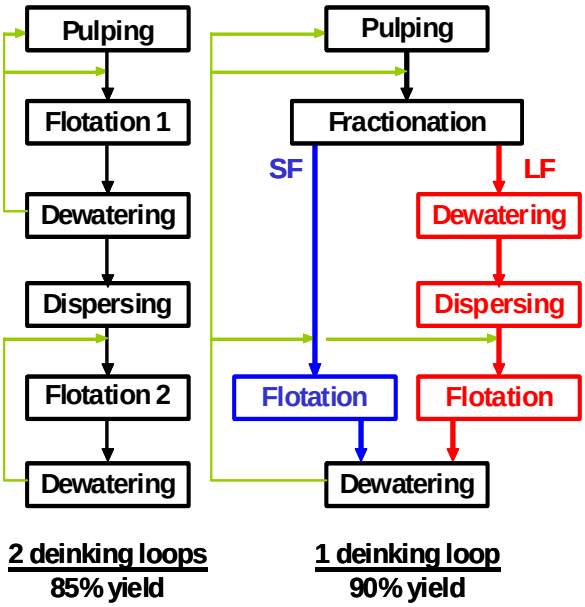

Figure 171: Classical 2 loop deinking line (left) and a simplified structure by use of fractionation techniques studied in the ECOTARGET project, from Carré [163]

The short fibre (SF) fraction containing majority of ink was treated with flotation operations while mechanical energy or dispersing operation was performed to detach ink on long fibre (LF) fraction followed by flotation operation. Comparing with classical 2 loop deinking line where all pulp flow was treated in all unit operations, the fractionation simplified deinking line showed advantages in loss reduction of 37%(at similar brightness) and energy reduction of 17%. However, the drawback was additional bleaching costs involved during the dispersing (bleaching not present in the 2 loops shown in Figure 170).

Continuing in similar concept, experimental trials were performed to approach the objective of deinking line optimization using fractionation. In the first series of trials, ink containing micro-hole accept fraction was treated in laboratory flotation cells to reduce the ink content. Analysis was made to understand the response of flotation operation and also how the fractionated system (simple simulation) performs with the reference trial. Moving further, in second series of 'complete' pilot plant trials, ink removal in pilot flotation cells was combined with hydrocyclone fractionation of fines and fibres to produce different fractions for sheet manufacture.

4.2.2. - Potential of micro-hole fractionation with dedicated treatment for DIP purpose

As stated earlier deinking line simplification necessitates separation of contaminants and their dedicated treatment. Pressure screening fractionation by a micro-hole screen plate offers high selectivity towards fines separation into the accepts. This has been analysed in the chapter N° 3.2. - Study of micro hole screen fractionation. As shown, the micro-hole accepts contain most of the ink; thus, their treatment by flotation can be envisaged, in order to remove ink particles and recover cellulosic material or fillers. This solution avoids the treatment by flotation of the whole pulp (generating fibre losses), with consequent cost and energy savings, as targeted by the simplification of deinking lines.

The approach for ink separation and ink treatment was investigated by performing 2-stage pressure screening of a 25%ONP 75%OMG mixture, enriching the accept fraction with ink (the fractionation

analysis of this pulp has been reported in Chapter n° 3.2.1.2. -Fractionation results). The complete experimental scheme is illustrated in Figure 172. Reject pulp obtained at 20% Rv of the 1st stage was diluted with tap water and used as inlet to the 2nd stage.

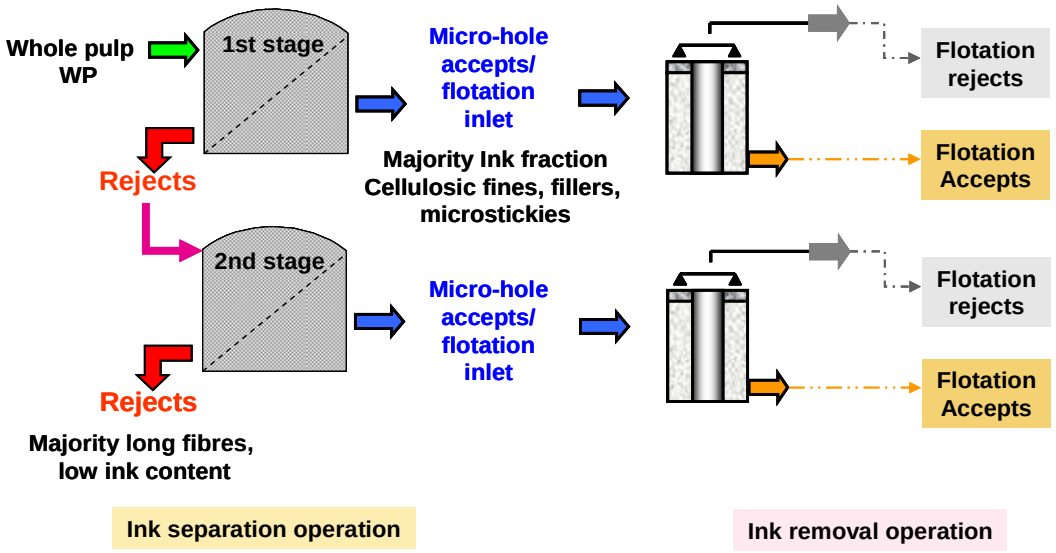

Figure 172: Micro-hole screening application in deinking pulp manufacture - feed forward set-up

The results were analysed in terms of efficiency of ink separation during screening operations and efficiency of ink removal during laboratory flotation experiments.

4.2.2.1. - Separation of ink in micro-hole pressure screening operations

The fractionation trials showed that the long fibres in the rejects get depleted and accepts get enriched with the ink particles. The results obtained for each pressure screen operating conditions are given in Figure 173 and Figure 174 for the ERIC and in Figure 175 and Figure 176 for the brightness.

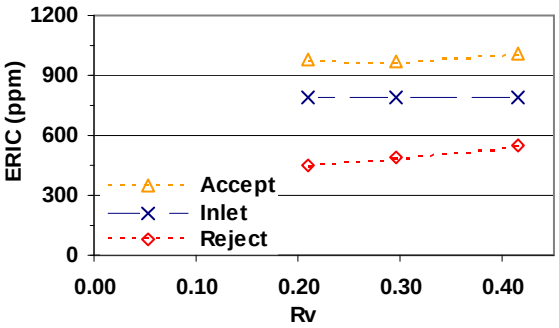

Figure 173: 1st stage ERIC evolution

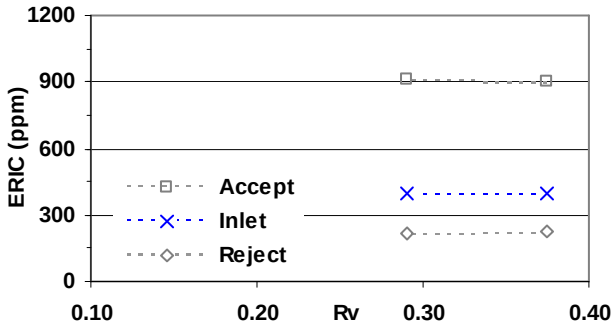

Figure 174: 2nd stage ERIC evolution

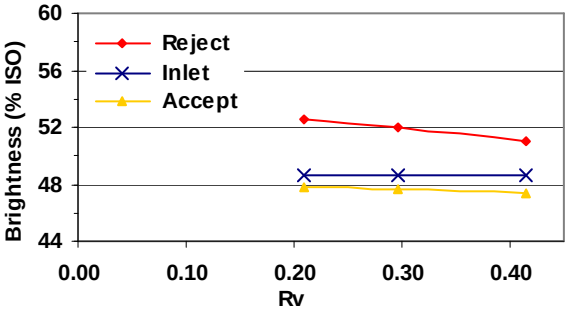

Figure 175: 1st stage brightness evolution

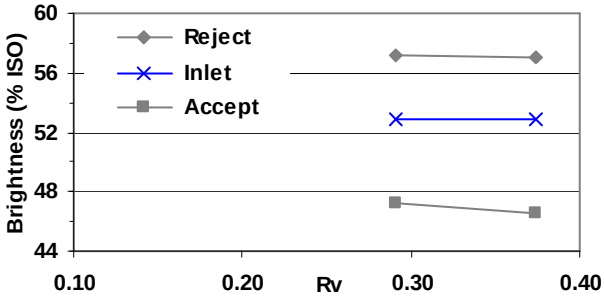

Figure 176: 2nd stage brightness evolution

Fines containing ink particles and mineral filler follow the flow split; lower volumetric reject ratio gives better results for reject pulp cleanliness. However, residual fines and ink particles still remain in 1st stage reject pulp even at lowest R_v. A 2nd stage micro-hole fractionation improves the reject pulp brightness and further lowers the ERIC content to ~200ppm as fines are separated into the accept fraction. But this is still not optimal as the hyper-washed pulp brightness and ERIC values are 63% ISO and 51ppm respectively.

This suggests that a further improvement of the final reject pulp could be possible. Among the solutions that should be tested, could be operating the 2nd stage pressure screening at lower R_v and /or the implementation of a 3rd stage.

Makinen *et al.* [108] also reported results for pressure screening fractionation of magazine rich (67.5%) raw material before deinking with a 3-stage feed forward set-up using 0.06mm slot basket. The final split was 35% rejects (or long fibres). The brightness and ERIC values for final rejects (long fibres) were 54% ISO and 426 ppm respectively. Using the author equation and data of thickening factor and pulp passage ratio for the 3 stages, the approximate R_v values were calculated. This helped in the comparison for the two basket types and is illustrated in Table 22 (values in brackets indicate ERIC for inlet and reject streams).

Table 22: Comparison of the ERIC reduction between inlet and reject streams at different fractionation stagesof two different screen plate types

		1st stage	2nd stage	3rd stage	Overall
Kumar (micro-hole)	$R_v \rightarrow R_m$ Water removal	21% → 57% 79%	29% → 82% 71%	-	06%→47% 94%
	% ERIC reduction (Inlet ↓ reject)	43% (790 ↓ 450ppm)	47.5% (400 ↓ 210ppm)	-	~73.4%
Makinen *et al.* (micro- slots)	$R_v \rightarrow R_m$ Water removal	~24.5%→51% 75.5%	~46.7%→74% 53.3%	~59.7%→85% 40.3%	07%→~32% 93%
	% ERIC reduction (Inlet ↓ reject)	35% (1140 ↓ ~740ppm)	26% (~740ppm ↓ ~550ppm)	22% (~550ppm ↓ 426ppm)	~52%

Indeed, for the equivalent water removal of ~94%, the results achieved with 2-stage micro-hole screen plate fractionation showed much better selectivity for ink separation into the accepts compared to 3-stage micro-slot fractionation, hence reduction in rejects. It must be noted also that the operating conditions (R_v) play a critical role in defining the ink reduction.

Specks contamination was calculated as their flow in inlet and reject streams. As their quantification was made by image analysis on hyperwashed pulp (long fibre content), the amount was re-calculated on the whole pulp using the long fibre content values. With the help of flow and concentration measurement on inlet and reject streams, it was possible to calculate the specks flow. This is illustrated in Figure 177, which represents the specks flow in number/h.

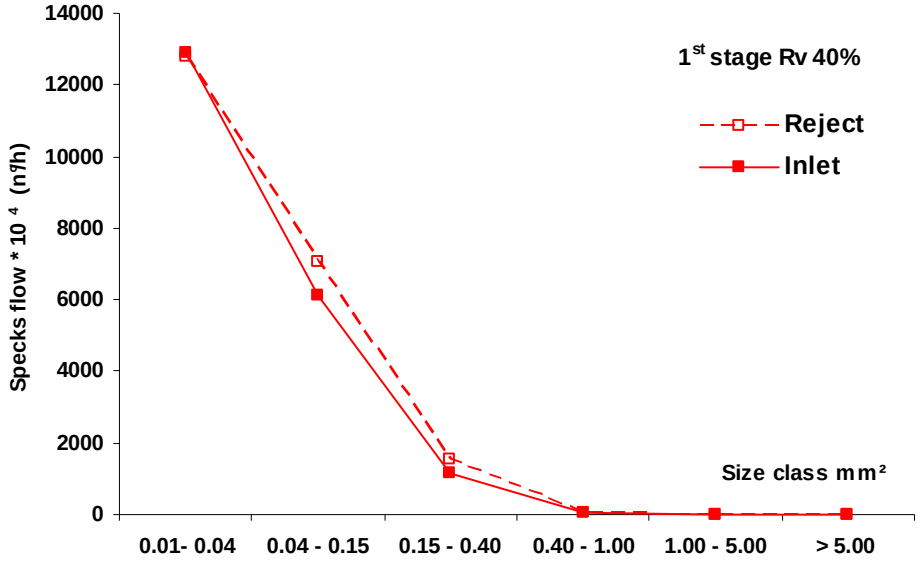

Figure 177: Specks flow in inlet and in rejects

The results show that specks contamination in the inlet gets rejected. Micro-hole screen plate was very effective in separation of specks. The slightly higher reject flow estimated in the rejects could be due to a slight over-estimation of the specks counted by image-analysis in the rejects as the pulp had higher brightness compared to the inlet so relatively more low-contrast specks may have been counted. Another hypothesis of their slight increase could be their fragmentation occurring during the pulp flow experimental trial circuit.

The main pulp characteristics at the flotation inlet are reported in Table 23 (fibre concentration is calculated by hyperwashing, fines here refer to cellulosic fines, which have been calculated from total, fibre and ash concentration). Micro-hole accepts had lower concentration than the reference pulp, due to the phenomenon of accept dilution occurring during the screening phase. 2nd stage accepts were more diluted, as the inlet pulp to this stage contained majority of long fibres, which were rejected.

				Total Solids	Fibres		Fines		Ash		ERIC
				(g/L)	(g/L)	(%of total solids)	(g/L)	(%of total solids)	(g/L)	(%of total solids)	(ppm)
Flotation Inlet	a		Reference	11.6	5.9	51%	2.07	18%	3.6	31%	904
	b	1 stage	R_V=40	3.28	0.28	8%	1.17	36%	1.83	56%	1204.0
	c		R_V=30	3.29	0.43	13%	1.06	32%	1.79	55%	1161.0
	d		R_V=20	3.35	0.56	17%	1.00	30%	1.79	53%	1180.0
	e	2nd stage	R_V=40	1.22	0.27	22%	0.45	37%	0.49	41%	1132.0
	f		R_V=30	1.21	0.28	23%	0.45	37%	0.48	40%	1055.0

Table 23: Micro-hole screening accept (flotation inlet) pulp characteristics

Concerning the impact of the variation in the operating conditions (volumetric reject rate during pressure screening operations), it can be seen that the total solid concentration is not really affected by this parameter, increasing slightly with decreasing R_v, whereas its composition (in terms of relative ratios of its components) is more modified: the increase in the R_v resulted in a decrease in the fibre concentration, while fines concentration decreased. Ash content remained quite constant.

These results observed with decreasing R_v and increasing reject thickening factor upto 2.7 could be analysed as follows: ash content remains constant as filler follow the flow split, fines concentration decreases slightly as the increasing consistency on the reject area tends to form a fibre mat which

retains more fibrillar fines, and fibre consistency increases more significantly by a factor of 2 as the shortest fibres with constant passage ratio are entrained in the accepts at higher consistency due to higher reject thickening, as far as their passage ratio is not too much reduced by increasing fibre interactions.

The variation of R_v during screening had no effect on the composition of the 2nd stage fractionation. However, in this case, the solid particle concentrations were very low, and R_v varied only from 0.4 to 0.3, so the impact could be within the experimental error.

4.2.2.2. - Laboratory flotation of ink containing micro-hole pressure screening accepts

The accept fractions obtained during the 2-stage micro-hole ONPOMG fractionation trials and one reference pulp after pilot pulping (i.e. the inlet to 1st stage micro-hole screening) were subjected to laboratory batch flotation in VOITH Delta 25L cell. The experiments were performed in absence of flotation chemistry as done in the reference mill of the BoostEff project. The operating conditions are reported in Table 24.

Table 24: Laboratory flotation conditions

Suspension volume for each test	**22.5L**
Air introduced	**7L/min (200%)**
Flotation time	**07min**

When performing flotation trials with the accepts of the 2nd stage micro-hole fractionation, very poor foaming was observed. This can be explained co nsidering that, as no chemical was added, pulp foaming was induced by the surface active substances released into the water phase from recovered papers at the repulping stage (Zeno [164]). During screening, accept pulp dilution occurs, and for the 2nd stage, there is a further dilution effect during pulp preparation that determines a strong decrease in the surface active substances concentration.

The flotation efficiency[3] (Figure 178) measured when treating the 1st stage accepts is close to that obtained when treating the pulp before screening, i.e, 80-85%. On the other hand, the flotation of the 2nd stage accepts was much less efficient. This is not due to a large difference in the ink inlet concentration (close to 1st stage, R_v=40%), it could be likely due a decrease in foaming and in collecting, due to the dilution of released substances at the repulper. The decrease in the foaming attitude is reflected by the low water losses (approximately 1% instead of 10% for reference and for 1st stage accepts).

Concerning the different samples for the 1st stage screening, a modest tendency to increase the ink removal is observed when accepts were obtained by increasing the R_v during screening. It could be explained by the increase in the fibre concentration, if such fibres contain attached ink. Unfortunately, this can be hardly verified with ERIC measurements, as the values are very low and the difference not significant (hyperwashed fibre for R_v=40%, ERIC = 59ppm; hyperwashed fibre for R_v=30%, ERIC = 56ppm).

[3] i.e., the ink mass removal. It has been calculated on pulp mass and the associated ERIC content in inlet and accepts stream

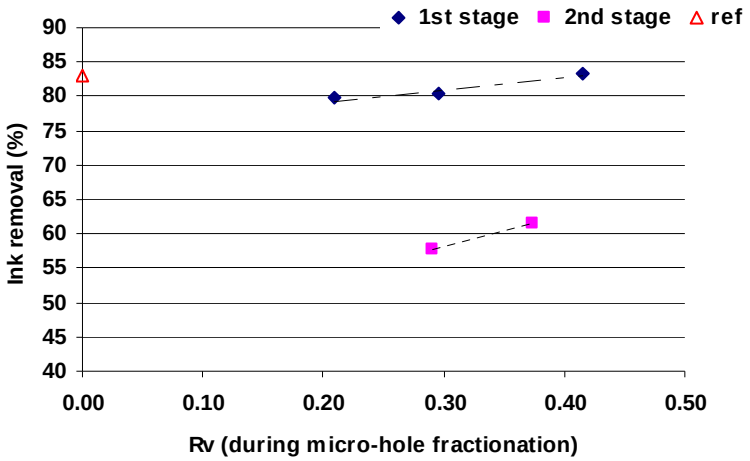

Figure 178: Flotation efficiency as a function of R_v (reference= R_v 0)

Figure 179 reports brightness gain after flotation, for the different pulps treated. The gain is slightly higher for the reference pulp, in agreement with slightly higher ink removal efficiency, but quite comparable with that of the 1st stage pulps. As expected the brightness gain for 2nd stage pulps, was much lower.

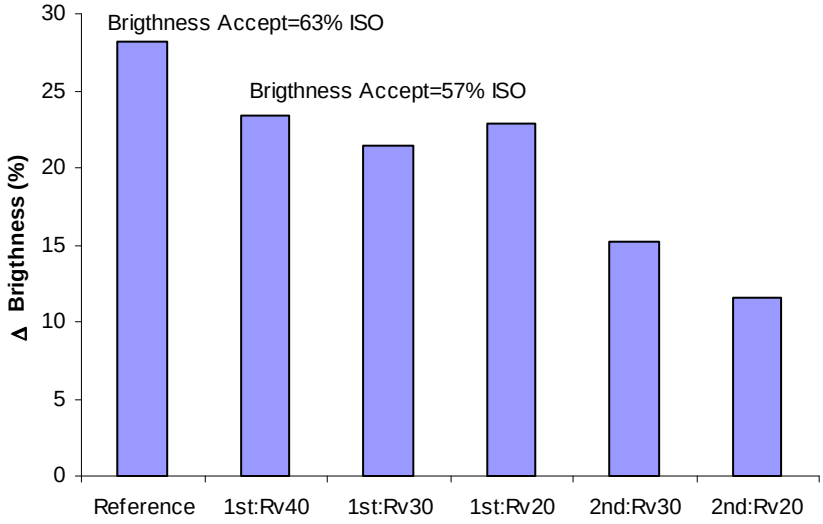

Figure 179: Brightness in flotation

Considering the poor flotation efficiency for 2nd stage accepts, and their negligible differences in composition (with consequently very similar flotation results, in term of losses), it was decided to report and discuss in the following only results for 1st stage accepts flotation.

Flotation losses reported in Figure 180 were generally lower for the screening accepts than for the reference pulp, at least for the fibres; fines and ash losses were quite similar. This is likely due to the differences in the fibre concentration between reference pulp and screening accepts (6g/L vs 0.3 to 0.6g/L respectively): screening accepts contain a lower fibre concentration, which results in a lower flocculation level and by consequence a lower loss by fibre entrainment (Allix *et al.*[165])

The variation during the screening R_v had a negligible impact on the losses, except for fibres: in that case, increasing R_v led to a decrease in the losses, that could be related again to the decrease in the fibre concentration (from 0.6 to 0.3g/L), even if the values are quite low.

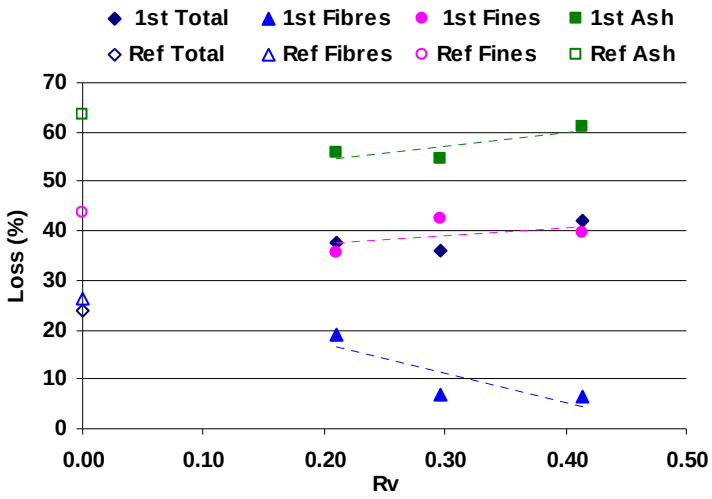

Figure 180: Total, Fibres, Fines and Ash losses for flotation of different pulp samples : reference and 1st stage screening accepts

When treating the accepts, flotation overall selectivity (defined as the ratio of the ink removal to total solid loss) reported in Figure 181 was almost constant, in agreement with the same pulp concentration values of all the samples (Table 23); surprisingly, it was lower than that for the reference pulp. However, the difference is quite negligible.

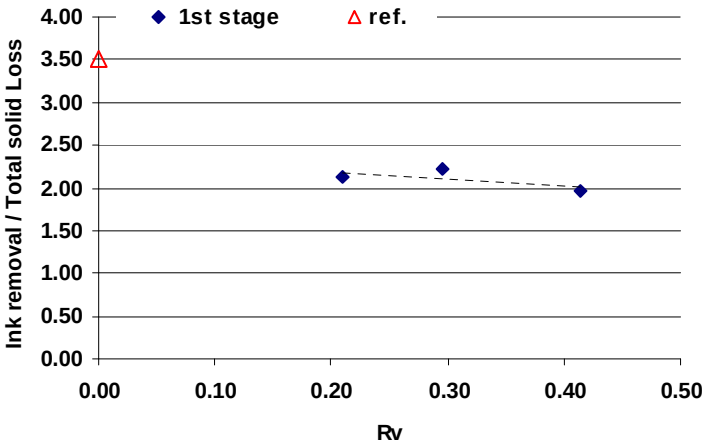

Figure 181: Flotation selectivity for reference pulp and 1st stage accepts

However, when considering the selectivity towards each single component of the pulp suspension (Figure 182), it can be observed that generally the values were close to those of the reference pulp, except for fibres. In this case, selectivity was much higher, especially for the highest R_v (corresponding to the lowest fibre concentration), then it rapidly decreased for samples obtained with decreasing R_v (and increasing fibre concentration). This is consistent with the fact that fibre losses are mainly due to fibre entrainment by bubble trapping in the flocs: thus, a lower fibre concentration leads to lower flocculation levels and consequently to lower fibre losses by entrainment. When considering the impact of the screening operating conditions (R_v) on the flotation selectivity towards fibres, it can be seen that the latter decreased as R_v decreased (from 13 to 4 when passing from 0.28 g/L to 0.56g/L).

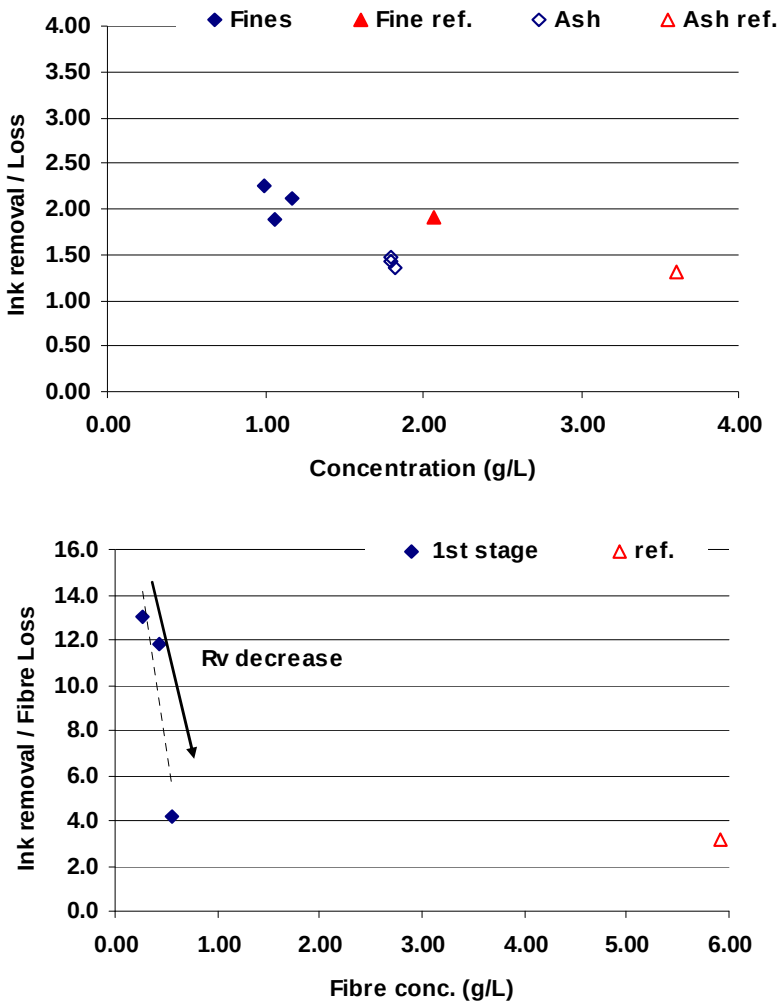

Figure 182: Flotation selectivity towards each pulp component

A host of variables, both operating and pulp conditions play an important role in flotation operations and selectivity. These include temperature, flotation chemical agents, flow, gas hold-up, air bubble size, pulp pH, concentration of pulp entities - fibre, fines, ash, etc. Air hold-up plays a very critical role in flotation yield and ink removal phenomenon. The upward movement of air bubbles and their interaction with other particles in the pulp suspension is strongly influenced by pulp concentration which in turns influences the fibre flocculation (through fibre concentration) and the entrapment of bubbles in flocs. Detailed discussion about these parameters is out-of-scope of this manuscript and can be found elsewhere ([166][167][168]).

Huber *et al.* [169], Zeno *et al.* [170][171] mentioned that the loss of cellulosic fibres is the result of their entrainment in flocculated state at higher pulp concentration. Large fibre flocs create large interstitial spaces and channels which favour bubble coalescence and collision. This condition reduces the ink particle removal. At lower flocculation levels, fibres are present in individualised state and fibre loss is less by entrainment, hence increasing the selectivity. Zeno *et al.* [170] showed decreasing pulp concentration decreased pulp flocculation and increased fibre flotation selectivity.

This situation is valid when the fibres are statistically in contact (high crowding) with each other. A second situation occurs when the fibre concentration is too low and there is 'no physical' contact between fibres, signifying that they are statistically isolated and cannot form flocs anymore. Indeed, researchers Mason [172][173], Kerekes & Schell [174] have defined a critical concentration; which defines the 'boundary' between isolated and crowded regimes. For 'N' number of fibres contained in

volume of diameter equivalent to the length of the given fibre, the theoretical critical concentration, C_m is represented in Eq. 26. For N=1, the fibres will be present in independent state and type of fibre contact would be a chance collision.

Eq. 26 :

$$N \approx \frac{5 C_m l_w^{\ 2}}{w}$$

N: Crowding factor
C_m: Critical concentration, %
l_w: Length weighted fibre length (mm)
w: Fibre coarseness (mg/m)

Table 25 reports the pulp characteristics and the value of N obtained with different fibre concentrations at different R_v. Also, the critical concentration, Cm, is calculated and reported on assuming N=1. The fibre coarseness was corrected with fines content, which was assumed to be equal to their surface area ratio reported by MorFi analyser [95].

Rv	0.41	0.30	0.21
Fibre conc g/L	0.28	0.43	0.56
Mean length-weighted fibre length, mm	0.53	0.56	0.56
Mean fibre coarseness (corrected), mg/m	0.15	0.16	0.16
N for different fibre concentrations	0.27	0.42	0.54
Remarks for N (calculated)	<<1	<1	≤ 1
for N=1 Cm (g/L)	1.02	1.03	1.04

Table 25: Value of N and critical concentration, Cm different pulp characteristics

At lower fibre concentration (R_v =40%), the value of N is very low (<<1) and 'approaches' 1 for higher fibre concentration (R_v =20%). For the 3 R_v values, critical concentration was ~1.0g/L, indicating that the fibre concentration (reported in Table 23) during the flotation operations is much lower than this critical value. This could explain why very high values of selectivity were observed at low fibre concentration level at R_v= 40% & 30%. When increasing the concentration we approach the theoretical critical concentration limit (and N=1) and it could be possible that the fibres exist in flocculated state at 0.6 g/l for R_v= 20%. This large decrease for a modest variation in the fibre concentration would require further investigations, in order to find out the evolution of the flocculation level as a function of the fibre concentration. Unfortunately, this was not possible in the frame of the present work, as raw material and time consuming experiments are required. Working at high total concentration but low fibre concentration would not only improve selectivity but also would be more economical.

4.2.2.3. - Comparison of fractionation deinking with whole pulp deinking

Fines and ink rich micro-hole accept fraction (at various R_v) was subjected to ink removal treatment in laboratory flotation cells. When treating the fine fraction the process efficiency is close to that of the whole pulp flotation. Rough calculations were done in order to verify if the new proposed process can potentially lead to the same pulp characteristics as for the conventional one (without screening and with whole pulp flotation).

As it can be seen in Figure 183, the (screening + fine flotation) process has slightly higher yield on addition of the 2 pulp streams than the full stream flotation process reported in Figure 184. If re-mixing the screening rejects and the screening accepts after their flotation (whatever the screening operating conditions (R_v), the final pulp has a similar composition as that of the pulp only treated by flotation, without prior screening.

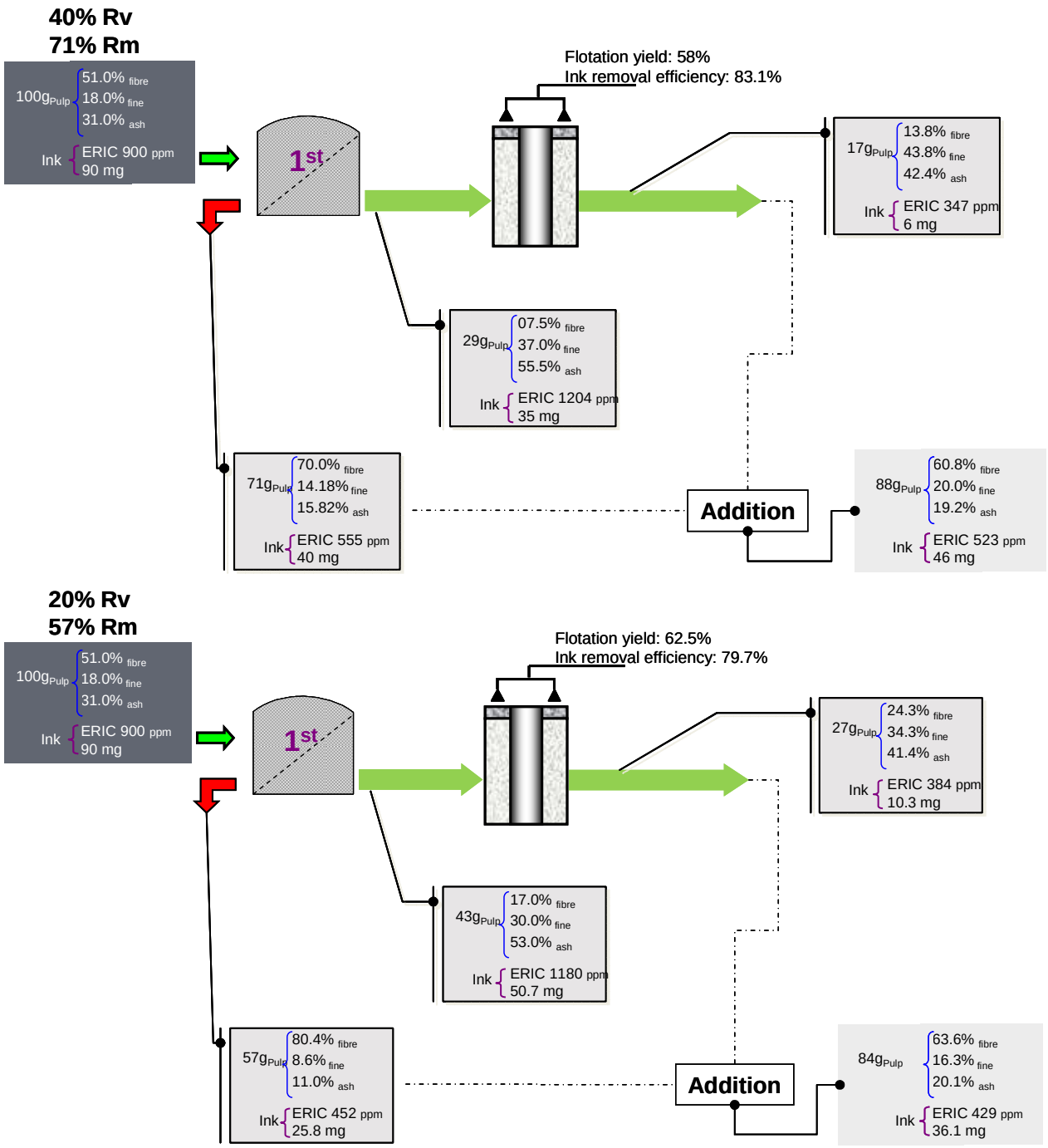

Figure 183: Final pulp characteristics -1 stage fractionation at 40% and 20% Rv and fine flotation

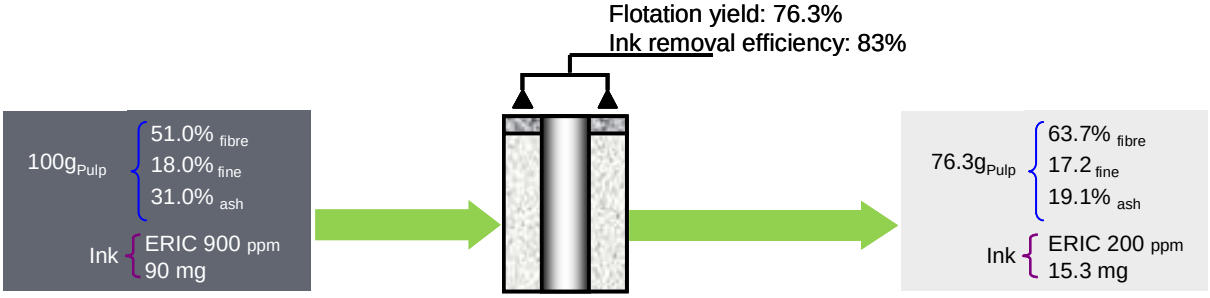

Figure 184: Pulp flotation without fractionation (reference)

The major difference between the two scenarios is the final ink content, higher for that obtained with the new process involving only 1-stage fractionation in the present case. When considering each step, the main origin of this additional ink amount is its presence in the screening rejects that were not treated by flotation to remove the residual ink. For this reason, the addition to the screening of a 2nd stage, and even of a 3rd stage, could be beneficial. This is analysed in Figure 185; the 3-stage screening with fines flotation) could give approximately the same yield than the whole pulp flotation, with the same residual ink. The values of mass reject ratio R_m and ERIC for 1st and 2nd stages are from the experimental trials at lowest volumetric reject ratio. For the 3rd stage, a value of 90% R_m and 50% reduction in ERIC content has been assumed considering a very high amount of long fibre at the 3rd stage inlet. Another hypothesis has been taken into consideration for flotation operations, which will treat the combined flow of the 3 stages with the accepted pulp ERIC being the average of the three stages found experimentally. The average value of yield and accept pulp ERIC as obtained in 1st stage experimental trial have been considered.

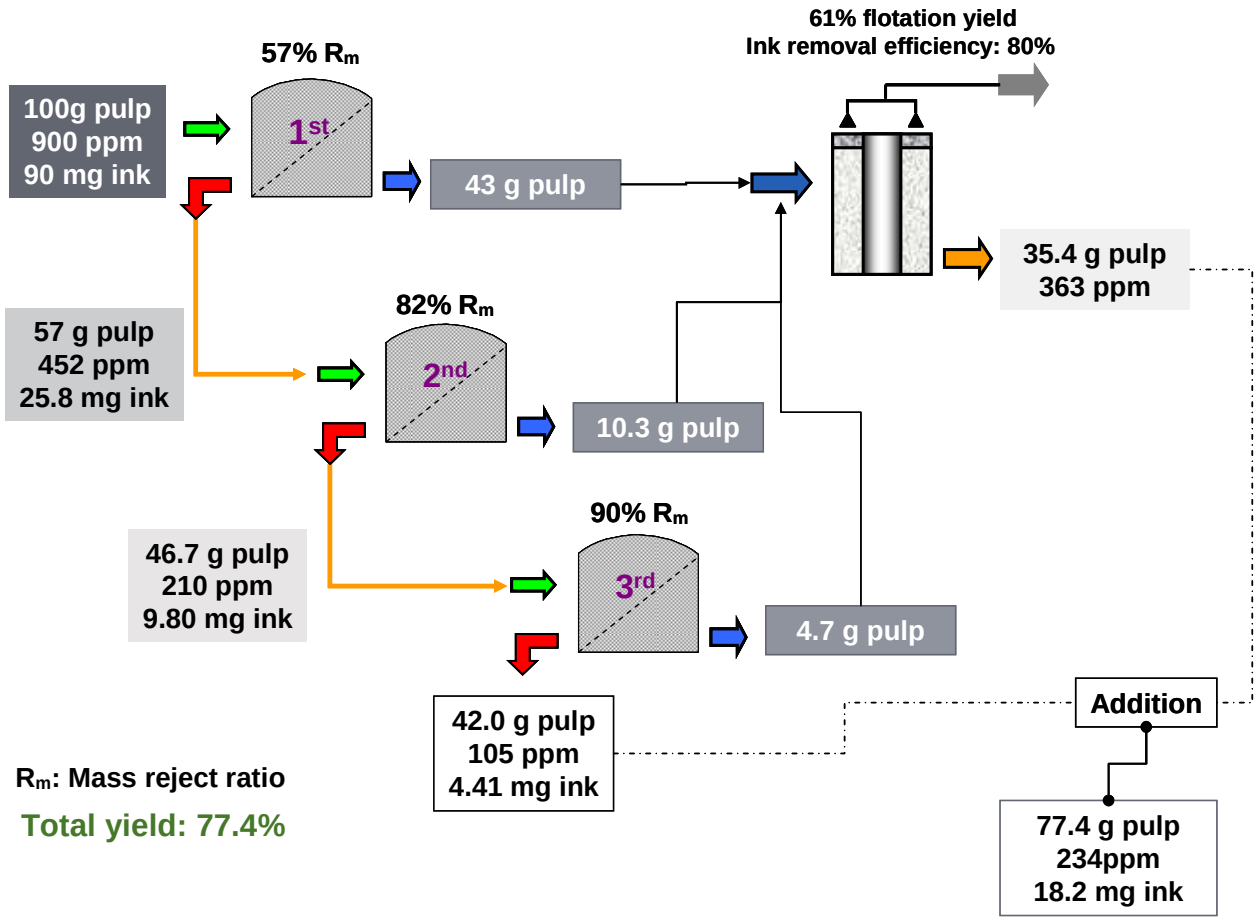

Figure 185: 3-stage micro-hole fractionation and fines flotation

4.2.3. - Summarising the experiments -deinking process optimisation

The results showed that fractionation with a micro-hole screen basket is effective in enriching the accepts with ink and specks into rejects. 2-stage micro-hole fractionation and operating the pressure screen at low R_v helps to obtain much cleaner reject fraction. Specks in the inlet pulp are very well retained and follow the screen rejects. This allows for dedicated treatment on each micro-hole fraction- application of mechanical energy on specks-rich reject fraction and ink removal operation on accept fraction. The reduction in energy consumption in these two unit operations could be possible, as only a

part of the whole pulp is treated. Further fragmentation of ink particles could be avoided as the accept fraction will not be treated with mechanical action.
Investigation of laboratory fines flotation showed low fibre losses in comparison to the whole pulp flotation, with similar ash and fines losses. Selectivity of ink removal to fibre loss was high at low screening accepts fibre concentration. In the situation where the flotation accepts and micro-hole rejects, were recombined, the total yield of the fractionation deinking process was higher than direct whole pulp flotation.

If this result is verified experimentally, a new process (pulp screening and fines flotation) could be proposed as an alternative for the present one (whole pulp flotation), with consequently several advantages: the use of the two pulp fractions, for different purposes (multilayer paper), a potential reduction in the required flotation capacity, or possibly a more efficient use of the available capacity. The latter could be used for further increasing the pulp final quality, in order to suppress the usual 2nd deinking loop, thus reaching a real process simplification, with the associated economical and environmental gains.

The approach of micro-hole fractionation and accepts flotation can be developed further if distinct fractions have to be produced for multi-layer manufacturing process. The next series of complete pilot plant experiments described in the following section illustrate the combined use of two different fractionation technologies and flotation operations to produce different fractions.

4.2.4. - Potential of micro-hole fractionation for DIP application associated with hydrocyclone fractionation for multilayer

Experimental trials at the pilot scale were performed with 25%ONP 75%OMG raw material, with the objective of simplification of deinking line and production of fractions. Studying the properties of single layer sheet could help to envisage the appropriate destination of fractions produced in a multi-layer sheet structure.

4.2.4.1. - Experimental set-up description and operating conditions

A ‘simplified’ pilot trial schematic is shown in Figure 186 and the operating conditions are reported in Table 16. The 2nd and 3rd stages of micro-hole fractionation were substituted by washing stages. This was done to ‘simulate’ a 3-stage micro-hole fractionation.

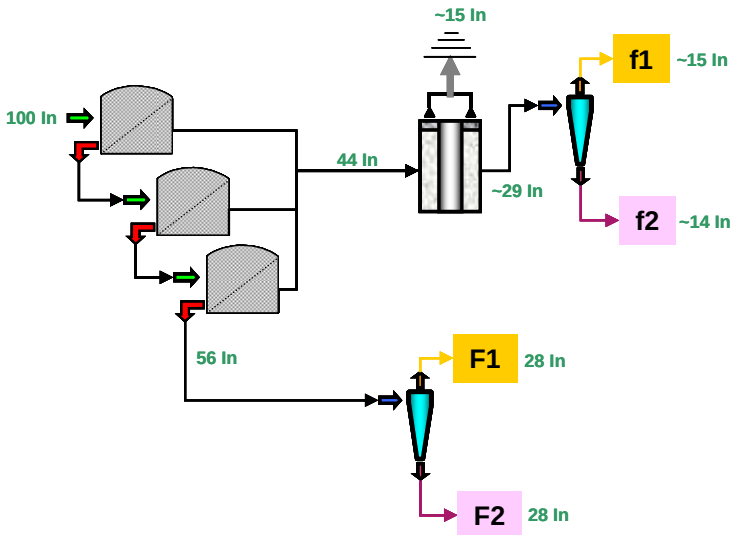

Figure 186: Experimental set-up for fraction productions
with corresponding mass flow (In=Inlet)

Table 26: Operating conditions of various unit operations

	Remarks
Pulping	16% concentration, 50℃, 15 minutes pulping time, 0 .4% of soap SERFAX MT90
Pressure screening fractionation	Micro-hole basket, 11g/L, 20% Rv (56.4% Rm), 0.3m/s
Pilot flotation	Verticel type, 4.4g/L, 50℃ temperature
Hydrocyclone	65mm head diameter, ~180kPa, 50℃, ▪ ~48% Rm or fine fractionation (at 42% Rv) ▪ ~50% Rm for fibre fractionation (at 22% Rv)

The micro-hole accepts containing majority of ink were treated in flotation cells. The flotation accepts containing majority of fines, were fractionated with hydrocyclone at an inlet concentration of 2g/L. As outlined earlier, this was done to separate the fines into fibrilar and flake type fractions. The rejects from screening were diluted with tap water and treated on a Classiflux washer (a wire washing technology, developed by CTP. The washing process takes place on an inclined open wire with 355 µm opening. The fibre mat formed due to dewatering is continuously unclogged by counter current moving bars located under the wire). For hydrocyclone fractionation the pulp was diluted with hot water to 5g/L concentration. Accept and reject hydrocyclone fractions were again washed on Classiflux washer. This was done to decrease the residual ERIC content of micro-hole rejects as only 1-stage pressure screening was performed. The addition of the various washing stage was implemented to simulate a 3-stage micro-hole fractionation. The trials led to production of 2 'fine' fractions f1 & f2 as they contained majority of fines and 2 'fibre' fractions as they contained majority of fibres.

The objective of these series of pilot plant trials was to obtain fines and fibre fractions; hence no detailed analysis is made with respect to flotation and hydrocyclone fractionation. The results described hereafter provide an indication that the approach outlined in experimental schematic can be developed (optimised) further. Complete process configuration could include fine screening operations on the micro-hole screening rejects to remove macro-stickies followed by application of mechanical energy to fragment the specks and detach residual ink from the fibres.

4.2.4.2. - Optical and morphological properties of fractions

Figure 187 shows the optical characteristics at selected positions of the experimental set-up. The final fine fractions, f1&f2, have a higher ink load in comparison to fibre fractions, F1&F2, which reach almost the hyper-washed pulp characteristics, thanks to the two-washing steps.

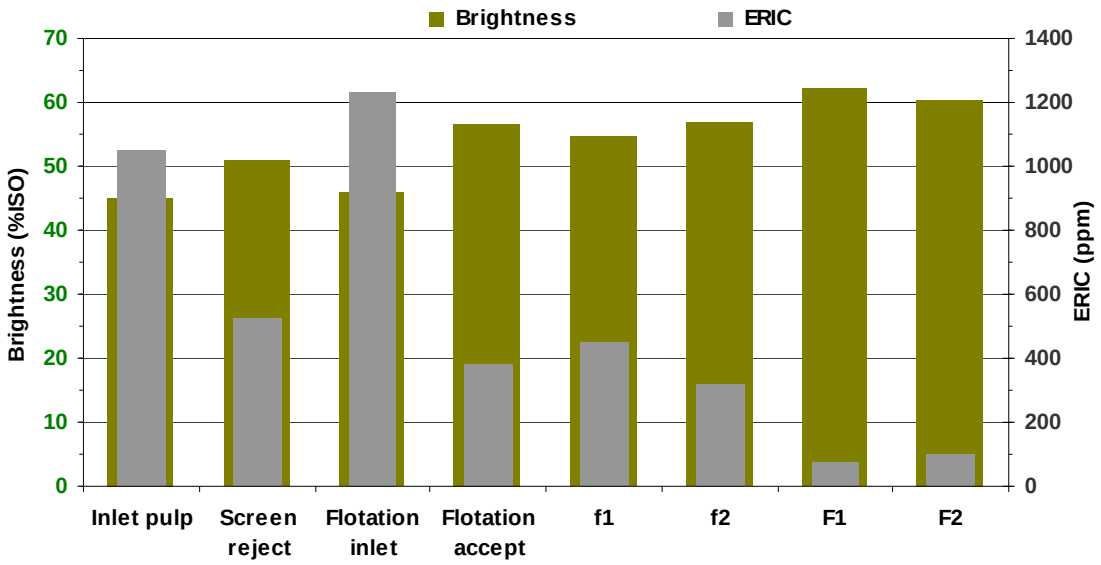

Figure 187: Brightness and ERIC values for various streams

The fractions f1&f2 contain majority of fines, short length and smaller width fibres and filler/pigments (ash content) as reported in Table 27, in comparison to the fibre fractions F1&F2, which are longer in length and have higher width. This is primarily due to efficient separation of fines and fibre fraction during micro-hole screening.

Table 27: Pulp characteristics

	Inlet pulp	Micro-hole reject	Flotation inlet	Flotation Accept.	f1	f2	F1	F2
Ash %	32	10.2	56	37.5	42	32.5	1.4	1.7
P200%	52.5	23.8	88.1	78	84.5	72.6	10.4	6.6
Fibre Length mm	1.12	1.26	0.52	0.52	0.48	0.54	1.23	1.24
Fibre width µm	24.4	26	22.2	23	22	24.3	25.4	26.8

Hydrocyclone fractionation of the flotation accepts or micro-hole screening rejects provides 4 pulp streams which do not have same morphological characteristics. Accepts (f1 or F1) contain fibres with small width diameters. This is explained further in examining the fibre width and length distributions of these fractions. Accept fractions have higher proportions of fibres in smaller width class as shown in Figure 188. High specific surface area fibrillar type fines and fibrillated fibres get concentrated in the accept fraction. Indeed, hydrocyclones do not fractionate on the basis of fibre length, this is evident from Figure 189, which shows the fibre length distribution in various size classes.

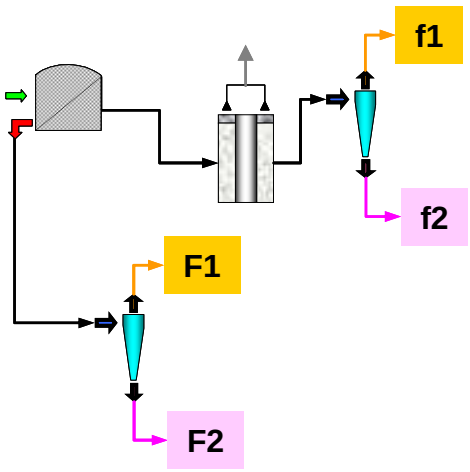

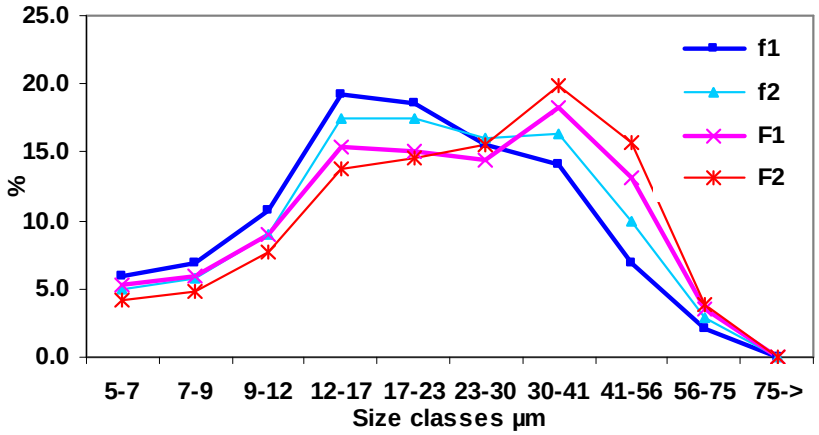

Figure 188: Deinking pulp hydrocyclone fractions fibre width distributions

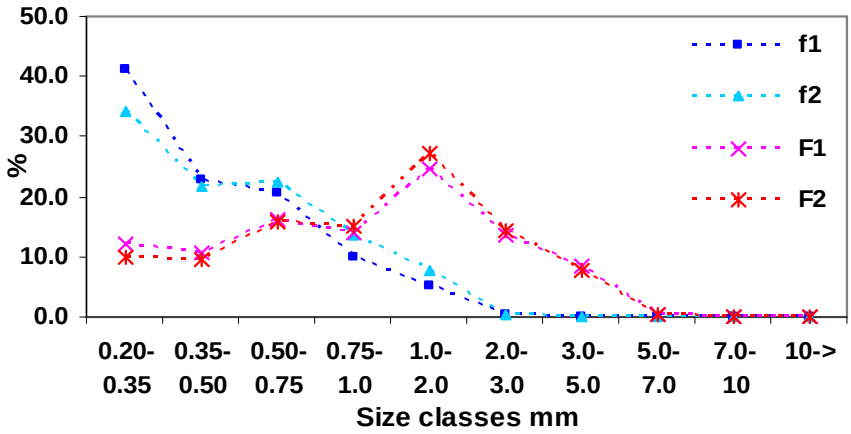

Figure 189: Deinking pulp hydrocyclone fractions fibre length distributions

Fractionation by hydrocyclone provides a very interesting scenario where the fractions produced could be put into different layers as envisaged in project BoostEff. The accept fractions (f1&F1) which have lower fibre width and more fibrillated fibres/fibrillated fines will provide better strength properties and can be directed to surface layers, whereas the reject (f2&F2) could be directed to middle layer. Indeed, from these four fractions various combinations are possible with different proportions of fractions in each layer. Additional benefits could also be achieved by performing separate bleaching treatment of the fractions. The bleaching costs could be reduced by studying the response of fractions to the bleaching dosage and chemicals.

4.2.4.3. - Mass balance and final pulp characteristics

Thanks to micro-hole fractionation, only 44% of the total pulp flow was treated in the flotation cells and 56% of the total pulp flow would be subjected to the screening stage (for macro-stickies removal with fine slots) and mechanical treatment. In the flotation operations, the volume losses amounted to 18% with a yield of 65%. The ink removal efficiency at flotation stage was 80% which is comparable to laboratory flotation trials described earlier. If all the 4 fractions are combined and considering no losses at washing and thickening stages (for example in industrial application the corresponding flow would be mixed with micro-hole accepts) of screening rejects, the total yield would be 85%. Addition of all 4 fractions results in an ERIC content of 187 ppm, shown in a simplified schematic in Figure 190.

The analysis also indicates that during hydrocyclone fractionation of the flotation accepts, the free ink and mineral filler fraction follows the flow split as R_{mink} and R_{mash} approximately equals R_v (42%). It is difficult to assume the same for fibre fractionation as the ink is attached to the fibres and not free.

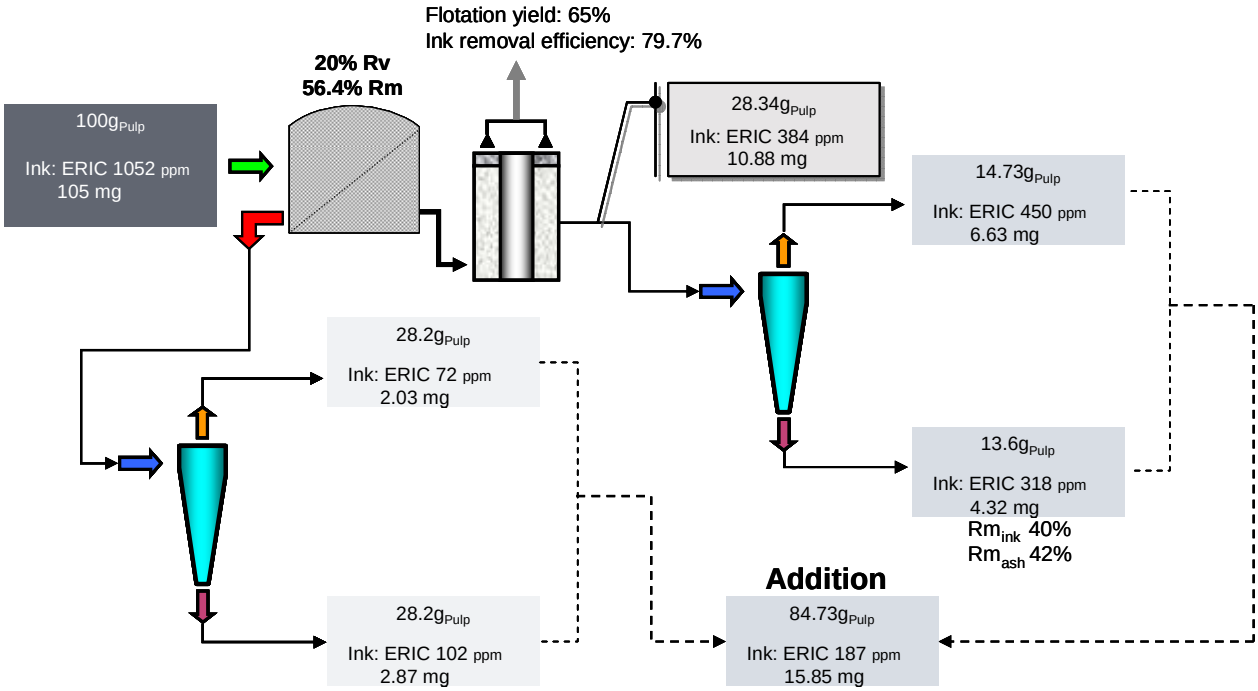

Figure 190: Combining all fractions leads to final ERIC of less than 200 ppm

The yield obtained by such a process is higher than the conventional single line deinking process with raw material studied.

4.2.5. - Summarising the pilot deinking experiments-optimisation and fractions

The results reported show that the combined micro-hole and hydrocyclone fractionation methodology could be applied on deinking line to achieve two distinct objectives- simplification of deinking operations and production of fractions for eventual multi-layer forming.

The trials showed the potential of micro-hole fractionation coupled with hydrocyclone fractionation providing 4 different fractions which could be utilised in optimised way for stratified sheet formation.

Ink-containing fines fraction firstly will have to be produced, and then treated in ink removal operations. Once treated these fines could then be fractionated into high specific area fibrilar fines and low specific area flake type fines. Separation based on cell wall characteristics could also be applied to the fibre fraction, leading to separation of fibrillated, thin cell wall fibres from coarse thick wall fibres in two different fractions. Such a strategy would lead to deinking line rationalization for energy efficiency and production of fractions for multi-layer sheet forming.

Sheet properties will depend on the type and quantity of fractions. With different optical and morphological characteristics, the fractions will provide varying degree of property enhancement.

4.3. - Conclusions

The objective of a series of experimental trials dedicated to fines fraction obtained by using micro-hole pressure screening was twofold.

1. In the case of pulp manufacture from recovered fibres:

- Performing right treatment to the right fibre type
- Producing fractions for possible multi-layer sheet structure as envisaged in BoostEff project.

This was done by the application of pressure screening fractionation with a micro-hole basket in deinking operations. This fractionation technology helped to produce two distinct fractions, which had different optical and morphological characteristics. 2-stage pressure screening was effective in separating fines and ink into accepts and retaining the majority of specks as well as clean long fibres with low ERIC content. This allowed performing dedicated treatments. One such treatment studied was ink removal operation in flotation cells. Ink removal efficiency during fines flotation was better than whole pulp flotation, with low fibre losses. It was demonstrated by simple simulation that an additional pressure screening stage could further reduce the ink content in the long fibres. The total yield of 3-stage pressure screening and fine flotation would be equivalent or slightly better than whole pulp flotation. In another test series fractionation of the flotation accepts and micro-hole rejects based on fibre fibrillation state or fines specific surface area with Hydrocylones lead to production of 4 fractions which had different morphological characteristics. Accepts were enriched with low fibre width fibrillated fibres and high specific surface area fibrillar fines whereas flake type fines and less fibrillated fibres were concentrated in rejects. The major advantage of fractionation in a deinking line would be firstly dedicated treatment to the right fraction and secondly possible energy savings in unit operations as only a fraction of the whole pulp would be treated.

2. In the case of pulp manufacture from virgin fibre SGW mechanical pulp:

- Hydrocyclone fractionation of fines obtained from micro-hole screening into flake and fibrillar type
- Investigating the effect of fines type on sheet properties, with the eventual integration of fines in a multi-layer sheet structure.

SGW pulp fraction containing majority of fines from pressure screening were fractionated using a small diameter hydrocyclone. The resulting two fine fractions resulted in different levels of sheet properties. In comparison to flake type fines, the fibrillar fines from hydrocyclone accept enhanced to a higher extent sheet mechanical (tensile index, scott bond) and optical properties (scattering, opacity). They reduced bulk and provided a much ‘closer’ structure (less air permeance). Effective separation and management of fines could be a possible option for the manufacture of multi-layer sheet structure, with fibrillated fines in surface layers providing sheet strength and flake type fines in middle layers providing bulk and possibly less paper defects in hiding elements linked to picking paper defect.

Fines separation and further treatment applied to pulp manufactured from either deinked or virgin pulp provides innovative strategies for process optimisation (deinking) or paper manufacture (sheet stratification). Segregation of optical impurities (specks and ink particles) in case of deinking pulp is possible with micro-hole pressure screening, thereby targeting the possibility of dedicated treatments to separated fractions. Indeed, the results showed that it is possible to limit the flotation to the fines fraction from the micro-hole screening accepts. The potential exists to improve the efficiency of the flotation operations for ink containing fine fraction.

Sheet properties are heavily influenced by fines and more importantly the fines type used for sheet making. For example in the case of virgin fibre pulp, the results of the sheet property evolution show the potential of fines separation by micro-hole screening and their subsequent fractionation by hydrocyclone. Production of fibre and fines types, which differ in their morphological development, provides flexibility in ‘configuring’ the multi-layer sheet structure.

5. - Final conclusions and perspectives

Paper recycling has spread worldwide over the past several decades, reaching a current recovery rate over 70% in the European Union (EU): hence, recovered fibres have become the major raw material for paper and board production, even over virgin fibres. Quite half of the recovered fibres are deinked, commonly by froth flotation, in order to remove ink besides other contaminants, and are used in almost all paper grades (even if the average utilisation rate is still very different from one category to another, as an example from 90% in newsprint to only 10% in graphic papers).

These facts already well comply with the requirements of the present socio-economic context, i.e. the sustainable use of resources, the waste reduction and re-use. However, there is still a window of opportunity to further promote the use of deinked pulp and optimise the paper recycling, also in order to maintain its competitiveness face to alternative solutions, as for example the exploitation of the recovered paper energy generation potential (by incineration).

Within this context, research efforts should be dedicated to optimise recycling/deinking technology, by increasing its efficiency, reducing costs and ecological footprint. This was the target of some National and European projects in the latest years, such as EcoTarget and BoostEff, which included research devoted to optimise and simplify the existing deinking lines, particularly by separating the different components of the pulp and applying dedicated treatments on each one.

Approximately 30-45% of the whole pulp is composed of the “fine fraction”, defined as the pulp fraction containing particles smaller than 75µm, mainly mineral fillers, cellulosic fines and ink particles. Most of the ink that should be removed from a pulp is present in the “fines”, under the form of isolated particles or linked to inorganic/organic surfaces. So, it would be possible to first separate this fraction and then to treat it by flotation, instead of treating all the pulp as presently done. Such an approach fitted in the general concept of right treatment to the right fraction, would lead to benefits in possible energy savings, as only a part of the whole pulp would be treated in various unit-operations, thanks to fractionation.

Moreover, cellulosic fines are an invaluable asset and very vital for the sheet mechanical properties, especially some specific types of fines that have higher augmentation capacity. Actually, fibrillar fines have higher bonding ability than flake fines, so that their incorporation in the paper structure would lead to additional advantages.

Thus, pulp fractionation appears as a crucial step, to first separate the fine fraction, and then to isolate the different types of fine, in order to optimise deinking and to open the way for controlled application of fines in single or multilayer paper with designed properties.

The work presented in this manuscript focuses on pulp fractionation with a pressurised screening system (at pilot plant scale) and particularly onto the characterization, separation and application of the “fine fraction”.

The first part of the work (Chapter n° 2 Characteri zation of fines) was devoted to the characterisation of the “fines”.

To investigate in more details the pulp fines, a specific manual method was developed which enabled to visualise and quantify fines sub-fractions. The procedure which can be applied to pulp from any

origin, involved washing of fines (collected via the Bauer McNett classifier) with a light pressure water jet on small aperture wire screens, with decreasing sizes (50µm-25µm-11µm), and the subsequent recovery and sample weighing for mass fraction and microscopic examination.

Whatever the initial pulp, observations revealed a majority of material (both organic and inorganic) of the fine fraction passing the 11µm openings. For a common DIP, the “fine fraction” 60-70% of particles smaller than 11 µm, corresponding to about 30% of the whole pulp. When considering deinking flotation rejects (secondary cells), 80-95% of the sample (composed by mainly mineral fillers) was contained in the <11µm fraction, indicating that only the finest particles were rejected during the flotation operations.

Besides the presence of a majority of finest elements, the mass distribution of fines in each sub-fraction is showed to be strongly dependent on the raw material.

Combining results from the new method developed with data from laboratory Bauer McNett classifier provides a complete analysis of the fibre and fines fractions, in terms of mass fraction and optical properties.

Microscopic observations revealed that slender, thin cellulosic fibrils were mostly free of ink in comparison to flakes where ink deposition was observed. Mineral flakes from coating had varying ink coverage, from uninked to partially or completely inked, and they were generally not linked to cellulosic fines. Cellulosic fibrils and flakes were present in each fine fraction, the lowest fraction category containing the finest of such particles.

An image analysis module was then developed in order to automatically analyse 3 categories of fines: cellulosic fibrils, flakes and inorganic mineral flakes. The distinction was possible thanks to the difference in the grey level intensities and introduction of a new intensity factor. Promising results were obtained, both in terms of differentiation and quantification.

Having established the presence of ink within the fines fraction, the second part of work (Chapter n 3. - Fractionation processes and separation of fines) focused on the selective separation of such fines with a micro-perforated screen basket and closed rotor configuration, proposed as a better alternative to available screening (fine slot) and working technology.

Since no studies were available on this screen plate-rotor combination, designed for industrial lines, a large part of the work dealt with the complete characterization of the screen, its functioning and its efficiency (selectivity), compared with that measured for screens with other aperture sizes.

The pressure screening system equipped with a 250µm smooth hole basket and solid core rotor was analysed with respect to reject thickening behaviour, morphological characteristics of fractions, the flow model of the screen-rotor configuration, and the degree of fractionation (β). A detailed analysis of the rotor pressure pulsations was also performed, to develop a better understanding of screening mechanisms.

The thickening factor which is primordially related to the screen aperture size (and design) had a direct impact on pressure screen operation. The micro-hole screen plate showed much higher thickening in comparison to a slot or a bigger perforation screen plate reported by other workers.

Fractionation led to an enrichment of fines into the accepts and long fibres in the rejects. Performing a two stage trial with deinking pulp reduced further the residual fines in the long fibre fraction and hence

the ink content. Analyses revealed that the mineral fillers and the cellulosic fines followed the flow split. On the other hand, the equipment was very selective for fibres, which were almost completely rejected.

It was also demonstrated that the screening system equipped with a closed rotor worked on a plug-flow model, as this model gave passage ratio distribution based on fibre length which were effectively independent of volumetric reject rate.

Moreover, as it was be expected, the fibre nature also had an impact on the selectivity. For a given fibre length, flexible chemical pulp fibres showed a higher passage ratio in comparison to rigid stone groundwood mechanical pulp fibres, the highest values being obtained for ONP/OMG pulp, and lowest for the screening rejects where stiff fibres concentrate.

The smooth micro-hole screen plate showed a degree of fractionation, β equal to 1.0 which was consistent with the results published with conventional smooth holes and significantly higher compared to profile slots (β equal to 0.5-0.6). This conclusively showed the high fractionation efficiency and the ability of the screen plate to selectively separate the fines into the accept stream.

Finally, to increase productivity, some additional studies were performed: unfortunately, the increase of the average passing velocity or the pulp concentration within the operating limit gave similar results on thickening factor. Also, it was not possible at higher pulp concentration to either increase the average passing velocity or decrease the volumetric reject rate. The reasons were determined by studying the pressure pulsations produced by the solid core rotor, namely the negative pressure pulses responsible for removing the accumulated debris on the upstream of the screen plate and thus expected to have the potential to increase screening capacity. Measurements showed indeed a high magnitude such pulses, which however did not translate into an increase of capacity. It was found that the effective passing velocity (resulting from effective volume passing the mico-holes during the screening phase, i.e. the volume backflushed during the negative pulse added to the volume fed in) did not increase to similar proportions as the increase of the average passing velocity. Further analysis revealed that (and especially on the reject section of the screen) at higher pulp concentration the amount of fibre mat formation between two passages of the pulsation element was high enough to disallow any increase of hydraulic loading. This was believed to explain the negligible effect of the operating condition variations, and the capacity constraints associated.

Additionally, the study revealed the existence of curves with truncated (flat end) negative pressure pulse followed by a very high pressure peak at the end of the negative pressure pulse. This highlighted the cavitation phenomenon which was occurring in the middle and reject sections of the screen. This also showed the importance of the feed pressure playing a decisive role in determining the cavitation risks.

The final part of the work (Chapter n°4. -Application of fractionation to deinking and paper layering) dealt with the purification (ink removal) and the utilisation of fines fractionated via micro-hole screen basket with the objective of deinking process simplification and of improving stratified paper manufacturing.

First, the fine fraction from deinking pulp was deinked by flotation, with an efficiency close that of the process performed on the whole pulp. The ink removal selectivity with respect to fibre loss was higher for the fine fraction flotation than for the whole pulp treatment (likely because of the very low fibre concentration of the fine fraction). Simple simulation analysis showed that comparable final pulp characteristics could be achieved by combining three stage micro-hole fractionation and fine fraction

flotation, instead of the conventional deinking line, that applies flotation on the whole pulp. A further advantage of the new line design would be that specks in the pulp follow the micro-hole pressure screening rejects (long fibres), and consequently the dispersion treatment could be applied only on this fraction. Results obtained showed also that the final pulp quality can be adjusted by lowering the volumetric reject ratio of the pressure screening system: this resulted in clean rejects with respect to ink contamination, as higher thickening values were achieved.

So, deinked pulp fractionationation is a viable strategy for deinking optimisation. However, fractionation can be also proposed for virgin pulps. In this latter case, its only purpose will be the isolation of fines and fibres, in order to subsequently add them in a controlled way, for a single or multilayer paper manufacturing.

Within this approach, an additional treatment of the fines could be also envisaged in order to isolate the most performing fines- the fibrillar type, i.e. as shown in literature, fines that have higher bonding capacity. In the present study, a small diameter hydrocyclone was used to further fractionate mechanical pulp fines into fibrillar and flake types. Their effect on sheet properties was studied. Incorporation of fibrillar fines (from the hydrocyclone base fraction) into long fibres from micro-hole screen resulted in handsheets with better mechanical strength and optical properties than those obtained when incorporating the flake type fines. For some sheet properties, similar values were achieved with the addition of a fibrillar fines amount half of that required when adding the flake fines.

These results confirmed the interest of fractionating fines in order to rationalize their use in papermaking, as for example to use them in multi-layer papers where fibrillar fines would find application mainly in top layers whereas flake type fines would be more appropriate for middle layers.

Such a fractionation strategy was also applied to the deinked fines: in this case, the fine fraction from the micro-hole screen was firstly deinked and then fractionated by hydrocyclone. After 2-stage washing operations to remove residual ink, the micro-hole rejects were fractionated with hydrocyclone. All the resulting 4 fractions were characterised morphologically and their optical properties assessed. At the end, four different fractions were available and they could be combined in a number of ways to produce new higher quality papers.

To conclude, it was shown that i) the pulp fractionation by pressure screens (with micro-holes basket) allows to optimise the deinking process (if subsequent fines and fibre treatments are optimised), ii) the combined use of the two fractionation technologies- the pressure screens (with micro-holes basket) and the hydrocyclone- could be efficaciously used for high quality stratified paper manufacture.

Crucial points of the advanced method of fractionation for deinking and for multi-layer sheet formation are:

a. Selective separation ink and its treatment:
    - This requires separation of fines from long fibres, followed by ink removal from fines.

b. Selective separation and treatment of fibre fraction:
    - This requires separation of long fibres from fines, followed by contaminant removal (specks, macro-stickies) and fibre upgrading operation (e.g. application of mechanical energy)

c. Generation of fractions for stratified forming:
    - This could require fractionation of fines obtained after their treatment (objective n°1a) into high and low specific area fines.
    - This could require fractionation of fibre fraction after their treatment (objective n°1b) based on their development- fibrillation & cell wall thickness.

The latter strategy can also be applied for mechanical pulps; in this case the fractionation will only address the multi-layer paper production.

Besides the advances in the pulp fractionation for deinking, the present work also pointed out the promising potential of a specific technology, not already available on the market, as the pressure screening with micro-holes basket. This kind of equipment will likely greatly contribute to 'increasing' the valorisation of fines, because it efficiently separates fines in pulp suspensions, leading to important advantages in future manufacturing concepts as it holds the key to deinking line rationalization and offers possibility to generate fractions for a multi-layer headbox. Indeed, a number of configurations of unit operations could be envisaged for a new rationalised deinking pulp manufacturing process. Treating only a fraction of the whole pulp would reduce energy demand and additional benefits could be thought of considering separate bleaching of fractions.

From the current study, new perspectives of work could be proposed.

With image analysis techniques it was highlighted to possibly separate different fines categories. Microscopic slide preparation demands time and there are various sources of error. It could be very much useful if the same technique of analysis could be performed directly with very dilute fines suspensions across a flow cell, enabling to distinguish and measure online, the cellulosic fibrils, flakes and mineral flakes.

The technique of soft-hyperwashing could be scaled up to treat higher amounts of fine fraction. Due to not effective agitation, equipping a Bauer McNett classifier with smaller apertures might not solve the situation as the smaller are the particles, the higher is their number which would then form a mat (higher upstream concentration) and offer a high resistance to flow across the apertures. New deplugging methods have to be ascertained to keep the apertures clear of the accumulated debris. One method could be vibrating plates as in the case of Somerville equipment.

Recovering sufficient quantifies of fibrils and fines would then enable the understanding of sheet properties with different fines sub-fractions especially with respect to deinking pulp where very little or no literature exists. This would also allow understanding the adsorption of colloids on the fine sub-fractions.

Though the micro-hole screen basked was effective in fines separation into accepts, a slight drawback was the inability to increase passing velocity (higher production) at high concentration (>15g/L) and low volumetric reject rates (for better long fibre cleanliness). Possibilities exists (working on both screen and rotor design) to achieve increased disruption and reduced formation of the fibre mat which forms over the screen plate surface and lowers the capacity. Indeed, higher accept concentration (with low fibre concentration) would be economically beneficial for any further treatment including chemical application (for example in deinking cells).

The 2-stage deinking pulp fractionation was performed with full feed forward configuration. This required reject dilution between stages. One possible solution to decrease or eliminate this input water is a full feed backward 3-stage screen configuration. In the 2nd and 3rd screening stages, the pulp

experiences a high mass reject ratio. Accepts have low total concentration. This eventually paves the way for studying the possibility of reusing them in preceding stages as reject dilution. Simulations based on the results gained in terms of fibre and fines passage ratio distributions should be used to optimise such screening systems.

Once each fraction separated, the dedicated treatment for both fines (flotation) and fibres (dispersion) should be optimised. As an example, numerous parameters (operating conditions and pulp properties) are associated with the flotation operations. Hence a vast field of work needs to be studied with respect to optimisation of fines flotation -chemistry and other flotation parameters, such as pulp concentration.

Similarly, the treatment of fibre fraction with application of mechanical energy has to be examined. Further fractionation of fibre fraction (micro-hole rejects) with a hyrocyclone and concentrating the specks in one fraction would again lead to less pulp fraction to be treated in high energy consuming dispersers.

Micro-hole and hydrocyclone fractionation offers the opportunity of examining the bleaching response of fibre and fines fractions. Avenues of energy and cost savings are possible by optimizing the bleachability of fractions.

Lastly, the effect of the fines and fibre fractions (produced by hydrocyclones) need to be analysed with respect to stratified sheet manufacturing. Such an analysis would put forward the high binding ability of the fibrillar fine fraction even at higher amounts of mineral content.

6. - Summary of the document in French

6.1. - Introduction

Les matières premières utilisées par l'industrie papetière correspondent principalement aux fibres générées à partir du bois (pâtes chimiques, blanchies ou non, et pâtes mécaniques) aux fibres recyclées (issues des papiers récupérations) et d'autres matières premières (principalement des charges et pigments minéraux ainsi que d'autres additifs), comme illustré par la Figure 191.

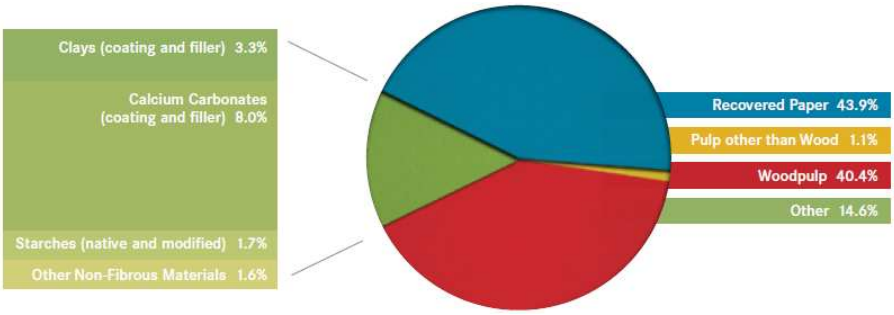

Figure 191: Consommation de matières premières de l'industrie papetière en Europe, CEPI 2010 [1]

Au cours des dernières décennies le développement croissant du recyclage a de fait fortement contribué à réduire l'intensité en matière première du secteur préservant ainsi la ressource forestière. L'industrie papetière européenne devra poursuivre ce développement pour atteindre le nouvel objectif de 70% de taux de recyclage qu'elle s'est fixé pour 2015, conformement à la dernière Déclaration Européenne sur le Recyclage des Papiers-Cartons [4].

Dans le domaine du désencrage des papiers de récupération, environ 30 à 45 % de la matière correspond à une « fraction fine ». Elle est définie comme la fraction des particules de taille inférieure à 75 µm, principalement constituée de charges minérales, de fines cellulosiques et de particules d'encre. L'essentiel de l'encre qui devra être éliminée se retrouve dans cette fraction fine sous la forme de particules isolées ou liées à la surface d'autres particules organiques ou minérales. Par ailleurs, une partie des éléments cellulosiques de cette fraction joue un rôle essentiel pour les propriétés du papier, notamment les éléments très fins de type fibrillaire dont la contribution au développement des propriétés mécaniques est très supérieure à celle des éléments fins de type granulaire.

Sur la base de ce constat, les travaux de recherche ont été concentrés sur le fractionnement de la pâte avec pour double objectif i) de séparer sélectivement la fraction fine de la pâte désencrée pour en éliminer les encres par flottation limitant ainsi l'opération à cette fraction avec pour conséquence des bénéfices économiques, et ii) de traiter les éléments fins cellulosiques pour en extraire les fines les plus pertinentes performantes en vue d'améliorer les propriétés mécaniques.

Dans un premier temps des méthodes de caractérisation des fines ont été mises au point pour déterminer dans quelle mesure les encres sont liées ou non aux fines cellulosiques et charges minérales. Dans un second temps une analyse très complète du procédé de fractionnement selon la technologie de classage sous pression sur tamis à micro-trous a été développé et pour finir des

applications de cette technologie sont exposées d'une part pour la rationalisation des procédés de désencrage et d'autre part pour la fabrication de papiers stratifiés.

6.2. - Caractérisation des éléments fins

Les fines ou éléments fins correspondent aux particules organiques ou minérales les plus petites qui sont présentes dans les suspensions fibreuses à l'exception des substances colloïdales et dissoutes. Conformément à la méthode TAPPI T-261-00 et comme le font de nombreux chercheurs, les fines sont définies comme des éléments passant (**P**) à travers un tamis de 75 µm d'ouverture de maille soit 200 mesh. L'unité "mesh" correspond au nombre d'ouverture par unité de longueur (exprimée en pouce). La partie de la suspension fibreuse qui est retenue sur le tamis est généralement noté **R**.

Les premières études fondamentales sur la caractérisation des fines ont été réalisées en 1939 par Brecht & Holl [19] puis en 1953 par Brecht & Klemm [20]. Les fines cellulosiques, classées sur un tamis de 135 mesh, ont été classifiées en deux catégories qui dépendent de leur forme et de leurs dimensions caractéristiques. Les "flour stuff – Mehlstoff" sont des bouts de fibres (farine ou éléments lamellaires) et les "slime stuff – Schleimstoff" correspondent à des éléments fibrillaires appelés fibrilles (cf.Figure 192). Les éléments lamellaires (ou flakes) sont présents dans les fines primaires (cellules de parenchyme, fragments de vaisseaux) et dans les fines secondaires (fragments de parois fibreuses) générées lors de l'application de contraintes mécaniques. Les fibrilles sont des particules qui se présentent comme de fins filaments et sont majoritairement produites pendant l'action de raffinage.

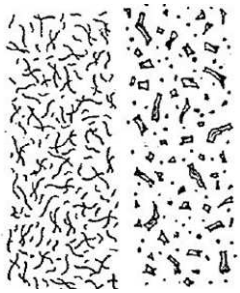

Longeur	To 200µm	20 – 300µm
Largeur	To 1µm	1 – 30µm

Figure 192: Eléments fibrillaires (gauche) et Eléments lamellaires (droite), selon Brecht & Klemm [20]

Les fibrilles augmentent la densité des papiers, ont un effet bénéfique sur leurs propriétés mécaniques, réduit la rugosité, le peluchage et l'arrachage fibreux lors de l'impression [20][26].

Parmi les éléments lamellaires , les cellules de parenchyme, fortement lignifiées et libérées lors de la fabrication de la pâte à papier, représentent 15 à 25% des fines primaires des pâtes chimiques alors que leur proportion n'est que de 5% dans le bois [25] [27]. Elles sont responsables du peluchage des papiers à cause de leur faible pouvoir de liaison [25][26][27]

En ce qui concerne le désencrage, l'un des constituants majeurs de la pâte correspond aux éléments fins. En fonction de la matière première utilisée, le taux de fines peut varier entre 25 et 55% [41][50] [51][52]. Ces fines sont constituées de fibrilles, d'éléments lamellaires et également d'éléments

inorganiques qui proviennent de la fabrication des papiers (charges minérales élémentaires ou agglomérées), de l'utilisation des papiers (particules d'encre en provenance de l'impression) ou encore de leur transformation (adhésifs). Avant d'être déposées sur le papier, la taille des particules élémentaires d'encre sont microscopiques voir sub-microscopiques et sont composées de pigments naturels ou de noir de carbone.

L'une des premières études utilisant l'analyse d'image pour caractériser les opérations de désencrage est celle de McCool & Silveri [46]. Ils ont décrits les efficacités d'élimination des "specks". Plusieurs chercheurs ont mentionné que les petites particules d'encre sont éliminées pendant l'étape très sélective de flottation [41][58] [59] (cf. Figure 193).

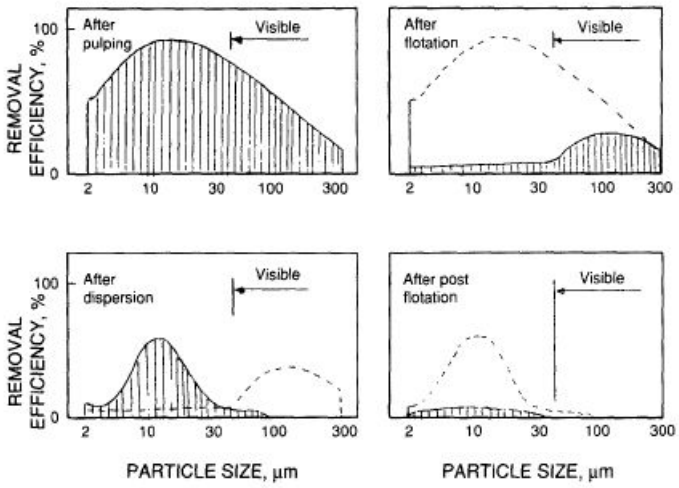

Figure 193: DIP unit operations particle size distribution and removal, selon Rangamannar & Silveri [59]

Les méthodes d'analyse d'image ont été largement utilisées pour déterminer les dimensions des particules d'encre et les efficacités des opérations unitaires [41][58][65][66][67][68][69]. Les particules les plus sombres sont détectées par un seuillage sur les niveaux de gris.

6.2.1. - Développement d'une méthode de soft-hyperwashing des fines

Comme vu prédédement, les fines issues des pâtes de récupération contiennent une grande variété de particules de différentes origines. Afin d'avoir une meilleure connaissance de ces particules, il est nécessaire de les séparer en fonction de leur taille et donc de les classer en sous-fraction. Une nouvelle méthode a été développée [73] pour séparer les éléments fins de désencrage préalablement collectées lors du test de fractionnement Bauer Mac-Nett. Basée sur le concept de l'hyper-lavage, la méthode utilise un jet d'eau à faible pression. Dans l'hyper-lavage, la totalité de la pâte est lavée avec un jet ou une douche à haute pression jusqu'à ce que le filtrat soit visuellement clair [61].

L'idée du "l'hyper-lavage doux" (soft-hyperwashing) est de ne pas forcer les particules à passer à travers le tamis. Dans cette nouvelle méthode, le jet d'eau utilisé est généré à partir d'une buse cylindrique de 1 mm de diamètre environ avec une pression de 70 ±10 kPa. La faible pression évite également les phénomènes de giclement et donc la perte des fines sur les tamis les plus fins. Le jet d'eau est maintenu tant que la turbidité du filtrat est supérieure à 15-18 FNU. Les tailles des tamis utilisés ont une ouverture de maille de 50 µm, 25 µm et 11µm.

6.2.1.1. - Principaux résultats du « soft-hyperwashing »

Pour des pâtes triturées en laboratoire à partir de 50%ONG+500%OMG et 100%ONP, la répartition massique selon des longueurs des fibres et des éléments fins est reportée sur la Figure 194. La fraction P11 µm correspond à la fraction la plus importante de la distribution soit 30% de la masse de la pâte entière pour une composition de 50%ONP et 50%OMG et à 13,4% pour une composition 100% ONP.

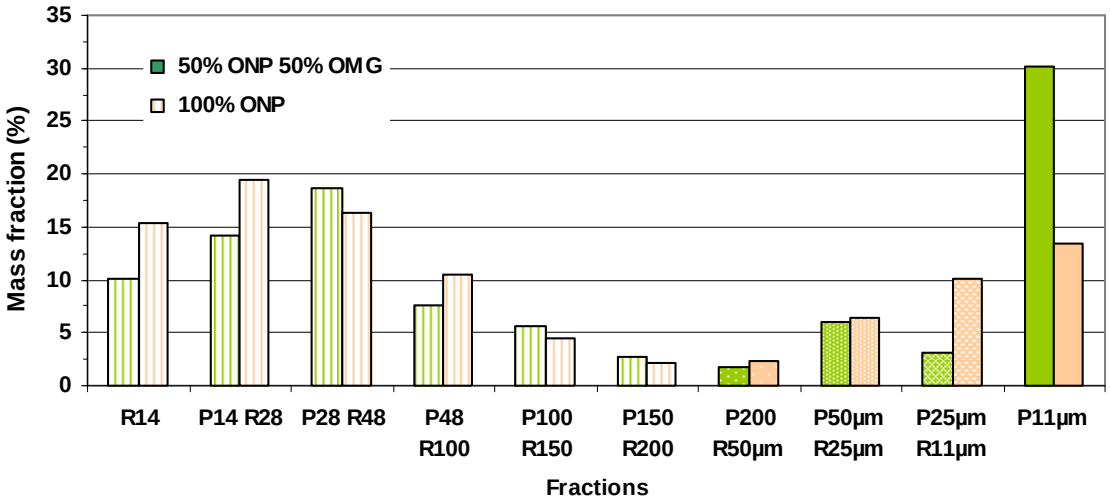

Figure 194: Fraction massique des fibres et des fines

Les Figure 195 et Figure 196 montrent l'évolution des blancheurs et des valeurs d'ERIC pour les différentes fractions. La quantité maximale de particules d'encre est contenue dans la fraction fine alors que les fractions fibreuses jusqu'à R200 contiennent peu d'encre résiduelle.

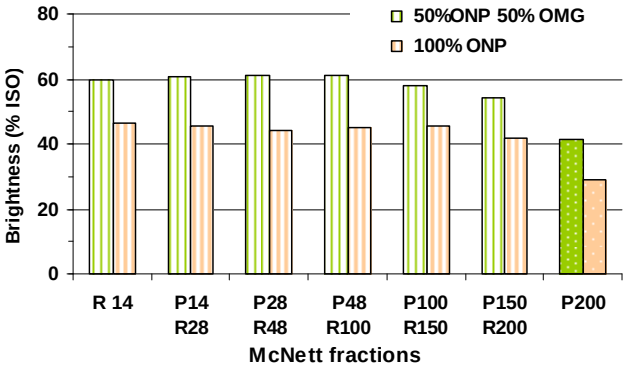

Figure 195: Blancheur des fractions McNett

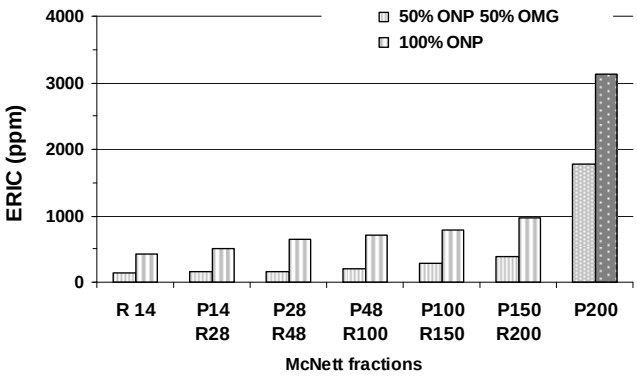

Figure 196: ERIC des fractions McNett

En ce qui concerne les "sous-fractions", les résultats sont reportés sur les Figure 197 et Figure 198 pour une pâte issue de 100% ONP.

Les fractions P200 µm R50 µm et P50 µm R25 µm ont des blancheurs légèrement inférieures et des valeurs ERIC supérieures à celles des fractions Bauer-McNett. Le nombre élevé de particules d'encre de petite taille augmente fortement les valeurs d'encre résiduelle. Les valeurs ERIC, pour la fraction P25 µm R11 µm, sont respectivement 3 et 2 fois supérieures à celles des fractions P200 R50 µm et P50 µm R25 µm avec une valeur de blancheur significativement plus basse. Cependant, la fraction P25 µm R11 µm encore une blancheur supérieure et une valeur ERIC inférieure à l'ensemble de la fraction P200. Cela prouve que la présence maximum d'encre résiduelle se trouve dans la fraction

P11 µm. Ce résultat est en accord avec celui de Ben *et al.* [50] qui indiquait une présence d'encre plus importante dans la fraction P400 que dans la fraction P200.

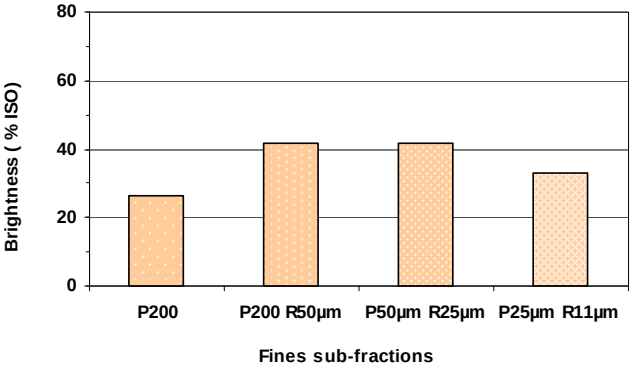

Figure 197: Blancheur des sous-fractions des fines, 100%ONP

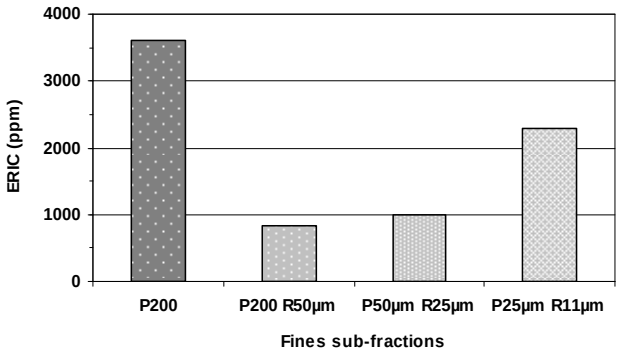

Figure 198: ERIC des sous-fractions des fines, 100%ONP

Dans le cas d'une pâte 50% ONP + 50% OMP, l'analyse microscopique des différentes "sous-fractions" révèle que 3 types d'éléments fins sont présents (cf.Figure 199).
les fibrilles : elles se présentent sous forme de filaments fins de cellulose plutôt linéaires.
- les particules lamellaires : elles regroupent les fragments de paroi fibreuse et les morceaux de cellules de parenchyme.
- les fragments de couche : ils sont issus de la couche minérale déposée à la surface des papiers.
La fraction P11 µm contient des fibrilles et des particules lamellaires de petites dimensions mais aussi de très petites particules colorées de dimensions inférieures au micromètre. Les charges minérales présentes ne semblent pas être associées à des fibrilles ou à des particules lamellaires.

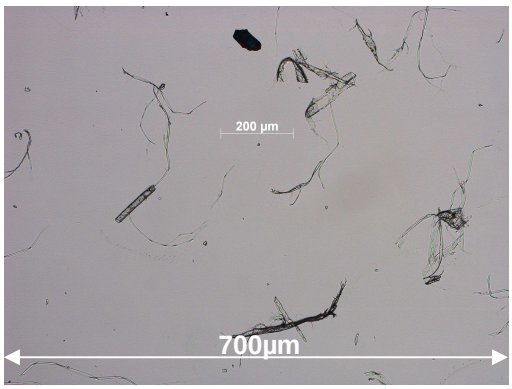

a) P200 R50µm

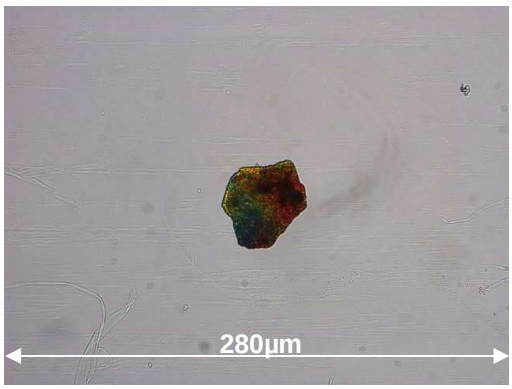

b) P50µm R25µm

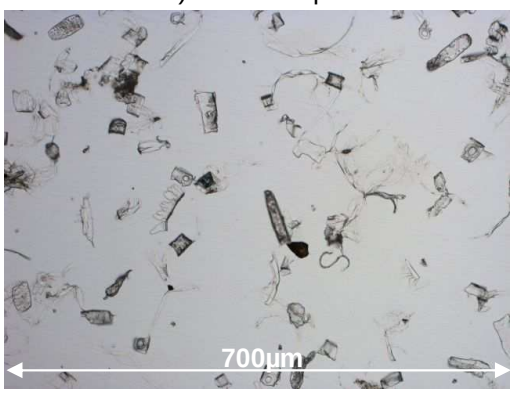

c) P25µm R11µm

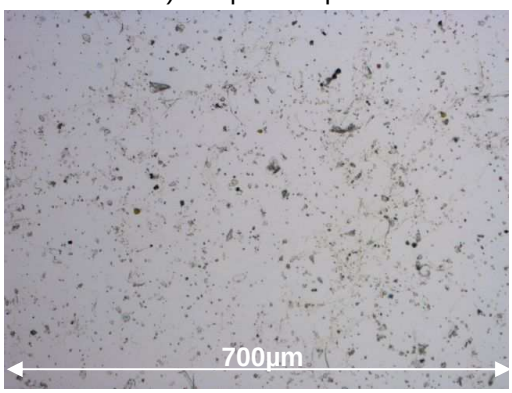

d) P11µm

Figure 199: Image microscopique des sous-fractions des fines

Des observations similaires ont été réalisées sur une pâte 100% ONP, imprimée pour la première fois sur un papier fabriqué à l'aide de fibres vierge de pâte mécanique et ne contenant pas de charges minérales. Comme précédemment, la fraction la plus fine contient les particules d'encre ainsi que les plus petites fines cellulosiques qui ont tendance à s'agglomérer pour former des amas. Les fibrilles des fractions supérieures semblent être libres de toutes particules d'encre.

La Figure 200 résume les résultats obtenus pour les fractions des rejets de flottation qui ont été prélevés sur site industriel. L'analyse des fractions massiques indique que 85 à 93% des particules fines sont dans la fraction P11 µm et une présence massive de particules minérales colorées (partiellement ou totalement) ou non dans cette même fraction (cf. Figure 201).

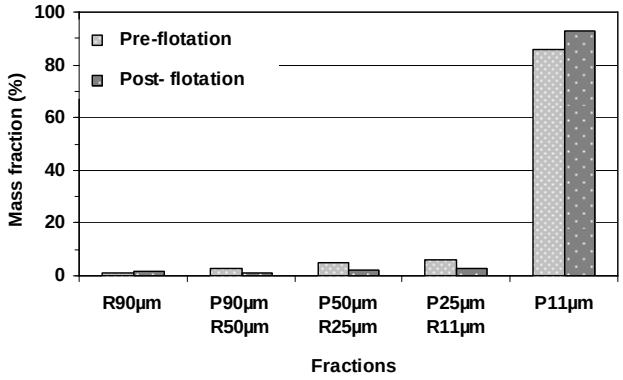

Figure 200: Refus de flottation

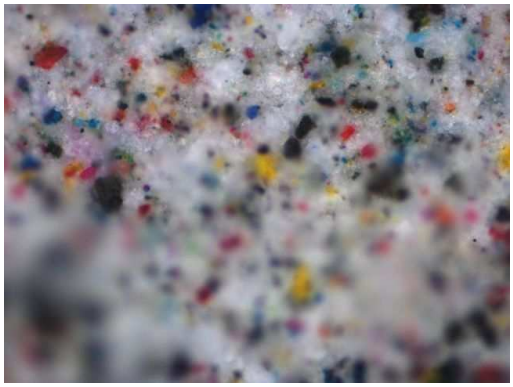

Figure 201: P11µm filter millipore

6.2.2. - Développement d'un module d'analyse d'image

Un module d'analyse d'image a été développé pour permettre de caractériser les fractions obtenues selon trois catégories de particules à savoir les fibrilles, les particules lamellaires et les charges minérales. Les images sont acquises en microscopie optique en lumière transmise et réfléchie puis elles sont traitées par lots.

La première étape consiste à éliminer les fibrilles par des fonctions de géométrie morphologique sur l'image en lumière transmise. Ensuite, les particules lamellaires cellulosiques et minérales sont identifiées en se basant sur le Facteur d'Intensité (cf. Eq. 27)

Eq. 27 : **Facteur d'intensité**

$$IF = \frac{(I_{max} - I_{min})}{I_{mean}}$$

I_{max}: niveau de gris maximum de la particule
I_{min}: niveau de gris minimum de la particule
I_{mean}: niveau de gris moyen de la particule

Les particules lamellaires ainsi identifiées sont supprimées de l'image obtenue en lumière réfléchie pour quantifier les fibrilles. La procédure complète est illustrée sur la Figure 202.

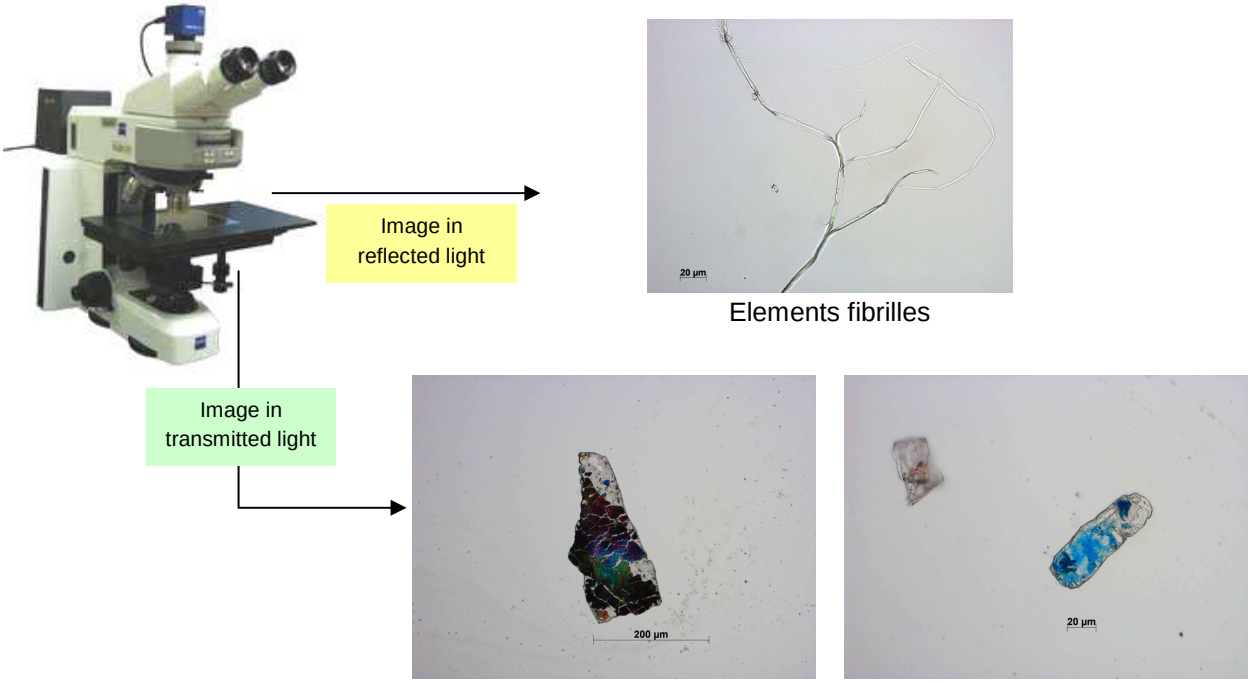

Figure 202: Principe de séparation en trois categories des particules fines.

6.2.3. - Conclusions sur la caractérisation des éléments fins

La méthode de laboratoire "Soft-Hyperwashing" a été développée pour obtenir des sous-fractionnements sur différents tamis ayant une ouverture de maille allant jusqu'à 11 µm. Elle a permis de mettre en évidence que concernant la fraction P200 (Bauer-McNett) la grande majorité des éléments fins (fibrilles et particules lamellaires) et des particules d'encre se retrouvent dans la fraction P11µm.

Les fibrilles qui sont fines, très flexibles et ayant un potentiel de gonflement important, sont pour la plupart libres de toutes particules d'encre résiduelle ; l'encre étant préférentiellement associée avec les particules lamellaires. Les charges minérales, colorées ou non, sont présentes majoritairement dans la fraction P11 µm.

Les cellules de désencrages fonctionnent selon le principe de la flottation qui est une opération unitaire très sélective pour les particules très petites et très fines. L'étude des rejets de flottation d'une installation industrielle a montré que 85 à 90% (en masse) des particules se trouvaient dans la fraction P11 µm.

Un module d'analyse d'image a été conçu afin de caractériser les différentes sous-fractions et de quantifier la proportion de particules lamellaires minérale, de particules lamellaires organiques et de fibrilles.

Une perspective intéressante serait de traiter spécifiquement la fraction des éléments fins qui contient un maximum de particule d'encre pour optimiser le procédé d'un point de vue énergétique et en terme de rendement matière. Ceci va être abordé dans la partie relative au fractionnement.

6.3. - Fractionnement

Le fractionnement de la pâte consiste à séparer la suspension de fibres en deux flux de pâte dont les propriétés diffèrent en termes de caractéristiques morphologiques des particules en suspension et donc de propriétés des papiers produits à base de ces fractions. La différence entre les opérations de classage et de fractionnement, réalisées sur tamis, réside dans le fait que la première est une opération d'épuration visant à éliminer les contaminants de la pâte (bûchettes, films plastiques, colles et adhésifs de type « stickies », etc.) alors que la seconde est dédiée à la séparation des constituants de la pâte selon notamment les caractéristiques des fibres. Le classage se traduit par des rejets de contaminants avec un minimum de fibres perdues et une pâte la plus propre possible alors que le fractionnement vise à produire deux fractions de pâte pour un usage séparé et/ou un traitement spécifique des fractions afin de réduire les coûts de traitement et/ou d'apporter de la valeur ajoutée au produit final par l'amélioration les propriétés des papiers.

Industriellement, le classage sous pression illustré par la Figure 203 et les cleaners ou hydrocyclones (cf. Figure 204) (permettant l'épuration de contaminants lourds et/ou légers) sont les deux technologies utilisées pour le fractionnement de la pâte.

6.3.1. - Fractionnement par classage sous pression

Dans le cas du classage sous pression, le fractionnement se produit au niveau d'un tamis (ou panier) avec l'aide d'un rotor équipé d'éléments générateurs de pulsation de pression assurant notamment le décolmatage du tamis. Les tamis de classage sont soit perforés (trous de 1.0 à 2.0mm de diamètre), soit équipés de fentes (typiquement de 0.10 à 0.15mm de largeur en épuration fine).

Dans le cas du cyclonage, ce sont les forces centrifuges et hydrodynamiques générées dans l'hydrocyclone qui, en relation avec la densité et la surface spécifique des particules en suspension, sont responsables du fractionnement de la pâte.

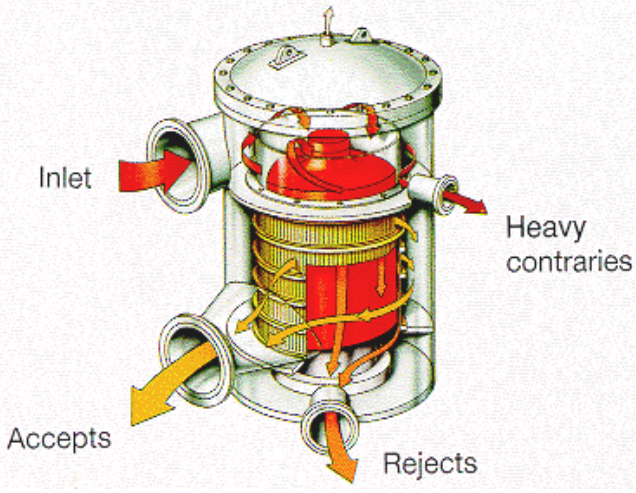

Figure 203: Exemple Voith - Escher-Wyss Omnisorter (notice commerciale). Le rotor, en rouge, générateur de pulsations de pression, se situe typiquement à l'intérieur d'un tamis cylindrique à fentes.

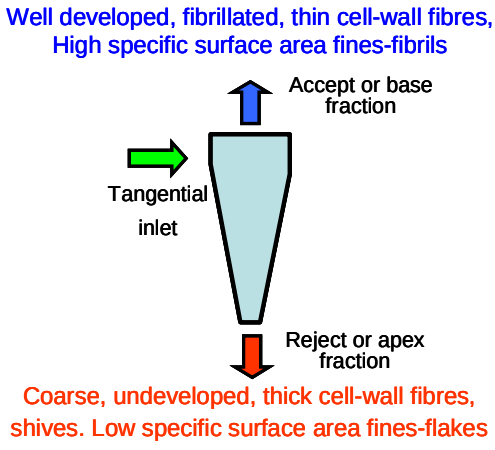

Figure 204: Représentation d'un hydrocylone pour le fractionnement de la pâte et caractéristiques des fibres dans les fractions

La Figure 205 illustre le principe de fonctionnement d'un équipement de classage.

Parmi les constituants de la pâte, l'eau rencontre le minimum de résistance pour traverser le tamis, suivi par les charges minérales, les fines cellulosiques, les fibres courtes et les fibres. De ce fait, les matières en suspension se concentrent dans les refus, les acceptés étant plus dilués conduisant ainsi à l'épaississement des refus, phénomène bien connu des industriels papetiers, que l'on exprime par le **facteur d'épaississement T**, tel que défini en Eq. 28.

Eq. 28 : $$T = \frac{C_r}{C_i}$$

C_r: concentration des rejets
C_i: concentration d'entrée

Concentration des rejets (**C_r**) > Concentration d'entrée (**C_i**) > Concentration des acceptés (**C_a**)

L'épaississement des refus dépend également duparamètre important de fonctionnement du classeur qui estde refus volumique défini par le rapport du débit de refus au débit d'entrée Eq. 29. Les classeurs industriels fonctionnent typiquement avec des taux de refus volumiques de 15 à 30%.

Eq. 29 : $$R_v = \frac{Q_r}{Q_i}$$

Q_i : débit volumique d'entrée
Q_r : débit volumique de refus

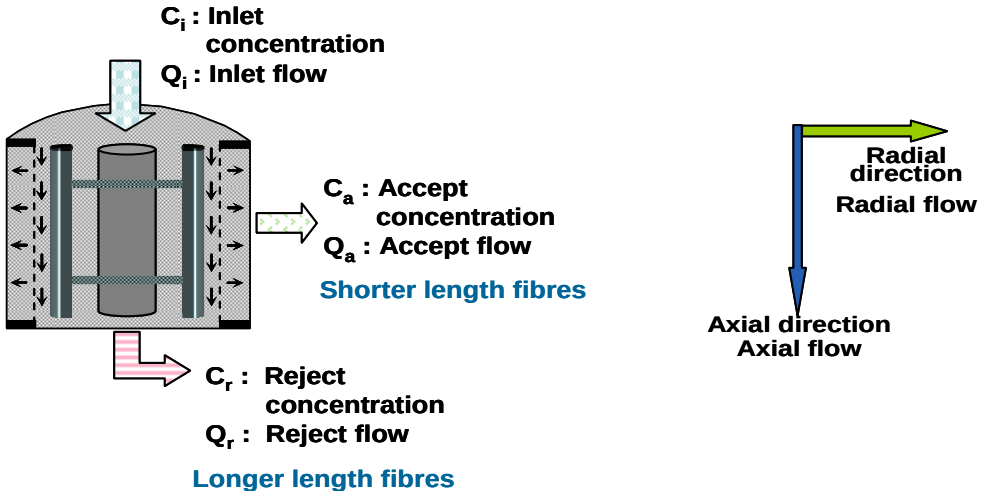

Figure 205: Equipement de classage et flux de pâte associés

L'épaississement plus ou moins important des constituants de la pâte selon leurs caractéristiques, notamment selon la longueur des fibres, conduit à un fractionnement de la pâte.

Le passage de particules à travers le tamis ou leur rejet est gouverné par de nombreux facteurs et phénomènes hydrodynamiques complexes à la surface du tamis. Les effets de fractionnement de la pâte sont plus prononcés dans le cas d'une pâte de résineux dont la distribution de longueur des fibres est plus étendue que celle d'une pâte de feuillus.

De nombreux travaux de recherche fondamentaux visant à mieux comprendre les mécanismes de fractionnement ont montré que les classeurs sous pression fractionnent principalement selon la longueur des fibres, la flexibilité/rigidité des fibres apparaissant comme un facteur secondaire [40][87][88][89] [90][91]. Les fibres les plus longues se retrouvent dans les refus alors que les fibres courtes et les fines parviennent à passer dans les acceptés.

6.3.2. - Elements d’un classeur sous pression

Tout classeur est constitué de deux éléments principaux, qui détermineront ses performances en termes d’efficacité, de capacité et de caractéristiques opérationnelles.

Le tamis, a pour fonction, principalement « barrière », d’éliminer les contaminants et autres particules indésirables qui nuiraient à la qualité de la pâte finale, en acceptant les fibres et éléments fins. Les tamis cylindriques ou paniers comportent des ouvertures, soit des trous (perforations cylindriques), soit des fentes généralement profilées, c'est-à-dire ménagées au fond de rainures parallèles à l’axe du tamis (perpendiculaires à l’écoulement) afin de favoriser le fractionnement de la pâte ou l’élimination des contaminants. Il existe différents types de tamis sur le marché, dont les caractéristiques sont définies en fonctions des applications aux pâtes mécaniques, chimiques ou recyclées.

Le rotor a pour fonction de contrôler les conditions hydrodynamiques complexes de l’écoulement au niveau du tamis, l’entraînement en direction tangentielle de la pâte à la surface du tamis et le passage radial au travers du tamis. Le rotor imprime une vitesse tangentielle à la pâte très supérieure à la vitesse d’écoulement dans le sens axial générée par l’évacuation des refus. Le rotor est équipé d’éléments de décolmatage du tamis générateurs de pulsations de pression.

Deux types de rotors sont principalement utilisés, les rotors « fermés » ou cylindriques caractérisés par une faible épaisseur d’écoulement entre le rotor et le tamis et les rotors « ouverts » équipés de foils présentant une forte épaisseur d’écoulement autour des foils.

La fonction essentielle du rotor est de maintenir suffisamment libre la surface amont du tamis où s’accumulent les contaminants ainsi que les éléments partiellement retenus de la pâte qui tendent à former une couche de fibres durant les phases de classage. Cette couche de fibres est éliminée régulièrement durant les phases de décolmatage du tamis générées par l’inversion du flux à travers le tamis, afin d’assurer l’efficacité de fonctionnement du classeur. Ce phénomène de re-pompage de la pâte vers le flux amont résulte de la dépression créée par les éléments de décolmatage après les phases de classage en surpression Figure 206. Le volume re-pompé s’ajoute ainsi au volume de pâte à tamiser durant les phases classage, ce qui conduit, durant cette phase de classage, à une vitesse moyenne cumulée de passage à travers le tamis, exprimée par la « vitesse de passage effective » Ve au niveau de fentes ou des trous du tamis qui peut être considérablement plus élevée que la vitesse de passage Vp classique, calculée à partir du débit d’acceptés et de la surface ouverte du tamis.

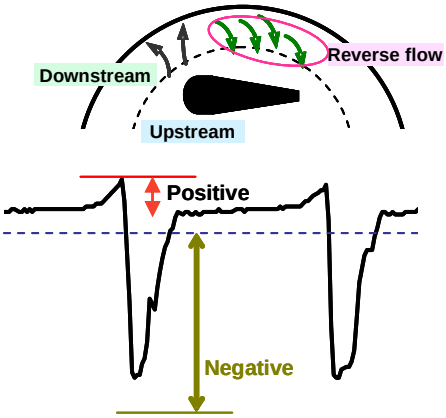

Figure 206: Représentation simplifiée de l’inversion de flux, ou re-pompage, généré par le rotor en relation avec les pulsations de pression produites

6.3.3. - Théorie de fractionnement par classage

Les phénomènes de classage et notamment l'épaississement des refus ont modélisés en 1989 par Gooding & Kerekes, sur la base d'un « taux de passage » P, défini pour des particules homogènes et des conditions hydrodynamiques de classage données au niveau d'une tranche élémentaire du tamis. Le taux de passage est défini par le rapport des concentrations en aval et en amont à ce niveau et pour chacune des classes de particules considérées (cf.Eq. 30).

Eq. 30 :

$$P = \frac{C_d}{C_u}$$

C_d : concentration aval
C_u : concentration amont
selon Gooding & Kerekes [143][146]

Ces relations exprimant le taux de passage de particules ont été étudiées par de nombreux auteurs afin de mieux comprendre les mécanismes de passage des fibres à travers les ouvertures du tamis. Un taux de passage nul exprime une rétention totale, une valeur de 1 un passage non entravé pour les particules qui suivent les flux hydrauliques, et des valeurs intermédiaires une rétention probabiliste des particules, notamment des fibres de diamètre très inférieur aux ouvertures (largeur de fentes ou diamètre de perforations) pour des longueurs très supérieures. Les relations entre longueur de fibres et taux de passage ont été établies par Olson [148]. Elles se présentent sous la forme d'une fonction exponentielle négative (cf.Eq. 31).

Eq. 31 :

$$P(l) = e^{-(\frac{l}{\lambda})^{\beta}}$$

λ: constante de taille
β: constant de forme
selon Olson [148]

Gooding et al. [149] ont analysé les courbes de taux de passage pour différentes valeurs de λ (qui représente le positionnement de la courbe selon la longueur de fibres en termes de seuil de coupure par rapport notamment aux ouvertures du tamis) et de β (qui se rapporte à la forme de la courbe) illustré dans Figure 98. Une valeur élevée de β traduit un fort degré de fractionnement, avec idéalement des courbes en S où l'essentiel des fibres de longueur inférieur à un seuil de coupure passent librement le tamis (acceptés) alors que celles de longueur supérieure sont essentiellement retenues (refus). Une bonne efficacité de fractionnement de la pâte selon la longueur des fibres est de ce fait indissociable d'un facteur d'épaississement élevé, du fait d'une rétention plus importante des fibres longues par rapport à des conditions de classage visant l'épuration des contaminants.

Gooding & Kerekes [143] ont établi, par intégration des relations d'une section élémentaire à l'ensemble du tamis, les expressions donnant le facteur d'épaississement en fonction du taux de refus volumique, ceci pour deux modèles d'écoulements en amont du tamis.

6.3.3.1. - Modèle mélange parfait

Ce modèle suppose un mélange parfait dans direction radiale comme dans la direction axiale de l'écoulement. L'expression du taux de passage est donnée par l'Eq. 32.

Eq. 32 :

$$T = \frac{1}{P - P.R_v + R_v} \quad \text{ou} \quad P = (\frac{1}{T} - R_v)(\frac{1}{1 - R_v})$$

6.3.3.2. - Modèle écoulement piston

Ce modèle suppose également un mélange parfait dans la direction radiale (concentration homogène dans une tranche de tamis), mais sans aucun mélange dans la direction axiale. L'expression du taux de passage est donnée par l'Eq. 33.

Eq. 33 : $$T = R_v^{(P-1)} \quad \text{ou} \quad P = \frac{Ln(T)}{Ln(R_v)} + 1$$

6.3.4. - Equipement et matières testées

Des essais de fractionnent ont été effectués à l'échelle pilote sur un classeur équipé d'un tamis à micro-trous de 0.25mm de diamètre et d'un rotor fermé comportant 3 pales et tournant à 25m/s en bout de pales. Le tamis d'un diamètre intérieur de 353mm pour une longueur de 257mm, avec une épaisseur de tôle de 2mm (cf. Image 9) présentait un taux de surface ouverte nominal de 10%.

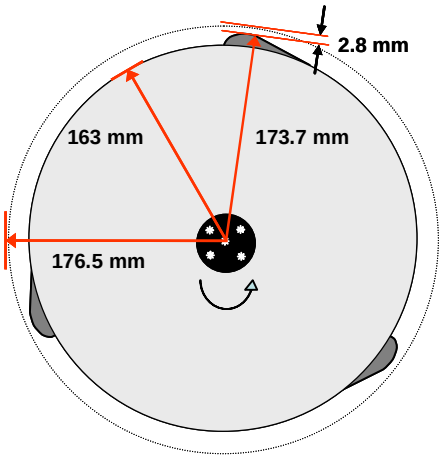

Image 9: Schéma et dimensions du rotor fermé équipant le classeur pilote.
Le tamis, d'un rayon intérieur 176.5mm, est représenté par les pointillés.

Trois types de pâte dont les caractéristiques sont indiquées dans le Table 28, ont été testés

Table 28: Pâtes étudiées

Pulp	Remarks
1. **Pâte mécanique de meule (SGW)**	❖ Pâte provenant d'une usine Scandinave
2. **Pâte chimique 65% résineux, 35% feuillus**	❖ Pâte raffinée et ajout de 23% de kaolin
3. **Pâté à désencrer (ONP/OMG)**	❖ Mélange de 75% de journaux (ONP) et 25% de magazines (OMG)

6.3.5. - Résultats

6.3.5.1. - Evolution du facteur d'épaississement

Dans le cas de la pâte chimique, et grâce de l'ajout de kaolin comme élément traceur, les facteurs d'épaississement ont pu être calculés pour la pâte mais aussi pour la fraction fibres (fraction organique) et pour les charges de kaolin (fraction minérale).

Les résultats (cf. Figure 107) indiquent que les charges suivent l'eau avec un facteur d'épaississement de 1 et donc un taux de refus massique égal au taux volumiques, contrairement aux fibres qui présentent un fort épaississement et conduisent donc un taux de refus massique élevé, même à faible R_v.

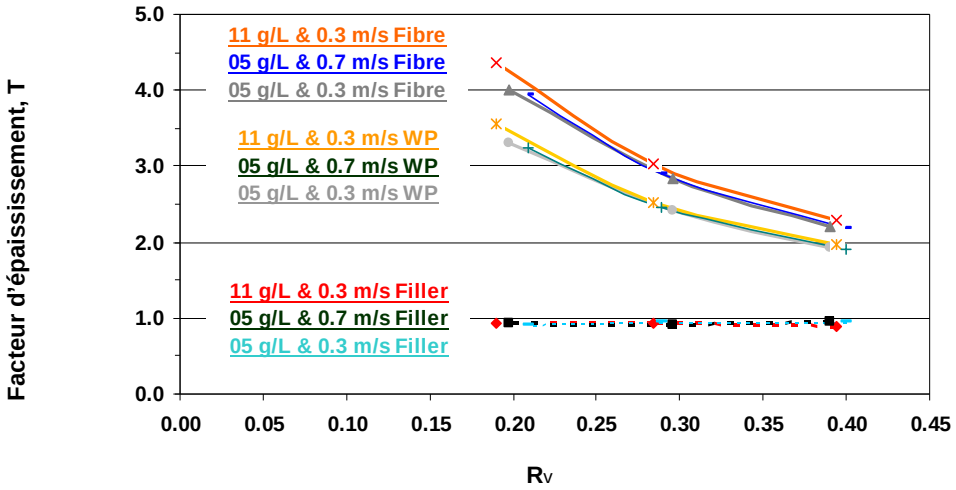

Figure 207: Facteur d'épaississement de la pâte chimique et de ses constituants

6.3.5.2. - Analyses Bauer McNett

Les Figure 208 and Figure 209 montrent les distributions de longueur Bauer McNett mesurées dans les acceptés et les refus pour différentes conditions de classage.

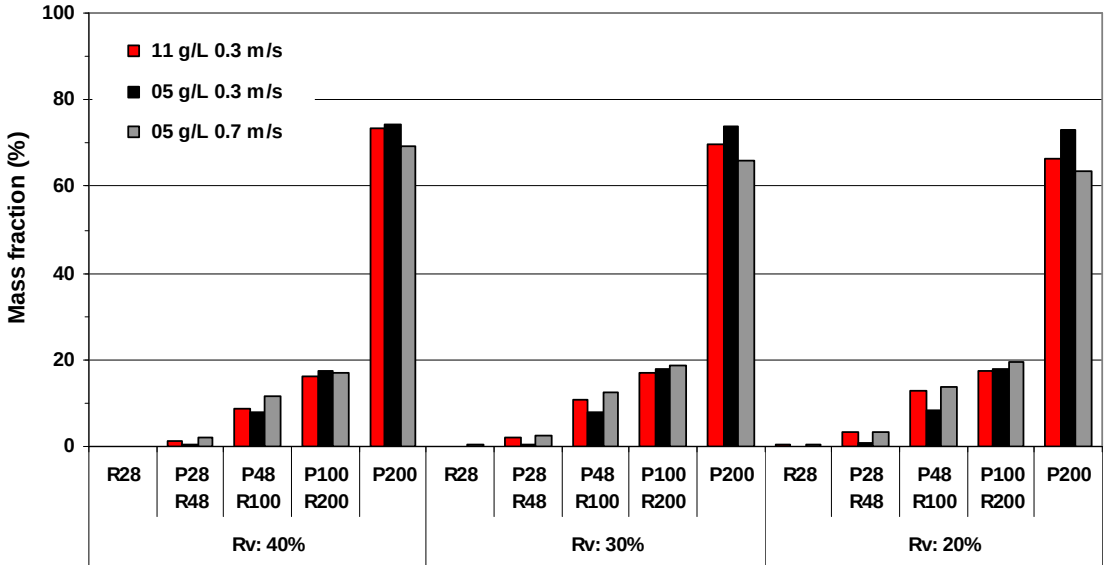

Figure 208: Répartition Bauer McNett pour la pâte SGW – Acceptés

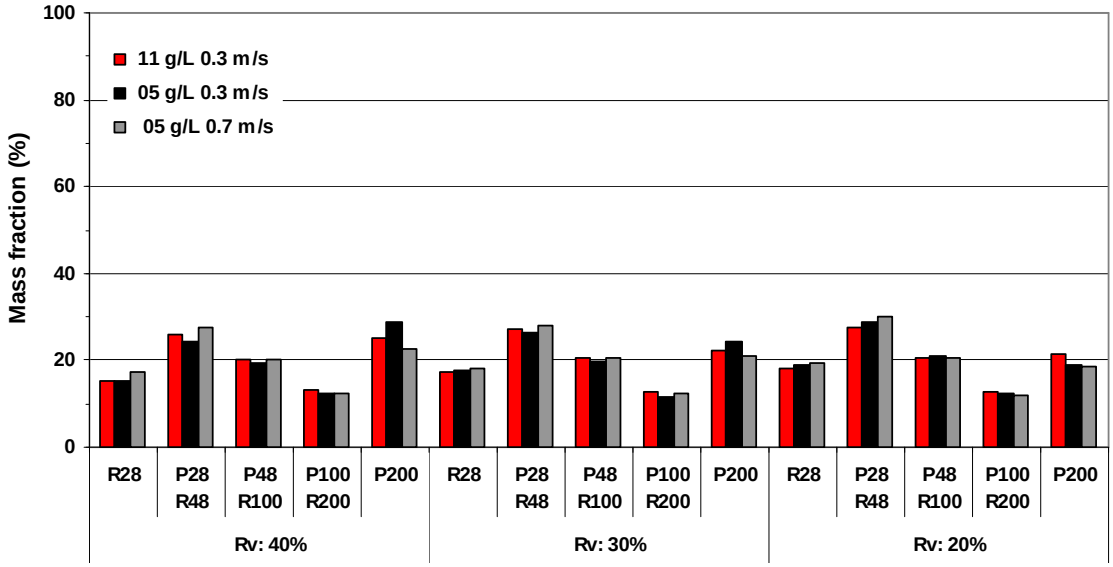

Figure 209: Répartition Bauer McNett pour la pâte SGW – Refus

Les résultats font apparaître logiquement l'enrichissement des éléments fins dans les acceptés et des fibres longues dans les refus. Cet enrichissent (fibres jusqu'à R200) est légèrement plus important à faible taux de refus du fait du « lavage » plus poussé des éléments fins. Les effets de la concentration et de la vitesse de passage n'apparaissent pas significatifs.

6.3.5.3. - Comparaison des taux de passage

La synthèse des résultats d'analyse des taux de passage des fibres en fonction de leur longueur et de leur nature est illustrée par la Figure 210. Pour une longueur de fibres donnée, la pâte chimique présente un taux de passage plus élevé que la pâte mécanique, du fait de la plus grande souplesse des fibres passant plus aisément à travers les micro-trous du tamis.

La comparaison des taux de passage obtenus, à longueur de fibre donnée, pour une même pâte désencrée (ONP/OMG) en premier et en second étage de classage fait apparaître un taux de passage plus faible au second étage du fait que les fibres les plus rigides sont préférentiellement rejetées au premier étage et conduisent donc à taux de passage plus faible lorsqu'elles sont traitées en second étage où elles se concentrent.

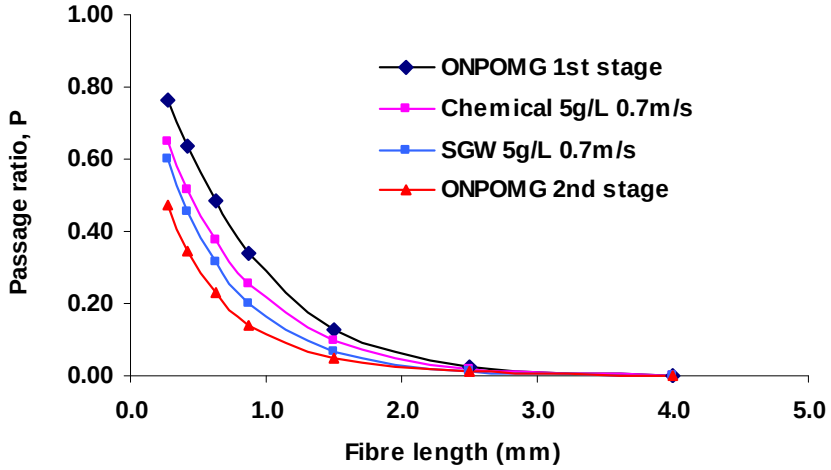

Figure 210: Comparaison des taux de passage de fibres de différentes natures en modèle d'écoulement piston (tamis à micro-trous de 0.25mm de diamètre)

L'analyse des résultats obtenus, a montré que le modèle piston représentait effectivement mieux la réalité de l'écoulement dans la configuration du classeur testé, avec un rotor fermé conduisant à une épaisseur d'écoulement faible par rapport à la distance axiale avec en conséquence relativement peu de mélange axial conforme au modèle d'écoulement piston. Les résultats ont mis en évidence un degré de fractionnement élevée, β, avec des valeurs proches de 1.0. Les tamis à micro-trous conduisent ainsi à des efficacités de fractionnement élevées entre fibres, fibres courtes, et éléments fins, comparativement aux tamis d'épuration conventionnels à fentes fines profilées dont les valeurs de β sont proches de 0.5. Les éléments fins sont ainsi séparés efficacement des fibres dans un flux de pâte acceptée, alors que le flux de rejets est enrichi en fibres.

6.3.6. - Capacité de classage

Des limites de capacité du classeur ont été observées lors des essais en particulier l'impossibilité d'augmenter la vitesse de passage à concentration accrue et faible taux de refus volumique. Ces observations ont conduit à effectuer des mesures de pulsations de pression créées par le rotor afin de comprendre les raisons de ces limites par rapport à des conditions de classage à fentes classiques. Sur la base de ces mesures, il a été possible d'évaluer, les débits de re-pompage à travers le tamis et donc les vitesses de passage effectives durant la phase de classage. Ceci a permis d'estimer, à partir des distributions de taux de passage des fibres selon leur longueur, les quantités de fibres déposées en fin de phases de classage. La Figure 211, représente ces quantités de fibres déposées en termes de grammage (poids déposer/m²), au niveau des sections d'entrée et de sortie (refus) du tamis et pour différentes concentrations d'alimentation. Ce grammage plus élevé à concentration d'entrée accrue (11g/L) l'est également davantage au niveau de la section de sortie du tamis du fait de l'épaississement des refus, indiquant que le colmatage du tamis se propage à partir de cette section de sortie. L'observation des limites de capacité de l'appareil résultant de ce colmatage, suggère que ce processus apparaîtrait à partir d'un grammage de fibres déposées de l'ordre de 80g/m², ce qui correspond effectivement à un matelas de fibres suffisant pour commencer à réduire de manière significative la vitesse de filtration à travers ce matelas.

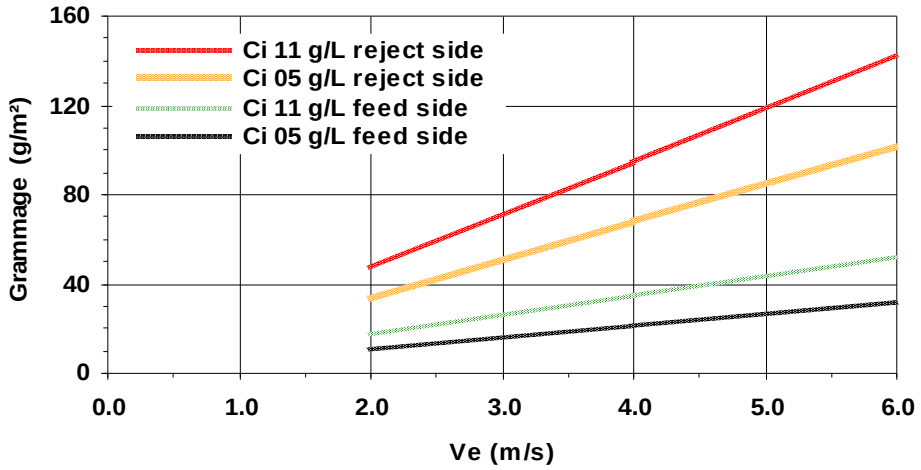

Figure 211: Grammage déposé sur le tamis en fin de phases de classage en fonction de la vitesse de passage effective au niveau des sections d'entrée et de sortie du tamis

6.3.7. - Application du fractionnement au désencrage et aux papiers stratifiés

Comme observé précédemment, le tamis µ-trous de 0.25 mm, qui possède une forte efficacité de fractionnement, permet d'enrichir préférentiellement les acceptés avec la fraction d'éléments fins. Une

fois séparés, ces fines peuvent être traités dans des cellules de flottation pour éliminer l'encre présente dans le cas du désencrage par exemple.

La génération de plusieurs fractions peut également trouver des applications dans la structure de papiers multi-couches où chaque fraction peut être mise dans la couche adéquate. Un tel concept est illustré par la Figure 212.

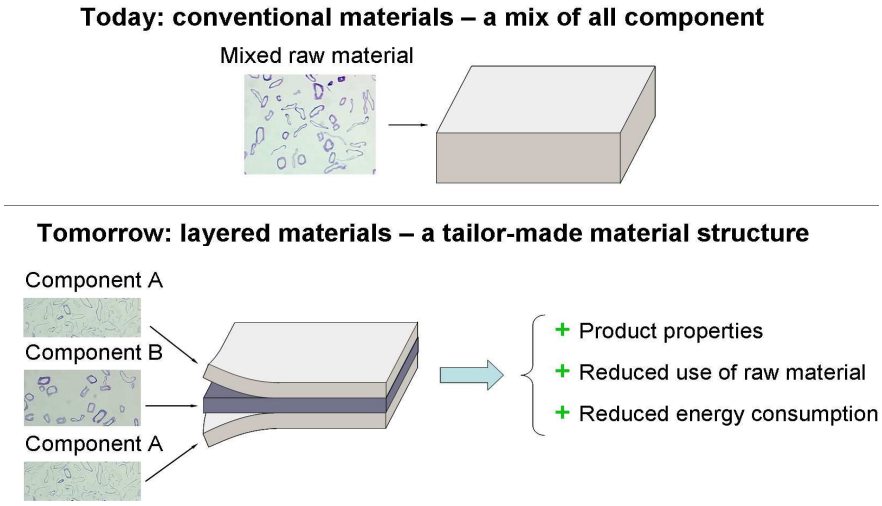

Figure 212: Concept de structure de papier simple ou multi-couches [6]

Dans le cas de pâte vierge, les fibres grossières et épaisses, ainsi que les fines de type lamellaires (ou « flakes ») peuvent introduite dans la couche interne pour masquer leur impact négatif sur l'état de surface du papier produit.

Dans ce manuscrit, deux situations expérimentales sont rapportées dans le cas d'une pâte mécanique de type SGW et dans le cas d'une pâte désencrée.

6.3.7.1. - Etude de fractionnement d'une pâte mécanique SGW

Dans le cas de la pâte mécanique SGW, les fines sont isolées grâce au classage µ-trous puis ensuite fractionnées à travers un hydrocyclone afin d'obtenir deux fractions enrichies soit en fines fibrillaires ($f1_{SGW}$), soit en fines lamellaires ($f2_{SGW}$). Le schéma de principe du fractionnement est schématisé par la Figure 213.A partir de ces fractions, des formettes ont été fabriquées en faisant varier la quantité de fractions fines re-mélangées avec la fraction fibre (rejet ou fraction longue du classeur) afin de déterminer l'impact sur les propriétés des formettes.

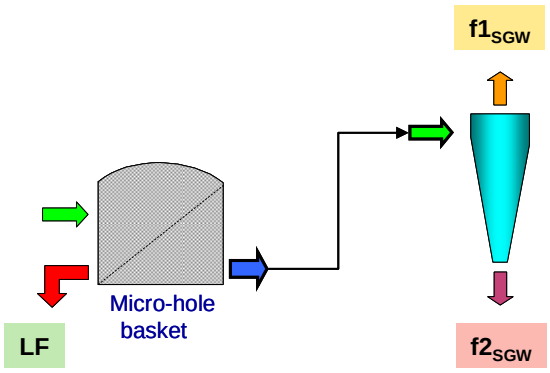

Figure 213: Descriptif du fractionnement des fines

Le résumé de l'ensemble des résultats est reporté dans le **Table 29**

Table 29: Résumé des propriétés des formettes en fonction du type de fines introduites

Property Fines fraction	Bulk (cm^3/g)	Breaking length (m)/ young modulus (MPa)	Tear ($mN.m^2/g$)	Opacity (%)	Light scattering coefficient (m^2/kg)	Air permeance ($cm^3/m^2.Pa.s$)	Scott bond (J/m^2)
f1	↘↘	↗	↘	↗↗	↗↗	↘↘	↗
f2	↘	No effect	↘	↗	↗	↘	No effect

Les résultats montrent que l'addition de la fraction fine fibrillaire ($f1_{SGW}$) développe des effets positifs sur les propriétés mécaniques (telles que la longueur de rupture et la cohésion interne dans le sens Z mesurée par Scott Bond) et optiques (opacité) ainsi que les propriétés de surface de la feuille (diminution de la rugosité). Ces résultats montrent que le management (et la production) de différentes fractions de fines pourrait permettre de les introduire dans la couche adéquate de papier stratifié pour améliorer et ajuster des propriétés à la demande.

6.3.7.2. - Optimisation du procédé de désencrage

Une rationalisation des lignes de désencrage nécessite la séparation des contaminants et leurs traitements dédiés. Le fractionnement par classage sous pression équipé d'un tamis µ-trous offre la possibilité d'une forte sélectivité de séparation des éléments fins dans la fraction dite acceptée. Cette fraction contient la majorité de l'encre qui pourrait alors être traitée par flottation dans le but de l'éliminer et de récupérer les éléments cellulosiques et les charges minérales. Cette solution permet d'éviter le traitement par flottation de l'ensemble de la pâte qui génère la perte de fibres cellulosiques et permet également de faire des économies d'énergies et de couts de production, comme visé par la simplification/rationalisation des lignes de désencrage.

L'approche pour la séparation de l'encre et son traitement spécifique a été étudiée en réalisant deux étages de fractionnement par classage µ-trous sous pression d'un mélange de journaux/magazines (25% journaux / 75% magazines) afin d'enrichir la fraction acceptée par les particules d'encre. Le schéma complet des expériences réalisées pour la production des différentes fractions est illustré par la Figure 214.

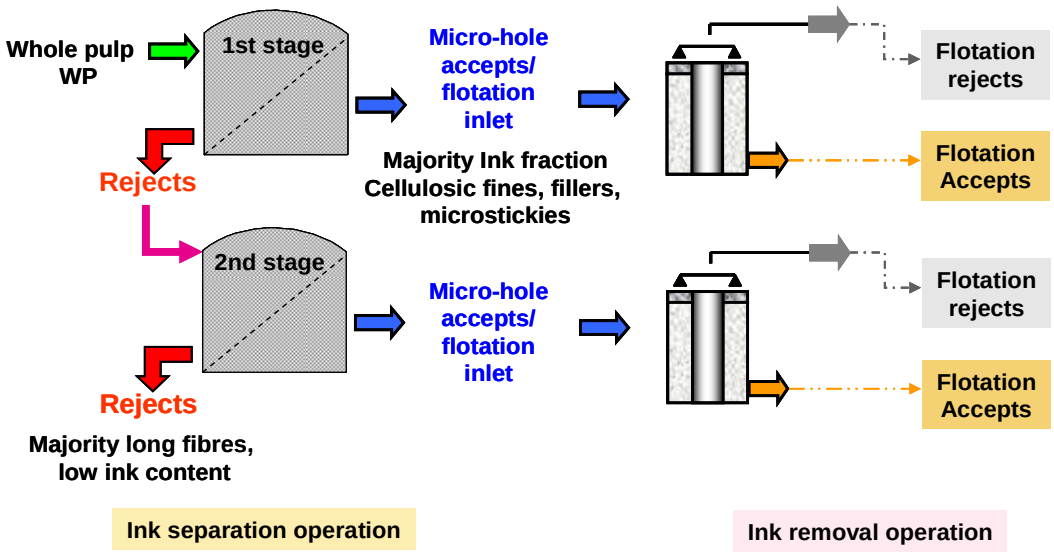

Figure 214: Application du fractionnement micro--trous pour une ligne de désencrage

6.3.7.3. - Séparation de l'encre par fractionnement à travers un tamis µ-trous

Les essais de fractionnement montrent que la quantité d'encre dans la fraction longue des rejets est réduite lors du fractionnement alors que la fraction acceptée s'enrichie en particules d'encre. Les résultats obtenus pour chaque condition de fractionnement sont donnés par les Figure 215 et Figure 216 en termes d'ERIC et par les Figure 217et Figure 218 pour la blancheur.

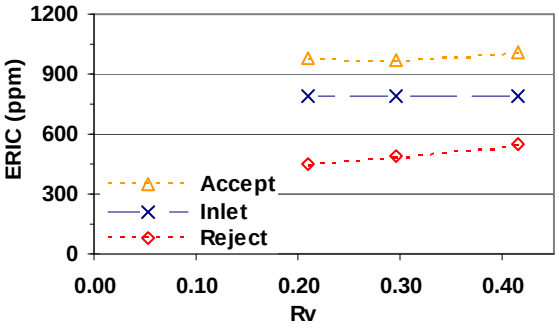

Figure 215: Evolution de l'ERIC lors du 1er étage de fractionnement

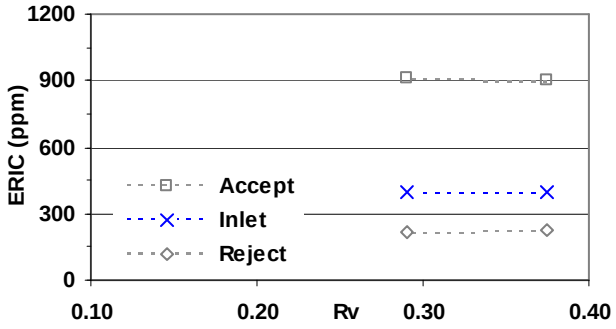

Figure 216: Evolution de l'ERIC lors du 2ème étage de fractionnement

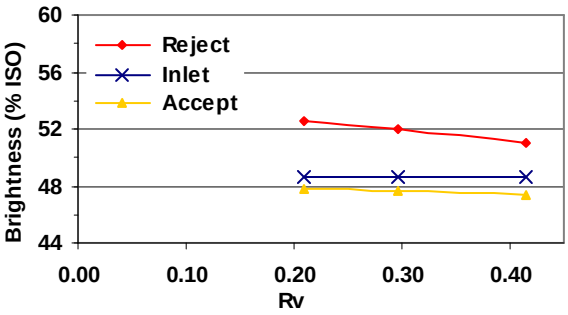

Figure 217: Evolution de la blancheur lors du 1er étage de fractionnement

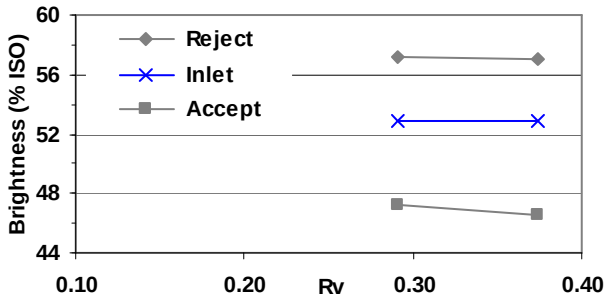

Figure 218: Evolution de la blancheur lors du 2ème étage de fractionnement

La fraction fine contenant les particules d'encre et les charges minérales suit le flux d'eaux. Deplus, plus le rejet volumique est faible, meilleure est la propreté des refus (fraction longue). Cependant, des fines et de l'encre résiduelle sont toujours présentes dans la fraction longue (refus) après le 1er étage de fractionnement, même au plus faible taux de rejets volumiques. Un deuxième étage de fractionnement par µ-trous améliore alors la blancheur de la fraction longue et diminue la quantité d'encre jusqu'à 200ppm (mesure d'ERIC). La qualité de la fraction longue n'est pourtant pas optimale dans la mesure où un hyperlavage (élimination de l'ensemble des éléments fins) conduit à des valeurs de blancheur de 63% et des valeurs d'ERIC de 51 ppm. Ceci montre qu'une amélioration de la qualité de la fraction longue est encore possible. Plusieurs solutions pourraient être envisagées pour des études ultérieures : (i) le deuxième étage de fractionnement pourrait travailler avec un taux de refus volumique plus faible et/ou (ii) introduire un 3ème étage de fractionnement sur la fraction longue.

6.3.7.4. - Comparaison du désencrage avec fractionnement et d'un désencrage conventionnel

Comme observé sur la Figure 219 le procédé combinant fractionnement et flottation de la fraction fine uniquement conduit à un rendement légèrement supérieur en recombinant les deux fractions (fines et longues) qu'un procédé conventionnel traitant l'ensemble de la pâte comme rapporté sur la figure 220.

Ce résultat est valide pour l'ensemble des conditions de fractionnement étudiées avec des taux de refus volumiques variable.

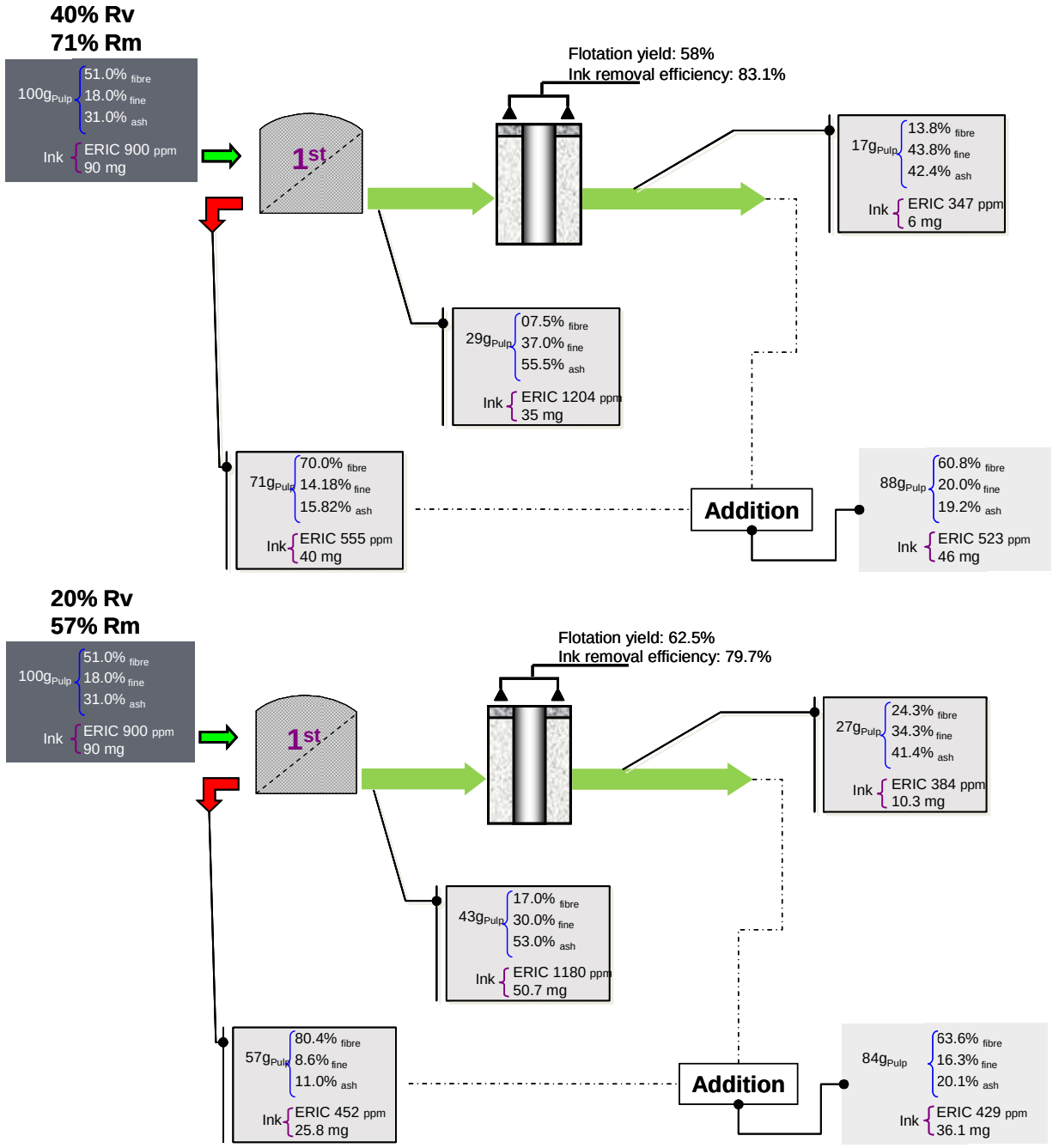

Figure 219: Caractéristiques finales de la pâte après 1ière stade de fractionnement à 40 et 20% de taux de refus volumique avec flottation de la fraction fine.

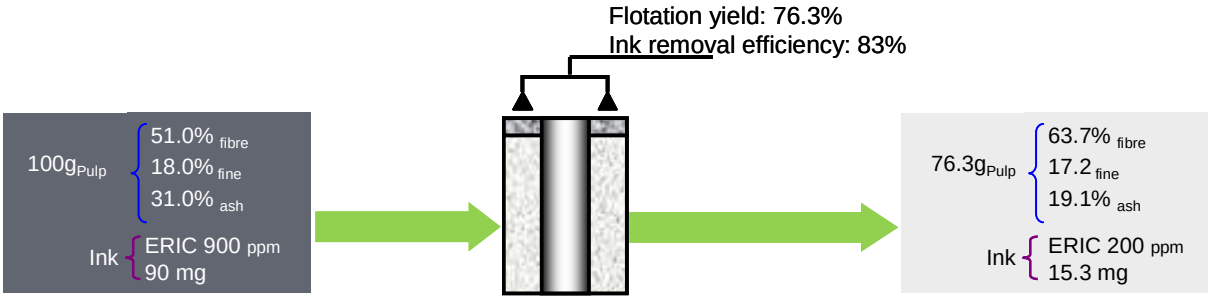

Figure 220: Flottation de la pâte entière sans fractionnement (référence)

La principale différence entre les deux scénarios (combinant fractionnement et flottation de la fraction fine et Flottation de la pâte entière sans fractionnement) est la quantité finale d'encre qui est plus importante pour celle obtenue avec le nouveau procédé mettant en œuvre un seul étage de fractionnement. En considérant chaque étape du procédé, la cause principale de cette différence est le fait que les refus du fractionnement (fraction longue) ne sont pas soumis à une étape de flottation pour éliminer l'encre résiduelle. Pour cette raison, l'addition d'un deuxième voir troisième étage de fractionnement pour transférer cette encre résiduelle vers la fraction fine qui sera flottée devrait être bénéfique. Ce scénario est analysé à travers la Figure 221; où trois étages de fractionnement sont envisagés avec la flottation sur les éléments fins. Il conduirait approximativement au même rendement que la flottation sur l'ensemble de la pâte avec la même quantité d'encre finale. Les valeurs de refus massiques Rm et d'ERIC reportées pour le 1er et 2ème étage correspondent aux valeurs expérimentales obtenues pour le plus faible taux de refus volumique. Pour le 3ème étage, un refus massique de 90% et une réduction de 50% de la mesure d'ERIC a été envisagée en considérant une forte proportion de fibre longue à l'entrée du 3ème étage. D'autre part, il a également été supposé que lors de la flottation qui va traiter les 3 flux de fraction fines, la valeur finale d'ERIC correspond à la moyenne des 3 valeurs d'ERIC obtenues précédemment avec plusieurs taux de refus volumique au 1er étage.

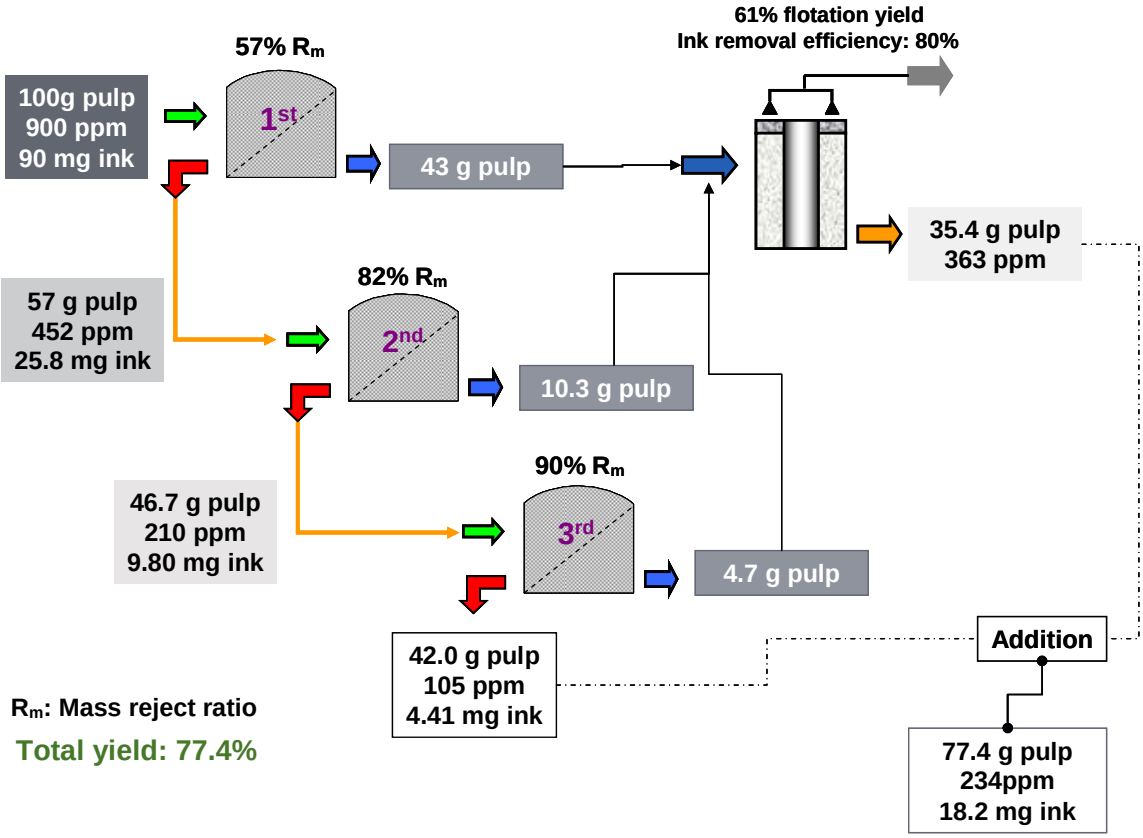

Figure 221: 3 étages de fractionnement par µ-trous avec flottation des éléments fins

6.4. - Conclusions de l’étude

Le recyclage des papiers s'est fortement développé dans le monde au cours des dernières décennies, pour atteindre un taux de réutilisation supérieur à 70% dans l'Union Européenne si bien que les fibres recyclées sont devenues, par rapport aux fibres vierges, la principale matière première pour la production de papier et de carton. Près de la moitié des fibres récupérées sont désencrées, souvent par flottation, afin d'enlever l'encre en plus d'autres contaminants, et sont utilisées dans presque toutes les sortes de papier (même si le taux d'utilisation moyen est encore très différent d'une sorte à l’autre, de 90% pour le papier journal à seulement 10% pour les papiers graphiques).

Cette évolution positionne parfaitement le secteur papetier face aux exigences environnementales et au contexte socio-économique actuel, à savoir l'utilisation durable des ressources, la réduction des déchets et le recyclage des matières premières. Il reste cependant encore des possibilités d’accroitre l’utilisation de la pâte désencrée et d'optimiser le recyclage du papier, aussi, afin de maintenir la compétitivité de ce secteur face à des solutions alternatives, comme par exemple l'exploitation du potentiel énergétique du papier (par incinération) qui ne devraient intervenir qu’en solution ultime.

Dans ce contexte, les efforts de recherche devraient être consacrés à optimiser les technologies de recyclage/désencrage, par l’amélioration de son efficacité et la réduction de ses coûts et de son empreinte écologique. Ce fut l’objectif de certains projets nationaux et européens dans les dernières années, comme EcoTarget et BoostEff, qui visaient à optimiser et simplifier les lignes de désencrage existantes, en particulier en séparant les différents composants de la pâte et en appliquant des traitements spécifiques sur chacun d’eux.

L’analyse de différentes fractions des éléments fins de la pâte par une nouvelle méthode de classification manuelle a montré que la l’essentiel de la contamination par les particules d’encres se retrouve dans la fraction non-retenue sur tamis de 11µm d’ouverture de maille. Cette fraction particulière contient aussi les fibrilles cellulosiques les plus fines et des particules lamellaires, ainsi que des charges minérales plus petites. L'analyse visuelle des images microscopiques a révélé que les fibrilles ne comportent pas d'encre, alors que la fines laminaires sont couvertes d'encre. Les charges minérales présentent divers degrés de couverture d'encre, partielle ou totale ou non-encrée. Un nouveau module d'analyse développé spécifiquement a montré la possibilité de distinguer les différentes formes de fines cellulosiques, fibrilles et fines lamellaires et les particules minérales.

L’étude d’un système de classage sous-pression pression équipé, en vue de séparer les fibres des éléments fins, d’un tamis à micro-trous de 250µm et d’un rotor fermé a mis en évidence une sélectivité élevée de séparation des fines dans les acceptés. Les fibres longues ainsi que les particules d’encre les plus grossières (specks) d’une pâte pour désencrage modèle sont rejetées et un second étage de fractionnement permet de réduire la teneur résiduelle d'encre fines dans les fibres longues retenues. Les essais ont révélé un comportement bien spécifique du classage sur tamis à micro-trous avec un épaississement des rejets élevé par rapport à l’utilisation de tamis d’épuration à fentes classiques. L'analyse des fractions a montré que la configuration de classage utilisée, avec tamis à micro-trous et rotor fermé, suivait un modèle d’écoulement piston et produisait un degré de fractionnement élevé, caractérisé par un coefficient de sélectivité élevé, β de l’ordre de 1.0, comparativement à des valeurs de 0.5 obtenues sur tamis à fentes classique. Les fibres de pâte chimique présentaient un taux de passage plus élevé par rapport aux fibres de pâte mécanique, plus rigides. Des pulsations de pression du rotor ont été mesurées en vue de mieux comprendre les limites de capacité et de charge hydraulique observées à concentration accrue, la vitesse de passage à travers le tamis ne pouvant être augmentée au niveau des valeurs habituelles (classage à fentes) même si les pulsation de

pression négative mesurées se sont avérées de magnitude élevée (environ 300 kPa). Deux raisons à ce comportement ont été avancées : d'une part l'augmentation de la vitesse de passage effective durant la phase de classage, forte et non proportionnelle à la vitesse moyenne de passage ; et d'autre part, du fait de cette vitesse de passage effective élevée et de la forte rétention des fibres, la formation rapide au cours de la phase de classage, d'un matelas de fibres compact à partir de la section de refus (compte tenu du facteur d'épaississement) avec pour conséquence un colmatage progressif du tamis réduisant de ce fait la capacité de production de pâte acceptée.

Des essais de flottation effectués sur la fraction fine du classage à micro-trous, ont mis en évidence des efficacités d'élimination de l'encre similaires par rapport à une flottation de l'ensemble de la pâte. Toutefois, la sélectivité du désencrage s'est avérée plus élevée, relativement aux pertes en fibres par rapport à la flottation de référence principalement du fait de la concentration en fibres très faible dans la fraction fine. Ces résultats offrent des perspectives prometteuses de rationalisation des chaines de désencrage par l'utilisation d'un classage à micro-trou en vue de limiter l'opération de désencrage à la fraction fine de la pâte contenant l'essentiel des encres. De même un traitement spécifique de la fraction fibres (dispersion) pourra être implanté, chacune des fractions ne recevant, en parallèle, que les traitements nécessaires. Une simple simulation d'une installation de fractionnement à micro-trous en 3 étages avec flottation sélective de la fraction fine a montré des propriétés de pâte comparables à celles obtenues par flottation de l'ensemble de la pâte.

Enfin, des essais de cyclonage effectués sur la fraction fine du classage à micro-trous ont permis de produire un fractionnement par hydrocyclone séparant les fractions fibrillaires et lamellaires des fines et de déterminer leurs influences respectives sur les propriétés de la feuille. L'incorporation de fines fibrillaires de surface spécifique très supérieure conduit à de meilleures propriétés mécaniques et optiques. Dans certains cas, ces fibrilles sont deux fois plus efficaces que les fines de type lamellaire.

Pour conclure, l'étude a souligné de nouvelles perspectives d'optimisation des lignes de désencrage par l'introduction d'une technologie de fractionnement spécifique des fines en vue de leur valorisation, notamment par leur répartition optimale dans l'épaisseur de la feuille dans le cadre de futurs concepts de fabrication des papiers par stratification.

References

[1] **CEPI** Sustainability report 2011

[2] **CEPI** Preliminary statistics 2011

[3] **CEPI** Key statistics 2010

[4] European Declaration on Paper Recycling 2011-2015, http://www.cepi.org

[5] ECOTARGET project, Contract n°500345 (NMP2-CT-2004 -500345), http://www.ecotarget.eu

[6] **BoostEff project (2010-2013):** 'Boosting raw material and energy efficiency using advanced sheet structure design and fibre modifications', collaborative project description, Part B of the proposal. Grant agreement n° 246059. (Theme NMP-200 9-4.0-4 Reducing environmental footprint of energy intensive industries), http://boosteff.com

[7] **Passas R., (2008),** Microscopy course, Grenoble – INP PAGORA, France.

[8] **Forsström J., (2004):** 'Fundamental aspects on the re-use of wood based fibres – Porous structure of fibres and ink detachment', PhD thesis, Mid Sweden University, Sundsvall, The Royal Institute of Technology, Stockholm, Sweden, ISSN 1652-2443, ISRN/KTH/FTP/R-2004/37-SE.

[9] **Ferreira P J., Matos S., Figueiredo M. M., (1999):** 'Size characterization of fibres and fines in hardwood kraft pulps', Particle and Particle Systems Characterization, 16(1), pp 20-24.

[10] **Laivins G .V., Scallan A. M., (1995):** 'The influence of drying and beating on the swelling of fines', 3rd Research Forum on Recycling, 20-22 November Vancouver, BC, Canada, pp 153-161.

[11] **Lindholm C.A., (1980):** 'Comparison of some papermaking properties of groundwood, pressure groundwood and thermomechanical pulps by means of artificial blends of pulp fractions - Part I : Primary results Part 1-Paperi Ja Puu, 62(10), pp 593-600, 603-606 and Part 2: "The fines fractions", Paperi Ja Puu, 62(12), pp 803-808.

[12] **Retulainen E., Luukko K., Fagerholm K., Pere J., Laine J., Paulapuro H., (2001 & 2002): '**Papermaking quality of fines from different pulp – the effect of size shape and chemical composition', 55th Appita annual conference, 30 April-2 May Hobart, Australia, pp 309-314, and APPITA journal, 55(6), pp 457-470.

[13] **Kang T., Paulapura H., (2006):** 'Characterization of chemical pulp fines', TAPPI Journal, 5(2), pp 25-28.

[14] **Paavilainen L., (1990):** 'Importance of particle size - fibre length and fines - for the characterization of softwood kraft pulp', Paperi Ja Puu, 72(5), pp 516-526.

[15] **Seth R. S., (2002):** 'The measurement and significance of fines', 88th Annual meeting, 29-31 January Montreal, Quebec, Canada, Preprints C, pp C97-C101.

[16] **Forgacs O.L., (1963):** 'The Characterization of mechanical pulps", Pulp and Paper Magazine of Canada, Convention issue, pp T-89 T118.

[17] **Retulainen E., Moss P., Nieminen K,. (1993):** 'Effect of fines on the properties of fibre networks', Paper presented at Products of Papermaking, 10th Fundamental Research Symposium, 20-24 September Oxford, UK, Vol. 2, pp 727-769.

[18] **Kartovaara I., (1989):** 'Mechanical pulp as coating base paper raw material – strength, weakness and developments needs', International Mechanical Pulping conference Helsinki, 6-8 June, V 1, pp 25-35.

[19] **Brecht W., Holl M., (1939):** 'Standard for evaluating the quality of groundwood pulps', Wochenblatt fur Papierfabrikation, 37(10), pp 74-86.

[20] **Brecht W., Klemm K., (1953):** 'The mixture of structures in a Mechanical pulp as a key to the knowledge of its technological properties', Pulp and Paper Magazine of Canada, 54(1), pp 72-79.

[21] **Luukko K., Maloney T C., (1999):** 'Swelling of mechanical pulp fines', Cellulose, 6(2), pp 123-136.

[22] **Alince B., Porubska J., Van de Ven T. G. M., (2001):** 'Effect of model and fractionated TMP fines on sheet properties', The science of papermaking, 12th Fundamental research symposium, Oxford UK 17-21 September, Vol. 2, pp 1343-1355.

[23] **Rundlöf M., (2002):** 'Interaction of dissolved and colloidal substances with fines of mechanical pulp – influence of sheet properties and basic aspects of adhesion', PhD thesis, KTH, SCA, Mid-Sweden University, Sweden.

[24] **Mohlin U.B., (1980):** 'Properties of TMP fractions and their importance for the quality of printing papers - Part 2: The influence of particle properties and particle size distribution on pulp properties', Svensk Papperstidning, 83(18), pp 513-519.

[25] **Westermark U., Capretti G., (1988):** 'Influence of ray cells on the bleachability and properties of CTMP and kraft pulps', Nordic Pulp and Paper Research Journal, 3(2), pp 95-99.

[26] **Krogerus B., Eriksson L., Sundberg A., Mosbye J., Ahlroth A., Östlund I., Sjöström L., (2002):** 'Fines in closed circuits - Final report', website consultation date 09 September 2010: http://www.nordicinnovation.net/_img/fines_in_closed_circuits_final_report.pdf.

[27] **Krogerus B., (2003):** 'Fines: Characterisation, interaction and effects in the papermaking stock', Scandinavian paper symposium. Quality improvement and management in the pulp and paper industry, 9-10 September Stockholm, Sweden, Paper 11, 9pp.

[28] **Bäckström M., Kolar M-C., Htun M., (2008):** 'Characterisation of fines from unbleached kraft pulps and their impact on sheet properties', Holzforschung, 62(5), pp 546-552.

[29] **Mancebo R M., Krkoska P., Blazej A., (1981):** 'The concept, properties and papermaking role of fines', Papir a Celuloza. 36(11) pp V75-V81.

[30] **Richardson J D., Wakelin R F., Corson S R., (1996):** 'The influence of fines on the energy demand of disc refined mechanical pulp', 5th International conference on new available techniques, World pulp and paper week, 4-7 June Stockholm, Sweden, Part 1, pp 203-215.

[31] **Luukko K., (1999):** 'Fines quantity and quality in controlling pulp and paper quality', TAPPI international mechanical pulping conference, 24-26 May Houston, Texas, USA, pp 67-75.

[32] **Luukko K., Paulapuro H., (1999):** 'Mechanical pulp fines: Effect of particle size and shape', TAPPI journal, 82(2), pp 95-101.

[33] **Rundlöf M., Höglund H., Htun M., Wågberg L., (1995):** 'Effects of fines quality on paper properties - new aspects', International Mechanical Pulping Conference, 12-15 June Ottawa, Canada, pp 109-118.

[34] **Rundlöf M., Htun M., Höglund H., Wågberg L;. (2000):** 'The importance of the experimental method when evaluating the quality of fines of mechanical pulps', Journal of Pulp and Paper Science, 26(9), pp 301-307.

[35] Luukko K., Kemppainen-Kajola P., Paulapuro H., (1997): 'Characterization of mechanical pulp fines by image analysis', Appita Journal, 50(5), pp 387-392.

[36] Rundlöf M., Htun M., Höglund H., Wågberg L., (2000): 'Mechanical pulp fines of poor quality – Characteristics and influence of white waters', Journal of Pulp and Paper Science 26(9), pp 308-316.

[37] Ferreira P J., Matos S., Figueiredo M. M., (2000): 'Primary and secondary fines from eucalyptus globulus Kraft pulp- characterization and influence', Paperi Ja Puu – Paper and Timber, 82 (6), pp 403 – 408.

[38] Hardell H.L., Westermark U., (1981): 'Techniques for separations of wood elements and cell wall layers', EUCEPA/TAPPI/CPPA/ACS International Symposium on Wood and Pulping Chemistry - "Ekman-Days ", Stockholm Vol. 5, pp. V17-V19.

[39] Westermark U., (1985): 'The occurrence of p-hydroxyphenylpropane units in the middle- lamella lignin of spruce (Picea abies)', Wood Science Technology, Vol. 19, pp. 223-232.

[40] Karnis A., (1997): 'Pulp fractionation by fibre characteristics", Paperi Ja Puu, 79(7), pp 480-488.

[41] Laitinen O., Löytynoja L., Niinimäki J., (2006): 'Tube flow fractionator – A simple method for laboratory fractionation', Papier Ja Puu - Paper and Timber, 88(6) pp 351 – 355.

[42] Lapierre L., Pitre D., Bouchard J., (2003): 'Fines from deinked pulp: effect of contaminants on their bleachability and on the pulp brightness', Pulp and Paper Canada, 104(8), pp T208-T211.

[43] Wood J.R., Grondin M., Karnis A., (1991): 'Characterization of mechanical pulp fines with a small hydrocyclone. Part 1: The principle and nature of the separation', Journal of Pulp and Paper Sciences, 17(1), pp J1-J5.

[44] Hirsch G., Schabel S., Feist M., Nirschl H., (2010): 'Separation of fibre fines and inorganic fines in recovered paper suspensions', Internationale Papierwirtschaft, No. 6, pp 20-23.

[45] Pelton R.H., Jordan B.D., Allen L.H., (1985): 'Particle size distributions of fines in mechanical pulps and some aspects of their retention in papermaking', TAPPI Journal, 68(2), pp. 91-94.

[46] McCool M.A., Silveri L., (1987): 'Removal of specks and non-dispersed ink from a deinking furnish', TAPPI Journal, 70(11), pp 75-79.

[47] Luukko K., (1999): 'Characterization and Properties of Mechanical Pulp Fines', PhD thesis; Helsinky University of Technology, Espoo, Finland.

[48] Jokinen M., Saharinen E., Luukko K., Hiltunen., Paulapuro H., (2003): 'Turbidity as a measure of specific surface of fibres and fines', 28th EUCEPA conference. Sustainable development for the pulp and paper industry, 2-4 April Lisbon, Portugal, Poster session, pp 366-367.

[49] Wood J.R., Karnis A., (1996): 'Determination of specific surface area of mechanical pulp fines from turbidity measurements', Papier Ja Puu – Paper and Timber, 78(4), pp 181-186.

[50] Ben Y., Dorris G. M., Page N., (2003 & 2004): 'Characterization of dissolved air flotation rejects', 89th Annual meeting, Montreal, Quebec, Canada, 27-30 January, Session 5D-1, 7pp. Pulp and Paper Canada, 105 (11), pp 246 – 251.

[51] Lapierre L., Pitre D., Bouchard J., (2001): 'Bleaching of deinked recycled pulp: benefits of fibre fractionation', Pulp and Paper Canada, 102(2), pp 35-38.

[52] Carré B., Vernac Y., Beneventi D., (2001): 'Reduction of Flotation Losses, Part 1: Is There Something Interesting to Recover in Flotation Deinking Froths?' Pulp and Paper Canada, 102(6), pp 33–36.

[53] Katsura T., Murakami K., (1986): 'How filler distribution affects paper properties (3) the influence of different fillers on optical and mechanical properties of paper', Japan TAPPI 40(12), pp 57-62.

[54] Ferguson L.D., (1992): 'Introduction to printing technology and ink chemistry', TAPPI deinking seminar notes, Atlanta, 22-24 June, 20 pp.

[55] Saari J., (2004): 'New process engineering for deinking- Part 1: The effects of inks on deinking', Paper Technology, 46(1), pp 30-31.

[56] Jordan B.D., Popson S.J., (1993): 'Measuring the Concentration of Residual Ink in Recycled Newsprint', 2nd Research Forum on Recycling, CPPA, October 5-7Ste-Adèle, Québec, pp. 153-169.

[57] Haynes R. D., (2000): 'Measuring ink content from pulper to deinked pulp', TAPPI Recycling symposium, 5-8 March Washington DC, USA, Vol. 2, pp 677-691.

[58] Julien Saint Amand F., Eymin-Petot-Tourtollet G., Perrin B., Sabater J., (1999): 'Advanced deinking process control using new on-line sensors', Progress in Paper Recycling, 8(3), pp 37-52.

[59] Rangamannar G., Silveri L., (1990): 'Effective secondary fibre treatment process for high quality deinked pulp', TAPPI Pulping Conference, 22-25 October Seattle, WA, USA, Book 1, pp 381-390.

[60] Laitinen O., Korkko M., Vahlroos S., Niinimaki J., (2006): 'Ink release and particle size analysis with combined use of a tube flow fractionator and microscope', 12th PTS CTP Deinking symposium, 25-27 April Leipzig, Germany, Paper N°2 4.

[61] Galland G., Bernard E., Sauret G., (1976): 'Aspects physico-chimiques du désencrage', Proceedings EUCEPA conference, 27-30 September Bratislava.

[62] Hanecker E., (2007): 'Treatment and utilisation of deinking sludges', 8th Advanced Training Course on deinking, CTP, 29-30 May, Grenoble, France.

[63] Ricard M., Dorris G., Lapointe C., Page N., Ben Y., (2008): 'Decontaminaton of whitewater fines by laboratory-scale flotation', 94th annual meeting preprints, 6-7 February Montreal, QC, Canada, pp A47-A56.

[64] Rao R.N., Stenius P., (1998): 'Mechanisms of ink release from model surfaces and fibre', Journal of Pulp and Paper Science, 24(6), pp 183-187.

[65] Godart A., Marmagne O., Fingerhut U., (2000): 'Characterization of residual ink particles by automated microscopy and image analysis. Part 1- Presentation of the equipment' TAPPI Recycling symposium, 5-8 March, Washington DC, Vol. 1, p 159-168.

[66] Kesti T., (2010): 'Measurement of ink content in recycled pulp suspension by polarized light microscopy', PTS-CTP Deinking symposium 2010, 27-29 April Munich, Germany, 17pp.

[67] Klein R., Wawrzyn H., Grefermann A., Grossmann H., (1995): 'Image analysis- an effective tool for quality assessment of secondary fibre furnish and recovered papers', Progress in Paper recycling, 4(4) pp 35 - 48.

[68] McCool M.A., Taylor C.J., (1983): 'Image analysis techniques in recycled fibre', TAPPI Journal, 66(08), pp 69-71.

[69] Ye C., Vilenius A., (2008): 'Evaluation of recycled pulp for distinguishing inks detached from and attached to fibres', PTS-CTP Deinking Symposium, 15-17 April Leipzig, Germany, Paper No. 7, 9pp.

[70] Borchardt J. K., (1995): 'Ink types: the role of ink in deinking', Progress in Paper Recycling, 5(1), pp 81-87.

[71] Ruzinsky F., Bennington C.P.J., (2001): 'The attachment force of ink to paper in paper recycling operations', 6th PAPTAC Research Forum on Recycling, 1-4 October Magog, Quebec, Canada, pp 19-27.

[72] Kumar S., Fabry B., Perrin B., Promonet G., Danièle G., (2008): 'Deinking operations and fibre removal selectivity?', 10th CTP recycled fibre research Forum 5-6 February, N°11, Grenoble France.

[73] Kumar S., Julien Saint Amand F., Passas R., Fabry B., Schelcher M., (2010): "Lab scale fine-fractionation of deinked pulp and particle microscopic analysis", Poster session, XXI TECNICELPA Conference and Exhibition / VI CIADICYP 2010 12-15 October, Lisbon, Portugal.

[74] Kress O., Brainerd F.W., (1934): 'A study of wood pulp fractionation', Paper Trade Journal, 95, pp 13-27.

[75] Mohlin U.B., (1980): 'Properties of TMP fractions and their importance for the quality of printing papers - Part 1: Large variations in properties within fractions are observed', Svensk Papperstidning, 83(16), pp 461-466.

[76] Felsvang K., Moller K., Norman B., A.D. Ruvo., (1977): 'Screening, cleaning and fractionation with an atomizer', Preprints 17th EUCEPA Conference, Vienna, Austria, 10-14 October, conference N°21, pp 30-42.

[77] Ora M., Hautala J., Paulopuro H., Saarinen A., (1993): 'Development of fractionating screening method for SC groundwood', Paperi Ja Puu, 75(5), pp 330-331, 334-336.

[78] Corson S. R., Wakelin R. F., Lloyd M., D., (1996): 'TMP furnish development strategies, part 1: fractionation and long fibre refining, Pulp and Paper Canada, 97(12), pp 129-132.

[79] Ferluc A., Lanouette R., Bousquet J-P., Bussiere S., (2010): 'Optimum refining of TMP pulp by fractionation after the first refining stage', Appita, 63(4), pp 308-314.

[80] Murton K., Richardson J., (2007): 'Low energy shive separation, evaluation of a new method of fibre processing', International Mechanical Pulping Conference, 6-9 May, Minneapolis, Minnesota USA.

[81] Zha Q., Lanouette R., Law K-N., Bousquet J-P., Bussieres S., (2008): 'Refining of long fibre fractions after fractionation', 94th annual meeting preprints, 6-7 February Montreal, QC, Canada, pp B481-B487.

[82] Amiri R., Yuan Z., Beaulieu S., (2010): 'Mechanical Pulp Quality and Fractionation. Part I: Upgrading Newsprint TMP for Value-Added Grades', Journal of Pulp and Paper Science, 36(3-4), pp 71-78.

[83] Sloane C M., (2000): 'Kraft pulp processing - pressure screen fractionation', 53rd Appita annual conference, 19-23 April Rotorua, New Zealand, vol. 1, pp 221-227.

[84] El-Sharkawy K., Koskenhely K., Paulapuro H., (2008): 'The fractionation and refining of eucalyptus kraft pulp', Nordic Pulp and Paper Research Journal, 23(2), pp 172-180.

[85] El-Sharkawy K., Koskenhely K., Paulapuro H., (2008): 'Tailoring softwood kraft pulp properties by fractionation and refining', TAPPI journal, 7(11), pp 15 -22.

[86] Koskenhely K., Ammala A., Jokinen H., Paulapuro H., (2005): 'Refining characteristics of softwood fibre fractions', Advances in Paper Science and Technology, 13th fundamental research symposium, 11-16 September Cambridge, edited by S J l'Anson, vol. 1, pp 427-456.

[87] Gooding R.W., Kerekes R.J., (1989): 'The motion of fibres near a screen slot', Journal of Pulp and Paper Science, 15(2), pp J59-J62.

[88] **Julien Saint Amand F., Perrin, B. (1998):** 'Screening: Experimental Approach and Modelling', TAPPI Pulping Conference Proceedings, 25-29 October Montreal, Canada, pp 1019-1031.

[89] **Julien Saint Amand F., Perrin, B. (1999):** 'Fundamentals of Screening: Effect of Rotor Design and Fibre Properties', TAPPI Pulping Conference, 31 October – 3 November Orlando, USA, Vol. 3, pp 941-955.

[90] **Kumar A., Gooding R.W., Kerekes R.J., (1998):** 'Factors controlling the passage of fibers through slots', TAPPI Journal, 81(5), pp 247-254.

[91] **Olson J.A., Kerekes R.J., (1998):** 'Fibre passage through a single screen aperture', Appita Journal, 51(2), pp 122- 126.

[92] **Lindqvist S., Moss C. (1993):** 'Advanced cleaner technology for the year 2000', Progress in Paper Recycling, 2(2), pp 35-40.

[93] **Pesch, A.W. (1963):** 'Process for preparation of fibres having different characteristics', International Paper Company US Patent n°3.085.927.

[94] **Julien Saint Amand F., Charuel, R. (1982):** 'Etude d'un épurateur à vortex libre en paroi tournante', Revue ATIP, 36 (6-7), pp 323-331.

[95] **Julien Saint Amand F., Perrin B., (2003):** 'Characterisation and simulation of fibre separation in screens and cleaners', International Mechanical Pulping conference, 2-5 June, Quebec, Canada, pp 245-257.

[96] **Paavilainen L., (1992):** 'The possibility of fractionating softwood according to cell wall thickness', Appita, 45(5), pp 319-326.

[97] **Panula-Ontto, S. (2002):** 'Fractionation of unbleached softwood kraft pulp with wedge wire pressure screen and hydrocyclone', Licentiate thesis, Helsinki University of Technology, Espoo, Finland.

[98] **Reyier, S. (2008):** 'Bonding ability distribution of fibres in mechanical pulp furnishes', Licentiate thesis, Mid Sweden University, Sundsvall, Sweden.

[99] **Shagaev O., Bergström B., (2005):** 'Advanced process for production of high quality mechanical pulps for value-added paper grades', International Mechanical Pulping Conference: IMPC 2005, 7-9 June Oslo, Norway, pp 169-179.

[100] **Vomhoff H., Grundstrom K-J., (2002):** 'Fractionation and separate refining of a bleached softwood pulp', STFI report PUB 6, Stockholm, Sweden, 23pp.

[101] **Niinimäki J., Ämmälä A., Jokinen H., (2007):** 'Fractionation of fibres: possibilities and limits', PulPaper 2007 conference. Fiber modifications and brightening, 5-7 June, Helsinki, Finland, pp 25-30.

[102] **Sandberg C., Shagaev O., (2010):** 'New fractionation technology gives better pulp quality and reduced energy consumption at Holmen Paper Braviken Mill', EXFOR and Annual Meeting, 2-3 February Montreal, QC, Canada, pp 110-114.

[103] **Floccia L., (1988):** 'Fractionation and separate bleaching of waste paper – A first', TAPPI international pulp bleaching conference, 5-9 June, Orlando, Florida, pp 181-198.

[104] **Eul, W., Meier J., Arnold G., Berger M., Suess H.U., (1990):** 'Fractionation prior to flotation - A new approach for deinking technology', TAPPI Pulping Conference, Toronto, Canada, vol. 2, pp 757-765.

[105] **Sauer A., Volk A., (2006):** 'Energy savings in stock preparation systems – efficient components, lean concepts', 12th PTS CTP Deinking symposium, 25-27 April Leipzig, Germany, Paper 29, 13pp.

[106] Lascar A., Fernandez de Grado A., Faul A., (2010): 'Deinking "2 in 1": an advanced approach to simplifying deinking systems', PTS-CTP Deinking symposium, 27-29 April Munich, Germany, 13pp.

[107] Lascar A., Fernandez de Grado A., (2009): 'Ink splitter technology, a good way to simplify deinking line design', 9th Advanced Training Course on Deinking CTP, 3-5 June, Grenoble, France.

[108] Makinen L., Ammala A., Vahlroos-Pirneskoski S., Korkko M., Sarja T., Niinimaki J., (2010): 'Fractionation prior to deinking: a study of optical properties and fractions', Internationale Papierwirtschaft, N°4-5, pp 14-20.

[109] Aregger H. J., Hertl E., Sket P., Janisch K. P., (2006): 'Fractionation in deinking plants: a new approach to recovered paper treatment', 12th PTS CTP Deinking symposium, 25-27 April. Leipzig, Germany, Paper 28, 16pp.

[110] Fabry B., Carré B., (2008): 'Importance of mechanical treatments prior to pre-flotation in order to simplify deinking lines', PTS-CTP Deinking Symposium, Leipzig, Germany, 15-17 April, Paper N°12, 18pp.

[111] Grundstrom K-J., Lucisano M.F.C., Bergstrom B., Bjarestrand A., Larsson E., Lindh H-O., Selin R., Sanneskog O., (2007): 'EcoFracSmart: a new stock-preparation process for testliner', 2007 TAPPI 8th Research forum on Recycling, 23-26 September Niagara Falls, ON, Canada.

[112] Scott G M., Abubakr S., (1994): 'Fractionation of secondary fibres – a review', Progress in Paper Recycling, 3(3), pp 50-59.

[113] Baptiste J., Lascar A., (2001): 'Improvement of mechanical properties with high consistency pulping and by fine removal', 2nd CTP PTS Packaging and Board Recycling International Symposium, 27-29 November, Grenoble, France.

[114] Brissaud M., Janin G., Scquizzato P., (1975): 'Le classage des fibre avec un classeur Bauer McNett', La Papeterie N°4, pp 194-207.

[115] Rienecker R. (1997): 'Sortierung von Altpapierstoff zur Herstellung von graphischen Papieren', Wochenblatt für Papierfabrikation, n°23/24 : 1149- 1159.

[116] Bride Mac, D., (1994): 'Deinking systems for Office Waste Paper 'Pay Now/Pay Later' Choices', Pulp and Paper, 68(4), pp 44-46, 49-51.

[117] Olson J. A., Pflueger C. D., Delfel S., Ollivier-Gooch C., Martin P., Vaulot F., Gooding R, W., (2008): 'High performance foil rotor improves de-ink pulp screening', Progress in Paper recycling, 17(4), pp 5-10.

[118] US Centennial Flight Commission website (Date consulted - 22/02/2012): http://www.centennialofflight.gov/essay/Dictionary/angle_of_attack/DI5.htm.

[119] Karvinen R., Halonen L., (1984): 'The effect of various factors on pressure pulsation of a screen', Paperi Ja Puu, 66(2), pp. 80-83.

[120] Levis S.H. (1991): 'Screening of Secondary Fibers', Progress in Paper Recycling, 1(1), pp 31-45.

[121] Yu C.J., (1994): 'Pulsation Measurement In A Screen, Part I: Pulse Signature And Magnitude Of S-Shape Rotor', TAPPI Engineering Conference; 19-22 September San Francisco, USA, Book 2, pp 767-782.

[122] Goldenberg P.H. (1987): 'Pressure screen improvements with new rotor design', 73rd Annual Meeting ofTechnical Section of Canadian Pulp and Paper Association, January Montreal, Canada, B275-B277.

[123] Niinimaki J., Dahl O., Kuopanportti H., Ammala A., (1998): 'A comparison of pressure screen baskets with different slot widths and profile highs - selection of the right surface for a groundwood application', Paperi Jaa Puu, 80(8), pp 601-605.

[124] Pinon V., Gooding R.W., Olson J.A., (2002): 'Measurements of pressure pulses from a solid core screen rotor', TAPPI Fall technical conference and trade fair, 8-11 September San Diego, CA, USA, Session 58, 11pp.

[125] Feng M., Gonzalez J., Olson J. A., Olliver-Gooch C., Gooding R. W., (2005): 'Numerical simulation and experimental measurement of the pressure pulses produced by pulp screen foil rotor', Journal of Fluid Engineering, 127 (2), pp 347-357.

[126] Feng M., Olson J. A., Olliver-Gooch C. F., Xia J., Gooding R. W., (2003): 'A computational fluid dynamics (CFD) tool for advanced pulp screen foil rotor design', 36th pulp and paper annual congress: ABTCP, Sao Paulo, Brazil, 13-16 October, 17pp.

[127] Olson J., Turcotte S., Gooding R., (2004): 'Determination of power requirements for solid core pulp screen rotors', Nordic Pulp and Paper Research Journal, 19(2), pp: 213-217.

[128] Gullichsen J., Paulapura H., (2000): 'Papermaking Science and technology', Book N°5- Mechanical pulping, Chapter Screening and cleaning, Publisher: Finnish Paper Engineers' Association.

[129] Jokinen H., Ämmälä A., Niinimäki J., Virtanen J.A., Lindroos K. (2006): 'Effect of bar geometry on screen plate performance – A laboratory study on pressure screening', Nordic Pulp and Paper Research Journal, 21(4), pp 435-443.

[130] Julien Saint Amand F., Perrin B., Gooding, R., Huovinen, A. (2004): 'Optimisation of screen plate design for the removal of stickies from deinking pulps', Revue ATIP, 58(4), pp 19-30.

[131] Kumar S., (2005): 'Effect of contour height on screen performance – Fibre fractionation and stickies removal', Masters Thesis, Institut National Polytechnique de Grenoble, France.

[132] Delfel S., Olson J. A., Martinez D. M., Regairaz A., Ollivier-Gooch C. F., Huovinen A., (2011): 'Influence of cylinder design and other factors on capacity and power consumption in a pressure screen', Apitta Journal, 64(1), pp 55-61.

[133] Grégoire G., Favre-Marinet M., Julien Saint Amand F., Serres A., Fernandez de Grado A. (1998): 'Modelling of the Productive and Reverse Flow at the Screen Surface', COST Workshop "Current Research on Multi-Phase Flows in Paper making", 12-13 November Paris.

[134] Mokamati S.V., Olson J.A., Gooding R.W., (2005): 'The effect of wire shape on the flow through narrow apertures in a pulp screen cylinder', ASME Fluids Engineering Division Summer Meeting & Exhibition, June 19-23 Houston, USA.

[135] Julien Saint Amand F., (1985): 'Epuration : limites techniques et économiques des technologies existantes - Perspectives nouvelles', 38th ATIP Congress preprints, November 5-7, Grenoble, France.

[136] Kumar, A., (1991): 'Passage of fibres through screen apertures', PhD thesis, Department of Chemical Engineering, University of British Columbia, Vancouver.

[137] Yu C.J., DeFoe R.J., (1994): 'Fundamental study of screening hydraulics Part 1: Flow patterns at the feed-side surface of screen baskets; mechanism of fiber-mat formation and remixing', TAPPI Journal, 77(8), pp 219-226.

[138] Gooding R.W., Craig D.F. (1992): 'The effect of slot spacing on pulp screen capacity, TAPPI Journal, 75(2), pp71-75.

[139] Hamann L., Cordier O., (2005): EU Project 'ScreenClean' Section 4.5- Pressure filtration, www.cost-e48.net/09_9_conferences/bruxelles/screenclean.pdf.

[140] Asikainen S., Fuhrmann A., Robertsen L., (2010): 'Birch pulp fractions for fine paper and board', Nordic Pulp and Paper Research Journal, 25(3), pp 269-276.

[141] Jokinen H., Ämmälä A., Julien Saint Amand F, Perrin B., Niinimäki J. (2006): 'Fractionation of pulp fine elements in cleaning, screening and flotation', 12th PTS-CTP Deinking Symposium, Paper n°30, 25-27 April Leipzig, Germany.

[142] Ammälä A., Dahl O., Kuopanportti H., Jouko Niinimäki J., (1999): 'Pressure screening: changes in pulp properties in the screen basket', TAPPI Journal, 82(10), pp 99-105.

[143] Gooding R.W., Kerekes R.J. (1992): 'Consistency changes caused by Pulp screening', TAPPI Journal, 75(11), pp 109-118.

[144] Pflueger C.D., Olson J., Gooding R. (2007): 'The performance of the EP Rotor in de-ink pulp screening', APPITA annual conference and exhibition, 6-9 May Gold Coast, Australia, pp 165-169.

[145] Kubat, J., Steenberg, B. (1955): 'Screening at low particle concentrations. Theory of screening III', Svensk Papperstidning, 58(9), pp 319-324.

[146] Gooding, R.W., Kerekes, R.J. (1989): 'Derivation of performance equations for solid-solid screens", The Canadian Journal of Chemical Engineering, 67(5), pp 801-805.

[147] Olson J., Wherret G., (1998): 'A model of fibre fractionation by slotted screen apertures', Journal of Pulp and Paper Science, 24(12), pp 398-403.

[148] Olson J.A., (2001): 'Fibre length fractionation caused by pulp screening, slotted screen plates', Journal of Pulp and Paper Science, 27(8), pp 255-261.

[149] Gooding R.W., Olson J., Roberts N., (2001): 'Parameters for assessing fibre fractionation and their application to screen rotor effects', International Mechanical Pulping Conference, preprints, session 4, Helsinki, June 4-8, 2001 and 2004 TAPPI Journal 3(3).

[150] Julien Saint Amand, F., Perrin B., Ottenio, P. (2007): 'Improvement of stickies removal through optimised screening', IPE-CTP-PTS-COST International Symposium- Present and Future of Paper Recycling Technology and Science, May 24-25Bilbao, Spain.

[151] Olson J., Roberts N., Allison B., (2000): 'Fibre length fractionation caused by pulp screening. Smooth hole screen plates', Journal of Pulp and Paper Science, 26 (1), pp 12-16.

[152] Julien Saint Amand, F., Perrin, B., Kolakowski, P. (2006): 'Stickies screening: influence of consistency and other screen operating and technological parameters', 4th CTP-PTS Packaging Paper & Board Recycling Symposium, Paper n°16, Marc h 21-23 Grenoble, France.

[153] Atkins M., Walmsley M., Weeds Z., (2007): 'Internal fibre length concentration in a pressure screen', Appita Journal, 60(1), pp 41-47.

[154] Walmsley M., Weeds Z., (2004): 'Plug flow versus mixed flow modelling of a pressure screen', Apitta Journal, 57(2), pp 121-127.

[155] Eymin-Petot-Tourtollet G., Petit-Conil M., Cochaux A., Cottin F., (2003): 'The use of MorFi analyser to characterise mechanical pulps', International Mechanical Pulping Conference, Proceedings, 2-5 June, Quebec, Canada, pp 225-232.

[156] Ämmälä A., (2001): 'Fractionation of thermomechanical pulp in pressure screenings - An experimental study on the classification of fibres with slotted screen plates', PhD thesis, University of Oulu, Finland.

[157] Chhabra R.P., Richardson J.F., (1999): 'Non-Newtonian flow in the process industries-Fundamentals and Engineering applications", Butterworth-Heinemann publisher, Book chapter 3, pp 74-77.

[158] Grégoire G., (2000): 'Etude et modélisation des écoulements dans un classeur en vue d'optimiser l'épuration de pâte à papier sur tamis à fentes', PhD thesis, Institut National Polytechnique de Grenoble.

[159] Julien Saint Amand F., (2001): 'Stock preparation Part II- Particle separation Processes', 12th Fundamental Research Symposium, September, Oxford, UK.

[160] Soderberg D., (2003): 'Method of forming a fibrous web and machine thereof', International Patent Application, WO 03/048452 A1.

[161] Soderberg D., (2008): 'A new technique for stratified forming', PaperCon '08. Sustainability: profits and performance for the pulp, paper and board industries, 4-7 May Dallas, Texas, USA, 35pp.

[162] Pande H., Gratton R. (2005): 'Impact of hydrocyclone fractionation of fibres on papermaking', Scientific and technical advances in refining and mechanical pulping, 28 February.-4 March Barcelona, Spain, Refining and mechanical pulping, Paper 11, 18pp.

[163] Carré B., (2008): 'Simplified Deinking Process: From Lab to mill trials', Final Open Conference ECOTARGET project, Stockholm November 12, www.ecotarget.eu.

[164] Zeno E., (2004): 'Influence of deinked pulp on wet-end chemistry', PhD, Grenoble INP, France.

[165] Allix J., Zeno E., Nortier P., Beneventi D., (2011): 'Roles of surfactant and fibres on fibre transport in a small flotation deinking column', Chemical engineering journal, 168(2), pp. 525-534.

[166] Allix J., (2011): 'Understanding and Modeling of the flotation mechanisms applied in de-inking of recovered paper', PhD thesis, University of Grenoble, France.

[167] Beneventi D., (2002): 'Selectivity in deinking flotation: physico-chemical aspects Sélectivité du procédé de désencrage par flottation: aspects physico-chimiques', PhD thesis, Institut National Polytechnique de Grenoble, France.

[168] Julien Saint Amand F., (1999): 'Hydrodynamics of deinking flotation', TAPPI Recycling symposium, 14-16 April, Chicago, IL, USA, pp 219-241.

[169] Huber P, Rousset X, Zeno E, Vazhure T (2011): 'Parameters of Deinking Efficiency in an Industrial Flotation Bank', Industrial & Engineering Chemistry Research. 50(7), pp 4021–4028.

[170] Zeno E., Huber P., Rousset X., Fabry B., Beneventi D., (2010): 'Enhancement of the Flotation Deinking Selectivity by Natural Polymeric Dispersants', Industrial & Engineering Chemistry Research; 49(19):9322–9329.

[171] Zeno E., Huber P., Rousset X., Beneventi D., Fabry B., (2011): ' Project INNODIP: Towards Optimisation of Flotation Deinking: Influence Of Pulp Flocculation", 13th CTP Recycled Fibres Forum , 1-2February, Grenoble, France.

[172] Mason S.G., (1950): 'The Flocculation of pulp suspensions and the formation of paper', TAPPI Journal, 33(9):440–444, (1950).

[173] Mason S.G., (1954): 'Fibre motions and flocculation', TAPPI Journal, 37(11):494–501.

[174] Kerekes R, Schell C., (1992): 'Characterization of fibre flocculation regimes by a crowding factor', Journal of pulp and paper science, 18(1), J32–J38.

Annexes

Annexe 1: Fines sub fractions by soft Hyperwashing

Object: To further fractionate the fines in sub-fractions for mass fraction analysis and microscopic study by soft Hyperwashing. Fines are washed using light water pressure on hand held sieves. The water jet impingement washing is done till the filtrate turbidity drops to below 15-18 FNU.

Fines contain a range of particles with 2 dimensions lower than an opening of 76 µm. For a better understanding of their various size distribution, it becomes evident to fractionate into smaller fractions i.e., fines sub-fractions. The smaller fractions could then be studied with optical and IR microscopy techniques

Material required :

- Hand held sieves with the following opening[4]:
  - 90µm opening
  - 50µm opening
  - 25µm opening
  - 11µm opening

- 2 glass beakers -150 to 200 mL capacity
- Portable turbidity meter with a clean vial (ex: HACH 2100 P)
- MilliQ water or distilled water (which leaves no residue on evaporation - eventual particle collection to perform microscopic analysis)
- 5L beakers or appropriate containers with single top edge rim. At least 2 in quantity.
- Millipore; preferably 47mm diameter, 0.8µm pore opening – Whatman make. At least 10 in number.
- Millipore filtering equipment.
- Weighing balance, with display accurate to (at least) 4 decimal places
- Stop watch or a simple timer.
- Graduated cylinder of 200mL volume
- Forceps
- Water supply in a flexible pipe having a plastic pipette attached to one end. The diameter of the plastic nozzle is 1mm ± 250µm and the water pressure in the tube is 70kPa ±10kPa. The flow could be controlled using a VFD pump, where a small by pass connection is made for the nozzle attached pipe. Please refer to Figure 224 and Figure 225 for more explanation.

Hand sieve | Turbidity meter | Millipore filter equipment | Plastic nozzle | Millipore filter

Figure 222: Equipment images

[4] *The user can choose the sieve opening according to the requirements.*

Method :

- ❖ Fines are collected by a sufficient quantity of pulp using a Bauer McNett classifier
- ❖ Using the series of 14 28 48 200 mesh.
- ❖ OD weight of Millipore should be taken.
- ❖ Wash the sieves carefully of previous particles residues which can lead to erroneous results.

To perform this, small quantities of fines are taken:

- Flotation rejects: 2 – 3g
- P200 pulp fines: 0.3 – 0.6g (up to 1g)

Suggested sieve combination for:

- Flotation rejects: 90µm → 50µm → 25µm → 11µm
- P200 pulp fines: 50µm → 25µm → 11µm

☞ **Step 1**

Calculate the O.D weight of millipore by placing them on the hot plate dryer between 2 blotting paper.

Calculate the fines concentration on (preferably) 2 millipore pads. More concentrated are fines, less volume to be treated.

☞ **Step 2**

With the help of the pressure gauge, adjust the reading to 70kPa ±10kPa.

Sample the required quantity of fines after thoroughly mixing the container onto the first hand sieve. Place a 5 L beaker under the sieve and then pour the sample at one corner of the sieve, slightly tilting it with one hand.

Using the flexible pipe and keeping at least 15-20 cm distance from the sieve mesh, start 'washing' the particles by moving the water jet in small circles. Every 2-3 minutes with the help of stop watch, collect the filtrate in the 150mL glass beaker (at least 50mL filtrate) after checking turbidity twice of 2 filtrate samples. Return the filtrate to the 5L beaker if the value if more than 15-18FNU. At these particular values of turbidity stop the soft-hyperwashing.

- ❖ It is important to keep the particles in a small area of the sieve. The particles will have a tendency to spurt to different parts of sieve mesh and on the rim (especially for flotation rejects). Hence from time to time wash the particles down to the small area where the majority of particles remain.

☞ **Step 3**

With the help of the water bottle pipette; collect the particles into a small area and recover them by slowly tilting the sieve on a wide mouth glass beaker. Mark the reference of the sample (for ex. R90µm date, sample type) on the edge of Millipore filter by using a ball-point pen. Then deposit the collected particles by filtering on the millipore by using the milipore equipment, example shown in Figure 222. The Millipore is dried at 105℃ overnight. The oven dry weight is taken on an appropriate balance, after at least 30 - 35 minutes by first placing them inside a dessicator.

- ❖ If the particles are to be collected for microscopic examination (and more importantly for preparation of dry slides) it is important to wash them by pouring 3-4 times 200mL distil or MilliQ water on the millpore filtering equipment itself. In this case recover the particles on the millipore filter into a small plastic container, by using distil or MilliQ water in the plastic bottle. It could however be possible to observe the presence of water line deposit after evaporation on slide warmer.

☞ Step 4

Continue the procedure with the next sieve in the series. If the volume of water cannot be poured in one time on the sieve, use the 150mL beaker to pour it in several times.

- ❖ When reaching 11µm sieve, the particle volume to be treated or washed becomes significant, could be 15-18L. Allow the suspension to settle down for 20-30 minutes. Then use a 200mL beaker, decant the top part (which after the sedimentation time will become clear) & pour carefully on the sieve. The water will drain slowly due to extreme small size of the aperture. By carefully holding the sieve, use the water jet to help pass the filtrate.

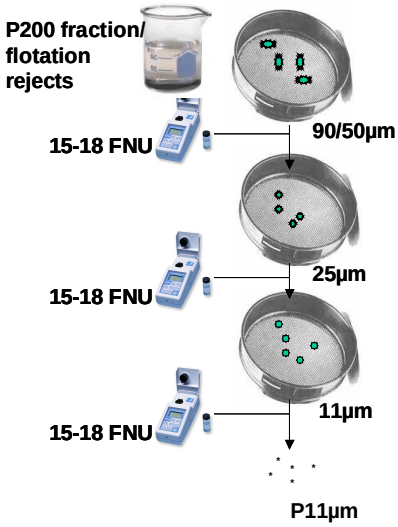

Figure 223: Soft-hyperwashing procedure

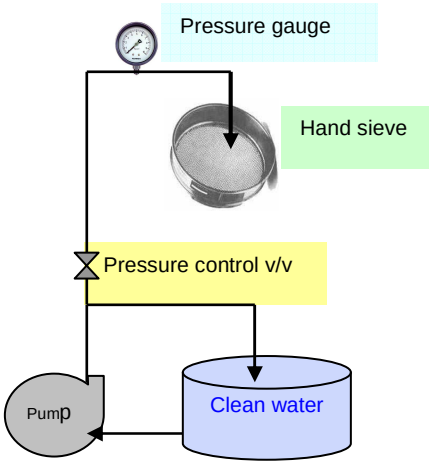

Figure 224: Expt. set up scheme

Figure 225: The actual set up

Annexe 2: Microscope slide preparation

Object: To visualise and observe fine particles – cellulosic fines, ink particles, fillers agglomerate; by the using reflection & transmission Optical Microscopy. (the images taken could be further treated by an image analysis software – ex.: Visilog 6.0)

For particle collection please refer to the protocol-Fines (P200) fractionation by soft – hyperwashing. The particles should be in suspension form in MilliQ or distil water (leaves no residue on evaporation)

Note

- One of the 'pre-requisites' of the microscope used in the study is dry samples for observation (using the protective cover glass causes light diffusion and hence hazy images, also the sample dried up due to heat generated by incident light causing water outlines) Figure 226

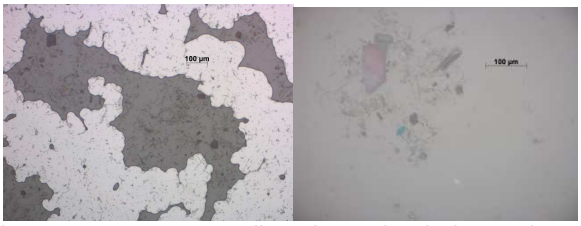

Figure 226: water outline (sample drying up) and hazy images (due to cover glass use)

Material required:

- Glass slides
- Slide warmer/dryer (for dry slides preparation)
- Plastic dropper ou 'compte – gouttes' (5mL capacity) with a wide mouth ~2-3 mm dia
- ~50mL conical glass beaker (for sample dilution)

Some equipment images are shown below:

Optical Microscope (PAGORA)

Plastic dropper

Slide warmer/dryer

Conical flask

Method:

- Please note that this protocol is not based or includes the particle concentration measurement
- Collect fines – sub fractions to be analysed as per Fines (P200) fractionation by soft – hyperwashing protocol.

☞ Step 1

Take 20 – 25mL of the sample in the conical glass beaker. Deposit gently 4 – 5 drops of a thoroughly shaken sample on the glass slide, as shown in. On complete drying, sample reference can also be mentioned on the slide edges.

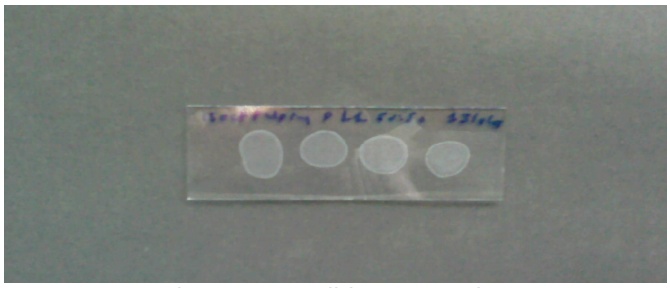

Figure 227: :Slide preparation

- Microscopic analysis of fine particles strongly depend on sample preparation (more observations & better understanding could be gained through a well distribution of particles) On visualization of images, if the particles are not well dispersed as shown in Figure 228, dilute the sample with MilliQ/Distil water to disperse the particles (as shown in Figure 229) in the conical glass beaker and prepare the slide as indicated in Step 1.

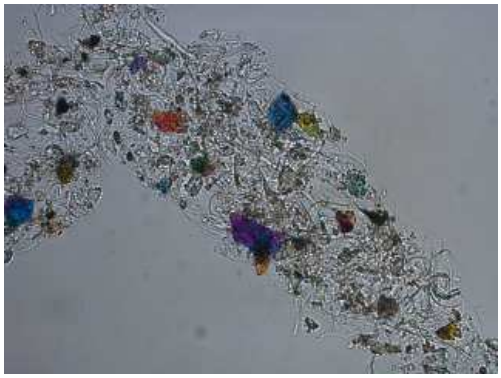

Figure 228: Not well dispersed particles

Figure 229: Dilute and dispersed particles

Annexe 3: Industrial DIP line results

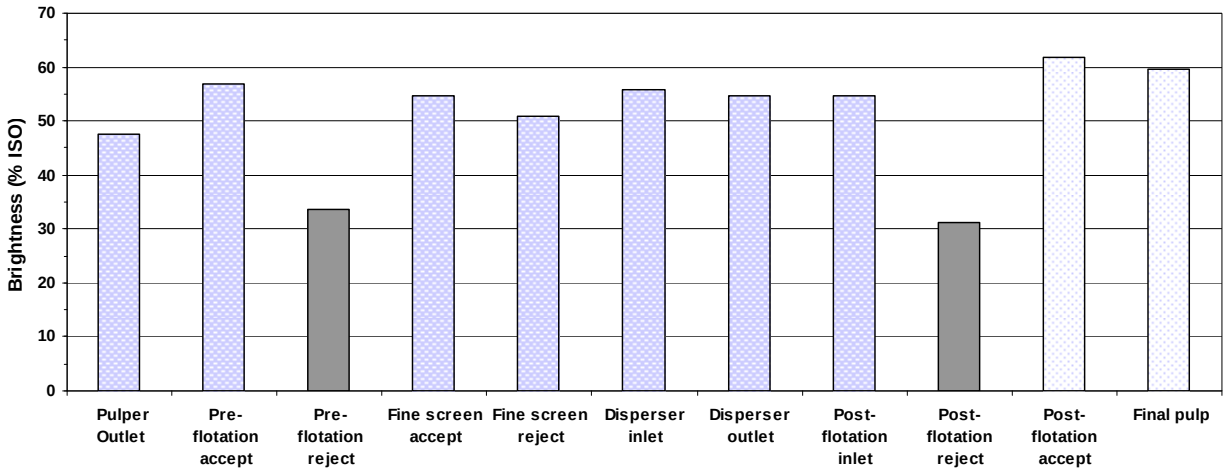

Figure 230: Industrial DIP line whole pulp brightness values

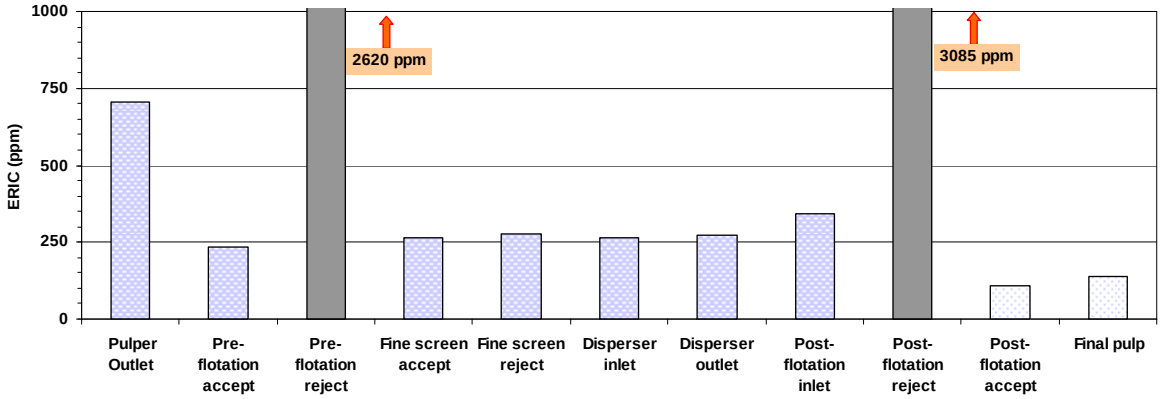

Figure 231: Industrial DIP line whole pulp ERIC values

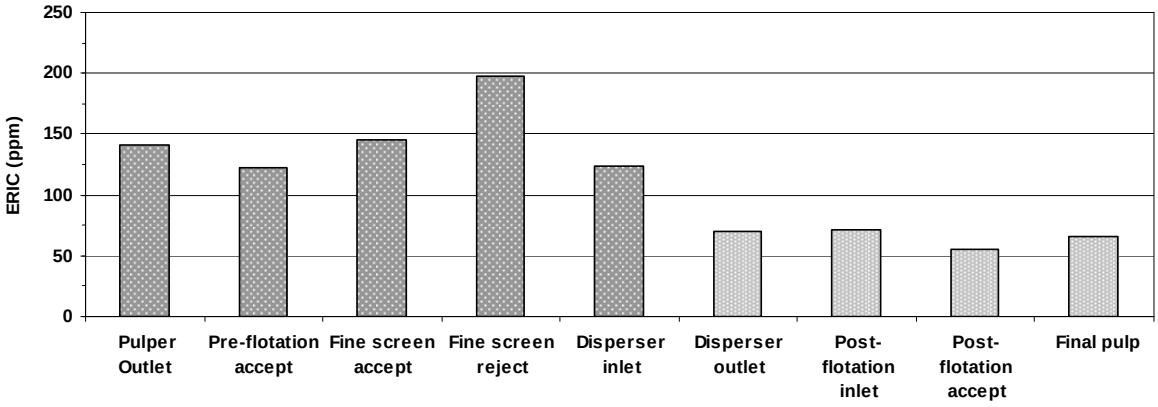

Figure 232: Industrial DIP line hyperwashed pulp ERIC

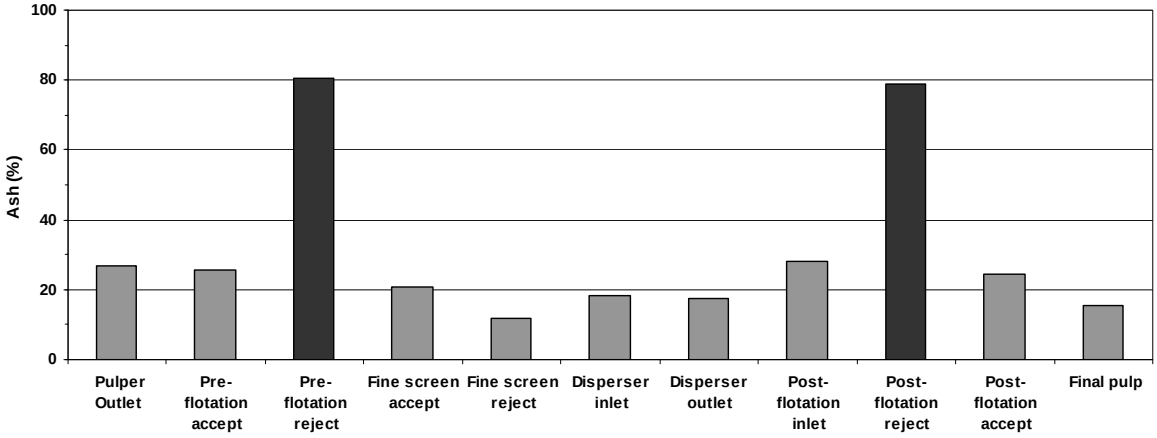

Figure 233: Industrial DIP line whole pulp ash content

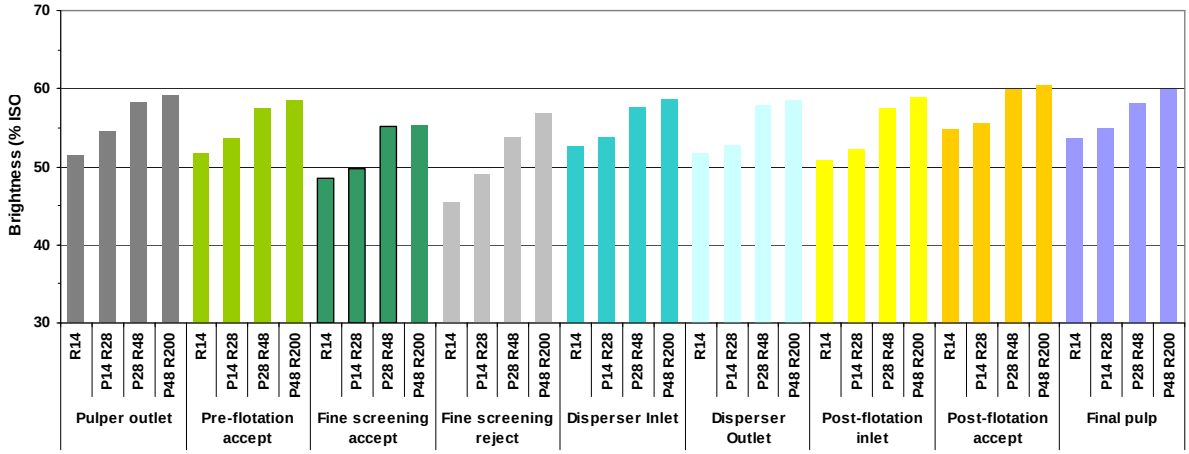

Figure 234: Bauer McNett series 14-28-48-200 brightness

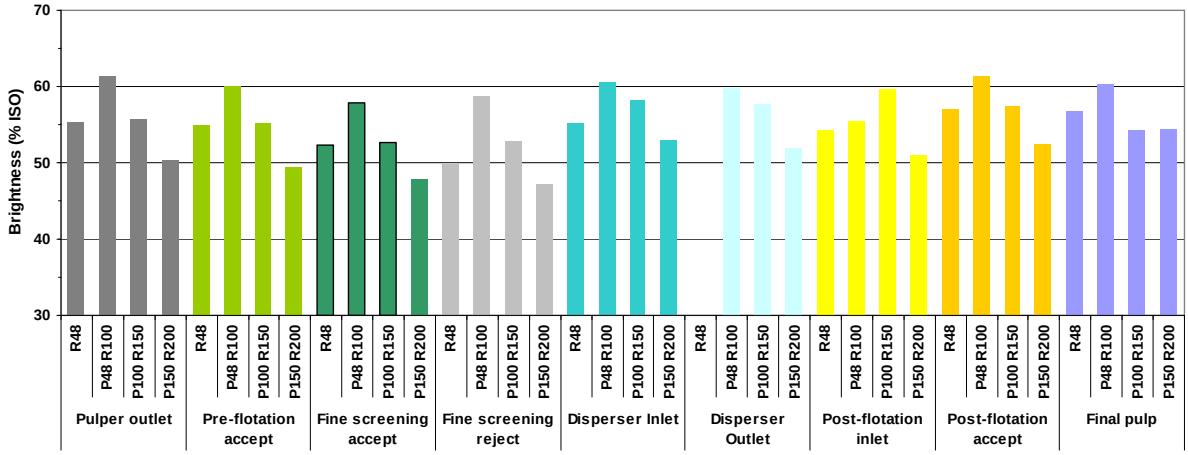

Figure 235: Bauer McNett series 48-100-150-200 brightness

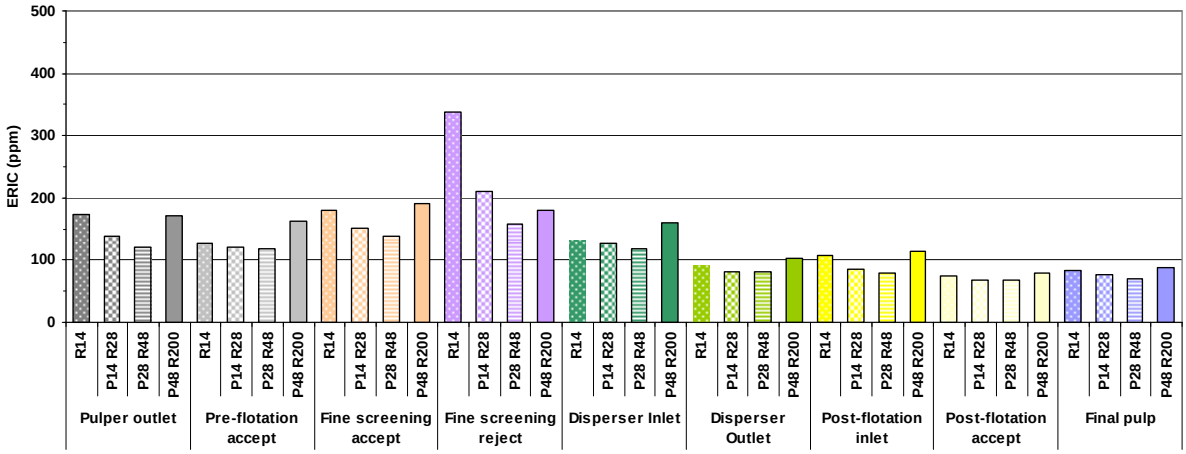

Figure 236: Bauer McNett series 14-28-48-200 ERIC

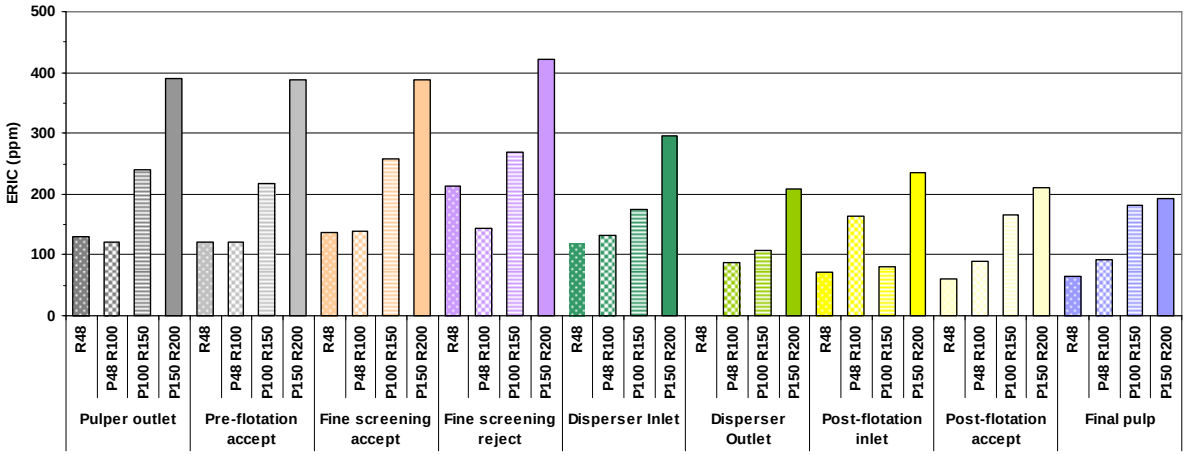

Figure 237: Bauer McNett series 48-100-150-200 ERIC

Annexe 4: Bauer McNett distributions - chemical pulp accepts and rejects

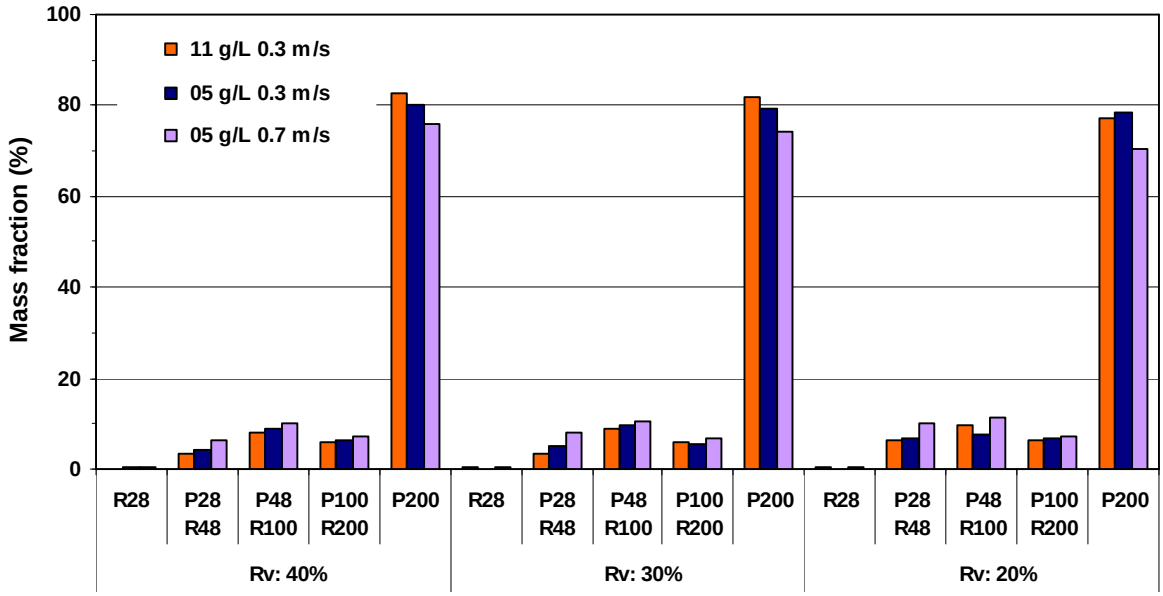

Figure 238: Chemical pulp accepts distributions

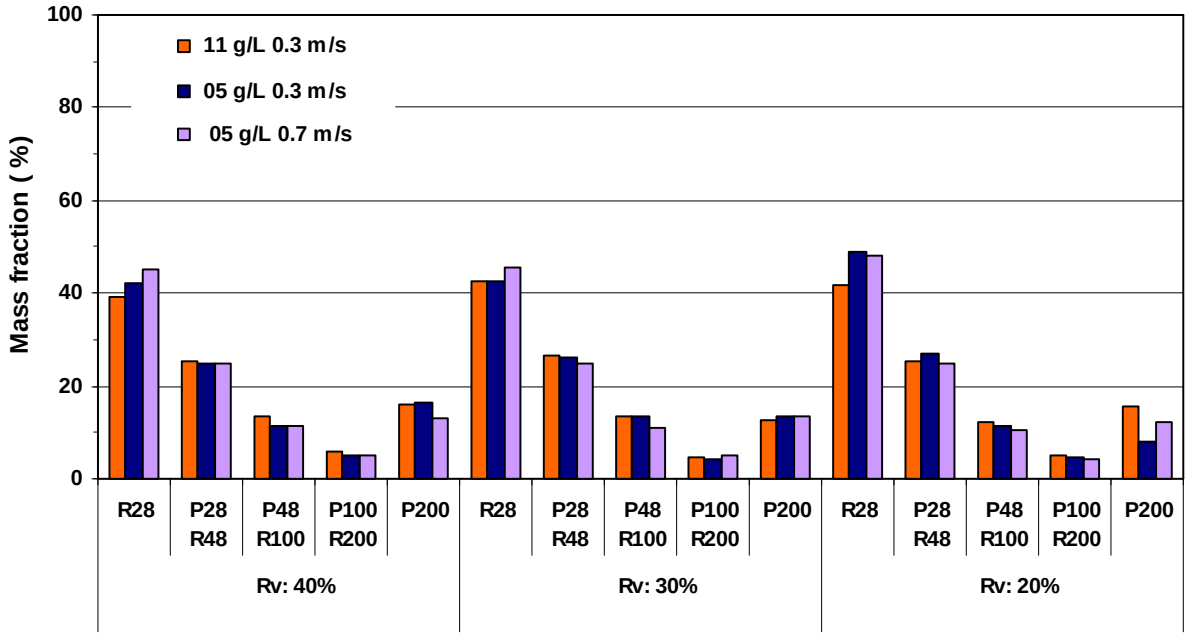

Figure 239: Chemical pulp rejects distributions

Annexe 5: Bauer McNett distributions- ONPOMG 1st and 2nd stages

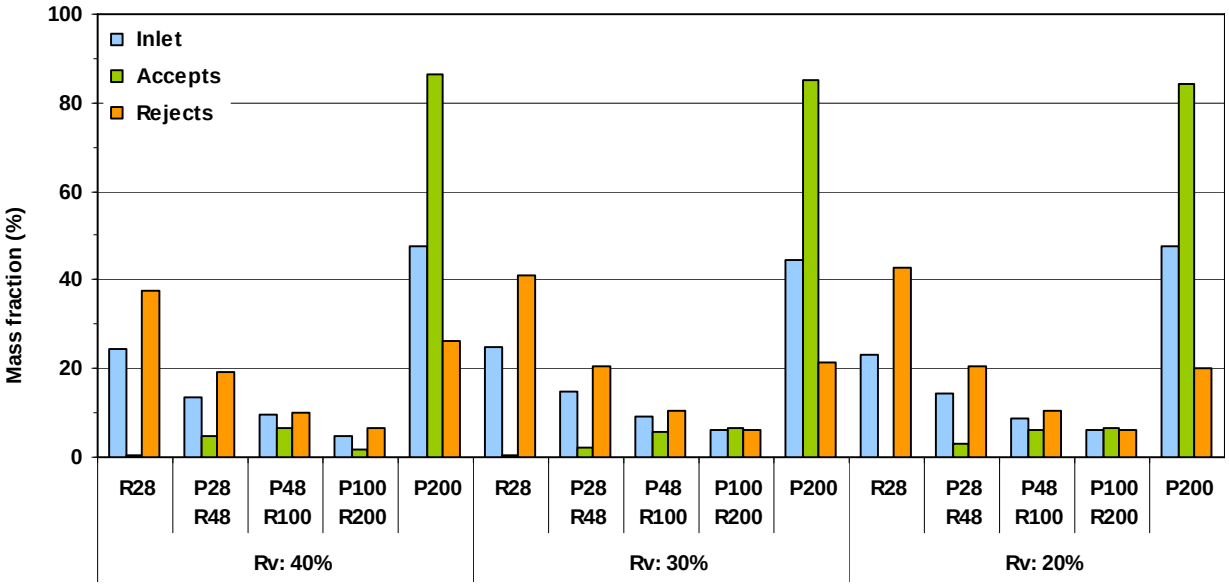

Figure 240: ONPOMG pulp Bauer McNett distributions – 6 g/L 0.6 m/s (1st stage)

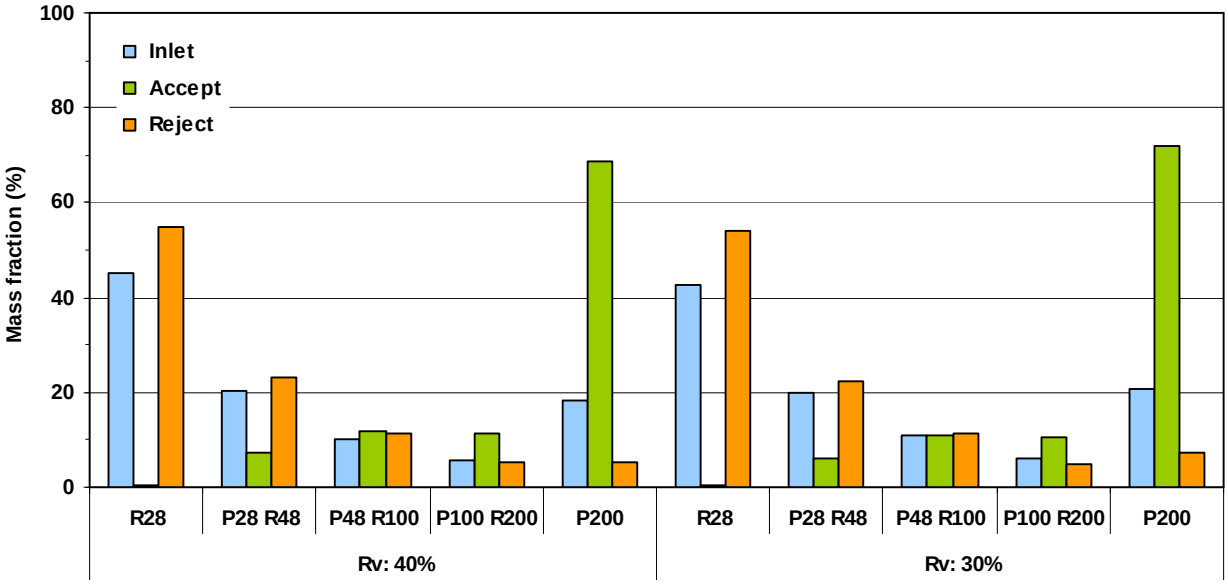

Figure 241: ONPOMG pulp Bauer McNett distributions – 5 g/L 0.5 m/s (2nd stage)

Annexe 6: Whole pulp fibre length - Chemical pulp, ONPOMG 1st & 2nd stage

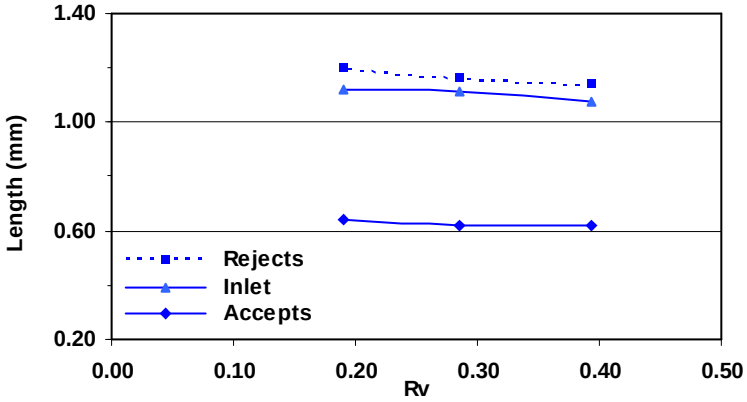

Figure 242: Fibre length for chemical pulp

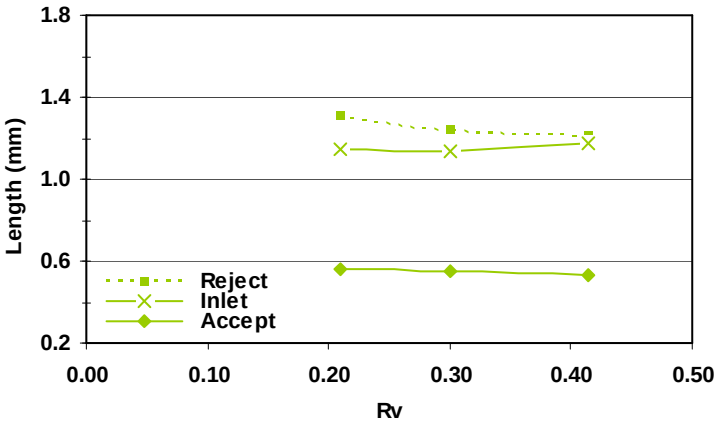

Figure 243: Fibre length for ONPOMG 1st stage

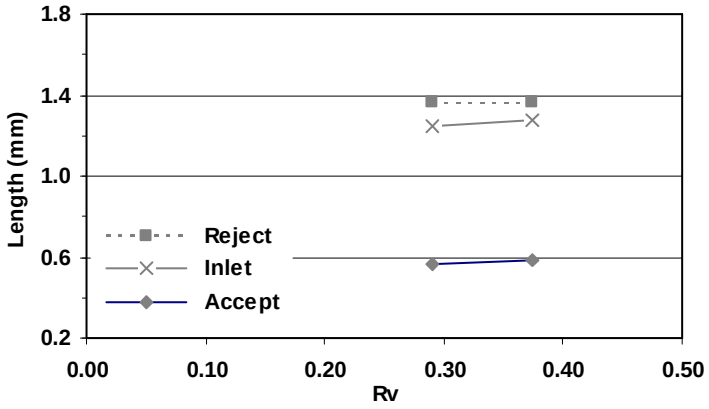

Figure 244: Fibre length for ONPOMG 2nd stage

Annexe 7: Whole pulp fibre length distribution- Chemical pulp, ONPOMG 1st & 2nd stage

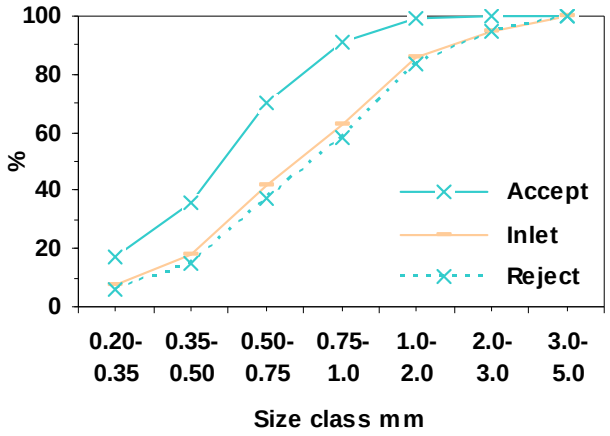

Figure 245: Fibre length distribution for chemical pulp

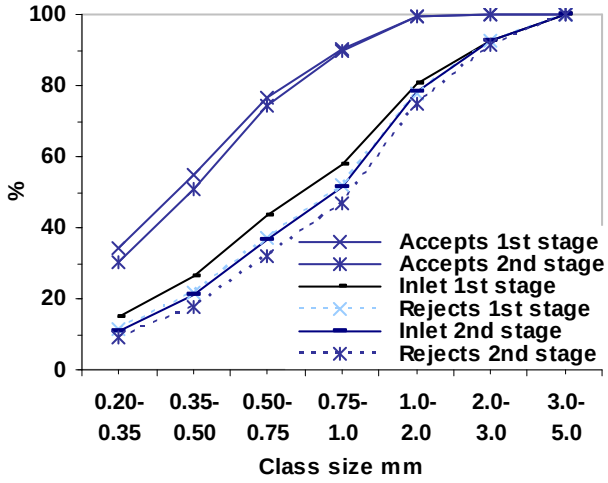

Figure 246: Fibre length distribution for ONPOMG pulp, both stages

Annexe 8: Length distributions for Bauer McNett mesh P48R100 and P100R200

Chemical pulp

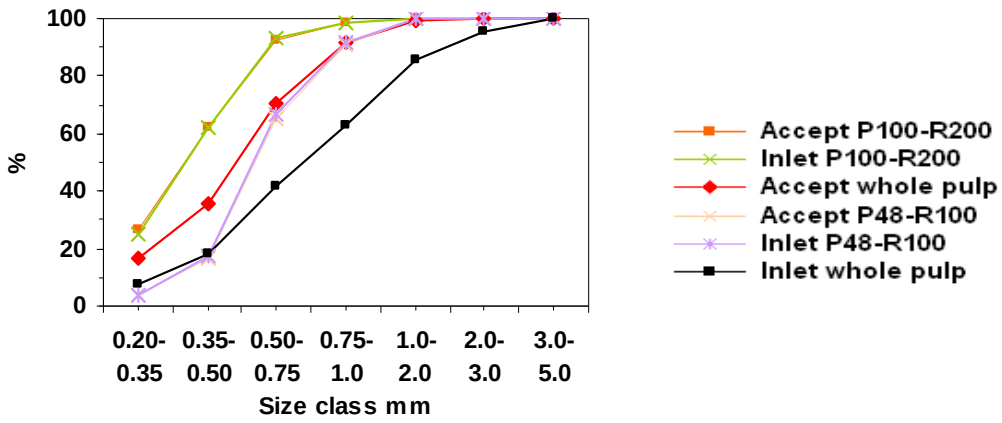

Figure 247: Fibre length for chemical pulp accept– P48-R100 & P100-R200

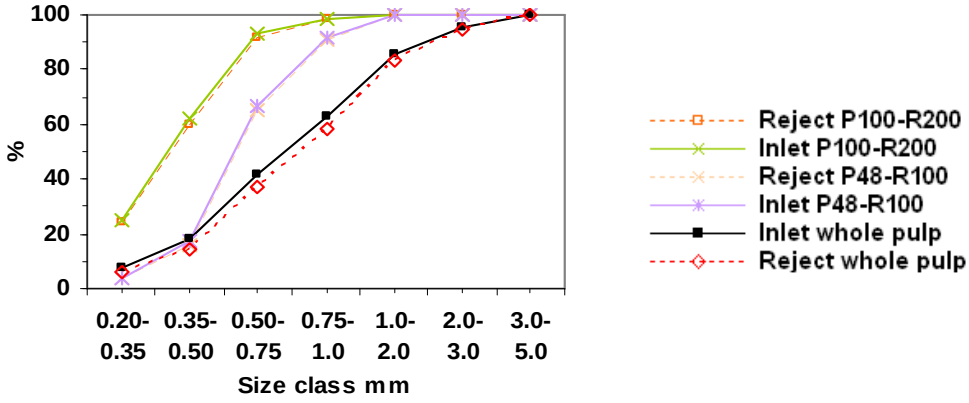

Figure 248: Fibre length for chemical pulp reject – P48-R100 & P100-R200

ONPOMG pulp

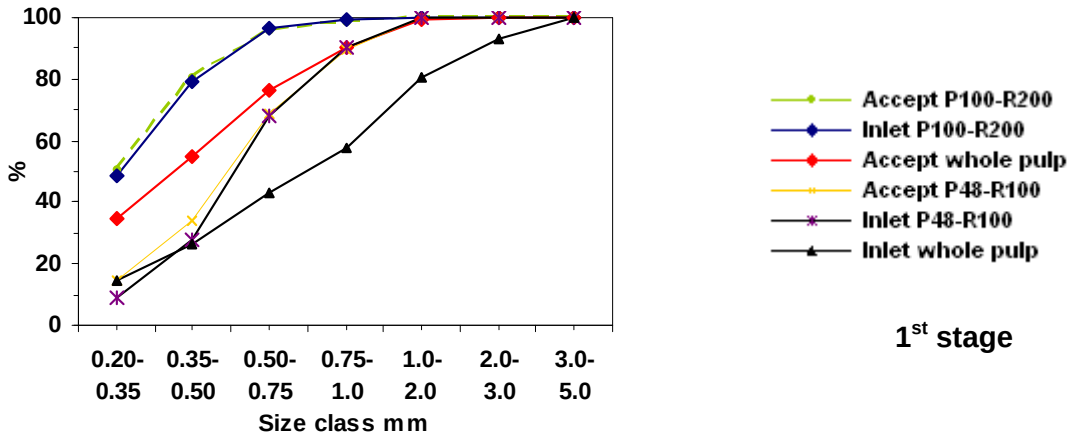

Figure 249: Fibre length for ONPOMG pulp accept 1st stage – P48-R100 & P100-R200

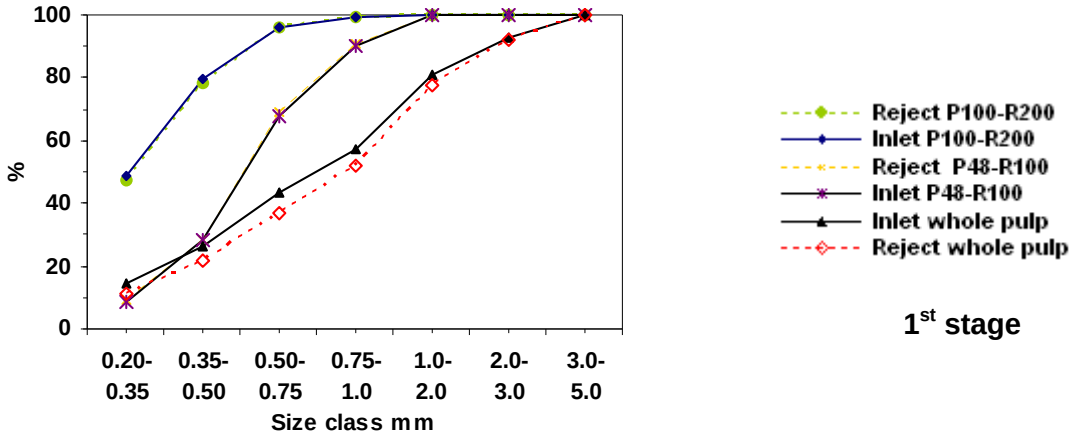

Figure 250: Fibre length for ONPOMG pulp reject 1st stage – – P48-R100 & P100-R200

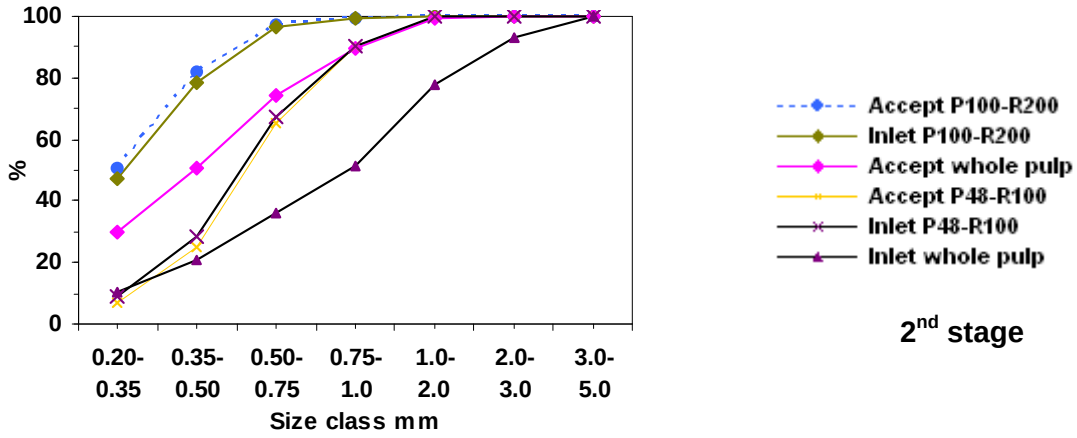

Figure 251: Fibre length for ONPOMG pulp accept 1st stage – P48-R100 & P100-R200

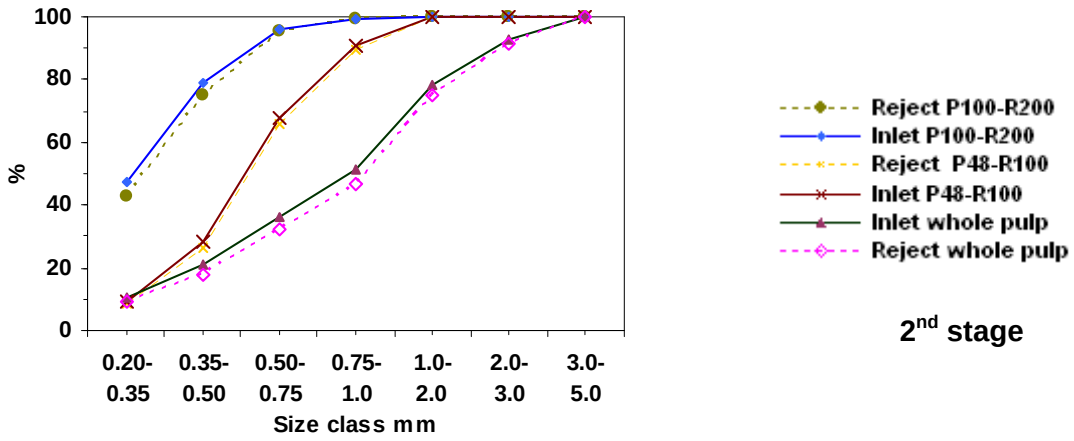

Figure 252: Fibre length for ONPOMG pulp reject 1st stage – – P48-R100 & P100-R200

Annexe 9: Passage ratio calculations for fibre length classes

Example: for SGW pulp

Ca-Concentration accepts:	2.8 g/L
Cr- Concentration reject	14.6 g/L
R_v- Volumetric reject ratio	20%

Length-weighted fibre length class size (MorFi analysis) mm	Average class size mm	Accepts		Rejects		Inlet recalculated Ca(1-R_v)+Cr*R_v	Thickening factor Cr/Ci
		MorFi		MorFi			
		%	g/L	%	g/L	g/L	
0.20-0.35	0.28	45.6	1.28	22.1	3.22	1.66	1.94
0.35-0.50	0.43	26.7	0.75	19.1	2.79	1.15	2.41
0.50-0.75	0.63	18.7	0.52	21.5	3.14	1.04	3.01
0.75-1.0	0.88	5.9	0.17	12.7	1.86	0.50	3.70
1.0-2.0	1.50	3.0	0.08	19.9	2.91	0.65	4.50
2.0-3.0	2.50	0.0	0.00	4.2	0.61	0.12	5.03
3.0-5.0	4.00	0.0	0.00	0.5	0.0762	0.015154	5.03
		∑100 %	∑2.8g/L	∑100 %	∑14.6g/L	∑5.2g/L	

Model

Average class size	Plug flow measured $P = \frac{Ln(T)}{Ln(R_v)} + 1$	Plug flow optimized (regression analysis) $P(l) = e^{-(\frac{l}{\lambda})^{\beta}}$	Mixed flow measured Ca/Cr	Mixed flow optimized (regression analysis) $P(l) = e^{-(\frac{l}{\lambda})^{\beta}}$
mm				
0.28	0.59	0.592	0.396	0.394
0.43	0.45	0.450	0.269	0.268
0.63	0.32	0.313	0.167	0.166
0.88	0.19	0.200	0.089	0.096
1.50	0.07	0.066	0.029	0.027
2.50	0.00	0.012	0.000	0.004
4.00	0.00	0.001	0.000	0.000
		λ: 0.536 β: 0.970		λ: 0.301 β: 0.798

Annex 10: Sheet properties with hydrocyclone fractionated fines

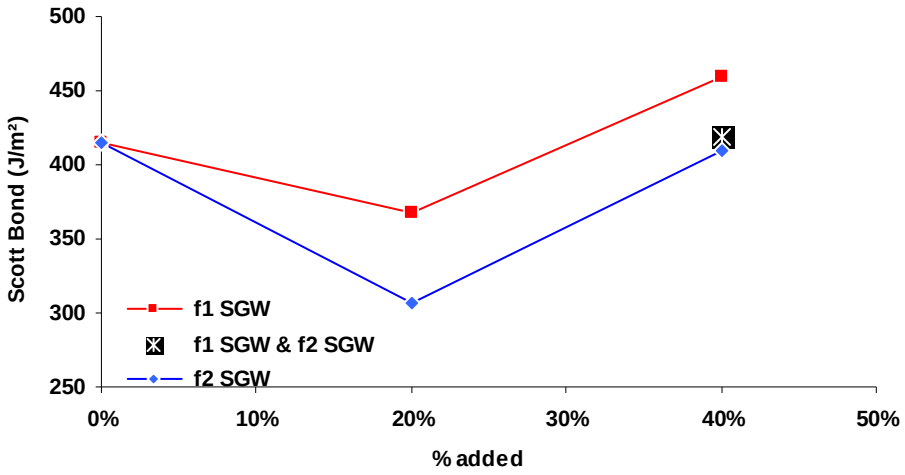

Figure 253: Z-directional strength evolution (Scott-Bond)

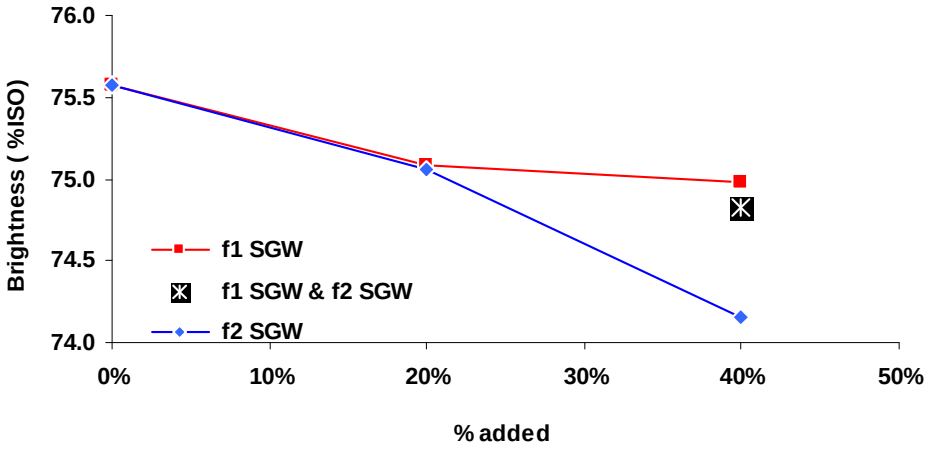

Figure 254: Brightness evolution (wire-side)

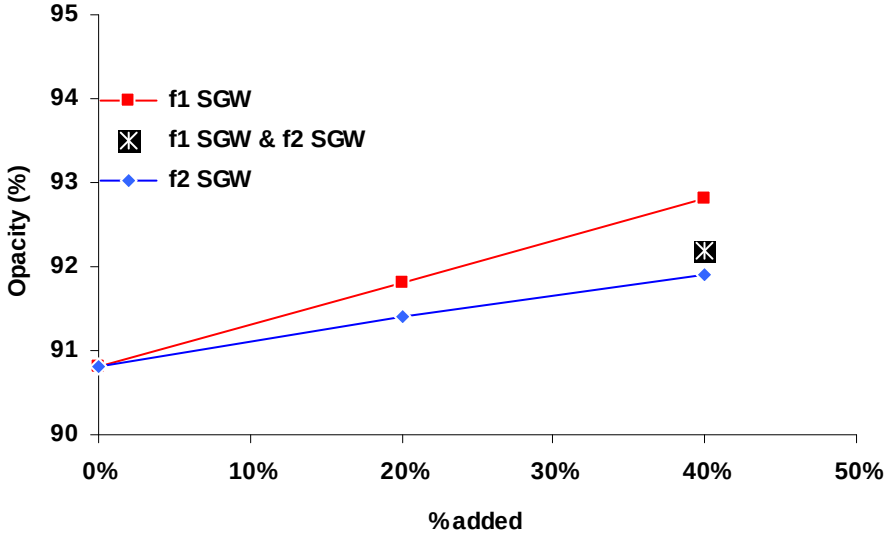

Figure 255: Opacity evolution

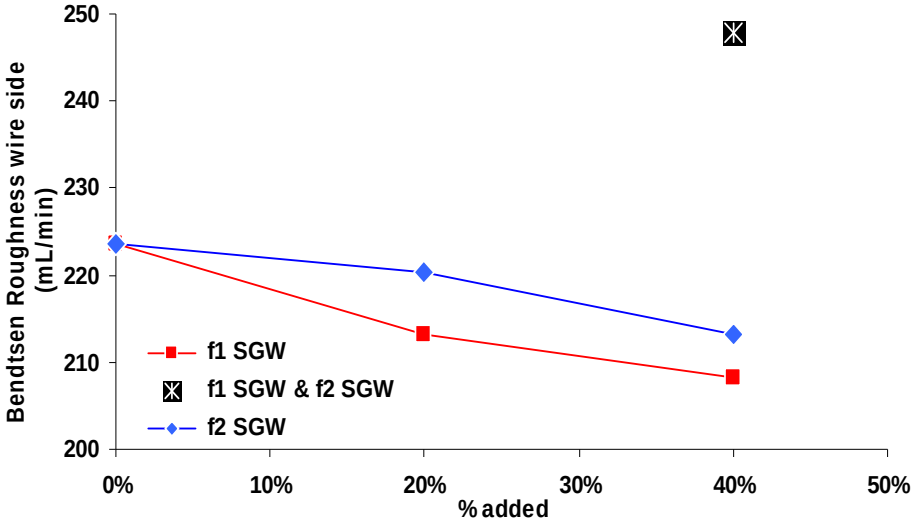

Figure 256: Roughness evolution (wire side)